National Institute of
Environmental Health Sciences

Development and Testing of a Novel Whole-body Exposure System for Investigative Studies of Radiofrequency Radiation in Rodents

August 2025

Development and Testing of a Novel Whole-body Exposure System for Investigative Studies of Radiofrequency Radiation in Rodents

August 2025

National Institute of Environmental Health Sciences
National Institutes of Health

Research Triangle Park, North Carolina, USA

Foreword

The National Institute of Environmental Health Sciences (NIEHS) is one of 27 institutes and centers of the National Institutes of Health, part of the U.S. Department of Health and Human Services. The NIEHS mission is to discover how the environment affects people to promote healthier lives. NIEHS works to accomplish its mission by conducting and funding research on human health effects of environmental exposures, developing the next generation of environmental health scientists, and providing critical research, knowledge, and information to citizens and policymakers to help in their efforts to prevent hazardous exposures and reduce the risk of preventable disease and disorders connected to the environment. NIEHS is a foundational leader in environmental health sciences and committed to ensuring that its research is directed toward a healthier environment and healthier lives for all people.

The environmental health sciences research described in this report was conducted by the Division of Translational Toxicology (DTT) at NIEHS. NIEHS/DTT scientists conduct innovative toxicology research that aligns with real-world public health needs and translates scientific evidence into knowledge that can inform individual and public health decision-making.

This report is available free of charge on the NIEHS website and cataloged in PubMed, a free resource developed and maintained by the National Library of Medicine (part of the National Institutes of Health).

Table of Contents

Tables

Figures

About This Report

Authors

Michael E. Wyde[a], Myles H. Capstick[b], Samantha M. Hall[c], Michelle J. Hooth[a], Niels Kuster[b], John M. Ladbury[d], Georgia K. Roberts[a], Kelly A. Shipkowski[a], Keith R. Shockley[a], Stephanie L. Smith-Roe[a], Matthew D. Stout[a], Nigel J. Walker[a]

[a]Division of Translational Toxicology, National Institute of Environmental Health Sciences, Research Triangle Park, North Carolina, USA

[b]IT'IS Foundation, Zürich, Switzerland

[c]ICF, Reston, Virginia, USA

[d]Spectrum Technology and Research Division, National Institute of Standards and Technology, Boulder, Colorado, USA

Division of Translational Toxicology, National Institute of Environmental Health Sciences, Research Triangle Park, North Carolina, USA
Michael E. Wyde, Ph.D., Lead Toxicologist[1,9,10]
Michelle J. Hooth, Ph.D.[1,10]
Georgia K. Roberts, Ph.D.[1,5,9,10]
Kelly A. Shipkowski, Ph.D.[5,10]
Keith R. Shockley, Ph.D.[1,2,5,10]
Stephanie L. Smith-Roe, Ph.D.[1,2,5,9,10]
Matthew D. Stout, Ph.D.[1,5,10]
Nigel J. Walker, Ph.D.[1,10]

IT'IS Foundation, Zürich, Switzerland
Myles H. Capstick, Ph.D.[1,3,4,6,9,10]
Niels Kuster, Ph.D.[1,3,4,6,9,10]

Spectrum Technology and Research Division, National Institute of Standards and Technology, Boulder, Colorado, USA
John M. Ladbury, M.S.[1,3,4,6,9,10]

ICF, Reston, Virginia, USA
Contracts 75N96025C00003 and GS00Q14OADU417 (Order No. HHSN273201600015U)
Samantha M. Hall, Ph.D.[9,10]

Contributors

Division of Translational Toxicology, National Institute of Environmental Health Sciences, Research Triangle Park, North Carolina, USA
Danica Andrews, B.S.[5]
Milene L. Brownlow, Ph.D. (currently at NIH Center for Scientific Review)[12]
Helen C. Cunny, Ph.D.[5]
Jennifer M. Fostel, Ph.D.[5]
Ronald A. Herbert, D.V.M., Ph.D.[5]
Angela P. King-Herbert, D.V.M.[5,9]

Ronald A. Herbert, D.V.M., Ph.D.[5]
Angela P. King-Herbert, D.V.M.[5,9]
Scott A. Masten, Ph.D.[10]
Jason P. Stanko, Ph.D.[5]
Pei-Li Yao, Ph.D.[5]
Mary S. Wolfe, Ph.D.[12]

Spectrum Technology and Research Division, National Institute of Standards and Technology, Boulder, Colorado, USA
Jason Coder, M.S.[10]

Battelle, Columbus, Ohio, USA
Contract HHSN273201400015C
Barney R. Sparrow, Ph.D., Principal Investigator[5,6]

AmplifyBio, West Jefferson, Ohio, USA
Subcontract to HHSN273201400015C
Sarah Shellenbarger, B.S.[3]
Amy M. Zmarowski, Ph.D.[3]

Taconic BioSciences, Inc., Germantown, New York, USA
Contract HHSN273201600020C
Jeffrey Lohmiller, D.V.M., Principal Investigator[5,6]
Emily Hackett[3]

Instem, Staffordshire, United Kingdom
Contract HHSN273201300004C
Mark Handley, Computing H.N.C., Program Manager[2,5,6]
Pam Reese, B.S.[2]
Martin Tyska, M.S.[2]

ASRC Federal, Research Triangle Park, North Carolina, USA
Contract 75N96023A00001
Julie Berke, B.S.[2]
Phyllis B. Brown, B.S.[2]
Erik Diffin, B.S.[2]
Karen S. Gilbert, B.S.[2]
Marcus A. Jackson, B.S.[2]
Tony Silver, B.S.[2]

Integrated Laboratory Systems, LLC, an Inotiv Company, Research Triangle Park, North Carolina, USA
Contract 75N96020C00001
Leslie Recio, Ph.D., Principal Investigator[5,6]
Cheryl A. Hobbs, Ph.D., Principal Investigator[3,5,6]
Lincoln Martin, M.S.[3]

CSS Corporation, Research Triangle Park, North Carolina, USA
Contract HHSN273201500006C
Steven Brecher, Ph.D., Principal Investigator[5,6,11]
Holly Dimig, B.S.[11]
Sudha Iyer, B.S.[11]
Varghese S. Tharakan, D.V.M.[11]

Social & Scientific Systems, a DLH Company, Research Triangle Park, North Carolina, USA
Contract GS-00F-173CA/75N96022F00055
Katherine N. Allen, Ph.D., Principal Investigator[2,5,6]
Laura J. Betz, M.S.[2]
Shawn F. Harris, M.S.[2]
Guanhua Xie, Ph.D.[2]

ICF, Reston, Virginia, USA
Contracts 75N96025C00003 and GS00Q14OADU417 (Order No. HHSN273201600015U)
David F. Burch, M.E.M., Principal Investigator[5,6]
Barrett D. Allen, Ph.D.[10]
Katherine S. Duke, Ph.D.[10]
Lindsey M. Green, M.P.H. [12]
Tara Hamilton, M.S.[10]
Cary E. Haver, M.P.H.[5]
Aishwarya Javali, M.S.[12]
Kevin T. O'Donovan, B.A.[10]
Lisa M. Prince, Ph.D.[10]
Swati Sriram, M.P.H.[10]
Nkoli Ukpabi, M.S.[10]
Jared Wang, M.E.M.[10]
Jessica A. Wignall, M.S.P.H.[5,6]

Author and Contributor Roles and Definitions[a]

No.	Role	Definition
1	Conceptualization	Ideas; formulation or evolution of overarching research goals and aims
2	Data Curation, Formal Analysis, and Software	Management activities to annotate (produce metadata), scrub, and maintain research data (including software code, when it is necessary for interpreting the data) for initial use and later reuse or Application of statistical, mathematical, computational, or other formal techniques to analyze or synthesize study data or Programming and software development; design of computer programs; implementation of computer code and supporting algorithms; testing of existing code components
3	Investigation	Conduct of the research/investigation process, specifically the performance of experiments or the collection of data/evidence
4	Methodology	Development or design of methodology; creation of models
5	Project Administration	Management and coordination responsibility for research planning and execution
6	Resources for Study Conduct	Provision of study materials, reagents, patients, laboratory samples, animals, instrumentation, computing resources, or other analysis tools
7	Validation	Verification, whether as a part of the activity or separately, of the overall replication/reproducibility of results/experiments and other research outputs
8	Visualization	Preparation, creation, and/or presentation of the published work, specifically visualization/data presentation
9	Writing: Original	Preparation, creation, and/or presentation of the published work, specifically the writing of the initial draft (including substantive translation)
10	Writing: Review and Editing	Preparation, creation, and/or presentation of the published work by those from the original research group, specifically provision of substantive critical review, commentary, or revision—including pre- or post-publication stages
11	Quality Assessment	Conduct of independent assessments of accuracy, consistency, and completeness of various aspects of research products and their components, including data; identification of areas in the conduct and documentation of studies that merit correction or improvement of the description of methodologies
12	Peer Review and Production	Coordination and management of external peer review and publication, including identification of experts, conflict-of-interest screening, correspondence with reviewers, preparation of review documents, and publication activities

[a]Developed using the Contributor Roles Taxonomy (CRediT) framework.[1]

Peer Review

The National Institute of Environmental Health Sciences Division of Translational Toxicology (NIEHS/DTT) secured the services of the experts listed below to conduct a peer review by letter of the draft report, *Development and Testing of a Novel Whole-body Exposure System for Investigative Studies of Radiofrequency Radiation in Rodents*, in November 2024. Reviewer selection and document review followed established NIEHS/DTT practices. The reviewers were charged to:

(1) Provide external peer review of the draft report, *Development and Testing of a Novel Whole-body Exposure System for Investigative Studies of Radiofrequency Radiation in Rodents*.

(2) Comment on whether the information in the draft report is clearly stated and objectively presented.

NIEHS/DTT carefully considered the reviewers' comments in finalizing this report.

Peer Reviewers

Frank Barnes, Ph.D.
Distinguished Professor Emeritus, Department of Electrical, Computer, and Energy Engineering
University of Colorado
Boulder, Colorado, USA

Asimina Kiourti, Ph.D.
Associate Professor, Department of Electrical and Computer Engineering
The Ohio State University
Columbus, Ohio, USA

J. Mark Cline, D.V.M., Ph.D.
Professor, Department of Pathology
Wake Forest School of Medicine
Winston-Salem, North Carolina, USA

Matthew LeBaron, Ph.D.
Toxicologist
The Dow Chemical Company
Midland, Michigan, USA

Susan Felter, Ph.D.
Vice President, Victor Mills Society
Procter & Gamble
Mason, Ohio, USA

Publication Details

Publisher: National Institute of Environmental Health Sciences

Publishing Location: Research Triangle Park, NC

DOI: https://doi.org/10.22427/NIEHS-RFR

Official citation: Wyde ME, Capstick M, Hall SM, Hooth MJ, Kuster N, Ladbury JM, Roberts GK, Shipkowski KA, Shockley KS, Smith-Roe SL, Stout MD, Walker NJ. 2025. Development and testing of a novel whole-body exposure system for investigative studies of radiofrequency radiation in rodents. Research Triangle Park, NC: National Institute of Environmental Health Sciences.

Acknowledgments

This work was supported by the Intramural Research Program (ES103374 and ES103380) at the National Institute of Environmental Health Sciences (NIEHS), National Institutes of Health and performed for NIEHS under contracts 75N96025C00003, 75N96023A00001, GS-00F-173CA/75N96022F00055, 75N96020C00001, HHSN273201800006C, GS00Q14OADU417 (Order No. HHSN273201600015U), HHSN273201600020C, HHSN273201500006C, HHSN273201400015C[1], and HHSN273201300004C.

[1]These studies were conducted under the NIEHS contract with Battelle Memorial Institute (HHSN273201400015C). The studies were initiated at the Battelle testing facility in West Jefferson, Ohio. On May 1, 2021, the testing facility was transferred to a new company, AmplifyBio. The study was transferred to AmplifyBio as a subcontract under HHS273201400015C. All of the installation and verification activities were conducted while Battelle was the testing facility. For the mouse study, all of the in-life, postmortem, and analytical portions of the study were conducted while Battelle was the testing facility; reporting was conducted under AmplifyBio as the testing facility. The rat studies were conducted under AmplifyBio as the testing facility.

Executive Summary

The predominant source of human exposure to radiofrequency radiation (RFR) occurs through the use of cell phone handsets. Previous toxicology studies on RFR, conducted in support of the National Toxicology Program (NTP) by researchers at the National Institute of Environmental Health Sciences (NIEHS), found exposure-related effects on body temperature and DNA damage. The studies reported herein were conducted by NIEHS researchers in the Division of Translational Toxicology to better understand the biological mechanisms that produced tumor development and DNA damage in exposed rodents. These studies were not conducted as part of the NTP.

The goals of the current research were to design, construct, and use a small-scale RFR exposure system to conduct toxicological research in rats and mice. One of the primary specific objectives of this research was to test and use new, experimental methods to collect physiological data from animals in real time during RFR exposures, including assessment of body temperature and use of videos for clinical observations. Previously, such data collections were not feasible without cessation of RFR exposure.

A new RFR exposure system based on the technical parameters of the system used in the previous NTP toxicology and carcinogenesis studies was developed for small-scale investigative studies with fewer animals. The system was designed with enhanced capabilities and more flexibility, including the ability to generate additional radiofrequency (RF) signals with frequencies and modulations used in more current wireless communication technologies. After development and installation, the system was rigorously tested and independently verified before animal studies were conducted. Following completion of the mouse study, several system modifications were required before the rat studies could be conducted. These system modifications required significant technical expertise and sometimes took several months to resolve successfully.

A series of 5-day studies was conducted in male or female Sprague Dawley (Hsd:Sprague Dawley® SD®) rats or B6C3F1/N mice to evaluate the effect of exposure to the same Code Division Multiple Access (CDMA)- or Global System for Mobile Communications (GSM)-modulated RF signals used in the previous NTP studies. Video from the cameras in the exposure chambers demonstrated no visible response in either rats or mice at the first time the exposure system was activated, at subsequent system on/off transitions, or during the periods of exposure. Exposure to RFR for 5 days did not induce DNA damage in brain cells (frontal cortex, hippocampus, and cerebellum), or in liver, heart, or blood cells of rats and mice, as measured using the comet assay. These investigative studies of RFR exposure were technically challenging to conduct and, unfortunately, measurement by two different methods did not yield data useful for assessing body temperature during exposure.

Despite a number of difficulties (i.e., engineering requirements, system modifications, measurement of body temperature during exposure), this small-scale RFR exposure system presents a prototype for investigative toxicological studies by researchers interested in conducting experimental RFR studies in rodent models. High-quality studies to understand the effects of RFR exposure on biological responses are needed given the widespread human exposure to RFR associated with cell phone use. The aim of this report is to share knowledge and facilitate advancement in research methodologies for investigating the potential health effects of RFR.

1. Overview

1.1. Introduction

Cell phones and other commonly used wireless communication devices transmit their signals via radiofrequency radiation (RFR). At high exposure levels, nonionizing RFR can produce a heating effect that can damage tissues and biological systems. However, little is known about the potential health effects of long-term exposure to low levels of RFR, and current exposure guidelines are based on protection from acute injury resulting from thermal effects.

Findings from some epidemiology studies suggest that exposure to RFR from cell phones is associated with brain tumors (gliomas and vestibular schwannomas) in heavy cell phone users,[2-6] while other studies have not consistently demonstrated a causal link between cell phone RFR and these same tumor types.[7-11] Interpretation of the results of these epidemiological studies is complicated by methodological issues such as confounding factors and potential recall biases. Additionally, exposures in the general population may not have occurred for a long enough period to account for the long latency period between exposure and the development of neoplasms.

The signal frequency and modulation of the radiofrequency (RF) signal may play a critical role in the potential interaction between RFR and biological tissues. RFR at the 900 and 1,900 MHz frequencies with signal modulating technologies, i.e., Code Division Multiple Access (CDMA) and Global System for Mobile Communications (GSM), used in 2G and 3G networks were previously evaluated in National Toxicology Program (NTP) studies. While 2G and 3G networks using these technologies were largely phased out in the United States in 2022, these networks continue to be used in other parts of the world. Additionally, the 900 and 1,900 MHz frequencies are used in 4G and 5G networks.

To assess the biological plausibility that nonionizing radiation may induce cancer, 2-year chronic toxicity and carcinogenicity studies were previously conducted as part of an NTP research program on cell phone RFR.[12; 13] These previous NTP studies found that exposure to GSM- or CDMA-modulated cell phone RFR at 900 MHz was associated with increases in the incidences of neoplastic lesions in the heart, brain, and adrenal glands of male Sprague Dawley (Hsd:Sprague Dawley® SD®) rats. Increased incidences of nonneoplastic lesions were also observed in the heart, brain, and prostate gland of male rats, and in the heart, thyroid gland, brain, and adrenal gland of female rats exposed to RFR. The results of these NTP studies supported an earlier assessment by the International Agency for Research on Cancer, which classified exposure to cell phone RFR as possibly carcinogenic to humans (Group 2B).[14]

1.2. NTP Toxicology and Carcinogenicity Studies

The previous 2-year chronic toxicity and carcinogenicity studies conducted under the auspices of NTP were led by National Institute of Environmental Health Sciences Division of Translational Toxicology (NIEHS/DTT) scientists who worked with technical experts at the Foundation for Research on Information Technologies in Society (IT'IS Foundation, Zürich, Switzerland) to design and construct a novel RFR exposure system that was used to conduct a series of in vivo studies, including 2-year chronic toxicity and carcinogenicity studies. The RFR exposure system

was tested and then independently verified by technical experts at the National Institute of Standards and Technology (NIST).

The approach used in the previous NTP studies included an early phase to investigate the thermal effects of RFR exposure and established maximal acute-exposure levels without significantly altering body temperatures. In these previous 5-day studies, exposure-related increases in body temperatures were observed at exposure levels ≥6 W/kg body weight (W/kg) in male and female Sprague Dawley rats, with exposure levels above 10 W/kg inducing increases in body temperature (≤3°C) and mortality in aged rats.[15] In B6C3F1/N mice, only sporadic increases in body temperature were observed regardless of sex or age when exposed to GSM or CDMA RFR up to 12 W/kg.[15]

In the previous 28-day studies, exposure of pregnant rats to GSM or CDMA RFR at 9 W/kg from gestation day (GD) 6 through postnatal day (PND) 21 resulted in decreased body weight and increased body temperatures of pregnant rats during gestation and of pregnant rats and their offspring during lactation.[13] These effects were not observed in male or female mice exposed to RFR up to 15 W/kg for 28 days.[12]

In the previous NTP chronic rat studies, exposure to GSM or CDMA RFR (≥1.5 W/kg) was associated with increased incidences of malignant schwannomas in the heart, malignant gliomas in the brain, and pheochromocytomas in the adrenal medulla.[13] Comet assay results in male rats after 19 weeks of exposure (CDMA) were positive for DNA damage in the hippocampus.[16] At the end of the study, survival was significantly increased in all groups of RFR-exposed males compared to control male rats.[13] In mice, no carcinogenic effects were observed in males or females exposed to RFR.[12] However, comet assay results in mice after 14 weeks of exposure were positive for DNA damage in the frontal cortex of the brain in males (GSM and CDMA) and in the blood in females (CDMA).[16] Positive findings in the brain of male mice were specific to the frontal cortex and were not observed in the hippocampus or the cerebellum.[16]

1.3. Research Rationale and Goals

The previous NTP experimental studies demonstrated that chronic, low levels of RFR exposure can induce biological changes in a mammalian system (rodents). These study findings were novel and provided biological plausibility for RFR-induced toxicity and carcinogenicity; however, critical knowledge gaps still existed. Evaluating the potential implications of RFR exposure on human health is dependent on understanding the interactions between RFR and biological tissues, the factors that affect those interactions, and the relationship to different magnitudes and patterns of RFR exposure. Appropriately designed experimental studies can provide insights into the relationship between RFR exposure and biological outcomes, such as carcinogenicity in rodents. These insights can then inform a framework for evaluating the potential for human responses given real-world patterns of exposure to lower levels of RFR. When extrapolating from animal studies to human risk assessments for the effects of RFR, many complicating factors make the evaluation of exposure challenging including the various ways people use their cell phones, such as via Bluetooth® headsets or speakerphone, or by putting the device directly next to their ear. Complicating factors also include variation in RFR exposure among individuals due to disparities in signal strength based on geographical location with respect to a cell phone tower.

The logistics and challenges of designing and carrying out high-quality studies on RFR exposure can be difficult. Because of inherent challenges in studying electromagnetic radiation, robust studies on RFR tend to be more complicated than toxicology studies of pharmaceuticals or environmental chemicals. Key considerations for the technical approach are ensuring that experimental animals are consistently exposed to constant levels of RFR, that the chamber design components and any equipment in the chamber do not interfere with delivery of the RFR signal to the animals, that the animals can be monitored in real time while the system is active, that the chamber design and amplification system do not cause undue stress on the animals, and that animal husbandry tasks can be easily performed.

In an effort to better understand some of the findings from the previous NTP studies and extend technical knowledge on the potential biological effects resulting from RFR exposure,[12; 13; 15; 16] scientists at the NIEHS/DTT worked with technical experts at IT'IS Foundation and the testing facility to design and develop a novel small-scale RFR exposure system based on many of the specifications of the large-scale system developed for the previous NTP studies, but with additional functionality required to conduct follow-on studies. This novel small-scale system was designed to generate multiple RF signals and frequencies used in 2G, 3G, and 4G long-term evolution (LTE) technologies and expanded exposure capabilities not available at the time the previous NTP studies were conducted. Similar to the previous NTP studies, experts from NIST provided independent verification of the system functionality following installation at the testing facility for the current NIEHS/DTT study.

The goal of the research presented in this report was to conduct a series of short-term investigative studies to assess the use of this new small-scale RFR exposure system for toxicological research. These studies aimed to use real-time physiological monitoring of rats and mice to evaluate the impact of RFR exposure on stress, heart rate, and body temperature, and further assess whether RFR exposure causes DNA damage.

To reduce the size of the overall study, a targeted combination of sex-species-modulation was selected to focus primarily on those that induced the most robust effects in the previous NTP studies. In the current studies, male rats were exposed to CDMA or GSM-modulated RFR, and female rats and male mice were exposed to CDMA-modulated RFR.

This report provides in-depth details on the design, construction, function, and testing of the novel small-scale RFR exposure system and the technical challenges associated with its construction and operation. It also provides findings from the investigative studies and compares them to findings from previously published NTP studies on RFR exposure.

2. Chamber Design, Exposure Generation, and Monitoring

2.1. Introduction

The radiofrequency radiation (RFR) exposure system was designed to produce exposure conditions identical to those utilized in the previous National Toxicology Program (NTP) studies. The reverberation chamber-based exposure design included an automatic control system with exposure and environmental condition monitoring and logging. Each reverberation chamber was a resonant box in which the resonances and field structure were continuously modified under the influence of metallic stirrers, while shielding the outside environment from the fields inside the chambers and preventing external RFR exposure into the chamber. The RFR exposures were generated and monitored by a computer-controlled system that comprised a radiofrequency (RF) source, signal amplifiers, and a data acquisition system. Each reverberation chamber was equipped with sensors that enabled the computer control system to monitor and record the exposure and environmental conditions. Like the large-scale system used in the previous NTP studies, the small-scale RFR exposure system included four chambers, each capable of delivering a different power level of RFR, but it was designed on a smaller scale to accommodate a smaller number of animals with a smaller facility footprint.

The exposure system was designed, constructed, and tested at the Foundation for Research on Information Technologies in Society (IT'IS) in Zürich, Switzerland. The system was then disassembled, shipped to the testing facility in West Jefferson, Ohio, reassembled, and installed before final system verification and qualification could be conducted.

2.2. Chamber Design

The final chamber design, including supporting information, tables, and figures are shown in Appendix A, Section A.3. A reverberation chamber exposure system was used for the studies for the primary benefit that controlled exposures can be achieved in unrestrained animals (e.g., rats and mice).

Each reverberation chamber (Figure 1) was designed to house 10 cages with one animal per cage in Thoren #7 cages (Hazleton, PA) with a cage floor area of 474 cm^2. Based on the homogeneity results of previous analyses that modeled the specific absorption rate (SAR) distribution of RFR across the whole body, rats were exposed at a frequency of 900 MHz, and mice were exposed at 1,900 MHz.[17] The chambers were constructed of stainless steel with fully welded seams to ensure no RF leakage. Additionally, a twin finger stock approach was used on the chamber doors to achieve the required shielding effectiveness, and a latch was used to secure the door in the closed configuration. Power and other electrical connections were fully shielded or filtered. Power was passed through a Mains filter (Schaffner, Luterbach, Switzerland) with suitable attenuation characteristics inserted into the chamber wall with a stainless-steel box on the inside of the chamber and a plastic box for protection on the outside. Each chamber contained two mode stirrers, one horizontal on the ceiling and one vertical on the rear wall; the stirred volume was 0.29 m^3 and the chamber volume was 2.31 m^3, corresponding to 12.5% stirred volume.

Figure 1. Internal View of a Reverberation Chamber

2.2.1. Stirrers

The stirrers were designed to have large reflecting surfaces, whereby the angles between surfaces and angles of rotation with respect to the main axis ensured no radial symmetry. The stirrers function like fans, rotating about their axes; however, the stirrers reflect the electromagnetic fields instead of moving air around with "blades." By avoiding symmetry, the scattered field has higher complexity over each rotation, leading to higher homogeneity of the field within the chamber volume. Each stirrer was driven by a motor and gear box that were mounted via rubber isolating mounts, which allowed some movement and decreased transmitted vibration. Supporting information, tables, and figures are shown in Appendix A, Section A.3.2.

While reviewing videos captured during exposure (see Section 4.2.3.5), it was noted that the stirrer on the back wall of the control chamber (Chamber 4) did not move throughout the four experiments (male mouse CDMA, male rat CDMA, female rat CDMA, male rat GSM). It is hypothesized that at an unidentified point in time after chamber characterization and before the start of the mouse experiment, the coupling between the motor and the stirrer came loose. As the stirrers were stopped during the animal care and observation periods for safety reasons, the issue was not identified by staff. Furthermore, while a problem with the motor or controller would have been detected by the control software, a mechanical issue like that hypothesized here would not have been detected.

2.2.2. Airflow and Vents

The temperature and humidity in the chambers were not independently controlled but relied on the control and sufficiency of airflow from the exposure room. Air was blown into and extracted

from the chamber by means of speed-controlled fans (Sanyo Denki, Tokyo, Japan). The fans were chosen to ensure that higher-than-required airflows could be achieved, and the correct number of air changes per hour was obtained by reducing the fan speed as required. By reducing the fan speed, the noise was kept to a minimum. The walls of the chamber had two integrated honeycomb vents, one located at the rear at the left and the other at the top front right. The inlet manifold had an air filter consisting of a coarse mesh material in front of the fans, followed by the honeycomb vents, which prevented the RF signal from propagating out of the chamber, while allowing the air to pass through. A sensor box was attached to the outlet manifold mounted to the top exterior of the chamber, with sensors projecting into the airflow to measure temperature, humidity, airflow, light, and noise. Sensor functionality is described in more detail below. Supporting information, tables, and figures are shown in Appendix A, Section A.3.3.

2.2.3. Lighting System

The chambers were equipped with halogen-based incandescent and light emitting diode (LED) lighting. The incandescent light fixtures were placed in the rear of the chamber. Incandescent lighting was used in the previous NTP studies, and the halogen incandescent bulbs used in this study were very similar. The chambers were also equipped with LED corner panels, 1.2 m in length, which were installed in both front corners of the chamber. While the chamber LED lights were not powered on during the animal studies described in this report, the LED lights were used during the system verification activities as the significantly higher light output allowed the LED lighting to be used as inspection lighting The LEDs were operated on 24 V direct current (DC) delivered by a small power supply installed inside the internal electrical filter box. A switch on the box allowed toggling between LED and incandescent lighting in each chamber. The chamber lights were connected to the main facility lighting circuit and hence the on/off timing was fully controlled by the facility, providing a controlled 12-hour light/dark cycle. Supporting information, tables, and figures are shown in Appendix A, Section 3.5.

2.2.4. Water System, Caging, and Cage Racks

Cages, cage racks, and watering systems for standard laboratory use contain metallic elements that can alter the exposure of the animals or introduce potential confounding factors. Because cage racks and the drinking water delivery system are contained inside the chambers during exposure periods, it was critical that these components be constructed of durable materials with minimal impact on the RF fields generated in the chamber. Because metal is incompatible with RFR and can interfere with RF signals, all metallic cage rack components (with exception of small rivets), cage lids, feed dispensers, and cage grommets had to be eliminated. Hence, custom engineering was required to overcome the challenges related to potential RFR exposure-altering aspects of all the components used to house the animals during the studies.

Water access through water bottles or a standard automatic watering system in the reverberation chambers would introduce the potential for enhanced exposure fields by metallic sipper tubes (lixits) or excessive, dose-dependent heating of stored water through the absorption of RFR energy by the water. The absorption of RFR energy by water could result in significant heating of the drinking water, thereby decreasing water palatability and increasing the required RF power to achieve the desired exposure field strength, potentially to the extent that the exposure levels could not be met. To overcome these challenges, adaptations were made to an automatic watering system so that the delivery of drinking water to the animals would not interfere with

RFR dosimetry. The water system was constructed from stainless steel to ensure no dose-dependent energy absorption occurred in the water (avoiding exposure-dependent water temperature) or in structures around the lixits, preventing the formation of enhanced fields that could lead to excessive increases in the SAR in the animals while drinking.

Two individual automatic water systems were installed: one for use at 900 MHz for rats and the other for use at 1,900 MHz for mice. The lixit (SE Lab Group, Hickory, NC) openings were at 57.5 mm and 82.5 mm above the bottoms of the cages for mice and rats, respectively. The cage grommets were ceramic and custom manufactured for use in these studies. Modifications to the cage grommets used in the rat studies are shown in Section 3.4.3. Two types of cages were provided for use in these studies. Cages for rats had grommets positioned correctly for operation at 900 MHz, and cages for mice had grommets positioned correctly for operation at 1,900 MHz. Supporting information regarding the water system is provided below under Section 2.5.4.

Both rats and mice were housed in reverberation chambers in Thoren #7 single rat-size cages with dimensions 308 × 222 × 222 mm (L × W × H) and a 474 cm^2 cage floor area. The cage rack was mounted internally, and each cage could be removed for cleaning. The cages with lids slid into the cage racks to a depth set by adjustable stops, ensuring that the grommet and lixit were aligned. Below the lixits and above the next cage was a U-shaped channel to catch water from any leaking lixits and ensure that the cage would not become flooded. Supporting information, tables, and figures are shown in Appendix A, Sections A.3.6 and A.3.10.

2.2.5. Video Cameras

Because of the closed design of the chambers and the desire to observe animals during exposure, the chambers were designed to incorporate video cameras. The infrared (IR) camera selected was the Transcend DrivePro Body 1080p camera. The cameras were placed within Faraday boxes to provide shielding to prevent errors or artifacts during operation in the RF field environment of the reverberation chamber. Furthermore, because of the all-metal construction, there was no absorption of energy, and the incident field was scattered. As the reverberation chamber environment was designed to give maximum scattering of the fields, the camera had no impact on the exposures provided. The cameras were placed more than half a wavelength from the nearest cage, and because the cameras were mounted on the metallic door, their presence had no impact on the RF field. These cameras were selected because they had a built-in recorder and did not need to transmit live data to an external device, which would have introduced additional challenges. Supporting information, tables, and figures are shown in Appendix A, Section A.12.

2.2.6. Safety

The system included multiple safety features to alert staff about the state of the system and avoid unwanted shutdowns or breaks in exposure. Each chamber was equipped with a set of warning lights that indicated the exposure status, and all amplifiers were connected to the chamber door interlock switches. In the event the door was opened during exposure, the switches would place the system in a safe state by turning off the power to the RF amplifiers. The software would then subsequently turn off all other elements of the RF generation signal chain. This functionality was hardwired; therefore, a software element was not required for the system to be placed into a safe state. In addition, emergency stop buttons installed in the exposure room and close to the control and amplifier racks allowed the RF power to be immediately removed from the system.

The monitoring software tracked and recorded all of the events described above in an exposure log; a summary of the exposure data during the animal studies is included in Appendix C. In the event of a power loss or software crash on the control computer, the system was placed in a safe state for the welfare of the animals. If the exposure field exceeded a given threshold above the target exposure level, the exposure was aborted. Supporting information, tables, and figures are shown in Appendix A, Section A.4.

2.3. Signal Generation and Amplification

2.3.1. Signal Generator

The signal generator (SMBV-100A, Rhode & Schwarz, Germany) chosen was capable of generating the types of signals used in the previous NTP RFR studies.[12; 13] The signal generator was also extremely flexible and could generate modulations with base bandwidths of up to 120 MHz and carrier frequencies of up to 3.2 GHz, and the software allowed any arbitrary complex modulation (32 Mb) to be generated. This signal generator is capable of providing modulation encompassing 2G, 3G, and 4G signals as well as Wi-Fi.

2.3.2. Modulation

Two different modulation and access schemes were utilized during these experiments, namely, those associated with the Global System for Mobile Communications (GSM) standard offset quadrature phase-shift keying (OQPSK) modulation with time division multiple access (TDMA) and the Interim Standard 95 (IS-95) standard using spread spectrum modulation with Code Division Multiple Access (CDMA). Throughout this report, these two modulations are referred to as GSM and CDMA when discussing the results from animals exposed to GSM- or CDMA-modulated RFR exposure.

GSM Modulation: The signal characteristics from GSM mobile handsets are mainly determined by the multiple access method applied. GSM supports both frequency division multiple access (FDMA) and TDMA. For FDMA, the GSM band is divided into 200 kHz-wide channels. Complementing FDMA, a TDMA mechanism enables up to eight time slots (voice channels) per frequency channel (i.e., a mobile handset transmits in only one out of eight available channels during voice communication), which introduces a pulsed signal shape with a pulse repetition rate of 217 Hz. This TDMA frame has a length of 4.6 ms, and 26 TDMA frames make up a multiframe with a duration of 120 ms. For GSM modulations, internal modulation with one time slot active was used.

CDMA Modulation: IS-95 (also known as TIA-EIA-95) was the first CDMA-based digital cellular communication standard. The system’s multiple access is based entirely on code division separation of mobile stations as well as base stations, which implies that the signal structure is significantly different from that of GSM. In the forward downlink, a set of 64 Walsh codes, which are deterministic and orthogonal, are applied to spread/separate the individual channels in the downlink of a cell. After orthogonal spreading, a short 16-bit pseudo noise code is applied to further spread the signal and identify the cell. For IS-95 systems, internal in-phase and quadrature modulation in the signal generator was used with a pseudo random modulation stream, a chip rate of 1.228 Mcps, and a cdmaOne (IS-95) baseband filter. The transmitter

transmits continuously, resulting in characteristics that differ substantially from those of the GSM signal.

2.3.3. Amplifiers

Each amplifier comprised two RF power modules of ≥175 W each combined with integrated circulators. The outputs were combined using a reactive power combiner followed by an integrated circulator to protect the modules from high reflected power. Reflected power occurs when the antennas in the chamber are not well matched; typically, this occurs when the stirrer blades cross near the antenna. At 900 MHz, the saturated power output of the completed amplifiers was approximately 320 W. The amplifiers had lower output power at 1,900 MHz with the lowest output power being >200 W. Additionally amplifiers were equipped with a limiter to ensure that the maximum output power level did not exceed the safe operation levels and that the maximum reflected power did not exceed the set threshold, as this would increase the dissipation within the amplifier with the potential for permanent damage.

2.3.4. Antennas

The antennas were designed to cover both the 900 MHz and 1,900 MHz frequency bands and did not need to be changed when switching from rat exposures at 900 MHz to mouse exposures at 1,900 MHz. Broadband log periodic antennas were designed and custom manufactured (SPEAG, Zürich, Switzerland) to meet the requirements; the maximum dimensions of these antennas were 40 cm long, 20 cm wide, and 2 cm deep. The system had seven antennas, with three antennas in each of the high- and medium-power chambers and one antenna in the low-power chamber. All antennas were placed such that their main beam was aimed at one of the stirrers to maximize the scattering of the field and avoid direct exposure of the animals. All antennas were placed in the rear of the chamber. In the case of the high- and medium-power chambers, antennas were placed in the top left and bottom right and aimed at the stirrer on the rear wall. The other antenna in the top right was aimed at the stirrer on the ceiling. In the low-power chamber, only the antenna in the top right was installed.

2.3.5. Exposure Control

The exposure level in any given chamber depended on (i) the number of amplifiers connected to the chamber and (ii) the output power from the amplifiers. The amplifiers that were connected to the different chambers depended on which time slot was being used. These chambers and the studies described in Section 4.2 utilized a 10-minute on/10-minute off alternating exposure paradigm by which animals in each chamber were exposed for 9 hours and 10 minutes per day over an 18-hour and 20-minute exposure period. The first 10-minute time slot had all three amplifiers connected to the high-power chamber (Chamber 1), with each amplifier connected to a different antenna. In the second 10-minute slot, two amplifiers were connected to the medium-power chamber (Chamber 2) and one amplifier was connected to the low-power chamber (Chamber 3). The exposure level in each chamber is a function of the input power to the chamber and the number of animals, weight of animals in the chamber, along with other accessory chamber contents (e.g., number of cages, amount of bedding, and feed). The exposure level was controlled by adjusting the input power to each chamber via a feedback control algorithm to maintain the measured field strength at the target exposure level. The software generated warnings if the measured fields and calculated SAR deviated from the target by more than 2 dB,

to alert staff to a potential problem. To ensure the safety of the animals, the exposure was aborted if the SAR exceeded a second set of programmable thresholds, set to 5 dB. Mean SAR levels for the exposures remained within 10% of target levels throughout the studies; summaries of the exposure data are provided in Appendix C. Supporting information, tables, and figures are shown in Appendix A, Section A.7.

2.3.6. Chamber Quality Factor and Stirring Performance

Using a vector network analyzer (VNA) connected to two antennas in the reverberation chamber, the loss in energy due to absorption in the individual chamber contents (e.g., racks, bedding, and feed) can be characterized by incrementally placing each component in the chamber and performing measurements over an integral number of stirrer rotations. These measurements were important for the calculation of the power needed to meet the required field strengths, and hence SAR level, in each chamber. The measurement repeatability was assessed and the maximum standard deviation observed at either 900 MHz or 1,900 MHz was 0.05 dB. Supporting information, including tables and figures, and information regarding the measurement of uncertainty is included in Appendix A, Section A.8.

2.3.7. Field Uniformity Measurement

Field uniformity was determined via a large number of measurements made over the working volume, both with the chamber empty and fully loaded with racks and phantoms (i.e., animal surrogates). Unlike VNA measurements, field measurements are time consuming. Thus, two elements of the measurement were assessed: the measurement repeatability and the increase in uncertainty as the number of points (i.e., measurement locations) is reduced and the measurement speed is increased. The standard deviation of sets of 900 MHz measurements was <0.2 dB for the total field and 0.3 dB for any given component of the field. The standard deviation of the sets of 1,900 MHz measurements was 0.22 dB for the total field and 0.37 dB for any given orthogonal field component. Supporting information, including tables and figures, and information regarding the measurement of uncertainty and determination of homogeneity is included in Appendix A, Section A.9.

2.3.8. Power-Control Simulation

GSM Modulation: To minimize interference between different cells (i.e., base stations), the output power of each handset connected to the GSM network is controlled to the lowest power to achieve reliable communication, which is based on feedback from the base stations. This action results in incremental steps in the power level. The power control has a dynamic range of 30 dB subdivided into 2 dB power-level steps. Power control is typically implemented by means of the slow associated-control channel, which facilitates a power-control update rate no faster than every four multiframes (i.e., 480 ms). Once a target power level is received, the mobile station is able to regulate its power in 2 dB steps every 60 ms (for example, a power regulation over 15 steps [full dynamic range] takes 900 ms). However, GSM base stations typically average the received signal strength from a mobile handset over 1 s, such that the actual power regulation usually takes place after multiples of 480 ms. In summary, the main low-frequency amplitude modulation components of the GSM signal are 217 Hz TDMA frame (provided by the modulation), 8.3 Hz multiframe, 2 Hz discontinuous transmission (DTx), and <1 Hz power control.

CDMA Modulation: In CDMA systems such as IS-95, efficient power control is crucial. Because all mobile stations transmit and interfere in the same frequency channel, each active mobile station decreases the signal to noise ratio of all the other mobiles. Hence, the output power of a mobile handset should be kept to the minimum level that guarantees good voice quality. On the other hand, when moving around, the mobile handset is subject to issues such as slow and fast fading, shadowing, and external interferences. To keep the output power low and compensate for the effects of changing communication channel loss, fast power control is necessary. When an IS-95 mobile station is actively communicating, a closed-loop power control is applied. The base station monitors the signal quality in the reverse link and inserts power control bits in the communication channel, which facilitates power control over a dynamic range of 48 dB in 1 dB steps with an update rate of 800 Hz. The power control is implemented by sending a binary value of 1 to regulate the transmit power down by 1 dB and a value of 0 to regulate the transmit power up by 1 dB. A quasi-static power level is therefore implemented with an alternating 0101 power-control pattern.

Stirrer Modulation for GSM and CDMA Modulations: In each reverberation chamber, field structure is randomly reflected in different directions from the surfaces of the stirrers, which are in turn continuously rotating, the result being that when averaged over time, the field is homogeneous throughout the volume occupied by the cages. By adjusting the rotation rate of the stirrers, the rate of change of the field strength is tuned to mimic the low-frequency amplitude modulation characteristic of each communication standard provided by the different power-control regimes employed. This stirrer-imposed amplitude variation is sometimes referred to as stirrer modulation. During study development, many combinations of stirrer speeds were measured, and those that best represented the extremely low-frequency components for GSM and IS-95 (i.e., CDMA) power control were selected for the exposure experiments. The faster power control of IS-95 CDMA resulted in faster stirrer speeds than those for GSM experiments. Supporting information is included in Appendix A, Section A.10.

2.4. Radiofrequency and Environmental Monitoring System

The RF monitoring system comprised two Four Channel Exposure Acquisition System (EASY4) field measurement devices from Schmid & Partner Engineering (SPEAG, Switzerland). Each EASY4 could monitor up to two chambers with two electric field (E-field) probes (EF3DV3, SPEAG, Switzerland) per chamber, with calibration traceable back to national standards. The use of two E-field probes rather than a single sensor greatly reduced the uncertainty. The probes were attached to custom-made DAEasy4 (SPEAG, Switzerland) data acquisition units, which in turn were connected via optical cables to the EASY4. It was important to measure the E-field for SAR control so that changes in losses (e.g., due to the bedding) did not influence the SAR in the animals. The EASY4 measurement server was connected by ethernet to the control computer. Data acquisition units from Keysight (Santa Rosa, CA) were used to collect all environmental data from the sensors and to control the various functions of the amplifiers and warning lights. The control computer included a fully featured control program for exposure and environmental monitoring, developed based on extensive experience with the operation of similar systems. The control program generated log files to document the operation of the system and, based on the most recent body weights of the animals and the SAR levels required, maintained the field strengths in each chamber at the target level.

The chambers were constructed from stainless steel, which has relatively low permeability and hence does not significantly shield or distort the incident magnetic fields. Therefore, all groups, including the room and chamber control animals, were exposed to similar static and extremely low frequency (ELF) fields. The magnetic fields were not explicitly measured within the context of the RF exposures.

Air, temperature, humidity, noise level, light level, and airflow sensors were included for environmental monitoring. Unless specifically requested otherwise, all sensor data were reported in International System of Units (SI units). The noise sensor microphone was housed outside the chamber, connected via a flexible tube into the chamber, to conduct sound out of the high-field environment. An Audix TM1 microphone was employed for the noise measurement, as it has a frequency response extended to approximately 30 kHz. The custom noise measurement was based on two metrics: the average noise level and the peak noise level.

Airflow through the chamber was measured using a F400 series sensor (Degree Controls, Inc, Nashua, NH), and the measured velocity could be related to the number of air changes per hour. Laminar flow elements were added to the outlet manifold (top right of the chamber) to reduce turbulence in the airflow and to increase measurement accuracy. According to the measured airflow, the speed of the fans, two at the chamber air inlet (bottom left of the chamber) and two at the chamber air outlet, could be adjusted using a fan speed controller (with one speed regulator per chamber). The temperature and humidity of the chamber air were measured using EE060 sensors (E+E Elektronik, Engerwitzdorf, Austria) and were assumed to be essentially the same as those of the air in the exposure room, as the power dissipation in each of the chambers increased the temperature in the RF chambers compared to the chamber control (i.e., the chamber without an active radiation antenna) by less than 0.1°C. Supporting information, tables, and figures are shown in Appendix A, Section A.6.

2.4.1. Noise Generators

It was observed that at very high-field strengths, the GSM signals created an audible noise at the 217 Hz TDMA slot frequency. The exact origin of this noise was not clear; however, the bright nature of the noise (i.e., the presence of high frequencies) ruled out thermal effects as the origin, as heating and cooling are slow processes. The noise was localized to an induced vibration in the stirrer blades produced by some force or stress on the relatively thin metal of the blades. This noise was present during GSM exposures in the previous NTP studies, as well. Because the modulation-related noise was exposure-dependent, a noise generator to generate “GSM” noise was linked to each sensor pack to mask any differences between the chambers and ensure that all environmental conditions, including noise, across chambers were similar. The GSM noise could be chosen to be employed only during GSM exposures. If used, the noise would be amplified to the required level to ensure approximately equal sound levels in each chamber. No noise was observed with the IS-95 (i.e., CDMA) signal as there is no on/off modulation associated with CDMA because of continuous transmission and a lack of time slots; thus, no noise generator would be used during CDMA exposures.

2.5. Detailed Dosimetry

Dosimetry in the fields of health physics and radiation protection is the measurement, calculation, and assessment of the internal exposure to the body. Nonionizing radiation

dosimetry within the radiofrequency range is quantified as the SAR. The SAR is expressed in W/kg. It is not possible to measure induced fields or SAR directly in a subject (human or animals), thus the electromagnetic fields that a subject is exposed to are measured and then numerical simulations using different postures of anatomical models are performed representing different species, sexes, and age groups (numerical dosimetry). If the incident field is well characterized, the correlation between incident field conditions and the fields induced in different tissues and organs can be established. However, the correlation needs to be verified experimentally using homogeneous phantoms (experimental dosimetry).

The numerical dosimetry for both rats and mice was reported in Gong et al.[18] and relates the SAR induced in the bodies (whole-body and tissue-specific) to a given incident field strength within a reverberation chamber environment as a function of the animal's body weight (Figure 2).

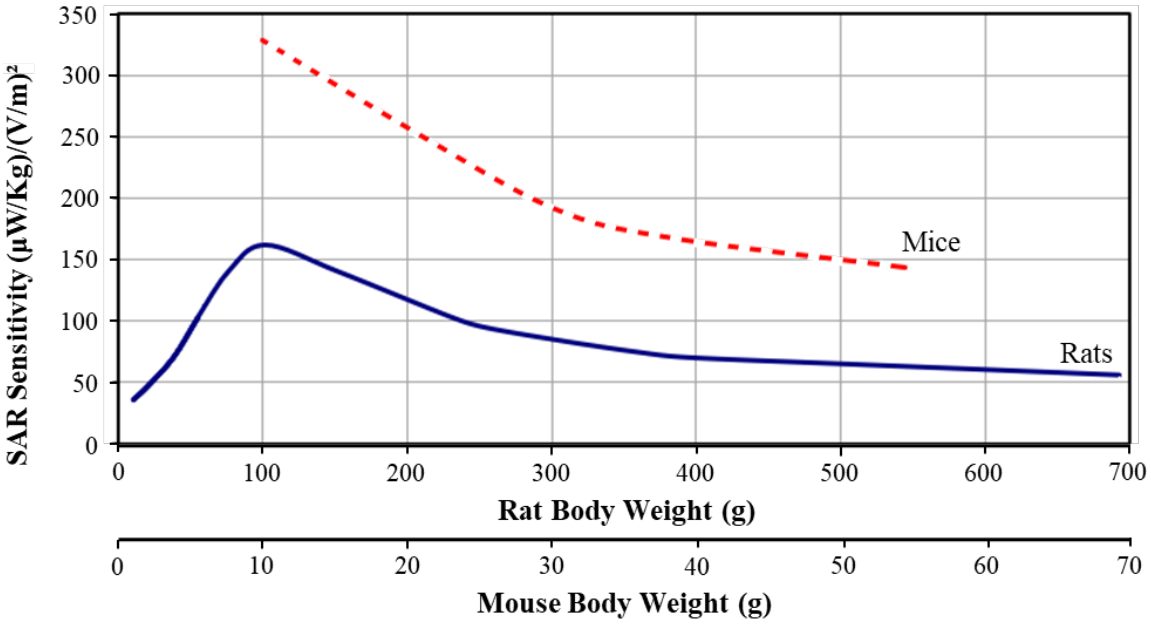

Figure 2. Specific Absorption Rate Sensitivity for Rats at 900 MHz and Mice at 1,900 MHz as a Function of Body Weight Based on Numerical Dosimetry Using Anatomical Models

Figure adapted from Gong et al.[18] SAR = specific absorption rate.

2.5.1. Experimental Verification of the Dosimetry

Experimental dosimetry was performed in the study chambers using the control system designed and fabricated for these studies. During system testing, animal surrogates, or "phantoms" were used. Each phantom consisted of a container of low-dielectric-constant, low-loss material filled with an appropriate volume of tissue-simulating liquid. The aim was to obtain the same whole-body average SAR (SAR_{WB}) in the phantom as in a rodent of the same weight. Simulations of full anatomical models of the rat or mouse provided the SAR distribution across all tissues, which was then averaged to provide the overall average SAR. The overall average SAR was then normalized to an incident field strength of 1 V/m to provide the SAR_{WB} sensitivity. Simulations of the phantoms filled with a selection of tissue-simulating liquids were performed, and the tissue-simulating liquid that provided the closest average SAR value was selected. The chosen

liquids were not meant to represent the average tissue properties of a rat or mouse but to represent the same absorption, which is related not only to individual tissue properties within the anatomical model but also the inhomogeneous field distribution.

For the male rats, a nominal 0.5 L bottle was filled to the top with approximately 550 mL head-simulating liquid (HSL) (HSL900; SPEAG, Switzerland), with properties $\varepsilon_r = 41.5$, $\sigma = 0.97$ S/m, which provided a good match to the whole-body anatomical rat. From the simulations, the average SAR_{WB} efficiency of the male rat phantom was determined to be 5.556×10^{-5} (W/kg)/(V^2/m^2).

For the physical mouse phantom, a nominal 50 mL conical centrifuge tube filled to the top with 55 mL of HSL1900 tissue-simulating liquid (SPEAG, Switzerland), with properties $\varepsilon_r = 40.0$, $\sigma = 1.40$ S/m, provided the best match to the SAR_{WB} efficiency of the mouse. The average SAR_{WB} efficiency for the mouse phantom was 1.50×10^{-4} (W/kg)/(V^2/m^2).

The SAR in the animal phantoms was assessed experimentally using the temperature method. In this method, animal phantoms were exposed to RFR in a chamber while the temperature of the liquid was monitored. When a liquid phantom was exposed to RF, the temperature change was measured during RFR application (i.e., the heating phase) and after RF was switched off (i.e., the cooling phase), and the heat transfer time constant τ was determined. By applying the lumped-heat-capacity method described in *Heat Transfer*,[19] the liquid temperature followed the differential equation below, based on cooling to the ambient temperature of the environment and RF heating, encompassing a cooling term due to heat loss to the environment and a heating term due to power absorption:

$$\frac{dT}{dt} = \frac{-\left(T_{liquid} - T_{ambient}\right)}{\tau} + \frac{SAR_{WB}}{C_{liquid}}$$

where C_{liquid} is the heat capacity of the tissue-simulating liquid, T is temperature, t is time, τ is the time constant, and ΔT is the temperature increase in the liquid (i.e., $T_{liquid} - T_{ambient}$). Two processes are possible: (1) when RF is on, the liquid temperature increases until an equilibrium state is reached, whereby the rate of heat absorbed due to the RF exposure and the rate of heat loss due to convection and conduction are equal; (2) when RF is off, the liquid cools through heat convection and conduction toward the lower temperature of the environment. The SAR_{WB} values were determined by solving the differential equation for long exposure times ($t >> \tau$) of the heating curve equation when the system was in an equilibrium temperature state:

$$SAR_{WB} = C_{liquid}\frac{\Delta T}{\tau}$$

where C_{liquid} is the heat capacity of the tissue-simulating liquid, τ is the time constant, and ΔT is the temperature increase in the liquid. The determination of SAR_{WB} required that the temperature of the environment was constant and also required measurements of the absolute temperature of the dummy liquid, measurements of the room temperature, and determination of the time constant (τ). The latter was determined by fitting the theoretical curve to the recorded temperature change in the phantom liquid during the heating process and separately for the cooling process. The time constant of the process can be calculated from either the heating or

cooling curve; however, the RF power during the warm-up phase of the power amplifiers can vary by several dB, resulting in increased uncertainty, therefore use of the cooling curve is preferred. The stated uncertainty of the temperature probes used in these measurements was ±0.2ºC.

2.5.2. Verification of Rat Dosimetry

The 10 male rat phantoms were placed in cages and positioned in the chamber. Two phantoms were equipped with fixed temperature sensors to evaluate the heating and cooling time constants; in the other phantoms only the temperature increase was measured at the end of the heating phase. The target field strength was set to 400 V/m. The E-field strength, air temperature, and phantom temperature were recorded during the course of the experimental dosimetry. To ensure that the ambient temperature did not change significantly, air was circulated through the chamber and cooler outside air let into the room intermittently. The SAR uniformity was determined by measuring the phantoms' temperature immediately after the power was shut off in as short a time as possible. The cooling of the phantoms was corrected via reference to the two phantoms with temperature probes that were present throughout the experiment. There was good concordance between the SAR calculated from the field strength present and the SAR measured (Appendix A). The uniformity in the male rat phantoms was assessed in the eight phantoms without fixed temperature sensors; the uniformity (standard deviation) in the SAR was 0.36 dB and was within ±0.6 dB of the mean for all phantoms.

2.5.3. Verification of Mouse Dosimetry

Ten mouse phantom positions within the chamber were measured using phantoms with temperature sensors installed. The temperature was monitored to determine when it approached a constant value at each location, and the time constant was determined from the cooling curve. The SAR uniformity was determined by measuring and estimating the final temperatures of all phantoms. The cooling time constant was then used to calculate the SAR with temperature probes present throughout the experiment. There was good concordance between the SAR calculated from the field strength present and the SAR measured (Appendix A). The uniformity (standard deviation) in the SAR was 0.5 dB and was within ±0.9 dB of the mean for all phantoms.

2.5.4. Verification of the Effect of the Water System on the Dosimetry

The fields around the water system were measured with respect to the fields measured by the two fixed probes in the chamber. At 900 and 1,900 MHz, the field strength at the lixit was well below the nominal chamber field strength, showing that the rats and mice (respectively) would be safe while drinking (i.e., that exposure would not be higher than the target SAR). The field at the flange was similar to the nominal field but within the variation measured during the homogeneity measurement of the empty chamber, which was up to ±3 dB compared to the average field strength.

Numerical and experimental dosimetry was conducted at 900 MHz for rats and at 1,900 MHz for mice using phantoms to assess the SAR when drinking water and when away from the water system. The relative magnitude of the SAR was determined by observing the rate of temperature change at different locations within the phantom, namely, at the mouth, the head, and the center of the body. A 3D-printed shell based on the anatomical models used for the numerical

dosimetry was utilized for the rat, whereas a simplified shape was used for the mouse. It was observed that evaporation from the exposed gel surface was a confounding process that could reduce the temperature rise at the mouth if the surface was not covered by a plastic membrane. The results of the rat water system dosimetry showed that the SAR in the mouth and head areas of the rat phantoms was lower when the phantom was "drinking water" than when the phantom was not close to the water system, confirming that the water system would be safe (i.e., that the exposure when the animal was drinking water was not higher than the target SAR). The results of the mouse dosimetry showed that the SAR in the head was the same when the phantom was "drinking water" compared to when the phantom was not close to the water system. In the mouse phantom, a small increase was observed in the mouth, but the SAR was still lower than in the head. The small increase in SAR observed in the mouse phantom mouth would not be sufficient to cause RF burns or other detrimental effects. Supporting information, tables, and figures are shown in Appendix A, Section A.11.

2.5.5. Evaluation of Implantable Temperature Sensors

These studies utilized temperature chips to record body temperature following RFR exposure. The devices were similar to those used in the previous NTP thermal pilot studies.[15] To build on these methods of measuring temperature, National Institute of Environmental Health Sciences Division of Translational Toxicology scientists identified another temperature recording device that was compatible with RFR exposure, namely nano-T data loggers (Star-Oddi, Gardebaer, Iceland). Larger devices, capable of measuring heart rate, from Star-Oddi (e.g., micro-HRT sensors) were also evaluated and were determined not to be compatible with RFR exposure. More information on that evaluation can be found in Appendix A, Section A.11.6.

In selecting this new method, safety and compatibility were evaluated prior to testing in animals. From a safety perspective, it was confirmed that the presence of the implanted data logger would not lead to an increase in SAR levels and subsequent increased temperature in the surrounding tissue. From a compatibility perspective, the implanted sensor was confirmed to report the correct temperature without interference from the RF fields. Benchtop experiments evaluating these two features are further described in Appendix A, Section A.11.6.

2.6. Summary

An RFR field exposure system was designed to enable equivalent exposure conditions to those utilized in the previous NTP 2-year studies[12; 13] and for a smaller number of animals with a smaller facility footprint.

The RF signal generator produced the modulated signals representative of mobile communication signals compliant with the desired standards. For these studies, either GSM or IS-95 (i.e., CDMA) signals were used. The output of the signal generator was split three ways. The level in each of the three paths was individually controlled before being amplified to the desired level and radiated into the desired chamber via antennas, with one antenna for each amplifier. Each chamber had two mode stirrers (rotating metallic structures) that scattered the field, producing a continuously variable field structure within the chamber. When averaged over time, this field was homogeneous and isotropic over the volume in which the rodents were housed.

The electromagnetic field level in each chamber was monitored using two isotropic E-field probes. Given the measured level and deviation from the target, the exposure level could be corrected by increasing or decreasing the power delivered to the chamber. Computer simulations and experimental verification using animal “phantoms” demonstrated that the RFR exposure parameters for both rats and mice were equivalent to those used in the previous NTP studies.

3. System Verification and Operations

3.1. System Verification

To verify the parameters of radiofrequency radiation (RFR) exposures recorded by the data-capture component of the exposure system, technical experts from the National Institute of Standards and Technology (NIST) conducted an independent verification of the system following installation and initial testing of the exposure system by the Foundation for Research on Information Technologies in Society (IT'IS) at the testing facility. NIST specifically evaluated RFR exposure fields, chamber characteristics (field uniformity), and signal quality. Full details of the procedures for measurements and calculations are available in Appendix B. The radiofrequency (RF) signals generated by the exposure system were within the estimated uncertainty bounds, indicating that the chamber fields measured by NIST agreed with the measurements provided by the exposure system's integrated probes. The magnitude of field variation throughout the volume of the chambers was also consistent with values reported for the chambers in the previous National Toxicology Program (NTP) studies. The quality of the modulated signals was found to be acceptable with regard to distortion and harmonic content. Overall, the NIST evaluation confirmed that the exposure system was operating correctly and RFR exposures were within specifications. These activities were conducted prior to the initiation of any animal studies.

3.2. Ambient Field Measurements

Additionally, NIST measured ambient levels of RFR at various locations in the facility to assess any potential differences at different locations across the facility. Measurements were taken at four separate locations within the testing facility, including the room housing the reverberation chambers and three other locations that represented a large geographic distribution throughout the facility. Data demonstrated that there were no marked differences in exposures among the sites evaluated across the facility.

3.3. System Qualification

Following installation of the exposure system and independent evaluation by NIST, the testing facility conducted a system qualification to ensure the accuracy and functionality of the system for the intended use. The qualification procedures were executed prior to initiation of the mouse study, and again after system repair prior to the rat studies being conducted. Qualification procedures were conducted with facility Wi-Fi enabled and with Wi-Fi disabled. Qualification included simulations to assess the following functionality:

- Initiate a test session using Global System for Mobile Communications (GSM) modulation and confirm program settings for exposure.
- Initiate a test session using Code Division Multiple Access (CDMA) modulation and confirm program settings for exposure.
- Confirm generation and readability of exposure log files from the IT'IS Evaluation Software.
- Confirm functionality of the emergency safety buttons and emergency door switch.

- Confirm functionality of all environmental sensors (temperature, humidity, airflow, noise, vibration, light), including testing of the alarm and abort functions by forcing parameters out of specification (min or max thresholds) for each parameter.
- Run a full simulated study similar to that planned for the rat exposures, including programming of animal body weights, reviewing the exposure configuration with the correct modulation, initiating exposure, stopping/pausing exposure, and generation and reading of the exposure log from the IT'IS Evaluation Software.

3.4. System Modifications for Rat Exposure Studies

This section describes system modifications and maintenance that were required after the system described above was installed and used to conduct the mouse study (the mouse study is described below in Section 4.2). These unanticipated modifications were required to conduct the rat studies detailed in Section 4.2. The section below was written based on correspondence between the National Institute of Environmental Health Sciences Division of Translational Toxicology (NIEHS/DTT), the testing facility, and IT'IS. Events are described in chronological order between August 2020 and November 2021 and are depicted in Figure 3.

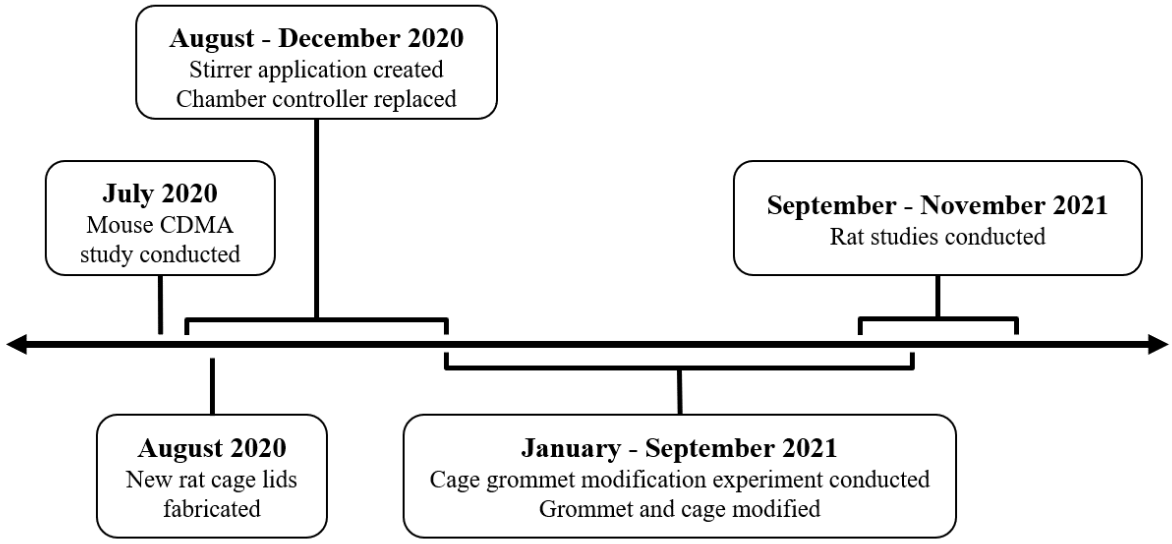

Figure 3. Timeline Diagram

3.4.1. Fabrication of Replacement Cage Lids

The in-life portion of the mouse study was completed in July 2020 (see Section 4.2 for study schedule). The in-life portion of the rat studies were originally scheduled to begin in early August 2020. During the acclimation period, prior to the start of exposure, it was discovered that the rats were able to chew through the cage filter tops and escape their cage units. This was not observed in the mouse study because the height of the cage units did not allow mice to access the filter tops. When the issue was discovered, the study animals were moved back to traditional housing. The testing facility, in consultation with NIEHS/DTT and IT'IS developed a plexiglass cage lid prototype. This cage lid prototype was evaluated for compatibility with the exposure system by measuring temperature and oxygen levels within the cage units during an hour of RF

generation. Following testing with acceptable results, the testing facility fabricated plexiglass cage lid replacements for the 40 cages needed for the rat studies. Figure 4 shows the original filter tops used in the mouse study and the replacement plexiglass lids used in the rat studies.

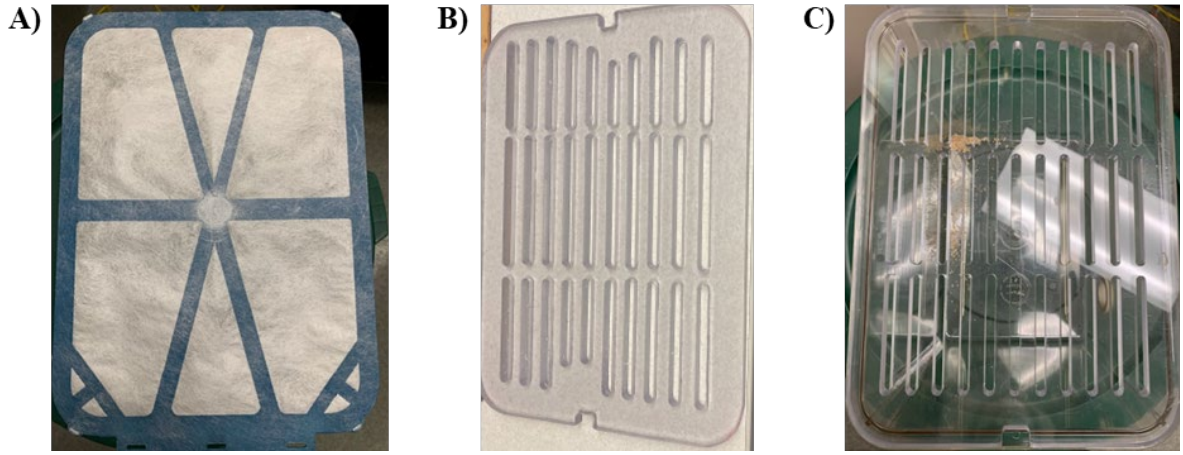

Figure 4. Cage Lids

Images of (A) the original filter tops used in the mouse study, and (B, C) the replacement plexiglass lids used in the rat studies.

3.4.2. System Maintenance

Following fabrication of new cage lids, the rat studies were rescheduled to begin in mid-August 2020. Upon restarting the first rat study, the exposure system was found to abort the scheduled exposure due to excursion of the electric field (E-field) probe measurements from the required specification. This issue resulted in animals often receiving less than the required exposure of 9 hours and 10 minutes per day (over the scheduled 18-hour and 20-minute period). A stirrer in the medium-exposure chamber (Chamber 2) also stopped working at the same time. After a review of the system files and exposure logs, it was originally hypothesized that the two events were related (i.e., the stirrer would malfunction and cause the E-field probe measurement to be out of specification), which in turn would cause the system to abort. In an attempt to resolve this issue, the motor for the stirrer in Chamber 2 was replaced at the end of August 2020. Following the motor replacement, the system functioned well for a couple of days before the stirrer malfunction and E-field measurement issues recurred.

Throughout September 2020, IT'IS provided remote support to evaluate options for resolving the stirrer malfunction. One option that IT'IS suggested would have required manual (e.g., power the system off and restart) operation of the exposure system by the testing facility. Another option required the development of automatic procedures that could be used when the stirrer malfunction occurred. The manual options were not preferred as they could not be employed during the night hours in which animals were exposed.

By mid-November 2020, a revised stirrer control program had been implemented. To allow the stirrers to be restarted independently and automatically, control of the stirrers was moved into a separate application from the main application that controlled the remainder of the exposure system. The main application controlled the stirrer application via a protocol that defined stirrer speed and acceleration. The main application monitored the speed of each stirrer. If the specified

speed was out of specification by more than 50% and for longer than 1 minute, then an error event was triggered.

When an error event was triggered for a stirrer, the stirrer application stopped all stirrers and sent an error message to the main application, which placed the system in pause mode. When the stirrer application sent an error to the main application, the main application waited 5 seconds and then restarted the stirrer application from off-mode. When the stirrer application came back online, it received information via the established protocol with the main application and restarted the stirrers at the specified speed and acceleration they were in before the error occurred.

In the September–November 2020 time period, one of the chamber controllers was replaced and adjustments were made to address the E-field measurement issue. For the E-field measurements, IT'IS expanded the sampling window used to determine whether the probe measurement was within specification. By expanding the window, the effects of minor excursions on the overall mean were reduced and better aligned with the intention of the specification. This modification resolved the issue by preventing minor excursions from affecting the system aborts.

During requalification testing, in late November–early December 2020, some additional software updates and program modifications were required to ensure compatibility with all the new hardware and software. By mid-December 2020, the revised system had been requalified (without animals) and was available for further RFR exposure evaluation.

3.4.3. Cage Grommet Modification

After the above system maintenance was completed, a final qualification study (with rats) was performed in January 2021 prior to rescheduling the 5-day investigative rat studies. During the January 2021 qualification, rats in all exposure chambers were observed to lose weight (including in the chamber control chamber). The first attempt to conduct the 5-day investigative studies (fall of 2020) with larger rats (>400 g) also provided indications (e.g., weight loss and animals observed pawing at the lixits) that larger rats had some water access issues in the chamber housing.

To better understand the observed weight loss and refine the study design (e.g., potentially extend chamber acclimation), an experiment was performed in February 2021. This experiment used rats of different weight ranges (250 g and >400 g) and included a period when animals were housed in normal caging for 1 week (study day 0–7) and then moved into the chamber caging on study day 7 for 2 weeks to assess changes in body weight and clinical observations. No RFR exposure was used in this experiment. The body weight results after animals were moved into the chamber housing recapitulated the weight loss findings from the January 2021 qualification study (Table 1). All animals in the >400 g chamber housing group lost weight starting on study day 9, and the magnitude of weight loss was higher than observed in the smaller rats. Weight loss in the 200 g chamber housing group was variable across study days and relatively minor.

Table 1. Body Weights of Male Rats in Different Housing Conditions

Study Day	200 g Rats Chamber Housing[a,b]	200 g Rats Room Control[a]	400 g Rats Chamber Housing[a,b]	400 g Rats Room Control[a]
n	20	5	20	5
2	232.6 ± 1.3[c]	234.7 ± 4.0	404.1 ± 2.8	408.8 ± 15.9
3	238.7 ± 2.0[c]	245.0 ± 2.1	415.6 ± 3.2	419.6 ± 18.1
4	242.3 ± 2.7	251.7 ± 1.8	424.0 ± 2.7	422.9 ± 20.0
7	257.8 ± 1.9	263.2 ± 2.2	433.5 ± 1.9	437.4 ± 13.4
8	264.8 ± 1.6	269.4 ± 1.5	439.7 ± 1.8	441.0 ± 14.9
9	261.7 ± 3.1	267.9 ± 2.5	415.1 ± 1.8	434.4 ± 12.5
10	268.8 ± 2.4[d]	272.9 ± 2.2	404.4 ± 2.4	442.8 ± 15.1
11	271.7 ± 2.4[d]	275.5 ± 2.3	396.3 ± 4.3	445.7 ± 14.8

[a]Data are presented as mean ± standard error. Body weight data are presented in grams.
[b]For study days 2–7, body weights were collected while all animals were in traditional housing. On study day 7, animals were moved into the cages within the radiofrequency radiation exposure chambers (no radiofrequency radiation was generated).
[c]n = 18. Two animal weights in the 200 g chamber housing group were excluded from the analysis as outliers.
[d]n = 19. One animal weight in the 200 g chamber housing group was excluded from the analysis as an outlier.

Following observations of the larger rats pawing at the lixits, veterinary staff and technicians suspected an issue with access to the watering system. To help confirm their suspicions, approximately half of the >400 g rats in chamber housing were provided hydrogels to supplement water intake. All animals that were provided hydrogels finished them within the first day and, with continued supplementation, started to gain weight. In light of this response, the study team was confident the weight loss issue was related to water access in the chamber housing. Animal technicians hypothesized that the larger animals were unable to maneuver into the correct position to activate the lixit with their lower jaw due to the position/opening size and their head sizes.

Drawing on the findings from the February 2021 experiment, the testing facility began working with IT'IS to evaluate options to improve water access for the larger rats. Between March and June 2021 the testing facility, IT'IS, and NIEHS/DTT evaluated the cage and water access parameters, taking into consideration differences between the exposure system used in the previous NTP studies and the exposure system designed for the current NIEHS/DTT studies. Figure 5 illustrates the construction of the water system including the cage grommets, lixits, and choke tubes. There were several adjustable parameters, and ultimately it was decided that new grommets with a wider opening would be the most appropriate modification to allow better access for the larger rats.

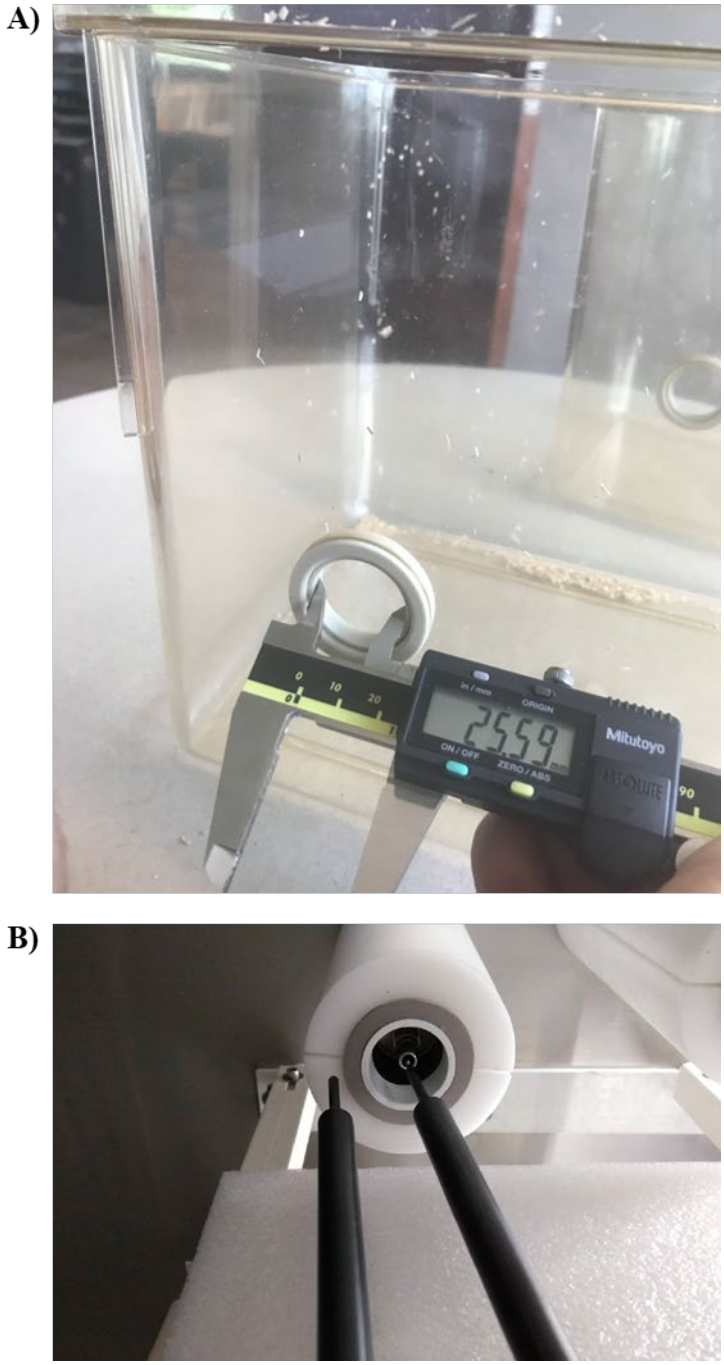

Figure 5. Water System Components

(A) The cage grommet which is an opening in the cage allowing access to the lixit. (B) The metal lixit within the choke tube that shields the lixit from radiofrequency radiation (RFR) exposure (also shown in Appendix A, Section A.11.5).

New grommets were custom manufactured and evaluated by IT'IS to ensure they were appropriate for use in an RF field. Following confirmation of acceptability within the RF field, IT'IS provided new grommets to the testing facility for testing with the large rats. The testing facility conducted two experiments (without exposure) between June and August 2021 to test the new grommets in modified cages. The experiments were designed to investigate water

accessibility for the larger rats with the new grommets by confirming animals did not experience body weight loss after being moved into the chambers in modified cages. The first small experiment using n = 2 rats looked promising and supported production and testing of a larger batch of new grommets/modified cages. Within the larger experiment (n = 20 per group, mean body weight >500 g) in August 2021 groups of rats housed in the modified cages were compared to rats housed in standard caging over the course of 2 weeks (Table 2). Both groups gained weight over the course of the experiment, with animals in the modified cages gaining slightly more weight than the room control animals. Following successful resolution of the water access issue, the 5-day investigative rat studies were rescheduled.

Table 2. Body Weights of Male Rats in Different Housing Conditions Following Cage Grommet Modifications

Study Day	500 g Rats Chamber Housing[a,b]	500 g Rats Room Control[a]
n	20	20
−4	515.8 ± 11.6	515.4 ± 11.6
1	508.2 ± 10.5	497.3 ± 13.9
5	524.2 ± 11.1	516.9 ± 13.2
8	522.5 ± 10.7	518.5 ± 12.8
12	532.7 ± 10.5	524.5 ± 11.9
15	531.2 ± 10.3	525.2 ± 11.4

[a]Data are presented as mean ± standard error. Body weight data are presented in grams.
[b]For study day −4, body weights were collected while all animals were in traditional housing. On study day 0, animals in the 500 g chamber housing group were moved into the cages within the radiofrequency radiation exposure chambers (no radiofrequency radiation was generated).

The rat studies were reinitiated and conducted between September and November 2021. Throughout the rat studies, additional technical challenges were encountered which required the system to be remotely reset by IT'IS prior to initiating each programmed exposure. Without coordinating this remote system reset, the system would abort exposure due to an error related to the EASY4 system monitoring. While these challenges did not significantly affect the overall schedule of studies conducted, it added a layer of complexity to scheduling and coordination. The root cause of the EASY4 system abort in this case was never identified.

3.5. Summary

The comprehensive verification and subsequent modifications of the RFR exposure system were crucial to ensure its accurate, reliable, and safe operation for animal studies. Following installation of the exposure system, experts from NIST independently confirmed the system's internal probe measurement of RFR, field uniformity, and signal quality. Following this verification, the testing facility developed and performed qualification procedures to confirm the system's functionality. These procedures included testing the system's performance under different modulation schemes (GSM and CDMA), verifying the environmental controls (temperature, humidity, airflow, noise, vibration, light), and confirming the proper functioning of emergency systems and safety protocols.

Unexpected technical issues were encountered requiring system modifications. Key modifications included designing new plexiglass cage lids to prevent rats from escaping, resolving stirrer and E-field probe issues through hardware and software updates, and improving water access for larger rats by modifying cage grommets. These detailed measures were essential to ensuring the integrity and reliability of the RFR exposure system and to facilitating accurate and dependable animal studies while maintaining high standards of animal care and safety.

4. Five-day Investigative Studies in Rats and Mice

4.1. Introduction

After system installation, verification, and qualification were completed, a series of four 5-day studies was conducted in Sprague Dawley (Hsd:Sprague Dawley® SD®) rats or B6C3F1/N mice. The goal of these studies was to further characterize radiofrequency radiation (RFR)-induced changes in body temperature and DNA damage observed in the previous National Toxicology Program (NTP) RFR studies and evaluate the use of new methods for collecting live, real-time data.

Changes in body temperature are important because the absorption of radiofrequency (RF) energy by biological tissues occurs in the form of heat transfer. It has been postulated that the absorption of RFR during exposure, even at power levels that do not lead to significant changes in body temperature, may constantly affect body temperature and challenge an animal's ability to thermoregulate and cause changes through this constant thermal stress. To understand the role of heat in the underlying mechanism of RFR-induced effects, it is critical to assess the impact of RFR exposure on body temperature in real time. Two different methods for measuring body temperature were selected for use in these 5-day studies. The first method was an implanted temperature chip analogous to those used in the previous NTP studies. The temperature chips can report temperature but are not able to record to the device. Therefore, the exposure system must be stopped and a temperature reader brought in close proximity with each chip to detect and report temperature for manual recording. The temperature chip has been shown to be accurate, although it does not allow measurement of temperature during exposure. In addition, there was criticism of the previous NTP studies that these temperature chips implanted into the subscapular region do not accurately reflect a core body temperature change. To help address both of these limitations, National Institute of Environmental Health Sciences Division of Translational Toxicology (NIEHS/DTT) scientists selected a second method to measure body temperature using an implantable temperature device (i.e., data loggers) for use in these 5-day studies. The data loggers are able to record temperatures at programmable intervals onto the device, allowing observation of temperature changes during exposure. The data loggers were implanted within the peritoneal cavity and were anticipated to better reflect internal core body temperature.

One noted limitation of the previous NTP studies was the lack of visual assessment of animal behavior during periods of exposure, and especially the moment the animals experienced the system initiation for the first time as well as during transitions between on/off exposure periods. Increased incidences in pheochromocytomas and other neuroendocrine changes in male rats from the previous NTP RFR studies suggest that there may be a potential stress response. In the current NIEHS/DTT studies, video from cameras inside of the exposure chambers was assessed for visible signs of a physical response at activation of the exposure system or during exposure to RF signals. In addition, a separate group of room control animals was included in the studies to assess the impact of housing within the RFR exposure chambers. Animals in this group were not exposed to RFR and were not housed within the RFR exposure chambers themselves at any time but were present in the same room where the RFR exposure chambers were located.

4.2. Materials and Methods

4.2.1. Animal Source

Male and female Sprague Dawley rats were obtained from the testing facility's holding colony, originally obtained from Envigo (Indianapolis, IN). Male B6C3F1/N mice were obtained from the testing facility's holding colony, originally obtained from the NTP colony maintained by Taconic Biosciences, Inc. (Germantown, NY).

4.2.2. Animal Welfare

Animal care and use were in accordance with the Public Health Service Policy on Humane Care and Use of Animals. All animal studies were conducted in an animal facility accredited by AAALAC International. Studies were approved by the testing facility (West Jefferson, OH) Animal Care and Use Committee and conducted in accordance with all relevant National Institutes of Health and NIEHS/DTT animal care and use policies and applicable federal, state, and local regulations and guidelines.

4.2.3. Five-day Studies

4.2.3.1. Exposure Level Selection Rationale

The previous NTP studies on RFR[12; 13; 15] utilized whole-body exposure levels of 0, 3, 6, or 9 W/kg body weight (W/kg) for rats, and 0, 5, 10, or 15 W/kg for mice. In the prior NTP 5-day studies, exposure-related increases in body temperatures were observed at exposure levels ≥6 W/kg in aged male and female Sprague Dawley rats, with exposure levels above 10 W/kg inducing increases in body temperature (≤3°C) and mortality in aged rats.[15] In the prior 28-day studies, reduced body weights and increased body temperature measurements occurred at 9 W/kg for rats; exposure to 6 W/kg resulted in some increases in core body temperature, but these increases were less than 1°C.[13] In male and female mice exposed for 5 days to RFR up to 12 W/kg, only sporadic increases in body temperature were observed and these changes were independent of the sex or age of the animals.[15]

In the current NIEHS/DTT studies, 15 W/kg was selected as the highest exposure level for the mouse study. The maximum capacity of the exposure system to generate high RF fields was intentionally limited to an achievable exposure capacity of 15 W/kg for mice. Because of the system capacity limitations and results of the published 5-day studies,[15] and the previous 28-day and 2-year NTP studies, the exposure levels selected for these NIEHS/DTT 5-day studies were 0, 3, 6, or 9 W/kg for rats and 0, 5, 10, or 15 W/kg for mice.

4.2.3.2. Body Temperature Measurements

Prior to exposure, each animal was surgically implanted with a Star-Oddi nano-T temperature logger (data logger; Star-Oddi, Gardebaer, Iceland) in the intraperitoneal cavity and an Implantable Programmable Temperature Transponder (temperature chip; IPTT-300, Bio Medic Data Systems, Seaford, DE) in the subcutaneous interscapular region to monitor individual animal body temperature. Animals were allowed to recover for at least 13 days (rats) or 8 days (mice) before exposure began.

The data generated by the data loggers and temperature chips during the rat and mouse studies were unusable. Below is the rationale for not summarizing and interpreting each temperature data set.

The data loggers recorded animal body temperature continuously throughout the study. A review of the continuous temperature data from the data loggers showed there were numerous instances of implausible data points. For example, some data loggers recorded single time-point body temperatures that were not considered biologically plausible (e.g., as low as 32°C, which was considered implausibly low), or they showed changes in body temperature of several °C from one minute to the next.

The temperature chips did not record animal body temperature on the implanted device and required a temperature reader wand to be placed in proximity of the chip to report and manually record a temperature. Collection of these temperature data required the reverberation chambers to be opened and animals to be removed from their cages to record a body temperature. On study days 0, 2, and 4, body temperature measurements were taken from the temperature chips at 10 minutes prior to exposure, after the first 10 minutes following the start of exposure (mice only), and after 1, 4, and 20 hours of exposure; body temperatures were also recorded on study day 5 for female rats. The intention was for body temperatures to be recorded immediately after a 10-minute "on" period of RFR exposure. Due to a methodological error with the temperature chips, body temperatures were taken at time points relative to the start of exposure without taking into account the on/off cycling. A review of the collection times of individual animal temperature against the exposure period determined that the majority of temperature recordings were taken too long (e.g., >5 minutes) after the most recent 10-minute "on" period ended. Immediately after RFR exposure ends, animals thermoregulate and return to a baseline temperature very quickly. Temperature recordings taken more than 5 minutes after exposure has ended cannot be interpreted regarding the effect of RFR exposure on body temperature.

4.2.3.3. Study Design

The rat and mouse studies were conducted between July 2020 and November 2021, as depicted in Figure 3. Rats were approximately 22 weeks (male) or 10 weeks (female) old on receipt. Mice were approximately 8 weeks old on receipt. Animals were quarantined for 7 days. Following the quarantine period, animals were aged onsite and maintained in a pre-exposure housing room prior to the study start. On the first day of the studies, rats were approximately 28–31 weeks (male) or 23 weeks (female) old, and male mice were approximately 33 weeks old. Rats and mice were randomly assigned to one of five exposure groups before the start of the study. Randomization was stratified by body weight that produced similar group mean weights using NTP Provantis software (Instem, Stone, UK).

Before the studies began, five male and five female rats, and five male mice were randomly selected for parasite evaluation and gross observation for evidence of disease. Additionally, the health of the animals was monitored during the studies according to the protocols of the NIEHS/DTT Sentinel Animal Program (Appendix F). All test results were negative.

Groups of 10 male and 10 female rats and 10 male mice were housed individually in reverberation chambers and exposed to whole-body RFR via Code Division Multiple Access (CDMA) (Interim Standard 95 [IS-95], 1,900 MHz) or via Global System for Mobile Communications (GSM) single modulation (900 MHz). Reverberation chambers are described in

further detail in Appendix A. Male mice were exposed to 0 (chamber control), 5, 10, or 15 W/kg of radiation via CDMA modulation for 5 days. Male and female rats were exposed to 0 (chamber control), 3, 6, or 9 W/kg of radiation via CDMA modulation for 5 days. Additional groups of male rats were exposed to 0 (chamber control), 3, 6, or 9 W/kg of radiation via GSM modulation for 5 days.

Exposures were scheduled to occur over the course of an 18-hour and 20-minute period each day, from 10:00 to 14:00 and from 15:40 to 06:00 the following day. Exposures did not occur during animal husbandry activities in the morning (06:00 to 10:00) or afternoon (14:00 to 15:40). Throughout the 18-hour and 20-minute period, each exposure group continuously cycled between 10 minutes of RFR exposure ("RFR ON") and 10 minutes of no exposure ("RFR OFF"), with a total exposure duration of 9 hours and 10 minutes per day (Figure 6). When the system started exposure at 10:00 each day, the stirrers in all four reverberation chambers started moving and continued to move throughout the 18-hour and 20-minute scheduled exposure period, regardless of whether RF was being generated or not. As described in Section 2 and Appendix A, if the chamber doors were opened (e.g., for unplanned activities), the stirrers and RF generation were paused for safety and would resume as scheduled once all doors were securely closed.

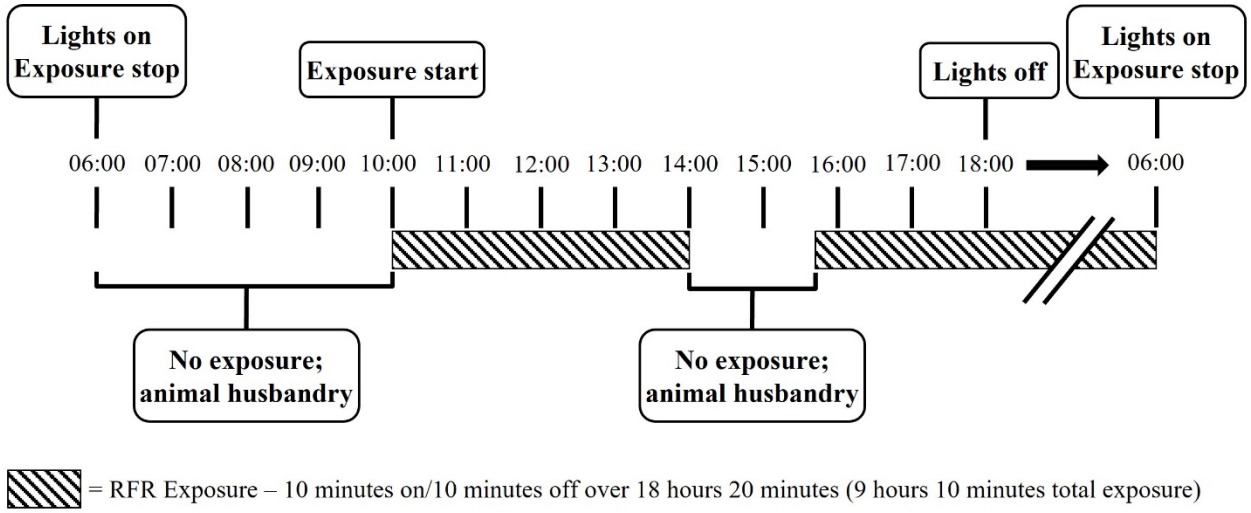

Figure 6. Exposure Regimen for Investigative Radiofrequency Radiation Studies

RFR = radiofrequency radiation.

Due to power constraints of the overall system, RFR groups were on opposite interval schedules across the two 10-minute periods of either "RFR ON" or "RFR OFF". During the first 10-minute period, the high exposure group was exposed, and the low and medium exposure groups were not exposed. During the next 10-minute period, the low and medium exposure groups were exposed, and the high exposure group was not exposed. This pattern continued throughout the 18-hour and 20-minute period. For the purposes of measurements taken as related to exposure status (e.g., video observations, RFR exposure log data), the chamber control group was considered to follow the same pattern as the high exposure group though this group received no RFR exposure. Table 3 demonstrates the exposure schedule using the hour of 10:00–11:00 as an example:

Table 3. Example Exposure Pattern

Time	Chamber Control and High Exposure Groups[a]	Low and Medium Exposure Groups[b]
10:00–10:10	RFR ON	RFR OFF
10:10–10:20	RFR OFF	RFR ON
10:20–10:30	RFR ON	RFR OFF
10:30–10:40	RFR OFF	RFR ON
10:40–10:50	RFR ON	RFR OFF
10:50–11:00	RFR OFF	RFR ON

RFR = radiofrequency radiation.
[a]The high exposure group was 9 W/kg for rats and 15 W/kg for mice. For the purpose of measurements taken as related to the status of RFR ON/OFF, the chamber control group followed the exposure pattern of the high exposure group.
[b]The low and medium exposure groups were 3 and 6 W/kg for rats and 5 and 10 W/kg for mice.

On study day 3, female rats were not exposed for the full duration due to improper closure of the chamber door; thus, female rats were exposed for an additional sixth day. To minimize time between the end of exposure and tissue collection for comet assay, animals were briefly exposed on the day of necropsy up until scheduled removal for necropsy. Subsets of animals were removed during successive "off" exposure periods, with representation across exposure groups during each "off" period. Exposures continued for animals that remained in the chambers until all animals were removed. For mice, individual animals had tissues collected within 8 minutes of euthanasia. For rats, individual animals had tissues collected within 13 minutes of euthanasia. All tissues of interest were collected from all animals within 2 hours and 50 minutes for rats, and within 2 hours and 4 minutes for mice.

Chamber control animals were housed in a reverberation chamber identical to that in which exposed animals were housed, except without an active RFR antenna, and were not exposed to RFR. Furthermore, the chamber shielded the animals from environmental RFR, with the exception of periods when the chamber door was opened for animal care activities. Room control animals were housed in the same room as exposed animals in standard polycarbonate cages and were similarly not purposefully exposed to RFR. Based on measurements over a 24-hour period at the location of the room control animals, the peak measured fields were 56 dB lower than those in the mouse high-power chamber (Figure B-5; Figure B-6) and resulted in specific absorption rate (SAR) levels more than 100,000 times lower in the room control animals than in the exposed animals. Mean SAR levels for the exposures remained within 10% of target levels throughout the studies; summaries of the exposure data are provided in Appendix C. Noise was monitored during all studies, and the minimum, maximum, and mean levels were similar for both average noise and peak noise across all exposure groups in all studies.

Feed and water were available ad libitum. To avoid interference with RFR dosimetry, feed was provided in ceramic (nonmetallic) bowls, and water was delivered in an adapted automatic watering system.[17] Rats and mice were housed individually during the 5-day studies. Details of the study design and animal maintenance are summarized in Table 4. Information on feed composition and contaminants is provided in Appendix E.

4.2.3.4. Clinical Examinations

Blood was collected immediately prior to study termination from the retroorbital plexus (rats) or sinus (mice) into cryotubes containing cold mincing solution for comet assay. Animals were anesthetized with a carbon dioxide/oxygen mixture and bled in a random order. Necropsies were performed on all animals. After rinsing in cold mincing solution, brain regions (frontal cortex, hippocampus, and cerebellum) and heart tissue were cut into small pieces, and all tissue pieces were flash frozen and stored at −80°C for the comet assay. Liver tissue underwent similar processing except that several small pieces were cut from a small strip of tissue taken from the left lobe of the liver. Samples were stored for a minimum of 3 days before shipment to Integrated Laboratory Systems, LLC, an Inotiv company (Research Triangle Park, NC) for analysis. Information on the comet assay sampling is provided in Appendix D.

Rats and mice were observed twice daily for signs of mortality or moribundity. Clinical observations were recorded initially, daily, and at study termination. Body weights were recorded prior to surgery for data-logger implantation, initially, and at study termination.

Table 4. Experimental Design and Materials and Methods in the Whole-body Exposure Studies of CDMA- and GSM-modulated Cell Phone Radiofrequency Radiation

Rats	Mice
Testing Facility	
Battelle/AmplifyBio[2] (West Jefferson, Ohio)	Same as rats
Strain and Species	
Sprague Dawley (Hsd:Sprague Dawley® SD®)	B6C3F1/N
Animal Source	
Envigo (Indianapolis, IN)	Taconic Biosciences, Inc. (Germantown, NY)
Time Held Before Studies	
CDMA: 59 (males) or 87 (females) days GSM: 38 days (males)	CDMA: 167 days (males)
Average Age When Studies Began	
CDMA: 31 (males) or 23 (females) weeks GSM: 28 weeks (males)	CDMA: 33 weeks (males)
Date of First Exposure	
CDMA: October 21, 2021 (males) or November 18, 2021 (females) GSM: September 30, 2021 (males)	CDMA: July 22, 2020 (males)

[2]These studies were conducted under the NIEHS contract with Battelle Memorial Institute (HHSN273201400015C). The studies were initiated at the Battelle testing facility in West Jefferson, Ohio. On May 1, 2021, the testing facility was transferred to a new company, AmplifyBio. The study was transferred to AmplifyBio as a subcontract under HHS273201400015C. All of the installation and verification activities were conducted while Battelle was the testing facility. For the mouse study, all of the in-life, postmortem, and analytical portions of the study were conducted while Battelle was the testing facility; reporting was conducted under AmplifyBio as the testing facility. The rat studies were conducted under AmplifyBio as the testing facility.

Rats	Mice
Duration of Exposure	
Nine hours and 10 minutes per day, over the course of an 18-hour and 20-minute period, in 10-minute-on, 10-minute-off intervals for 5 (males) or 6 (females) days	Nine hours and 10 minutes per day, over the course of an 18-hour and 20-minute period, in 10-minute-on, 10-minute-off intervals for 5 days
Date of Last Exposure	
CDMA: October 26, 2021 (males) or November 24, 2021 (females) GSM: October 5, 2021 (males)	CDMA: July 27, 2020 (males)
Necropsy Dates	
CDMA: October 26 (males) or November 24 (females), 2021 GSM: October 5, 2021 (males)	CDMA: July 27, 2020 (males)
Average Age at Necropsy	
CDMA: 32 weeks (males) or 24 (females) weeks GSM: 29 weeks (males)	CDMA: 33 weeks (males)
Size of Study Groups	
CDMA: 10 males and 10 females GSM: 10 males	CDMA: 10 males
Method of Distribution	
Animals were distributed randomly into groups of approximately equal initial mean body weights	Same as in rats
Animals per Cage	
1	Same as in rats
Method of Animal Identification	
Tail tattoo and cage card	Tail marking with permanent pen and cage card
Diet	
Irradiated NTP-2000 wafer feed (Zeigler Brothers Inc., Gardners, PA), available ad libitum, ceramic feed bowls	Same as in rats
Water	
Tap water (Village of West Jefferson, OH municipal supply) via automatic watering system (Edstrom Industries, Waterford, WI) or via Lixit® in exposure chambers, available ad libitum	Same as in rats
Cages	
Solid polycarbonate (Lab Products, Inc., Seaford, DE), for room control animals	Solid polycarbonate (Lab Products, Inc., Seaford, DE), for room control animals
Solid polycarbonate (Thoren #7, Thoren Caging Systems, Hazleton, PA) for exposed animals with plexiglass lids	Solid polycarbonate (Thoren #7, Thoren Caging Systems, Hazleton, PA) for exposed animals with filter top lids

Rats	Mice
Bedding	
Irradiated Sani-Chips® (Envigo, Madison, WI)	Same as in rats
Environmental Enrichment	
None	Natural crinkled kraft paper (Crink-l'nest™, The Andersons, Maumee, Ohio)
Racks	
Stainless steel (Lab Products, Inc., Seaford, DE) for room control animals Custom-designed fiberglass cage racks integrated within the reverberation chambers (Foundation for Research on Information Technologies in Society [IT'IS], Zürich, Switzerland) for exposed animals; reverberation chambers held up to 10 cages	Same as in rats
Rack Filters	
Spun-bonded polyester (National Filter Media Corporation, Olive Branch, MS)	Same as in rats
Reverberation Chambers	
Fully shielded, stainless-steel chamber equipped with a stainless-steel door to eliminate leakage of RFR signals, RFR excitation antennas, and two rotating stirrers	Same as in rats
Animal Room Environment (*Room control animals)*	
Temperature: 75°F to 78°F Relative humidity: 48% to 53% Room fluorescent light: 12 hours/day Room air changes: at least 10/hour	Temperature: 75°F to 76°F Relative humidity: 48% to 53% Room fluorescent light: 12 hours/day Room air changes: at least 10/hour
Reverberation Chamber Environment *(Chamber control and exposed animals)*	
Temperature: 69°F to 75°F Relative humidity: 47.0% to 60.2% Chamber incandescent light: 12 hours/day Chamber airflow: 0.0 to 1.7 m/sec (adjusted to achieve the target air changes per hour)	Temperature: 69°F to 72°F Relative humidity: 49.0% to 59.5% Chamber incandescent light: 12 hours/day Chamber airflow: 0.0 to 1.6 m/sec (adjusted to achieve the target air changes per hour)
Exposure Level	
Time-averaged whole-body SAR levels of 0 (chamber control), 3, 6, or 9 W/kg CDMA- or GSM-modulated cell phone RFR	Time-averaged whole-body SAR levels of 0 (chamber control), 5, 10, or 15 W/kg CDMA-modulated cell phone RFR
Type and Frequency of Observation	
Observed twice daily; animals were weighed prior to implantation surgery, initially, and at study termination, and clinical observations were recorded daily. The body temperature data generated by the temperature chips and data loggers were unusable.	Same as in rats

Rats	Mice
Method of Euthanasia	
100% carbon dioxide, followed by exsanguination	70% carbon dioxide/30% oxygen, followed by exsanguination
Necropsy	
Necropsies were performed on all animals	Same as in rats
Genetic Toxicology	
At study termination, samples were collected from blood, brain (frontal cortex, hippocampus, cerebellum), heart, and liver for analysis by comet assay.	Same as in rats

CDMA = Code Division Multiple Access-modulated cell phone radiofrequency radiation; GSM = Global System for Mobile Communications-modulated cell phone radiofrequency radiation; RFR = radiofrequency radiation; SAR = specific absorption rate.

4.2.3.5. Video Clinical Observations

To support the planned evaluations, cameras were added to the exposure chambers for select time periods to generate recordings of animals during exposure. As described in Section 2 and Appendix A, each chamber had 10 cage locations in a design of five rows with two cages per row. For each exposure chamber, cameras (five per chamber) were positioned on the chamber door such that one video camera would be directly in front of one cage on each of the five rows when the chamber doors were closed. The room control group similarly had cameras (five per group) positioned directly in front of the cages. Based on video recordings, animals with cameras directly in front of their cage (five animals per exposure group) were evaluated on study days 0, 1, 2, 3, and 4 (mice), or on study days 0 and 4 (rats). Due to the short duration of the studies, cage locations were not rotated throughout the chamber, and the same animals were evaluated at each timepoint. Recorded video was evaluated to gauge whether there were visible changes in animal activity during the first on and off exposure cycles in the morning/light hours (AM ON, AM OFF) and in the first on and off exposure cycles of the evening/dark hours (PM ON, PM OFF). Infrared light was used for illumination during nighttime recording. Table 5 shows the days and times that each video observation was recorded for the four studies.

Table 5. Scheduled Times of Video Recording

	AM ON		AM OFF		PM ON		PM OFF	
CDMA Male Mice	**0, 15 W/kg**	**5, 10 W/kg**	**0, 15 W/kg**	**5, 10 W/kg**	**0, 15 W/kg**	**5, 10 W/kg**	**0, 15 W/kg**	**5, 10 W/kg**
Day 0, 22Jul2020	10:00	10:30	10:10	10:40	18:00	18:10	18:10	18:20
Day 1, 23Jul2020	10:00	10:10	10:10	10:20	18:00	18:10	18:10	18:20
Day 2, 24Jul2020	10:00	10:30	10:10	10:40	18:00	18:10	18:10	18:20
Day 3, 25Jul2020	10:00	10:10	10:10	10:20	18:40[a]	18:30[a]	18:30[a]	18:40[a]
Day 4, 26Jul2020	10:00[b]	10:30	10:10[b]	10:40	18:00	18:10	18:10	18:20
CDMA Male Rats	**0, 9 W/kg**	**3, 6 W/kg**	**0, 9 W/kg**	**3, 6 W/kg**	**0, 9 W/kg**	**3, 6 W/kg**	**0, 9 W/kg**	**3, 6 W/kg**
Day 0, 21Oct2021	10:00	10:10	10:10	10:00	18:00	18:10	18:10	18:00
Day 4, 25Oct2021	10:00	10:10	10:10	10:00	18:00	18:10	18:10	18:00
CDMA Female Rats	**0, 9 W/kg**	**3, 6 W/kg**	**0, 9 W/kg**	**3, 6 W/kg**	**0, 9 W/kg**	**3, 6 W/kg**	**0, 9 W/kg**	**3, 6 W/kg**
Day 0, 18Nov2021	10:00	10:10	10:10	10:00	18:20[c]	–[c]	–[c]	18:20[c]
Day 4, 22Nov2021	10:00	10:10	10:10	10:00	18:00[b]	18:10	18:10	18:00
GSM Male Rats	**0, 9 W/kg**	**3, 6 W/kg**	**0, 9 W/kg**	**3, 6 W/kg**	**0, 9 W/kg**	**3, 6 W/kg**	**0, 9 W/kg**	**3, 6 W/kg**
Day 0, 30Sept2021	10:00	10:10	10:10	10:00	18:00	18:10	18:10	18:00
Day 4, 4Oct2021	10:00	10:10	10:10	10:00	18:00	18:10	18:10	18:00

CDMA = Code Division Multiple Access-modulated cell phone radiofrequency radiation; GSM = Global System for Mobile Communications-modulated cell phone radiofrequency radiation; AM = morning light hours; PM = evening dark hours.

[a]Lights were scheduled to turn off at 18:00. On Day 3 (July 25, 2020) of the CDMA male mouse study, lights did not turn off until 18:24; therefore, the PM ON and PM OFF evaluations for all groups were delayed to evaluate the first cycles in the dark period.

[b]There are three instances in which a video clinical observation was recorded, but the corresponding video files are no longer available due to file corruption. The recorded observations for which videos are not available include a CDMA male mouse (animal 33, day 4, AM ON and AM OFF) and a CDMA female rat (animal 364, day 4, PM ON).

[c]There was an unscheduled system pause at 18:02 on Day 0 (November 18, 2021) of the CDMA female rat study; therefore, the PM ON and PM OFF video recordings were delayed or unavailable.

Animals were evaluated according to a reaction rating scale of normal, minimal, mild, moderate, and severe (Table 6). Animals were also evaluated over the subsequent full 10-minute "on" period to determine whether there was any change in activity over the 10-minute exposure window; no changes in activity were observed during these observations. Videos used to generate the observations described here are available in the Chemical Effects and Biological Systems (CEBS) database: https://doi.org/10.22427/NIEHS-DATA-NIEHS-RFRB. Videos have been edited to protect privacy by removal of human faces and voices.

Table 6. Reaction Rating Scale for Video Clinical Observations

Score[a]	Rating Used in Report Narrative	Description
NT	NV	No video available
−1	Normal	No reaction
0	Minimal	Slight reaction; ear flinching or flicking within normal limits
1	Mild	More energetic response than Minimal
2	Moderate	Exaggerated reaction (e.g., jumps, bites, attacks)
3	Severe	Rodent freezes, actual muscle contractions

NT = not assigned; NV = no video.
[a]Numerical score as reported in the individual animal video observations. The individual animal data can be found in Appendix G.

4.2.4. Statistical Methods

Statistical methods were chosen based on distributional assumptions. Unless specifically mentioned, all endpoints were tested for a trend across exposure groups, followed by pairwise tests for each exposed group against the chamber control group. Significance of all trend and pairwise tests is determined by a p value of ≤0.05 and is reported at both 0.05 and 0.01 levels. The room control group was analyzed only by a single pairwise comparison to the chamber control group. The room control analysis was kept separate from that of the other exposed groups and was excluded from all trend tests.

4.2.4.1. Analysis of Continuous Variables

Two approaches were employed to assess the significance of pairwise comparisons between exposed and control groups in the analysis of continuous variables. Body weight data, which historically have approximately normal distributions, and body temperatures were analyzed with the parametric multiple comparison procedures of Dunnett[20] and Williams.[21; 22] The Jonckheere test[23] was used to assess the significance of the exposure-related trends and to determine whether a trend-sensitive test (the Williams' test) was more appropriate for pairwise comparisons than a test that does not assume a monotonic exposure-related trend (the Dunnett test). Before statistical analysis, outliers identified using the Dixon and Massey test[24] were examined by NIEHS/DTT personnel, and biologically implausible values (likely due to experimental error) were eliminated from the analysis.

4.2.5. Quality Assurance Methods

The 5-day studies were conducted in compliance with U.S. Food and Drug Administration Good Laboratory Practice Regulations.[25] In addition, the 5-day study reports were audited retrospectively by an independent quality assurance contractor against study records submitted to

the NTP Archives. Audit procedures and findings are presented in the reports and are on file at NIEHS. The audit findings were reviewed and assessed by NIEHS/DTT scientists, and all comments were resolved or otherwise addressed during the preparation of this report.

4.2.6. Genetic Toxicology

The genetic toxicity of whole-body GSM- and CDMA-modulated cell phone RFR was assessed by testing whether the exposure increased DNA damage in cells from the brain (frontal cortex, hippocampus, and cerebellum), liver, heart, and blood of rats and mice following 5 days of exposure. The protocol for these studies and the results are given in Appendix D.

The genetic toxicity studies have evolved from an earlier effort to develop a comprehensive database permitting a critical anticipation of a test article's carcinogenicity in experimental animals that was based on numerous considerations, including the relationship between the molecular structure of the chemical and its observed effects in short-term in vitro and in vivo genetic toxicity tests (structure-activity relationships). The short-term tests were developed originally to clarify proposed mechanisms of chemical-induced DNA damage, given the relationship between electrophilicity and mutagenicity,[26] and the somatic mutation theory of cancer.[27; 28] Not all cancers, however, arise through genotoxic mechanisms.

4.2.6.1. Comet Assay

The alkaline (pH > 13) comet assay,[29] also known as the single cell gel electrophoresis assay, detects DNA damage in any of a variety of eukaryotic cell types[30-33]; cell division is not required. The type of DNA damage detected includes nicks, adducts, strand breaks, and abasic sites that are converted to DNA strand breaks after treatment of cells in an alkaline (pH > 13) solution. Transient DNA strand breaks generated by the process of DNA excision repair might also be detected. DNA damage caused by crosslinking agents has been detected as a reduction of DNA migration.[34; 35] The fate of the DNA damage detected by the comet assay is varied; most of the damage is rapidly repaired and results in no sustained effect on the tissue, but some damage might result in cell death or be incorrectly processed by repair proteins and lead to a fixed mutation or chromosomal alteration. In these studies, brain (frontal cortex, hippocampus, and cerebellum), liver, heart, and blood samples from rats and mice were tested in the comet assay. The protocol for these studies and the results are given in Appendix D.

4.3. Results

4.3.1. Data Availability

All study data were evaluated. Data relevant for evaluating findings are presented here. Body temperature data were unusable because of data quality or data collection issues. All study data are available in the CEBS database: https://doi.org/10.22427/NIEHS-DATA-NIEHS-RFRA.[36]

4.3.2. Five-day Study in Male Mice Exposed to CDMA-modulated Cell Phone Radiofrequency Radiation

4.3.2.1. Survival and Body Weights

All animals survived until the scheduled termination on study day 5. There were no exposure-related effects on survival or body weights with CDMA-modulated RFR exposure up to 15 W/kg

for 5 days in male mice. Body weights of exposed animals were within 5% of the chamber control (0 W/kg) animals and did not reach statistical significance throughout exposure (Table 7). The body weight of the room control group was also within 5% of the chamber control group.

Table 7. Summary of Body Weights of Male Mice in the Five-day Study of CDMA-modulated Radiofrequency Radiation

Study Day	Room Control	0 W/kg	5 W/kg	10 W/kg	15 W/kg
n	10	10	10	10	10
0[a,b,c]	40.8 ± 0.5	40.7 ± 0.6	40.5 ± 0.6	41.3 ± 0.5	39.5 ± 0.5
5	42.6 ± 0.5	41.6 ± 0.8	43.0 ± 0.6	43.3 ± 0.5	42.3 ± 0.6

CDMA = Code Division Multiple Access-modulated cell phone radiofrequency radiation.
[a]Data are presented as mean ± standard error. Body weight data are presented in grams.
[b]Statistical analysis performed by Jonckheere (trend) and Williams or Dunnett (pairwise) tests. Statistical analysis for the room control group compared to the 0 W/kg chamber control group was performed using the t-test. No statistically significant findings were noted at $p \leq 0.05$.
[c]Study day 0 is the day animals were placed on study.

4.3.3. Five-day Study in Male Rats Exposed to CDMA-modulated Cell Phone Radiofrequency Radiation

Prior to conducting the rat studies described here in Sections 4.3.3, 4.3.4, and 4.3.5, a number of system modifications and maintenance occurred. These activities are described in more detail in Section 3.4.

4.3.3.1. Survival and Body Weights

All animals survived until the scheduled termination on study day 5. There were no exposure-related effects on survival or body weights with CDMA-modulated RFR exposure up to 9 W/kg for 5 days in male rats. Body weights of exposed animals were within 5% of the chamber control animals and did not reach statistical significance throughout exposure (Table 8). The body weight of the room control group was also within 5% of the chamber control group.

Table 8. Summary of Body Weights of Male Rats in the Five-day Study of CDMA-modulated Radiofrequency Radiation

Study Day	Room Control	0 W/kg	3 W/kg	6 W/kg	9 W/kg
n	10	10	10	10	10
0[a,b,c]	394.2 ± 5.3	382.4 ± 5.5	384.7 ± 4.8	388.1 ± 4.4	388.8 ± 4.4
5	400.7 ± 6.0	401.2 ± 5.1[d]	388.2 ± 6.4	394.5 ± 3.1	387.7 ± 4.7

CDMA = Code Division Multiple Access-modulated cell phone radiofrequency radiation.
[a]Data are presented as mean ± standard error. Body weight data are presented in grams.
[b]Statistical analysis performed by Jonckheere (trend) and Williams or Dunnett (pairwise) tests. Statistical analysis for the room control group compared to the 0 W/kg chamber control group was performed using the t-test. No statistically significant findings were noted at $p \leq 0.05$.
[c]Study day 0 is the day animals were placed on study.
[d]n = 9. One animal weight in the 0 W/kg chamber control group was excluded from the analysis as an outlier.

4.3.4. Five-day Study in Female Rats Exposed to CDMA-modulated Cell Phone Radiofrequency Radiation

4.3.4.1. Survival and Body Weights

All animals survived until the scheduled termination on study day 6. There were no exposure-related effects on survival or body weights with CDMA-modulated RFR exposure for 6 days up to 9 W/kg in female rats. On study day 6, body weights showed a positive trend compared to the chamber control group; however, no pairwise comparisons for exposed groups reached statistical significance, and body weights of the exposed animals were within 10% of the chamber control animals throughout exposure (Table 9). The body weight of the room control group was also within 10% of the chamber control group.

Table 9. Summary of Body Weights of Female Rats in the Five-day Study of CDMA-modulated Radiofrequency Radiation

Study Day	Room Control	0 W/kg	3 W/kg	6 W/kg	9 W/kg
n	10	10	10	10	10
0[a,b,c]	275.6 ± 5.2	266.5 ± 6.1	267.0 ± 4.5	275.1 ± 5.0	277.0 ± 3.5
6	277.6 ± 4.8	264.0 ± 5.0*	266.5 ± 4.8	273.6 ± 5.6	279.1 ± 5.1

CDMA = Code Division Multiple Access-modulated cell phone radiofrequency radiation.
Statistical significance for the 0 W/kg chamber control group indicates a significant trend test; the room control group was excluded from trend test. All comparisons are made to 0 W/kg chamber control.
*Statistically significant at $p \leq 0.05$.
[a]Data are presented as mean ± standard error. Body weight data are presented in grams.
[b]Statistical analysis performed by Jonckheere (trend) and Williams or Dunnett (pairwise) tests. Statistical analysis for the room control group compared to the 0 W/kg chamber control group was performed using the t-test.
[c]Study day 0 is the day animals were placed on study.

4.3.5. Five-day Study in Male Rats Exposed to GSM-modulated Cell Phone Radiofrequency Radiation

4.3.5.1. Survival and Body Weights

All animals survived until the scheduled termination on study day 5. There were no exposure-related effects on body weights with GSM-modulated RFR exposure up to 9 W/kg for 5 days in male rats. On study day 5, body weights showed a negative trend and a significant decrease in the 6 W/kg group compared to the chamber control group. However, body weights of all exposed groups were within 10% of the chamber control group (Table 10). The body weight of the room control group was also within 5% of the chamber control group.

Table 10. Summary of Body Weights of Male Rats in the Five-day Study of GSM-modulated Radiofrequency Radiation

Study Day	Room Control	0 W/kg	3 W/kg	6 W/kg	9 W/kg
n	10	10	10	10	10
0[a,b,c]	374.2 ± 4.7	377.7 ± 5.2	377.4 ± 5.0	360.2 ± 7.7	373.2 ± 3.4
5	379.0 ± 4.0	382.5 ± 3.7*	381.9 ± 5.5	352.7 ± 13.5*	368.2 ± 5.0

GSM = Global System for Mobile Communications-modulated cell phone radiofrequency radiation.
Statistical significance for an exposed group indicates a significant pairwise test compared to the 0 W/kg chamber control group. Statistical significance for the 0 W/kg chamber control group indicates a significant trend test; the room control group was excluded from trend test. All comparisons are made to 0 W/kg chamber control group.
*Statistically significant at $p \leq 0.05$.
[a]Data are presented as mean ± standard error. Body weight data are presented in grams.
[b]Statistical analysis performed by Jonckheere (trend) and Williams or Dunnett (pairwise) tests. Statistical analysis for the room control group compared to the 0 W/kg chamber control group was performed using the t-test.
[c]Study day 0 is the day animals were placed on study.

4.3.6. Video Clinical Observations

Another factor in assessing the use of the exposure system for conducting toxicological research was to understand the extent to which animals were aware of or stressed by the RF signal itself, the GSM-associated noise, or movement of stirrers in the chambers. Video cameras were placed within the exposure chambers to capture video footage of animals during exposure. Recorded video was evaluated during the first RFR ON and first RFR OFF cycle during the morning/light hours (AM ON, AM OFF) and during the first RFR ON and RFR OFF cycle during the evening dark hours (PM ON, PM OFF). Across nearly all animals and all time points evaluated, there were no consistent, exposure-related, and visible changes in activity that would indicate the animals were aware of or stressed about the initiation or cessation of exposure in the chambers.

A summary of the frequency of normal video clinical observations in mice and rats is presented in Table 11 and Table 12 below. The tables combine observations across exposure groups within each study.

For the CDMA mouse study, all video clinical observations were recorded as normal, with the exception of one animal in the 5 W/kg group that was recorded as having a minimal response on study day 0 during the first AM ON evaluation (Table 11). A minimal response was considered a slight reaction with ear flinching or flicking within normal rodent activity limits.

For video clinical observations in the rat studies, most recordings were within normal limits (Table 12). In a few instances, animals were observed to show some changes in activity. Two

CDMA male rats in the 9 W/kg group during the first AM ON evaluation were recorded as having a minimal or mild response; specifically, one 9 W/kg CDMA male rat was recorded as having a minimal response, and one 9 W/kg CDMA male rat was recorded as having a mild response. A mild response was considered more energetic than the minimal response.

Video clinical observations showed that all CDMA female rats in the chambers had normal responses at the time points evaluated (Table 12). Two GSM male rats (one each in the 6 and 9 W/kg groups) were recorded as having responses greater than normal during the exposure signal transitions on study day 0. One 9 W/kg GSM male rat during the first AM ON evaluation was recorded as having a mild response, and one 6 W/kg GSM male rat during the first PM OFF evaluation was recorded as having a mild response.

In addition to evaluating animals at AM ON, AM OFF, PM ON, and PM OFF, animals were evaluated over a full 10-minute "on" period during the morning and evening exposures to determine whether there was any change in activity over the exposure period. No changes in activity were observed during these observations.

Table 11. Frequency of "Normal" (i.e., −1 Reaction Score) Recordings in Male Mice in the Five-day Study of CDMA-modulated Radiofrequency Radiation[a]

	Day 0	Day 1	Day 2	Day 3	Day 4	Total Across Days (%)
AM ON	12/13[b]	23/23	20/20	25/25	23/23	103/104 (99%)
AM OFF	13/13	23/23	20/20	25/25	23/23	104/104 (100%)
PM ON	23/23	18/18	19/19	23/23	19/19	102/102 (100%)
PM OFF	23/23	18/18	19/19	23/23	19/19	102/102 (100%)

CDMA = Code Division Multiple Access-modulated cell phone radiofrequency radiation; AM = morning light hours; PM = evening dark hours.
[a]Reported observations in this table are combined across all five exposure groups. All observations not recorded as "normal" are described in footnotes. A subset of animals (goal of five animals per exposure group) was monitored for each period. Video observations were sometimes unavailable for all animals (e.g., animal was not visible in video or infrared illumination was inadequate for video capture).
[b]One animal (#29, 5 W/kg) had a recording of 0 on Day 0 at the first AM ON period.

Table 12. Frequency of "Normal" (i.e., −1 Reaction Score) Recordings in Male and Female Rats in the Five-day Studies of CDMA- and GSM-modulated Radiofrequency Radiation[a]

	Day 0	Day 4	Total Across Days (%)
CDMA Male Rats			
AM ON	21/23[b]	22/22	43/45 (96%)
AM OFF	23/23	22/22	45/45 (100%)
PM ON	22/22	21/21	43/43 (100%)
PM OFF	22/22	21/21	43/43 (100%)
CDMA Female Rats			
AM ON	25/25	24/24	49/49 (100%)
AM OFF	25/25	24/24	49/49 (100%)

	Day 0	Day 4	Total Across Days (%)
PM ON	12/12[c]	24/25[d]	36/37 (97%)
PM OFF	12/12[c]	25/25	37/37 (100%)
GSM Male Rats			
AM ON	16/17[e]	22/22	38/39 (97%)
AM OFF	17/17	22/22	39/39 (100%)
PM ON	21/21	22/22	43/43 (100%)
PM OFF	20/21[f]	22/22	42/43 (98%)

CDMA = Code Division Multiple Access-modulated cell phone radiofrequency radiation; GSM = Global System for Mobile Communications-modulated cell phone radiofrequency radiation; AM = morning light hours; PM = evening dark hours.
[a]Reported observations in this table are combined across all five exposure groups. All observations not recorded as "normal" are described in footnotes. A subset of animals (goal of five animals per exposure group) was monitored for each period. Video observations were sometimes unavailable for all animals (e.g., animal was not visible in video or infrared illumination was inadequate for video capture).
[b]One animal (#300, 9 W/kg CDMA male rat) had a recording of 0, and one animal (#297; a second 9 W/kg CDMA male rat) had a recording of 1 on Day 0 in the AM ON period.
[c]For CDMA female rats, video cameras did not capture the entire RFR ON and RFR OFF cycles in the PM period on Day 0. As a result, video observations are unavailable for the first PM ON for the 3 W/kg group, the 6 W/kg group, and some room control animals. Video observations are also unavailable for the first PM OFF transition for the 0 W/kg chamber control group, the 9 W/kg group, and some room control animals.
[d]One animal (#355, room control CDMA female rat) had a recording of 0 on Day 4 at the first PM ON period.
[e]One animal (#197, 9 W/kg GSM male rat) had a recording of 1 on Day 0 at the first AM ON period.
[f]One animal (#182, 6 W/kg GSM male rat) had a recording of 1 on Day 0 at the first PM OFF period.

4.3.7. Genetic Toxicology

DNA damage from exposure to RFR was assessed in frontal cortex, hippocampus, cerebellum, liver, blood, and heart cell samples from male mice and male and female rats using the comet assay (Table D-1, Table D-2, Table D-3, and Table D-4). For CDMA male mice, there were no significant increases in DNA damage, measured as the percent tail DNA, in cells sampled from the three brain regions, blood, and heart tissue; there was a significant trend test for the percent tail DNA in liver cells that is of uncertain biological significance. For CDMA male and CDMA female rats, no significant increases in the percent tail DNA were observed for any tissue. For GSM male rats, there were no significant increases in DNA damage, measured as the percent tail DNA, in cells sampled from frontal cortex, cerebellum, liver, blood, or heart tissue; there was a significant trend test for the percent tail DNA in hippocampal cells that is of uncertain biological significance.

The percent tail DNA for room control animals and chamber control animals was not significantly different for 20 of the 24 tissues examined in the 5-day studies. For CDMA male mice, the percent tail DNA was lower in the frontal cortex and higher in the heart in the room control group compared to the chamber control group. For GSM male rats and CDMA female rats, the percent tail DNA in heart tissue was lower in the room control group compared to the chamber control group. For these four instances in which significant differences in the percent tail DNA were detected between the two control groups, the differences did not reach twofold (1.5–1.6-fold) except for the frontal cortex cells in CDMA male mice, which showed a twofold difference in the chamber control group over the room control that may be considered biologically relevant. Notably, negative results were observed in the dose-response studies for

each of these four tissues (i.e., heart and frontal cortex in CDMA male mice and heart in GSM male rats and CDMA female rats).

4.4. Summary

Five-day studies were conducted in male mice or male or female rats to evaluate the effect of exposure to the same CDMA- or GSM-modulated RF signals used in the previous NTP studies. Video from the cameras in the exposure chambers demonstrated no consistent, exposure-related, and visible changes in activity in either rats or mice the first time the exposure system was activated, at subsequent system on/off transitions, or during the periods of exposure. There were no exposure-related effects on survival or body weights following exposure to RFR for 5 days. There was no increase in DNA damage following exposure to RFR for 5 days, as measured using the comet assay, in brain cells (frontal cortex, hippocampus, and cerebellum), or in liver, heart, or blood cells of mice and rats. Body temperature measurements were collected during the studies using two different devices; however, the data were unusable.

5. Conclusion

The generation of well-controlled and well-characterized radiofrequency radiation (RFR) exposures is a critical factor in carrying out experimental studies to assess the interactions between RFR and biological tissues. Such research requires the development of an exposure system that can generate radiofrequency (RF) signals that mimic human exposure, which can vary because of the continued use of frequencies and modulations in older cell phone technologies (2G, 3G, 4G long-term evolution [LTE]) and the implementation of evolving mobile communication technology (5G and beyond) that utilizes different frequencies and modulations.

The development of a small-scale RFR exposure system with expanded capabilities was a major goal for this investigative research to understand the effects of RFR exposure on biological responses in rats and mice. The studies reported herein were conducted by researchers in the Division of Translational Toxicology (DTT) at the National Institute of Environmental Health Sciences (NIEHS). These studies were not conducted as part of the National Toxicology Program (NTP).

This report describes the development of a small-scale exposure system by NIEHS/DTT that was based on the one used in previous NTP studies[12; 13; 15-18] and presents data from short-term investigative studies on RFR exposure. Working with the same technical experts as those who supported the previous NTP toxicology and carcinogenesis studies, an RFR exposure system with four exposure chambers capable of housing 10 animals each was designed, constructed, and tested for its performance in generating the desired RFR exposures (i.e., RF field strength, uniformity, and homogeneity). Technical staff from the National Institute of Standards and Technology also independently tested the system to verify the RF field strengths, signal quality, and signal parameters recorded by the internal components of the exposure system in a process analogous to that used in the previous NTP studies.[12; 13; 17] Field uniformity and signal quality were acceptable, and the overall conclusion of the technical experts was that the small-scale exposure system operated correctly and was capable of performing the exposure study.

The small-scale exposure system had greater flexibility for evaluating different characteristics of RF signals and increased functional capabilities compared to the system developed for the previous NTP studies.[17; 18] Although it was state of the art for the time, the exposure system used in the previous NTP studies was based on technology that was only capable of generating Global System for Mobile Communications (GSM)- and Code Division Multiple Access (CDMA)-modulated RF signals at 900 and 1,900 MHz, which are older, less used cell phone technologies such as 2G and 3G. Additionally, each chamber had to be permanently designated for a specific modulation at a specific frequency, and, as a result, a greater number of chambers was required. The new small-scale RFR exposure system described in this report was developed by NIEHS/DTT to overcome those limitations with a signal generator capable of generating a broader array of RF signals. In addition to the GSM and CDMA signals at 900 and 1,900 MHz used in the previous NTP studies, the small-scale exposure system could generate signals reflective of more current wireless communications (e.g., Third Generation Partnership Project [3GPP] LTE Frequency Division Duplex [FDD] and Time Division Duplex [TDD], LTE-Advanced, 3GPP FDD/ High-Speed Packet Access [HSPA]/HSPA+, GSM/Enhanced Data rates for GSM Evolution [EDGE]/EDGE Evolution, Time Division-Synchronous CDMA [TD-

SCDMA], Wireless Local-area Network [WLAN]) with frequencies between 9 kHz and 3.2 GHz, modulations with base bandwidths of up to 120 MHz, and carrier frequencies of up to 3,200 MHz. With these broader exposure flexibilities, a single chamber could be used for different signal frequencies, and the same chambers could be used at different times for studies in different animal strains, with different signals, and at different frequencies. Chambers were also equipped with the ability to toggle between two different light sources—halogen-based incandescent bulbs in these NIEHS/DTT studies, for consistency with the light source in the previous NTP studies, and newer light emitting diode (LED) bulbs. In addition, the system was designed to accommodate video recording during RFR exposure to enable monitoring of animals during exposure. Recorded video was used to observe if there were any changes in animal activity associated with RFR exposure or the physical functioning of the system.

After development and verification of the new RFR exposure system, unanticipated challenges were encountered that required extensive technical expertise to resolve. Following successful completion of the mouse CDMA study but prior to conducting the rat studies, numerous system modifications were required. These modifications included the fabrication and testing of new cage lids, evaluation and modification of the animal drinking water system, and reprogramming of the stirrer operations. Additional technical issues occurred during the conduct of the rat studies that required continued remote support from the Foundation for Research on Information Technologies in Society (IT'IS).

The new small-scale RFR exposure system was used to conduct an array of studies to investigate the role of heat, stress, and specific exposure parameters on the underlying potential mechanisms of RFR-mediated toxicity and carcinogenicity. The overall goals of this investigative project included evaluating cellular and molecular changes of DNA damage in the heart, brain, liver, and blood; measuring real-time changes in physiological parameters and animal response to RFR exposure; and investigating newer telecommunications technologies. Four 5-day investigative studies (three in Sprague Dawley (Hsd:Sprague Dawley® SD®) rats and one in B6C3F1/N mice) were conducted by NIEHS/DTT to evaluate the performance of the new RFR exposure system; compare the function of the new exposure system with the original system used in the previous NTP studies; and evaluate the effects of RFR exposure on body weight, body temperature, and DNA damage, as well as observe animals during exposure using video cameras.

In these studies, evaluation of video from the cameras in the exposure chambers demonstrated no consistent, exposure-related, and visible changes in activity in either rats or mice the first time the system was activated, during subsequent system on/off transitions, or during the periods of exposure. It has been hypothesized that the RF signal itself, noise generated during exposure periods, or the physical motion of the chamber components, such as the stirrers that serve to generate a homogeneous RF field, may startle the animals or otherwise induce a stress response.[37-39] A question raised during peer review of the previous NTP studies was whether the physical components of the reverberation chamber RFR exposure system or the signal itself had any effect on the animals. The previous NTP studies did not capture video of the animals during periods of exposure to observe changes that would indicate awareness of or reaction to RFR exposure; therefore, there was specific interest in capturing any awareness or reaction by the animals the first time they experienced the system's activation and the slow physical rotation of the vertical and horizontal stirrers. The potential effect of RF signal, noise, or physical/mechanical activity during exposures has never been evaluated in toxicological studies of RFR in animals. The lack of observable reaction in the current studies using the small-scale

system with RFR exposure levels up to 9 W/kg body weight (W/kg) in rats and 15 W/kg in mice suggests that operation of the system did not subject the animals to stress or discomfort.

A key goal for these investigative studies was to assess temperature changes during exposure, which was not conducted in the previous NTP chronic toxicity and carcinogenicity studies. The data generated by the data loggers and temperature chips during the rat and mouse studies were unusable.

Implanted data loggers were used to record changes in internal body temperature in real time while the RFR system was operational. The previously established method of temperature measurement using the implanted-temperature-chip approach required complete shutdown of the RFR system before animals could be assessed. After the system was shut down and chambers opened, a handheld sensor was used to collect individual animal temperatures from the implanted chips. Because animals are constantly thermoregulating, time between cessation of exposure and measurement of temperature could be a key factor affecting data collection and accuracy (as was the case with temperature-chip measurements in this study). The data loggers, if demonstrated as a viable method to collect body temperature, would allow for a robust real-time assessment of the effects of RFR exposure on body temperature during exposure. Unfortunately, data recorded by the data loggers in this study were inconsistent over short periods of time, and often not physiologically possible. As a result, the data-logger approach proved to be technically unfeasible.

As a component of the current NIEHS/DTT 5-day studies, the comet assay was used to explore whether genotoxic effects of RFR could be observed following a short duration of exposure. To reduce the influence of inter-animal variation, 10 animals per group were evaluated instead of 5, as was done for the previous 90-day NTP comet assay study. Exposure to RFR for 5 days did not induce DNA damage in brain cells (frontal cortex, hippocampus, and cerebellum), or in liver, heart, or blood cells of rats and mice. Equivocal results, showing limited statistically significant effects, were observed for male mouse liver cells (CDMA) and male rat hippocampal cells (GSM) in these 5-day studies. Although it is not possible to directly compare the 5-day and 90-day comet assay studies, it is interesting to note that a positive result for hippocampal cells from male rats exposed to CDMA was observed in the 90-day study. In addition, the unusually low baseline for the percent tail DNA reported for the frontal cortex of male mice in the chamber control group of the previous 90-day NTP study (1.32% ± 0.21% when 150 cells were assessed)[16] was also observed in the current 5-day study for male mice (0.46% ± 0.11% for the room control group and 0.91% ± 0.10% for the chamber control group). These observations appear to be consistent with previous studies indicating that shorter durations of exposure may not induce significant levels of DNA damage.[40; 41]

In summary, researchers at the NIEHS/DTT developed a small-scale RFR exposure system to investigate the effects of RFR exposure on biological responses in rats and mice and to better understand the potential mechanisms of RFR-mediated toxicity and carcinogenicity reported in the previous NTP studies. The investigative studies to test the exposure system found that the animals showed no visible response during operation of the system, and exposure to RFR for 5 days did not induce DNA damage in rats and mice.

These investigative studies of RFR exposure were technically challenging to conduct and, unfortunately, did not yield data useful for assessing body temperature in real time. Despite these

difficulties, this small-scale RFR exposure system presents a prototype for investigative toxicological studies by researchers interested in conducting experimental RFR studies in rodent models. High-quality studies to understand the effects of RFR exposure on biological responses are needed given the widespread human exposure to RFR associated with cell phone use. This report presents information about the design and conduct of this novel, small-scale RFR exposure system to facilitate advancement in methodologies and raise awareness about technical challenges associated with studying RFR.

References

1. National Information Standards Organization (NISO). CRediT (Contributor Roles Taxonomy). Baltimore, MD: National Information Standards Organization; 2024. [Accessed: July 26, 2024]. https://credit.niso.org/

2. Choi YJ, Moskowitz JM, Myung SK, Lee YR, Hong YC. Cellular phone use and risk of tumors: Systematic review and meta-analysis. Int J Environ Res Public Health. 2020; 17(21):8079. https://doi.org/10.3390/ijerph17218079

3. Coureau G, Bouvier G, Lebailly P, Fabbro-Peray P, Gruber A, Leffondre K, Guillamo JS, Loiseau H, Mathoulin-Pélissier S, Salamon R, et al. Mobile phone use and brain tumours in the CERENAT case-control study. Occup Environ Med. 2014; 71(7):514-522. https://doi.org/10.1136/oemed-2013-101754

4. Hardell L, Carlberg M, Söderqvist F, Mild KH. Pooled analysis of case-control studies on acoustic neuroma diagnosed 1997-2003 and 2007-2009 and use of mobile and cordless phones. Int J Oncol. 2013; 43(4):1036-1044. https://doi.org/10.3892/ijo.2013.2025

5. INTERPHONE Study Group. Brain tumour risk in relation to mobile telephone use: Results of the INTERPHONE international case-control study. Int J Epidemiol. 2010; 39(3):675-694. https://doi.org/10.1093/ije/dyq079

6. INTERPHONE Study Group. Acoustic neuroma risk in relation to mobile telephone use: Results of the INTERPHONE international case-control study. Cancer Epidemiol. 2011; 35(5):453-464. https://doi.org/10.1016/j.canep.2011.05.012

7. Benson VS, Pirie K, Schüz J, Reeves GK, Beral V, Green J, Million Women Study Collaborators. Mobile phone use and risk of brain neoplasms and other cancers: Prospective study. Int J Epidemiol. 2013; 42(3):792-802. https://doi.org/10.1093/ije/dyt072

8. Feychting M, Schüz J, Toledano MB, Vermeulen R, Auvinen A, Harbo Poulsen A, Deltour I, Smith RB, Heller J, Kromhout H, et al. Mobile phone use and brain tumour risk – COSMOS, a prospective cohort study. Environ Int. 2024; 185:108552. https://doi.org/10.1016/j.envint.2024.108552

9. Pettersson D, Mathiesen T, Prochazka M, Bergenheim T, Florentzson R, Harder H, Nyberg G, Siesjö P, Feychting M. Long-term mobile phone use and acoustic neuroma risk. Epidemiology. 2014; 25(2):233-241. https://doi.org/10.1097/ede.0000000000000058

10. Repacholi MH, Lerchl A, Röösli M, Sienkiewicz Z, Auvinen A, Breckenkamp J, d'Inzeo G, Elliott P, Frei P, Heinrich S, et al. Systematic review of wireless phone use and brain cancer and other head tumors. Bioelectromagnetics. 2012; 33(3):187-206. https://doi.org/10.1002/bem.20716

11. Yoon S, Choi JW, Lee E, An H, Choi HD, Kim N. Mobile phone use and risk of glioma: A case-control study in Korea for 2002-2007. Environ Health Toxicol. 2015; 30:e2015015. https://doi.org/10.5620/eht.e2015015

12. National Toxicology Program (NTP). NTP technical report on the toxicology and carcinogenesis studies in B6C3F1/N mice exposed to whole-body radio frequency radiation at a

frequency (1,900 MHz) and modulations (GSM and CDMA) used by cell phones. Research Triangle Park, NC: U.S. Department of Health and Human Services, Public Health Service, National Toxicology Program; 2018. NTP Technical Report No. 596. https://doi.org/10.22427/NTP-TR-596

13. National Toxicology Program (NTP). NTP technical report on the toxicology and carcinogenesis studies in Sprague Dawley (Hsd:Sprague Dawley SD) rats exposed to whole-body radio frequency radiation at a frequency (900 MHz) and modulations (GSM and CDMA) used by cell phones. Research Triangle Park, NC: U.S. Department of Health and Human Services, Public Health Service, National Toxicology Program; 2018. NTP Technical Report No. 595. https://doi.org/10.22427/NTP-TR-595

14. International Agency for Research on Cancer (IARC). Non-ionizing radiation, part 2: Radiofrequency electromagnetic fields. (IARC monographs on the evaluation of carcinogenic risks to humans; vol. 102). Lyon, France: International Agency for Research on Cancer; 2013. https://publications.iarc.fr/126

15. Wyde ME, Horn TL, Capstick MH, Ladbury JM, Koepke G, Wilson PF, Kissling GE, Stout MD, Kuster N, Melnick RL, et al. Effect of cell phone radiofrequency radiation on body temperature in rodents: Pilot studies of the National Toxicology Program's reverberation chamber exposure system. Bioelectromagnetics. 2018; 39(3):190-199. https://doi.org/10.1002/bem.22116

16. Smith-Roe SL, Wyde ME, Stout MD, Winters JW, Hobbs CA, Shepard KG, Green AS, Kissling GE, Shockley KR, Tice RR, et al. Evaluation of the genotoxicity of cell phone radiofrequency radiation in male and female rats and mice following subchronic exposure. Environ Mol Mutagen. 2020; 61(2):276-290. https://doi.org/10.1002/em.22343

17. Capstick MH, Kuehn S, Berdinas-Torres V, Gong Y, Wilson P, Ladbury JM, Koepke G, McCormick DL, Gauger J, Melnick RL, et al. A radio frequency radiation exposure system for rodents based on reverberation chambers. IEEE Trans Electromagn Compat. 2017; 59(4):1041-1052. https://doi.org/10.1109/temc.2017.2649885

18. Gong Y, Capstick MH, Kuehn S, Wilson PF, Ladbury JM, Koepke G, McCormick DL, Melnick RL, Kuster N. Life-time dosimetric assessment for mice and rats exposed in reverberation chambers of the 2-year NTP cancer bioassay study on cell phone radiation. IEEE Trans Electromagn Compat. 2017; 59(6):1798-1808. https://doi.org/10.1109/temc.2017.2665039

19. Holman JP. Heat transfer. 7th ed. New York, NY: McGraw-Hill; 1990.

20. Dunnett CW. A multiple comparison procedure for comparing several treatments with a control. J Am Stat Assoc. 1955; 50(272):1096-1121. https://doi.org/10.1080/01621459.1955.10501294

21. Williams DA. A test for differences between treatment means when several dose levels are compared with a zero dose control. Biometrics. 1971; 27(1):103-117. https://doi.org/10.2307/2528930

22. Williams DA. The comparison of several dose levels with a zero dose control. Biometrics. 1972; 28(2):519-531. https://doi.org/10.2307/2556164

23. Jonckheere AR. A distribution-free k-sample test against ordered alternatives. Biometrika. 1954; 41(1-2):133-145. https://doi.org/10.1093/biomet/41.1-2.133

24. Dixon WJ, Massey FJ. Introduction to statistical analysis. 2nd ed. New York, NY: McGraw-Hill; 1957.

25. U.S. Food and Drug Administration (FDA). 21 CFR Part 58. https://www.ecfr.gov/current/title-21/chapter-I/subchapter-A/part-58

26. Miller JA, Miller EC. Ultimate chemical carcinogens as reactive mutagenic electrophiles. In: Hiatt HH, Watson JD, Winsten JA, editors. Origins of Human Cancer. Cold Spring Harbor, NY: Cold Spring Harbor Laboratory; 1977. p. 605-627.

27. Crawford BD. Perspectives on the somatic mutation model of carcinogenesis. In: Flamm WG, Lorentzen RJ, editors. Mechanisms and Toxicity of Chemical Carcinogens and Mutagens. Princeton, NJ: Princeton Scientific Publishing; 1985. p. 13-59.

28. Straus DS. Somatic mutation, cellular differentiation, and cancer causation. J Natl Cancer Inst. 1981; 67(2):233-241. https://doi.org/10.1093/jnci/67.2.233

29. Organisation for Economic Co-operation and Development (OECD). Test no. 489: In vivo mammalian alkaline comet assay. OECD guideline for the testing of chemicals. Paris, France: OECD Publishing; 2014. https://doi.org/10.1787/9789264224179-en

30. Brendler-Schwaab S, Hartmann A, Pfuhler S, Speit G. The in vivo comet assay: Use and status in genotoxicity testing. Mutagenesis. 2005; 20(4):245-254. https://doi.org/10.1093/mutage/gei033

31. Burlinson B, Tice RR, Speit G, Agurell E, Brendler-Schwaab SY, Collins AR, Escobar P, Honma M, Kumaravel TS, Nakajima M, et al. Fourth International Workgroup on Genotoxicity Testing: Results of the in vivo comet assay workgroup. Mutat Res. 2007; 627(1):31-35. https://doi.org/10.1016/j.mrgentox.2006.08.011

32. Collins AR. The comet assay for DNA damage and repair: Principles, applications, and limitations. Mol Biotechnol. 2004; 26(3):249-261. https://doi.org/10.1385/mb:26:3:249

33. Tice RR, Agurell E, Anderson D, Burlinson B, Hartmann A, Kobayashi H, Miyamae Y, Rojas E, Ryu JC, Sasaki YF. Single cell gel/comet assay: Guidelines for in vitro and in vivo genetic toxicology testing. Environ Mol Mutagen. 2000; 35(3):206-221. https://doi.org/10.1002/(sici)1098-2280(2000)35:3<206::aid-em8>3.0.co;2-j

34. Hartmann A, Agurell E, Beevers C, Brendler-Schwaab S, Burlinson B, Clay P, Collins A, Smith A, Speit G, Thybaud V, et al. Recommendations for conducting the in vivo alkaline comet assay. Mutagenesis. 2003; 18(1):45-51. https://doi.org/10.1093/mutage/18.1.45

35. Pfuhler S, Wolf HU. Detection of DNA-crosslinking agents with the alkaline comet assay. Environ Mol Mutagen. 1996; 27(3):196-201. https://doi.org/10.1002/(SICI)1098-2280(1996)27:3<196::AID-EM4>3.0.CO;2-D

36. National Toxicology Program (NTP). Chemical Effects in Biological Systems (CEBS) data repository: Development and testing of a novel whole-body exposure system for investigative

studies of radiofrequency radiation in rodents. Research Triangle Park, NC: U.S. Department of Health and Human Services, Public Health Service, National Institute of Environmental Health Sciences, National Toxicology Program; 2025. https://doi.org/10.22427/NIEHS-DATA-NIEHS-RFRA

37. Bosquillon de Jenlis A, Del Vecchio F, Delanaud S, Bach V, Pelletier A. Effects of co-exposure to 900 MHz radiofrequency electromagnetic fields and high-level noise on sleep, weight, and food intake parameters in juvenile rats. Environ Pollut. 2020; 256:113461. https://doi.org/10.1016/j.envpol.2019.113461

38. Broom KA, Findlay R, Addison DS, Goiceanu C, Sienkiewicz Z. Early-life exposure to pulsed LTE radiofrequency fields causes persistent changes in activity and behavior in C57BL/6 J mice. Bioelectromagnetics. 2019; 40(7):498-511. https://doi.org/10.1002/bem.22217

39. Spandole-Dinu S, Catrina AM, Voinea OC, Andone A, Radu S, Haidoiu C, Călborean O, Popescu DM, Suhăianu V, Baltag O, et al. Pilot study of the long-term effects of radiofrequency electromagnetic radiation exposure on the mouse brain. Int J Environ Res Public Health. 2023; 20(4):3025. https://doi.org/10.3390/ijerph20043025

40. Ruediger HW. Genotoxic effects of radiofrequency electromagnetic fields. Pathophysiology. 2009; 16(2-3):89-102. https://doi.org/10.1016/j.pathophys.2008.11.004

41. Verschaeve L, Juutilainen J, Lagroye I, Miyakoshi J, Saunders R, de Seze R, Tenforde T, van Rongen E, Veyret B, Xu Z. In vitro and in vivo genotoxicity of radiofrequency fields. Mutat Res. 2010; 705(3):252-268. https://doi.org/10.1016/j.mrrev.2010.10.001

42. Hill DA. Electromagnetic theory of reverberation chambers. Gaithersburg, MD: U.S. Department of Commerce, Technology Administration, National Institute of Standards and Technology; 1998. NIST Technical Note 1506. https://purl.fdlp.gov/GPO/gpo103869

43. Ladbury J, Koepke G, Camell D. Evaluation of the NASA Langley Research Center mode-stirred chamber facility. Gaithersburg, MD: U.S. Department of Commerce, National Institute of Standards and Technology; 1999. NIST Technical Note 1508. https://nvlpubs.nist.gov/nistpubs/Legacy/TN/nbstechnicalnote1508.pdf

44. ITU Radiocommunication Study Groups. Annex 1: Unwanted emission characteristics for IMT-2000 CDMA direct spread radio interface. In: Generic Unwanted Emission Characteristics Associated with the Terrestrial Radio Interfaces of IMT-2000, Revision 1. Geneva, Switzerland: International Telecommunication Union; 1999. 8-1/TEMP/271(Rev.1)-E. https://www.3gpp.org/ftp/tsg_ran/tsg_ran/TSGR_06/Docs/Pdfs/RP-99828.pdf

45. European Telecommunications Standards Institute (ETSI). GSM Technical Specification: Digital cellular telecommunications system (Phase 2+); radio transmission and reception. Sophia Antipolis, France: European Telecommunications Standards Institute; 1996. GSM 05.05 Version 5.1.0: May 1996. https://www.etsi.org/deliver/etsi_gts/05/0505/05.01.00_60/gsmts_0505v050100p.pdf

46. U.S. Food and Drug Administration (FDA). 21 CFR Part 11. https://www.ecfr.gov/current/title-21/chapter-I/subchapter-A/part-11

47. Dunn OJ. Multiple comparisons using rank sums. Technometrics. 1964; 6(3):241-252. https://doi.org/10.1080/00401706.1964.10490181

Appendix A. Chamber Design, Exposure Generation, and Monitoring

Table of Contents

Tables

Figures

A.1. Introduction

This appendix describes the chambers and control system for the whole-body radiofrequency radiation (RFR) exposure studies. The health and safety features of the system are introduced, along with descriptions of the reverberation chambers, RFR generation and monitoring systems, Global System for Mobile Communications (GSM) and Code Division Multiple Access (CDMA) signal generation, and maintenance of the environmental conditions. This appendix also includes documentation to demonstrate that the chambers function as required with regard to both exposure (including field uniformity) and environmental parameters.

Signal generation and chamber characterization activities were performed by the Foundation for Research on Information Technologies in Society (IT'IS Foundation) at its laboratories in Zürich, Switzerland. Dosimetry was performed in the completed system on phantom (i.e., animal surrogate) rats and mice to determine the influence of the implanted temperature sensors and water system.

A.2. System Overview

The rodent electromagnetic field exposure system was based on reverberation chambers and included an automatic control system with exposure and environmental condition monitoring and logging. Each reverberation chamber (Figure A-1) was a resonant box in which the resonances and field structure were continuously modified under the influence of metallic stirrers, while shielding the outside environment from the fields inside and vice versa. The system comprised four reverberation chambers: one high specific absorption rate (SAR), one medium SAR, one low SAR, and one with no RFR exposure (i.e., the chamber control). The computer-controlled system consisted of a radiofrequency (RF) source, amplifiers, and data acquisition components. The chambers were equipped with sensors to monitor the exposure and environmental conditions; the computer control system both monitored and recorded the conditions and controlled exposure using these sensors.

An RF signal generator produced the modulated signals representative of mobile communication signals compliant with the desired standards. In these studies, either GSM or Interim Standard 95 (IS-95; i.e., CDMA) signals were used. The output of the signal generator was split three ways and the level in each of the three paths was individually controlled before being amplified to the desired level and radiated into the desired chamber via antennas, with one antenna for each amplifier. Each chamber had two mode stirrers (rotating metallic structures) that scattered the field, producing a continuously variable field structure within the chamber that when averaged over time was homogeneous and isotropic over the volume within which the rodents were housed.

The electromagnetic field level in each chamber was monitored using two isotropic electric field (E-field) probes based on the measured level, and deviation from the target exposure level could be corrected by increasing or decreasing the power delivered to each chamber.

Figure A-1. Internal View of a Reverberation Chamber

A.3. Chamber Design

Each reverberation chamber was designed to house 10 cages with one animal per cage in Thoren #7 cages with a cage floor area of 474 cm^2. Based on the homogeneity results of previous analyses that modeled the SAR distribution of RFR across the whole body, rats were exposed at a frequency of 900 MHz, and mice were exposed at 1,900 MHz. Each chamber contained two mode stirrers, one horizontal on the ceiling and one vertical on the rear wall; the stirred volume was 0.29 m^3 and the chamber volume was 2.31 m^3, corresponding to 12.5% stirred volume. The doors in two of the chambers were hinged on the right and two were hinged on the left to aid easy access when installed in the exposure room.

The fully welded construction of the chambers ensured no RF leakage from the seams. Internal and external components were shipped separately and were installed onsite so as to:

- Minimize the possibility of damage during transport

- Reduce the external dimensions of the shipping containers to facilitate transport through the hallways at the testing facility from the loading dock to the exposure room

External views of the chamber are depicted in Figure A-2. The features of the chamber design are shown and described in detail in the following sections.

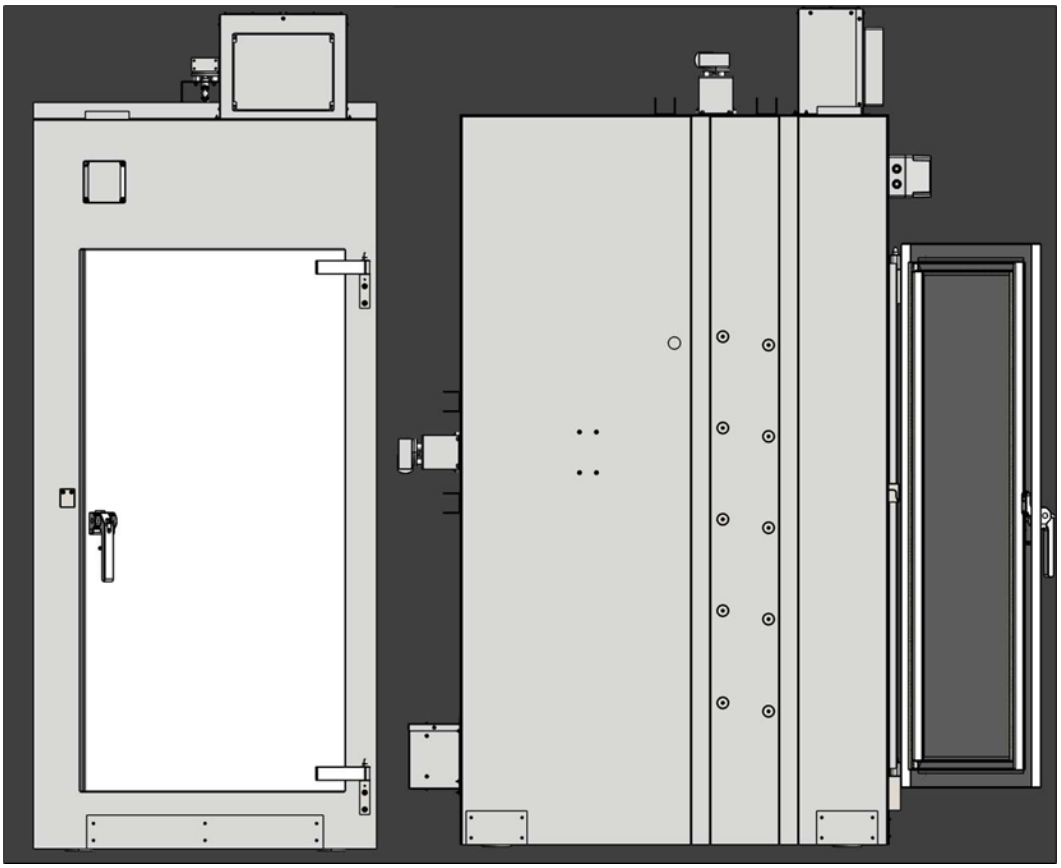

Figure A-2. Front (Left) and Side (Right) Views of the Chamber Designed for the Investigative Studies

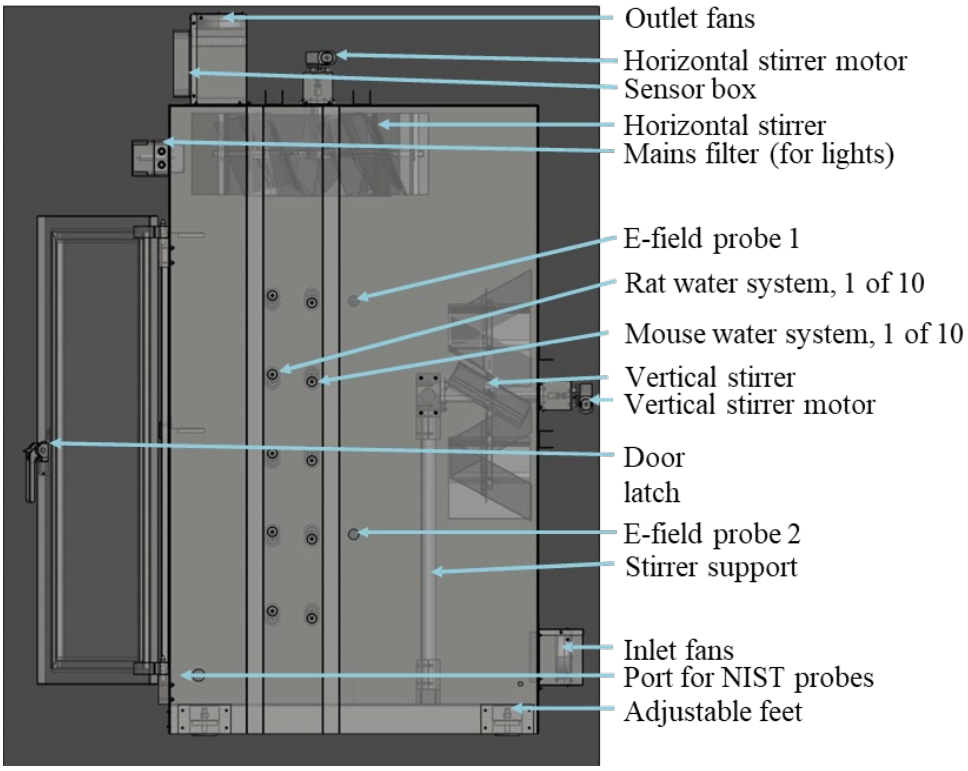

Figure A-3. Detailed Features of the Chamber Design (Side View)

NIST = National Institute of Standards and Technology.

A.3.1. Undercarriage Features

The underside of the chamber (Figure A-4) was designed with integrated U-shaped channels to allow a trolley jack to be slotted in from the front. The channels, which allow the unit to be transported through the facility to the exposure room upon arrival, could be revealed by the removal of a decorative panel that was reinstalled after final positioning in the exposure room. Integrated into the four corners were large adjustable feet that could be used to level the chamber at its final resting position. The feet were accessed for adjustment by removing small side panels. These panels were designed to ensure that any animal that managed to escape could not hide under the chamber.

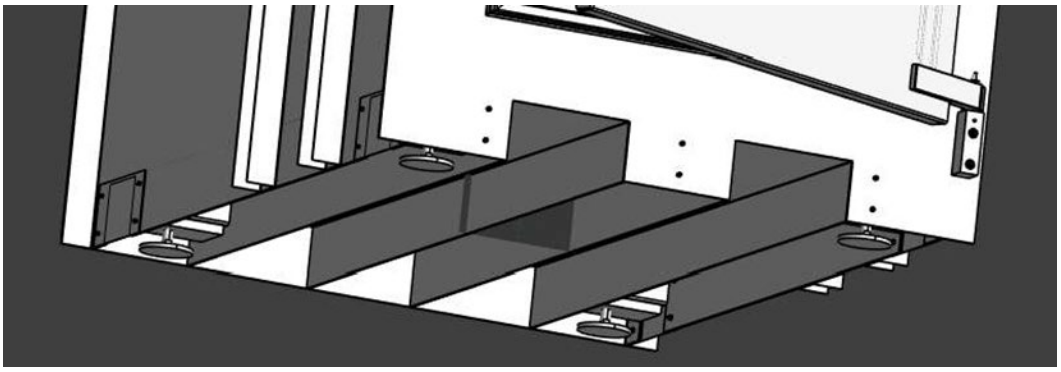

Figure A-4. View of the Underside of the Chamber Showing the Four Adjustable Feet and the Slots to Allow a Trolley Jack to Be Used for Transport

A.3.2. Stirrers

The stirrers were designed to have large reflecting surfaces, whereby the angles between the surfaces and angles of rotation with respect to the main axis ensured no radial symmetry (Figure A-5). The mode stirrers were designed like fans, rotating about their axes, but the stirrers reflected electromagnetic fields instead of moving air around with "blades." By avoiding symmetry, the scattered fields could have higher complexity (Figure A-6) and excite more modes within the chamber volume. The stirrer had six radial elements, each of which was inserted into a hub and held in position with set screws, which allowed individual elements to be removed and replaced.

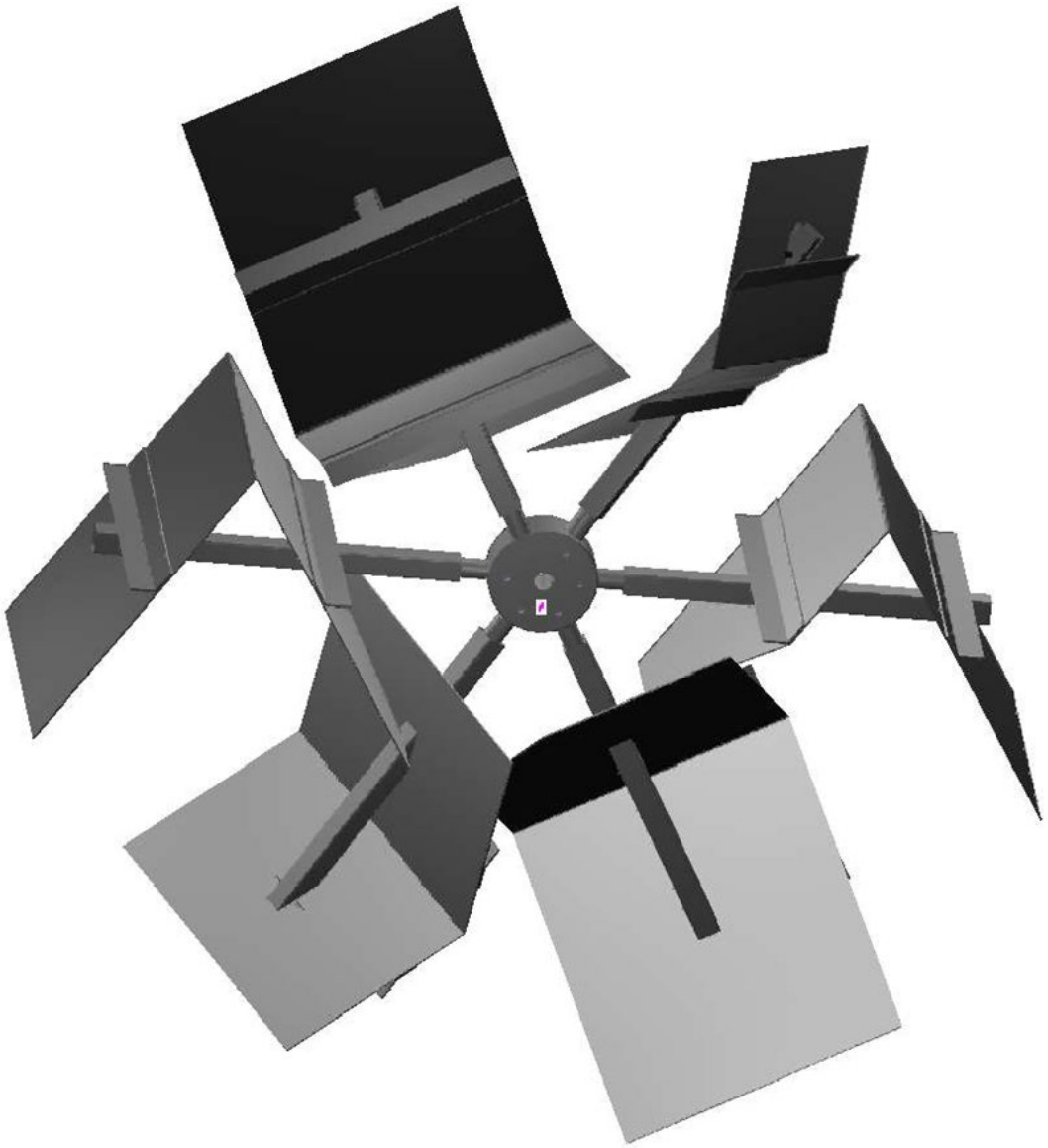

Figure A-5. Mode Stirrer, Designed with No Symmetry about the Rotational Axis

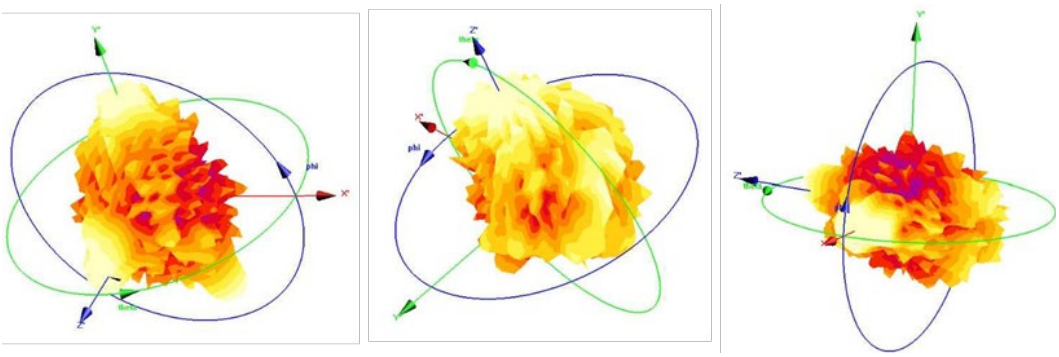

Figure A-6. Typical Scattered Fields for Different Stirrer Angles (the Lighter the Color, the Higher the Amplitude of the Scattered Field at That Angle)

Each stirrer was driven by a maxon servo motor connected via a 90:1 worm gear. The motor and gear box were mounted by means of rubber isolating mounts that allow some movement and decrease transmitted vibrations. The gear was connected to the stirrer drive shaft via a universal joint that can correct for slight misalignments without causing excessive force or wear. The drive shaft, which was fabricated from a glass-fiber composite, passed through a tube that was sufficiently long and small in radius to provide excellent isolation (Figure A-7). The weight of the stirrers was supported, in the case of the horizontal stirrer, by a conical thrust bearing and, in the case of the vertical stirrer, by two ball bearings. The second bearing was supported by a fiberglass support inside the chamber in front of the stirrer.

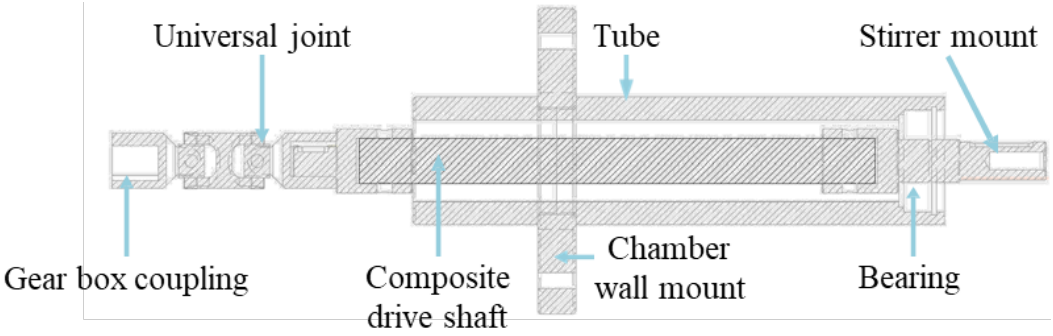

Figure A-7. Stirrer Drive Shaft and Bearing

While reviewing videos captured during exposure (see Section 4.2.3.5) it was noted that the stirrer on the back wall of the control chamber (Chamber 4) did not move throughout the four experiments. It is hypothesized that at an unidentified point in time after chamber characterization and before the start of the mouse experiment, the coupling between the motor and the stirrer came loose. As the stirrers were stopped during the animal care and observation periods for safety reasons, the issue was not identified by staff. Furthermore, while a problem with the motor or controller would have been detected by the control software, a mechanical issue like that hypothesized here would not have been detected.

A.3.3. Airflow and Vents

The temperature and humidity in the chambers were not individually controlled but relied on the control of and sufficient throughput of air from the exposure room. Air was blown into the chamber and extracted from the chamber by means of speed-controlled fans. The fans were

chosen to ensure that higher-than-required airflows could be achieved, and the correct number of air changes per hour was obtained by reducing the fan speed as required. Reduction of the fan speed ensured the noise was kept to a minimum. The walls of the chamber had two integrated honeycomb vents (Figure A-8): one located at the rear left and the other at the top front right (Figure A-3). The attenuation of the RF by the honeycomb vent is summarized in Table A-1.

Figure A-9 shows the details of the inlet and outlet manifolds. The inlet manifold had an air filter consisting of a coarse mesh material in front of the Sanyo Denki (Tokyo, Japan) fans, followed by the honeycomb vent, which prevented the RF from propagating out of the chamber.

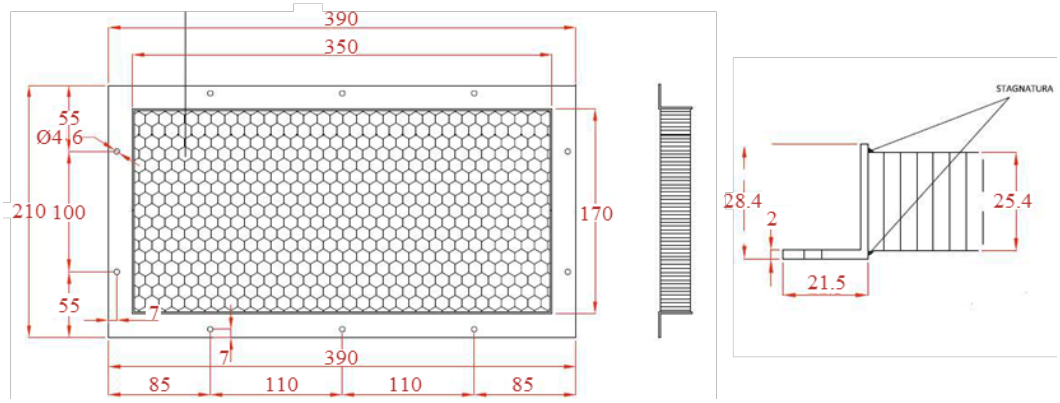

Figure A-8. Dimensions of the Air Vent (mm)

Table A-1. Attenuation of the Radiofrequency Provided by the Air Vents

Frequency	Field	Shielding dB[a]
0.4 GHz	Plane wave	130
1 GHz	Plane wave	120
10 GHz	Plane wave	120

[a]Shielding effectiveness for stainless-steel honeycomb with 3/16-inch hexagonal cell size and 1-inch length.

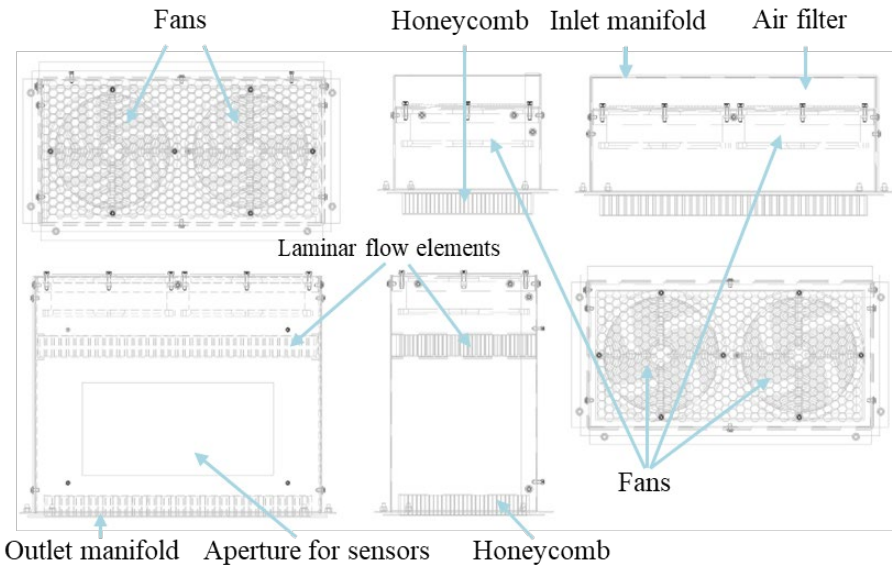

Figure A-9. Structure and Components of Inlet Manifold (Top) and Outlet Manifold (Bottom)

The length of the outlet manifold was larger than that of the inlet to accommodate the environmental sensors. Air passed through the honeycomb air vent at the outlet; the sensor box was attached to the manifold, with sensors projecting into the airflow to measure temperature, humidity, airflow, light, and noise. The airflow sensor could make reliable readings only when in a laminar flow region. If the fans were mounted directly at the outlet, the airflow would be more turbulent; hence a laminar flow element was placed in front of the fans to maintain a relatively straight flow of air between the honeycomb and laminar flow element.

A.3.4. Mains Filter

Power was required within the chamber for the lighting. Power and any other electrical connections must be either fully shielded or filtered, and the power must pass through a filter with suitable attenuation characteristics. The mains filters (Schaffner, Luterbach, Switzerland) were inserted into the chamber wall with a plastic box for protection on the outside and a stainless-steel box on the inside of the chamber (Figure A-10). Attenuation characteristics for the installed filter (FN7612-10-M3) are available from the manufacturer.

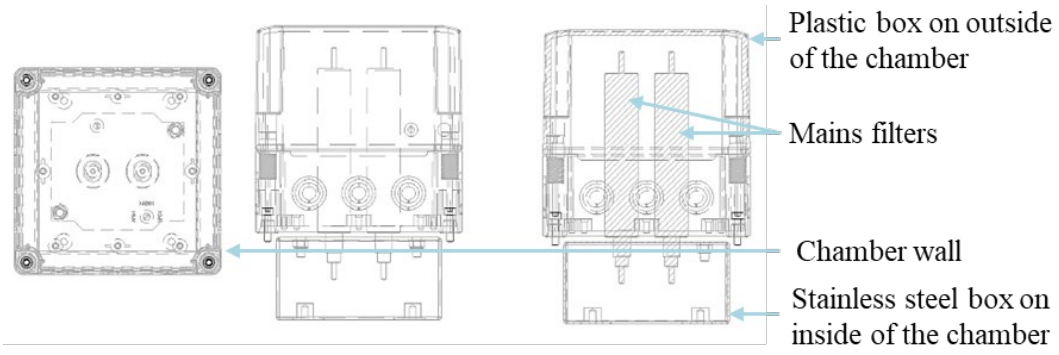

Figure A-10. Mains Filter Installation

A.3.5. Lighting

The original intention was to install only flat light emitting diode (LED) lighting panels inside the door of the chamber for direct illumination of the cages. However, after review and discussion, the decision was made to install additional incandescent lighting. A review of available fixtures revealed that the industry has largely progressed to the use of low energy lighting, with a far more limited selection of incandescent fixtures. Especially given the available amount of space in the chambers, few options were available. Two light fixtures were required to achieve the required light levels in the animal cages; rough-service 60 W incandescent bulbs, with a color temperature of 2,700 K and light output of 480 Lumens each, should provide sufficient light. These bulbs nominally have long lifetimes of 20,000 hours, whereas the lifetime of a standard incandescent bulb is typically 2,500 hours. As the efficiency of these bulbs is <5%, approximately 115 W of heat would have been expected to be generated per chamber. Ultimately, halogen-based incandescent bulbs were utilized, improving the efficiency and reducing the heat dissipation without degrading the lifetime of the bulbs. The halogen incandescent bulbs used in this study were very similar to those used in the previous NTP studies and reduced energy consumption by one-quarter to one-third compared to standard incandescent light bulbs. For the mouse study, halogen light bulbs (Philips, Model Number 458018) were used, and for the rat studies, halogen light bulbs (GE, Model Number 70335) were used. Both types of halogen light bulbs were 53 W, with an A19 bulb shape and 120 V. Figure A-11 shows the angled bulkhead light fixture.

Figure A-11. Angled Bulkhead Fixture

The incandescent light fixtures were placed in the rear of the chamber, in front of the stirrers to avoid modulation of the light level as the stirrers rotate. This location was the only location able to accommodate the two 10-inch × 6.13-inch fixtures. The two fixtures were placed on opposite sides of the chamber, with one on the rear right side and another on the rear left side, to provide even illumination; Figure A-12 shows the approximate locations of the two fixtures.

LED corner panels, 1.2 m in length, were installed in both front corners of the chamber. Figure A-13 shows the profile and the frosted diffuser used with these elements, which have a rated power of approximately 25 W. The efficiency of the LEDs was approximately 10-fold higher than that of incandescent lights, and the significantly higher light output allowed the LED lighting to be used as inspection lighting. The LEDs were operated on 24 V DC delivered by a small power supply installed inside the internal electrical filter box. A switch on the box allowed toggling between LED and incandescent lighting in each chamber.

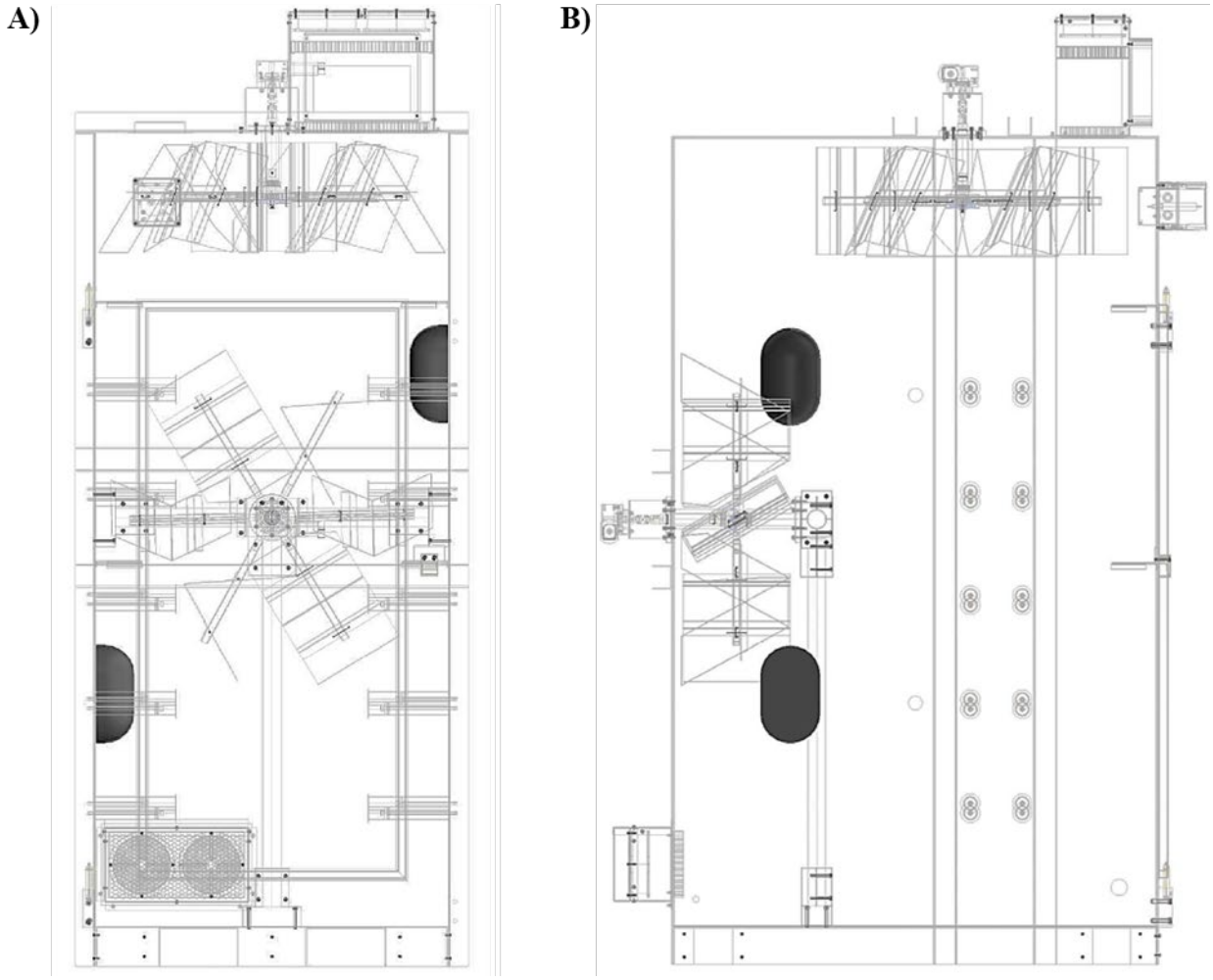

Figure A-12. Locations of Two Angled Bulkhead Light Fixtures

The two angled bulkhead light fixtures are depicted as black ovals. Light fixtures were placed at the rear of the chamber in front of the stirrers. Panel (A) shows the chamber from the front view. Panel (B) shows the chamber from the side view.

A)

B)

Figure A-13. (A) Light Emitting Diode Corner Profile and (B) Typical Waterproof Lighting Strip

A.3.6. Water System

Two individual water systems were installed, one for use at 900 MHz and the other for use at 1,900 MHz. The water system used during any exposure was dependent on the animal cage chosen. Half of the cages had grommets positioned correctly for operation at 900 MHz for use with rats; the remaining cages had grommets that allowed access to the 1,900 MHz water system for mice. See Section A.11 for more details of the performance.

A.3.7. National Institute of Standards and Technology Probes

A port was provided on the lower right-hand side of each chamber to allow the electromagnetics expert of the National Institute of Standards and Technology (NIST) to insert probes for verification procedures. Figure A-14 shows such a waveguide port (WGF-12) before installation.

Figure A-14. Waveguide Port for Probes and Optical Fibers

A.3.8. Chamber Door

A twin finger stock approach was used to achieve the required shielding effectiveness for the door. A rectangular cross section was welded onto the front panel around the location of the door opening, with a U-shaped section on the door itself and finger stock on both inner and outer surfaces (Figure A-15).

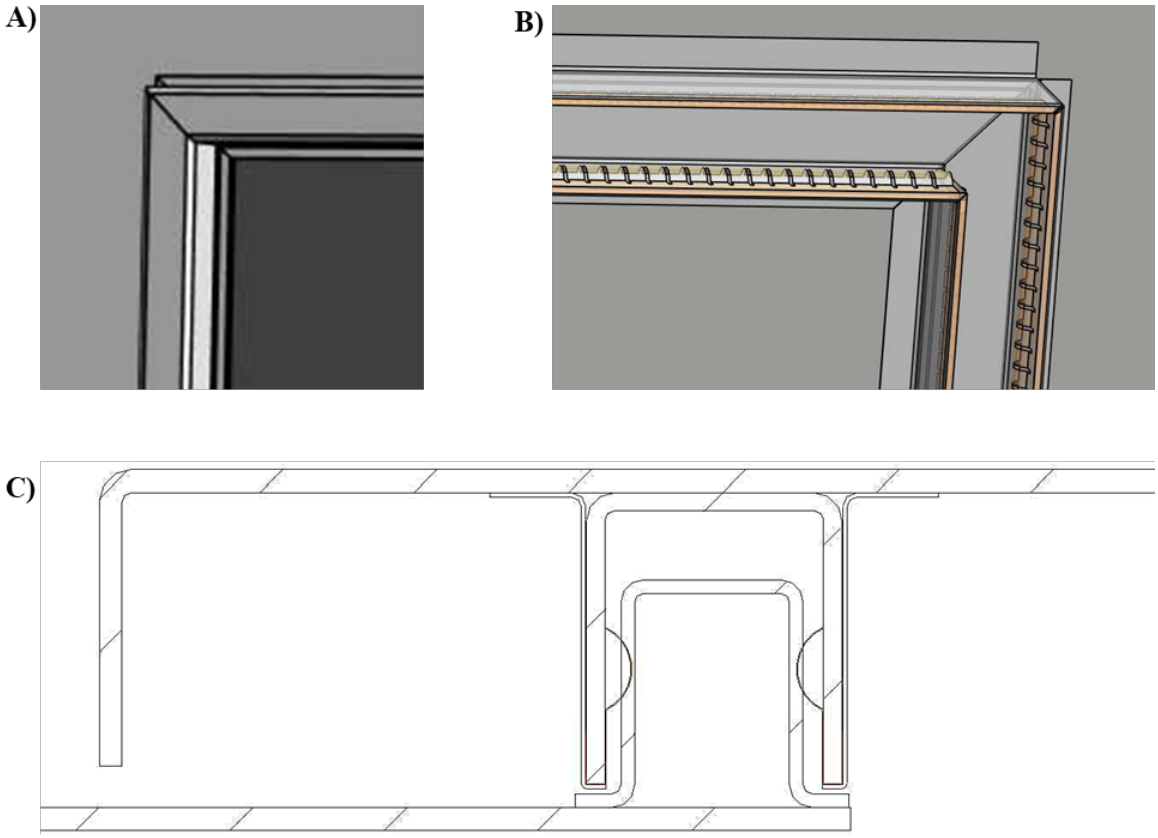

Figure A-15. Frame Around Chamber Opening and Finger Stock Gasket Installed on the Door

Panel (A) shows the frame around the chamber opening. Panel (B) shows the finger stock gasket installed on the door. Panel (C) shows a cross-sectional view from above of the relative positions when closed, with the frame of the chamber opening shown at the bottom of the image and the door shown at the top.

Figure A-15 also shows the relative positioning of the door and the fixed frame. Figure A-16 shows the door on the chamber in partially open and closed configurations. The hinges were placed 125 mm away from the closest finger stock gasket, so that the finger stock gasket engaged with the mating frame around the door, allowing it to close with a more linear rather than rotational motion. A latch was used to secure the door in the closed configuration. Triangular strengthening members were placed inside the chamber corners to provide rigidity in proximity to the hinges and the latch.

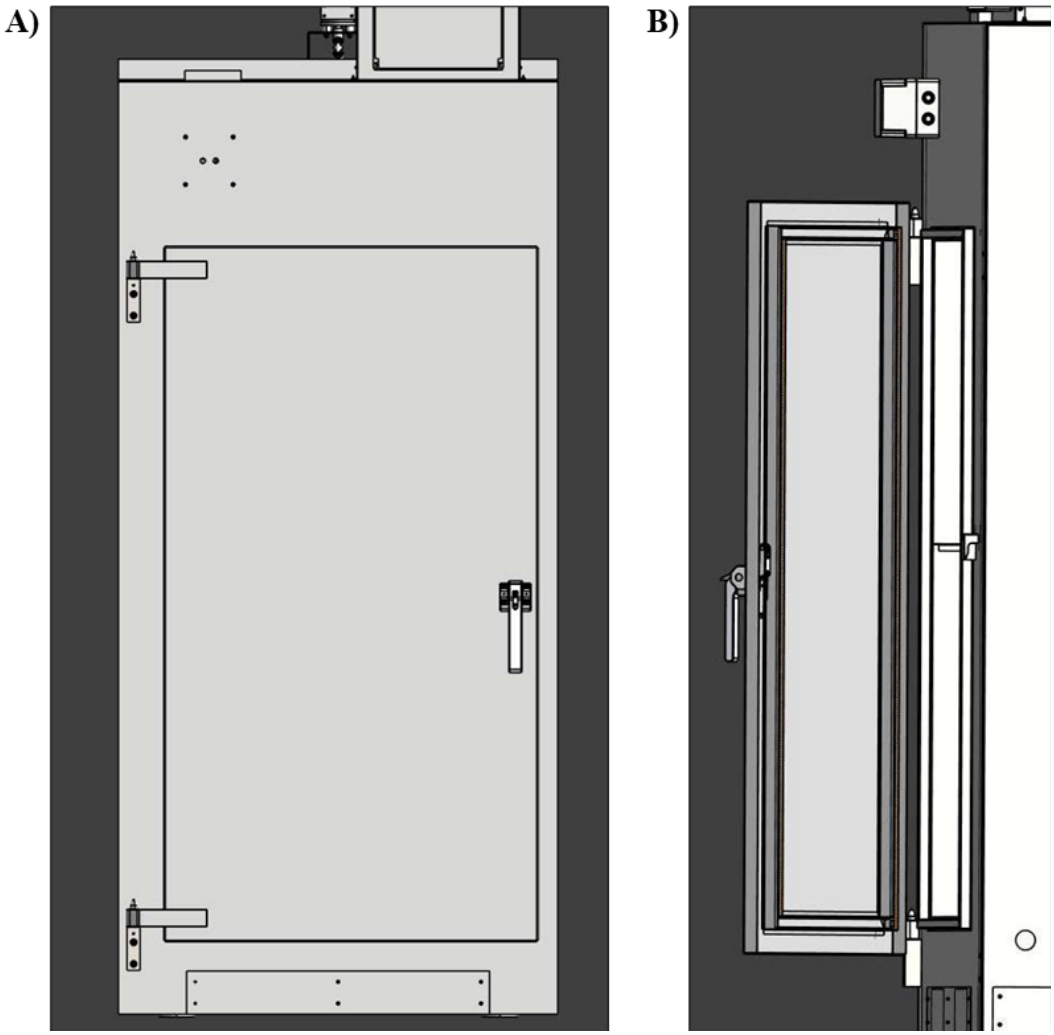

Figure A-16. Door Installed on the Chamber

Panel (A) shows the front view with the door closed. Panel (B) shows the side view with the door open.

A.3.9. Chamber Strengthening

The final chamber design is shown in Figure A-17; the left image shows the view from the front without the front panel and door, and the cut-away on the right shows the internal features. Rigidity was provided by the side panels and the base through the bending of the panels around the periphery. However, certain features of the chamber required that the panels remained flat to ensure the connected parts were positioned in orthogonal orientations. To this end, additional U-shaped bracing was added to the external surfaces on either side of the vertical and horizontal stirrers as well as the water system to prevent buckling or rippling of the panels caused by the welding process.

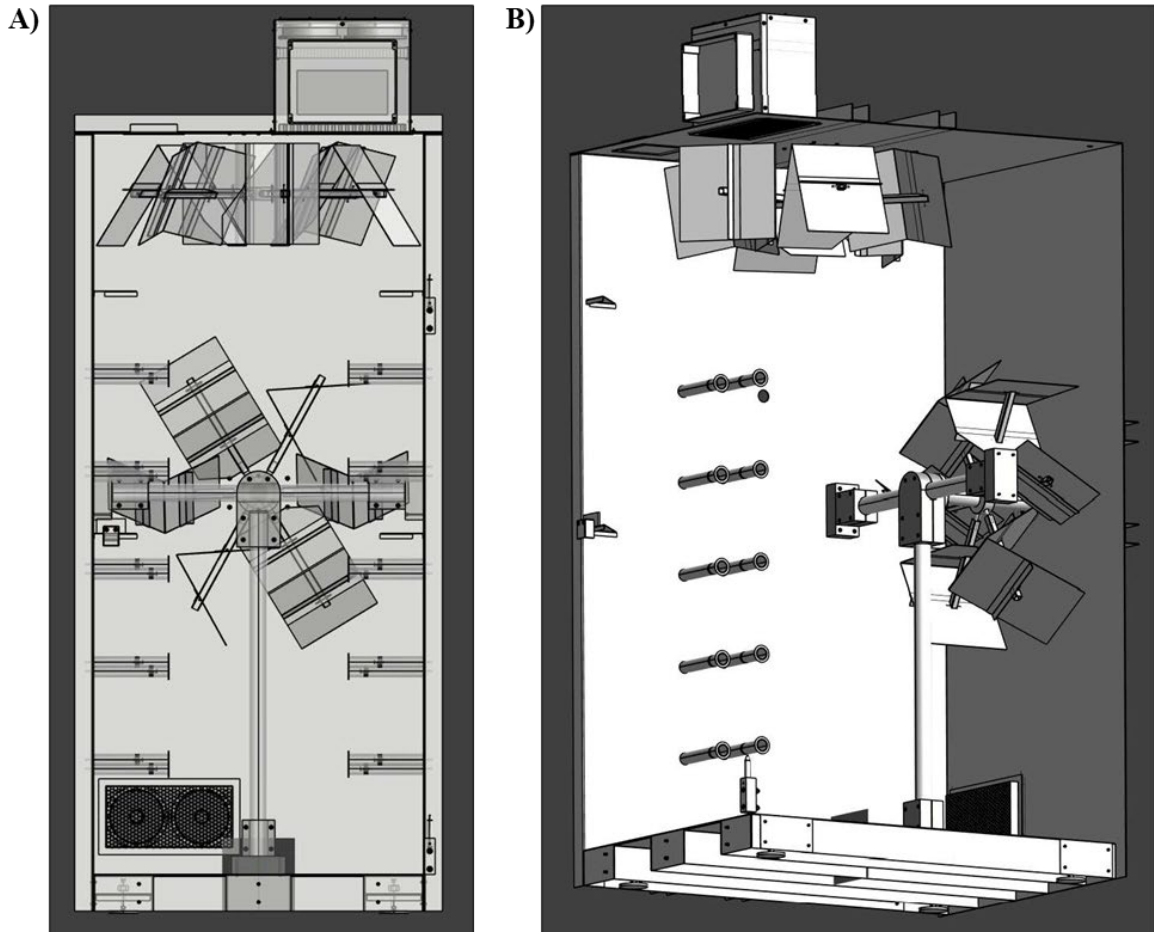

Figure A-17. Views of the Complete Chamber Including the Internal Features

Panel (A) shows the front view of the complete chamber with the front removed. Panel (B) shows the internal features of the chamber with the front wall and one side wall removed.

At connection points on the side of the chambers (i.e., to the field probes or antennas), stainless-steel cable trunking was used to protect cables and connections from damage.

A.3.10. Caging and Cage Racks

Both rats and mice were housed in the chambers in #7 single rat-size cages from Thoren with dimensions of 308 × 222 × 222 mm (L × W × H) and a cage floor area of 474 cm^2. The lixit openings were at 82.5 mm and 57.5 mm above the bottoms of the cages for rats and mice, respectively. The cage grommets were ceramic.

The cage rack was mounted internally to the chamber walls, and each cage could be removed for cleaning. The cages with lids slid into the cage racks to a depth set by adjustable stops, ensuring that the cage grommet and lixit were aligned. Below the lixits and above the next cage, a U-shaped channel was added to catch water from any leaking lixit and ensure that the cage below did not become flooded.

A.4. Safety Features

The system included many safety features. To alert staff to the state of the system and avoid unwanted shutdowns or breaks in exposure, each chamber was equipped with a set of warning lights, shown in Figure A-18. The state of the system was indicated by the colors red for "exposure in progress," blue for "exposure imminent" or "exposure paused by operator," and green for "the system is idle and the doors can be safely opened" (e.g., for animal care tasks); a flashing blue light indicated that the door needed to be closed.

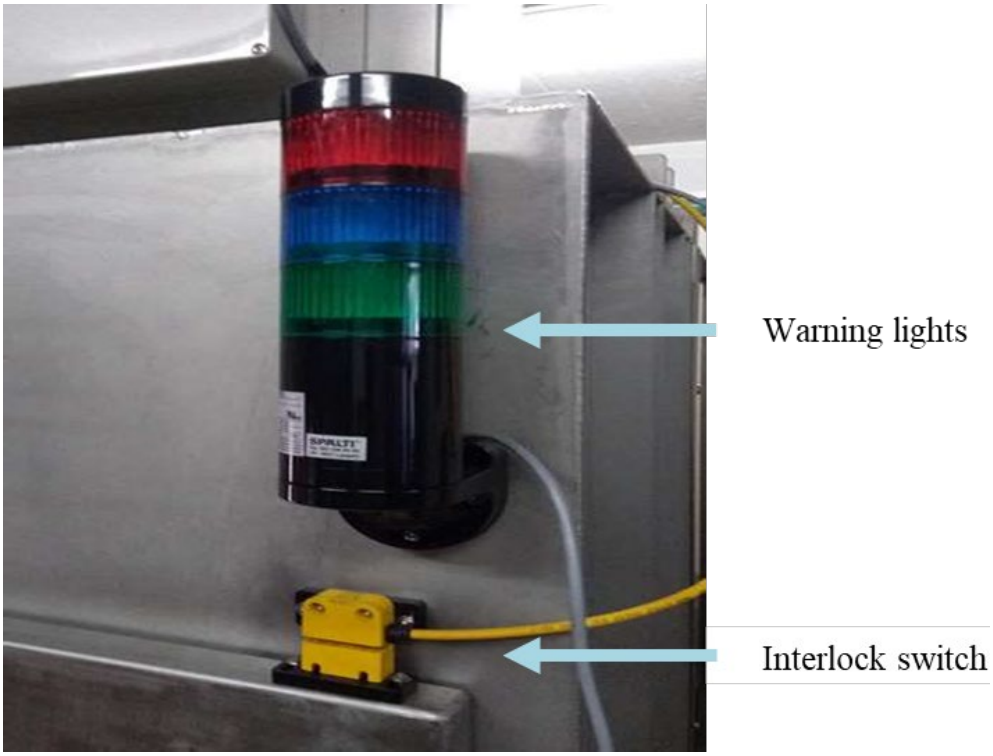

Figure A-18. Warning Lights and Interlock Switch

All amplifiers were linked to interlock switches on all chambers (Figure A-19) so that if a situation arose whereby the warning lights were not or could not be heeded, the switches would place the system in a safe state by turning off the power to the RF amplifiers (e.g., RF generation was stopped when a door was open or was not properly closed after animal care functions). The software would then subsequently turn off all other elements of the RF generation signal chain. The interlock circuitry relied on safety switches from Pilz mounted on each chamber door and Pilz safety relays for control of the power to the amplifiers. Figure A-19 shows the wiring diagram used as well as the available indicators. This circuit was hardwired and therefore did not require any software element for the system to be placed in a safe state. Safety was ensured by the removal of main power to the amplifiers in the event that a door was opened. In addition, emergency stop buttons installed in the exposure room and close to the control and amplifier racks allowed the RF power to be immediately removed from the system. The monitoring software tracked any of the events described above and recorded them in the log file.

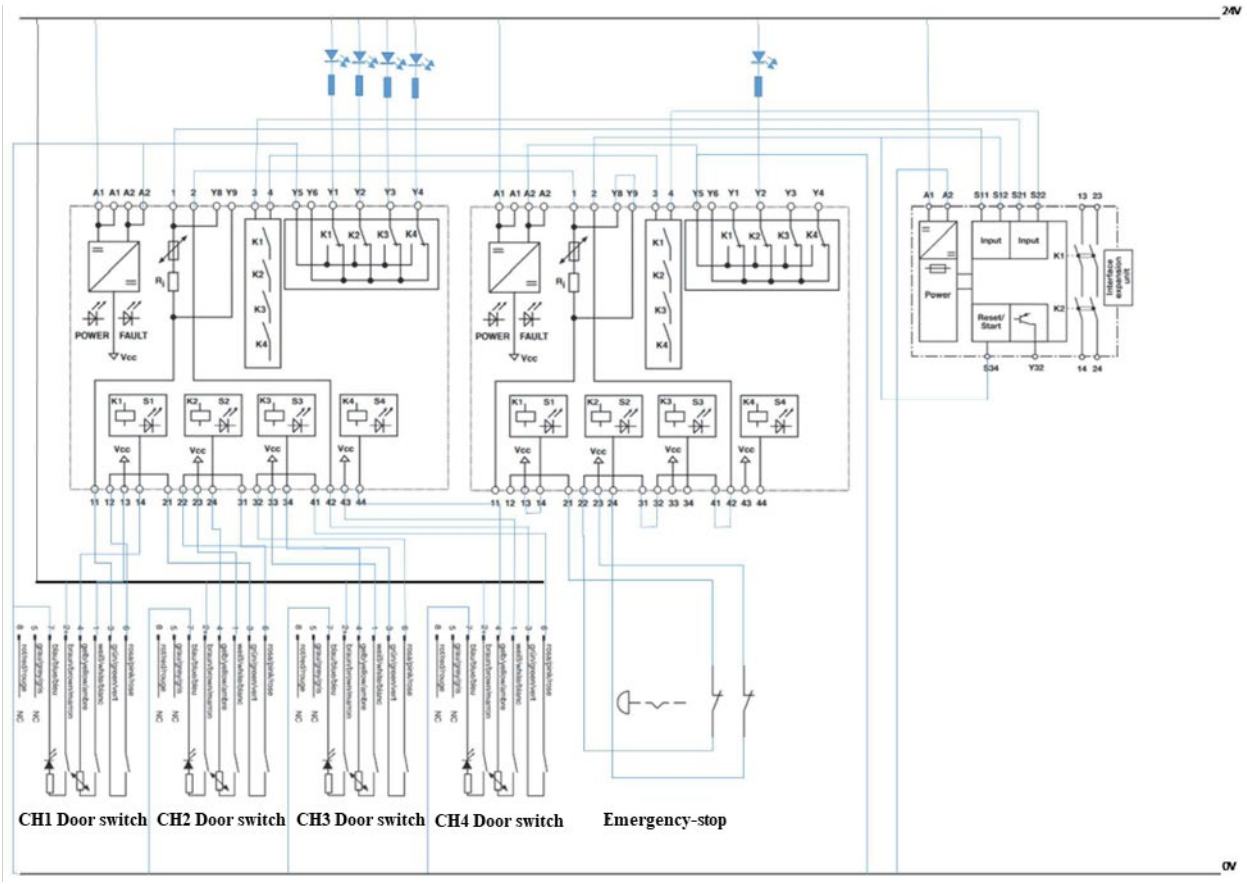

Figure A-19. Safety Interlock System with Pilz Safety Components

A "watchdog" ensured the system was placed in a safe state for the welfare of the animals if the control computer were to lose power or suffer a software crash. The watchdog was a hardware timer that needed to be reset every 20 seconds by the software control program; if this did not happen, the RF power amplifiers were switched off, ensuring the exposure was terminated.

The airflow through the chambers was monitored to ensure sufficient ventilation for the animals, and warnings/alarms were sounded if the flow were to be reduced below the defined minimum.

Other measured environmental parameters were linked to warning and exposure thresholds (e.g., temperature, humidity, and exposure field strength), designed to abort the experiment if the thresholds were exceeded. In particular, if the exposure field exceeded a given threshold above the target exposure level, the exposure would be aborted. The appropriate thresholds were defined at the time of installation.

A.5. Illumination

The illumination was assessed using a Voltcraft BL10L light meter. The light levels were lower for the incandescent halogen bulbs than for the LED lighting; however, both were in line with the required light level needed for animal housing.

A.6. Monitoring System

The monitoring system (Figure A-20) comprised two Four Channel Exposure Acquisition System (EASY4) field measurement devices from Schmid & Partner Engineering (SPEAG), Switzerland. Each EASY4 could monitor up to two chambers with two EF3DV3 electric field (E-field) probes (SPEAG, Switzerland) per chamber, with calibration traceable back to national standards. The use of two E-field probes rather than a single sensor greatly reduced the uncertainty. The probes were attached to custom-made DAEasy4 (SPEAG) data acquisition units, which were in turn connected via optical cables to the EASY4. It was important to measure the E-field for SAR control so that changes in losses (e.g., caused by the bedding becoming wet), did not influence the SAR in the animals. The EASY4 measurement server was connected by ethernet to the control computer. Data acquisition units from Keysight (Santa Rosa, CA) were used to collect all environmental data from the sensors and to control the various functions of the amplifiers and warning lights. The equipment rack is shown in Figure A-21.

The chambers were constructed from stainless steel, which has relatively low permeability and hence does not significantly shield or distort the incident magnetic fields. Therefore, all groups, including the room and chamber control animals, were exposed to similar static and extremely low frequency (ELF) fields. The magnetic fields were not explicitly measured within the context of the RF exposures.

The control computer included a fully featured control program for exposure and environmental monitoring, developed on the basis of IT'IS' extensive experience with the operation of similar systems. The control program generated log files to document the operation of the system and maintained the field strengths in each chamber at the target level according to the most recent weights of the animals and the SAR levels required. The control computer was capable of generating email messages to notify the staff of the status of the system and produced alarms when any given parameter drifted outside predefined limits, stopping exposure when other limits were exceeded.

Software was provided to process the log files to provide daily and monthly reports on the exposures and environmental parameters. In addition, tools to export particular data from the log files to text files (e.g., .csv format), were provided.

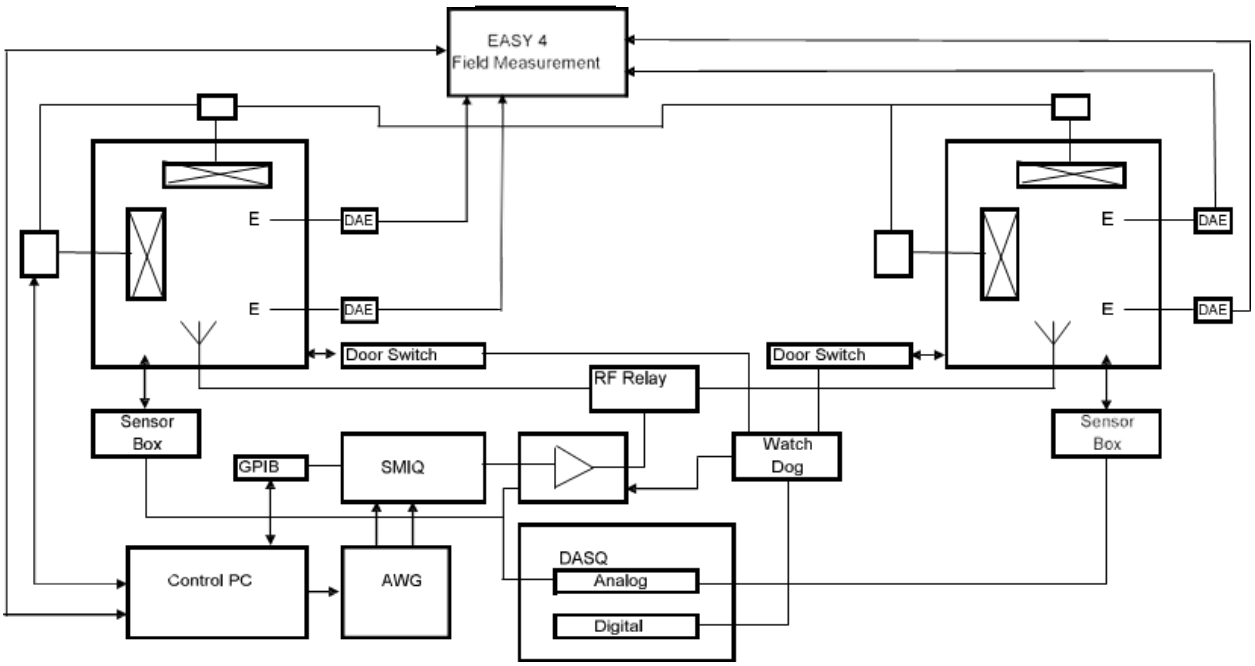

Figure A-20. Example of the Control System (Only Two Chambers Shown)

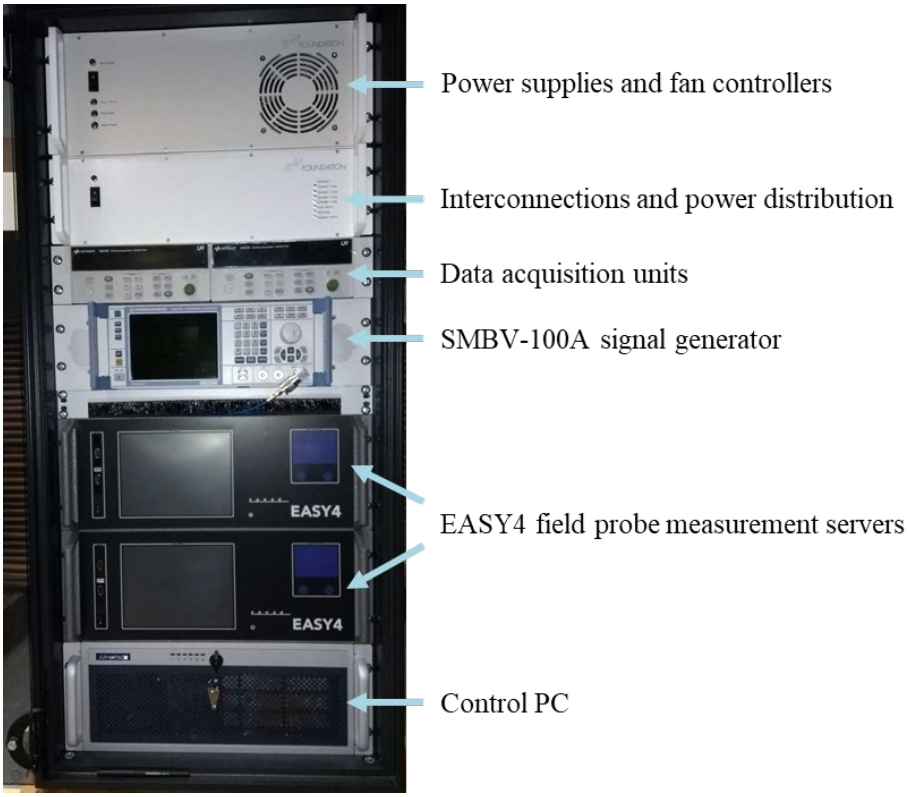

Figure A-21. Equipment Rack Configuration, Dimensions 1,567 × 553 × 600 mm (H × W × D)

A.6.1. Sensors

In the outlet manifold for circulated air, temperature, humidity, noise level, light level, and airflow sensors were included for environmental monitoring. Unless specifically requested otherwise, all sensor data were reported in the International System of Units (SI units).

The noise sensor microphone was housed outside the chamber, connected via a flexible tube to the chamber, to conduct sound out of the high-field environment. Different possible weightings could be applied to the noise measurement; dBA (A-weighted), a common measure, is the weighting used in the previous NTP studies on RFR exposure. For example, A-weighting represents the relative sensitivity of the human ear, whereas Z-weighting gives equal weight to all frequencies. An Audix TM1 microphone was employed for noise measurement, as it has a frequency response that extends to approximately 30 kHz (Figure A-22, Figure A-23), with a modification of A-weighting at low frequencies of up to 2.5 kHz and Z-weighting modified by the microphone frequency response at high-end frequencies. This extended frequency range was used to address questions raised in the public review of the previous NTP studies related to the hearing range of rodents in the range from 400 Hz to 75 kHz for rats and 900 Hz to 79 kHz for mice. The custom noise measurement was based on two metrics: the average noise level and the peak noise level.

The light sensor was fed from a plastic optical fiber, which was also inserted into the chamber. In each chamber, two E-field probes that were calibrated and traceable to national standards were placed close to the exposure volume.

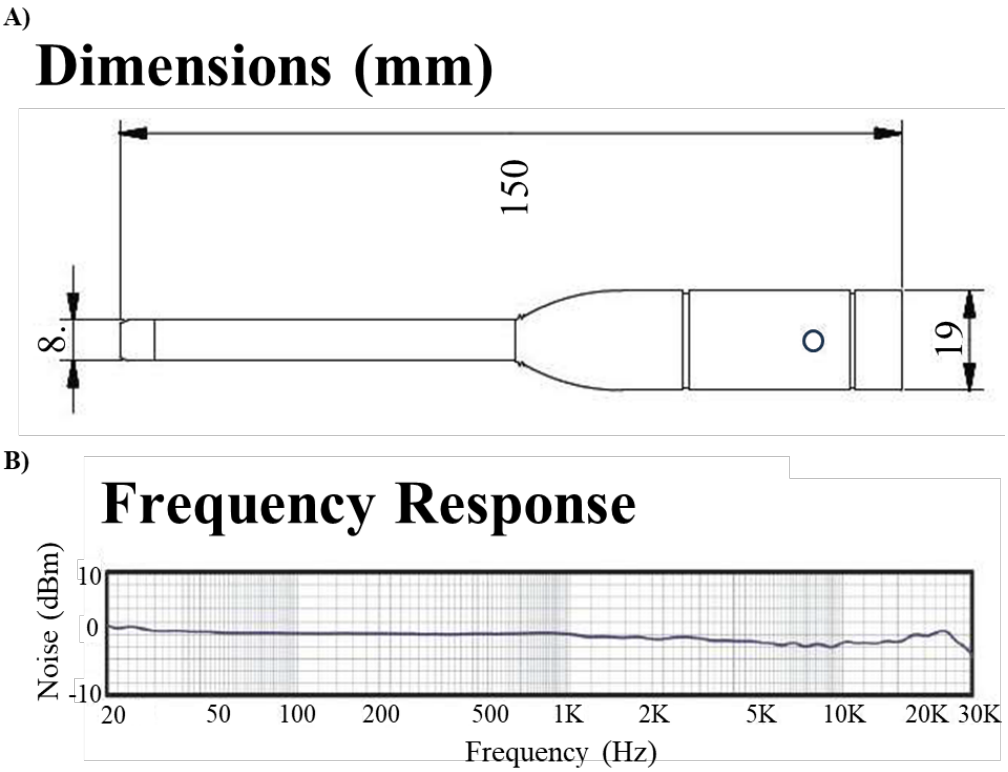

Figure A-22. Audix TM1 Microphone Used for Noise Measurement

Panel (A) shows the dimensions of the microphone in millimeters. Panel (B) shows the frequency response of the microphone.

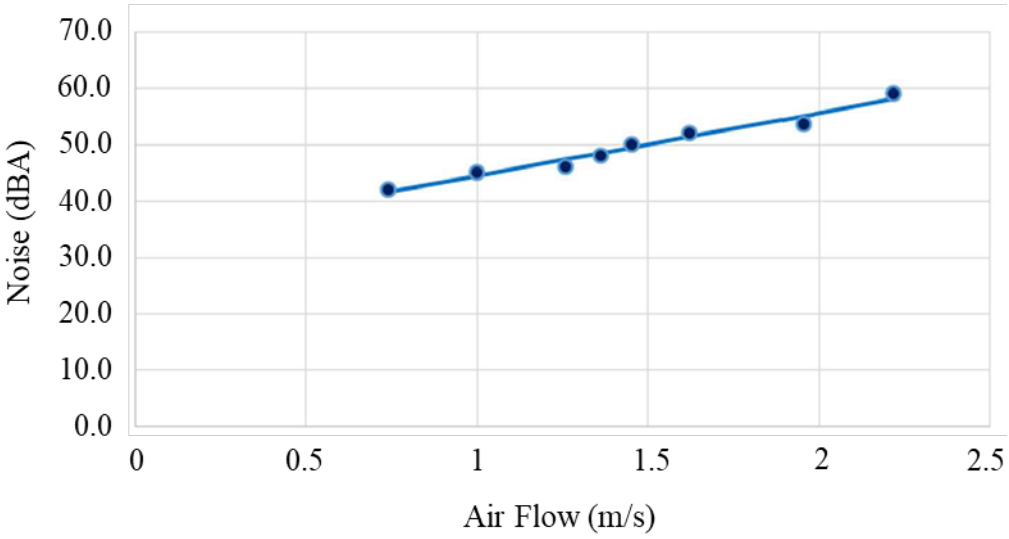

Figure A-23. Noise as a Function of Airflow (Fan Speed)

Linked to the sensor pack was a noise generator, which generated "GSM" noise to mask any differences between the chambers. The GSM noise could be selectively employed only during GSM exposures. The noise was amplified to the required level and played back using a Ci130QS (45 Hz–34 kHz) speaker (KEF, Maidstone, United Kingdom) placed outside the chamber, connected via a dedicated 130 × 130 mm honeycomb vent to deliver sound into the chamber.

A.6.2. Airflow

Airflow through the chamber was measured by means of an F400 series sensor (Degree Controls, Inc, Nashua, NH) as shown in Figure A-24, and the measured velocity was related to the number of air changes per hour. Laminar flow elements were added to the outlet manifold (top right of the chamber) to reduce turbulence in the airflow and to increase measurement accuracy.

Figure A-24. F400 Series Airflow Sensor

According to the measured airflow, the speed of the fans, two at the chamber air inlet and two at the chamber air outlet, could be adjusted using a fan speed controller, with one speed regulator per chamber. The temperature and humidity of the chamber air were essentially the same as those of the air in the exposure room, which were in turn controlled by the facility. As the power dissipated in each of the chambers, the temperature increase in the RF chambers compared to the control chamber was less than 0.1°C.

A.6.3. Ventilation

The environment in terms of temperature and humidity in the chamber was not controlled by the exposure system but relied on the building control systems. Airflow was maintained at a sufficiently high level to ensure approximately identical conditions in the chamber as in the animal room by virtue of fans integrated into the inlet and outlet plenums.

Ventilation was provided by two Sanyo Denki (Tokyo, Japan) fans on the inlet and two on the air outlet; the air then passed through a honeycomb vent with dimensions of 160 × 340 mm (3/16-inch cell size) to provide RF isolation.

All sensors, including the air speed sensor, were contained in the outlet manifold for circulated air. The cross section of the box was 190 × 360 mm; therefore 1 m/s flow corresponded to 0.068 m^3/s or approximately 4 m^3/min. The chamber volume was approximately 2.35 m^3, hence even the lowest airflows provided much higher turnover than the minimum required by the National Institute of Environmental Health Sciences Division of Translational Toxicology (NIEHS/DTT). Higher airflow was highly desirable for systems fitted with incandescent lighting, to remove the additional heat generated by the lighting and help maintain the chamber temperature consistent with that of the animal room.

A.6.4. Sensor Summary

The environmental parameters measured are summarized in Table A-2 along with the nominal accuracy where applicable.

Table A-2. Sensors, Ranges, and Accuracy

Sensor	Range	Uncertainty
Airflow	0.5–10 m/s	4% + 0.1 m/s
Temperature	−40°C–60°C	±0.3°C at 20°C
Humidity	0%–100%	±2.5% at 20°C
Noise	−30 to 90 dBA	±1.2 dB
Light	on/off	
Vibration	relative dB	

The inherent uncertainty associated with the field sensors related to the calibration process includes elements caused by variations in the field within the chamber and the temporal variation caused by the stirrer rotation. By virtue of having two field sensors in each chamber, the effects of chamber homogeneity were mitigated. The contributions to the uncertainty in the measurement of the field at 900 MHz and 1,900 MHz are described in Table A-3 and Table A-4, respectively.

Table A-3. Field Measurement Uncertainty at 900 MHz

Equipment/Factor	Uncertainty Distribution	Divisor ×	Coverage	Standard Uncertainty
Absolute Accuracy of the E-field Probe	±0.26 dB	Normal	1	±0.26 dB
Frequency Linearity	±0.2 dB	Rectangular	√3	±0.12 dB
Dynamic Range Linearity	±0.2 dB	Rectangular	√3	±0.12 dB
Isotropy	±0.4 dB	Rectangular	√3	±0.12 dB
Field Control	±0.2 dB	Normal	1	±0.20 dB
Homogeneity	±0.7 dB	Normal/2 Probes	1/√2	±0.49 dB
Combined Standard Uncertainty				±0.65 dB

Table A-4. Field Measurement Uncertainty at 1,900 MHz

Equipment/Factor	Uncertainty Distribution	Divisor ×	Coverage	Standard Uncertainty
Absolute Accuracy of the E- and H-field Probes	±0.26 dB	Normal	1	±0.26 dB
Frequency Linearity	±0.2 dB	Rectangular	√3	±0.12 dB
Dynamic Range Linearity	±0.2 dB	Rectangular	√3	±0.12 dB
Isotropy	±0.4 dB	Rectangular	√3	±0.12 dB
Field Control	±0.2 dB	Normal	1	±0.20 dB

Equipment/Factor	Uncertainty Distribution	Divisor ×	Coverage	Standard Uncertainty
Homogeneity	±0.42 dB	Normal/2 Probes	1√2	±0.30 dB
Combined Standard Uncertainty				±0.53 dB

A.7. Signal Generation and Amplification

A.7.1. Signal Generator

The signal generator chosen—Rhode & Schwarz model SMBV-100A with frequency option SMBV-B103 covering 9 kHz–3.2 GHz (Figure A-25)—is extremely flexible and can generate modulations with base bandwidths of up to 120 MHz at carrier frequencies of up to 3.2 GHz. The SMBV-B10/B92 combination in conjunction with the R&SWinIQSIM2 software allowed any arbitrary complex modulation (32 Mbyte) to be generated.

For GSM modulations, internal modulation with one time slot active was used. For IS-95 (i.e., CDMA) systems, internal in-phase and quadrature (I/Q) modulation for offset quadrature phase-shift keying (OQPSK) was used, with a pseudo random modulation stream, a chip rate of 1.228 Mcps, and the cdmaOne (IS-95) baseband filter to produce a baseband constellation and modulated spectrum identical to those of the IS-95 (i.e., CDMA) setup used in the previous NTP studies (Figure A-26).

The Rhode & Schwarz signal generator could also provide modulations such as 3G and 4G signals. 5G signal modulation was expected to be similar to 4G in terms of modulation; however, the carrier frequencies at that time were not known, and it was thought to be outside the design scope of this exposure system. The signal generator supports several modulations, including Third Generation Partnership Project (3GPP) Long-Term Evolution (LTE) Frequency Division Duplex (FDD) and Time Division Duplex (TDD), LTE-Advanced, 3GPP FDD/High-Speed Packet Access (HSPA)/HSPA+, GSM/Enhanced Data rates for GSM Evolution (EDGE)/EDGE Evolution, Time Division-Synchronous CDMA (TD-SCDMA), and Wireless Local-area Network (WLAN).

Figure A-25. Rhode & Schwarz Signal Generator SMBV-100A

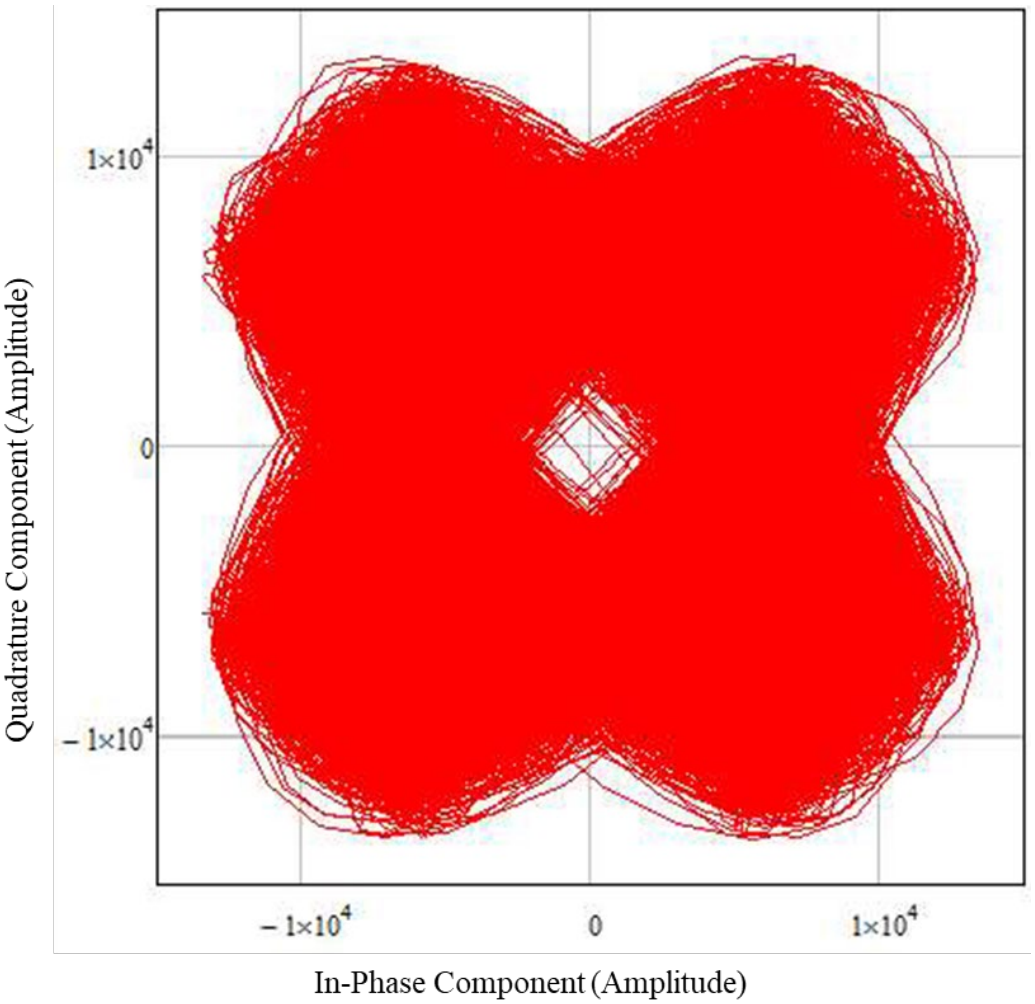

Figure A-26. Interim Standard 95 (i.e., CDMA) In-phase and Quadrature (I/Q) Constellation

CDMA = Code Division Multiple Access-modulated cell phone radiofrequency radiation.

A.7.2. Amplifier Performance

Figure A-27 shows the amplifiers with the controller. Each amplifier comprised two RF power modules of ≥175 W each combined with integrated circulators. At 900 MHz, the saturated power output of the completed amplifiers was approximately 320 W. The amplifiers had lower output power at 1,900 MHz, with the lowest output power being >200 W.

Figure A-27. Three Amplifiers and the Amplifier Controller

A.7.3. Amplifier Linearity and Spectral Regrowth

Figure A-28 shows the IS-95 (i.e., CDMA) signal spectrum at the highest expected output power for both 900 and 1,900 MHz; the performance at each frequency was the same within approximately 2 dB. Figure A-29 shows a comparison of the performance of broadband amplifiers in the current study to that achieved in the previous NTP studies with single band amplifiers. The comparison showed that linearity was about the same at 1,900 MHz and slightly worse at 900 MHz. However, all unwanted spectral components were <l/l,000 of the power within the intended bandwidth and at most 5 dB higher than the spectral mask.

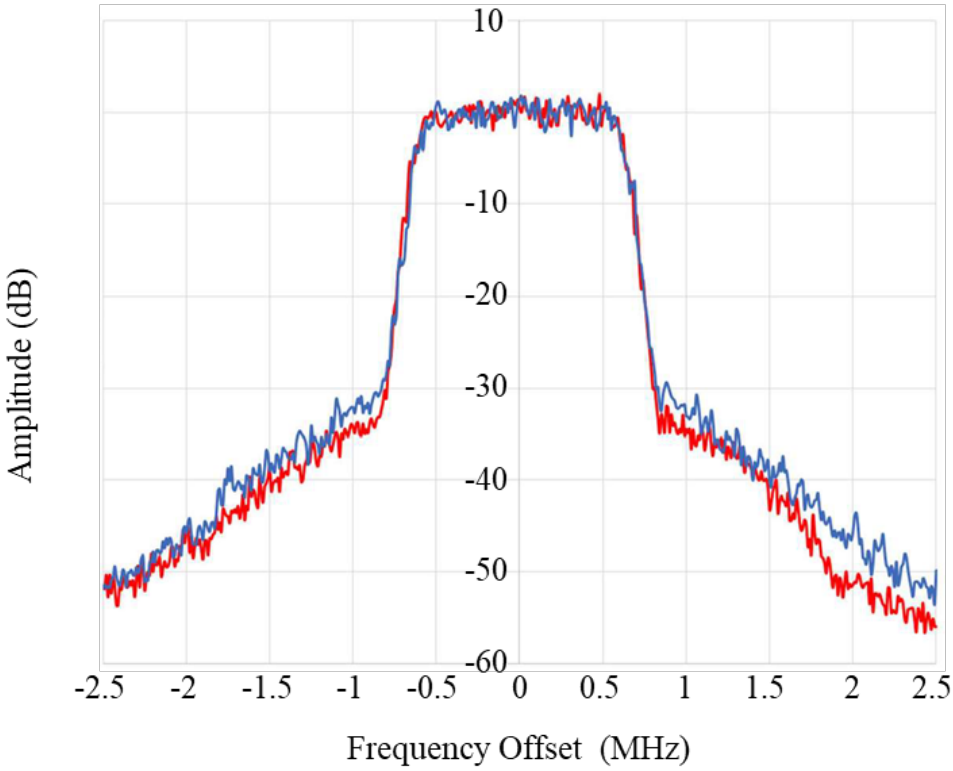

Figure A-28. Interim Standard 95 (i.e., CDMA) Spectra for 900 MHz (Blue) and 1,900 MHz (Red)

CDMA = Code Division Multiple Access-modulated cell phone radiofrequency radiation.

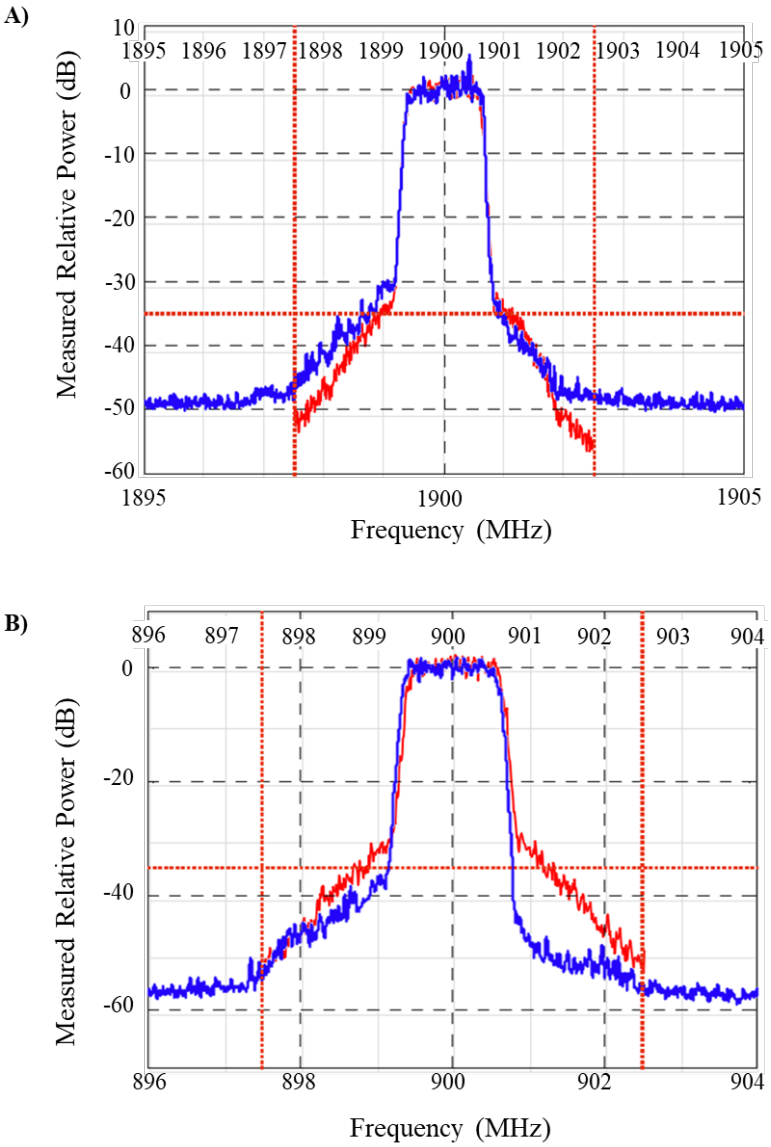

Figure A-29. Comparison of the Interim Standard 95 (i.e., CDMA) Spectra from the Amplifiers

Panel (A) shows the response for 1,900 MHz. Panel (B) shows the response for 900 MHz. Blue indicates the spectra from single band amplifiers used in the National Toxicology Program radiofrequency radiation studies, and red indicates the spectra from broadband amplifiers used in the current studies. The spectral mask limits for Interim Standard 95 CDMA transmissions are denoted by the red, dotted lines on the plots. CDMA = Code Division Multiple Access-modulated cell phone radiofrequency radiation.

A.7.4. Antennas

The antennas were designed to cover both the 900 MHz and 1,900 MHz frequency bands and did not need to be changed when switching from rat exposures at 900 MHz to mouse exposures at 1,900 MHz. Broadband log periodic antennas were designed and custom manufactured to meet the requirements; the maximum dimensions of these antennas were 40 cm long, 20 cm wide, and 2 cm deep. The simulation model and predicted performance are shown in Figure A-30, and the physical antenna is shown in Figure A-31. The high-power chamber had three antennas, the medium-power chamber had three antennas, and the low-power chamber had one antenna, for a

total of seven antennas within the system. All antennas were placed such that their main beam was aimed at one of the stirrers to maximize the scattering of the field and avoid direct exposure of the animals. All antennas were placed in the rear of the chamber. In the case of the high- and medium-power chambers, antennas were placed in the top left and bottom right and aimed at the stirrer on the rear wall. The other antenna in the top right was aimed at the stirrer on the ceiling. In the low-power chamber, only the antenna in the top right was installed.

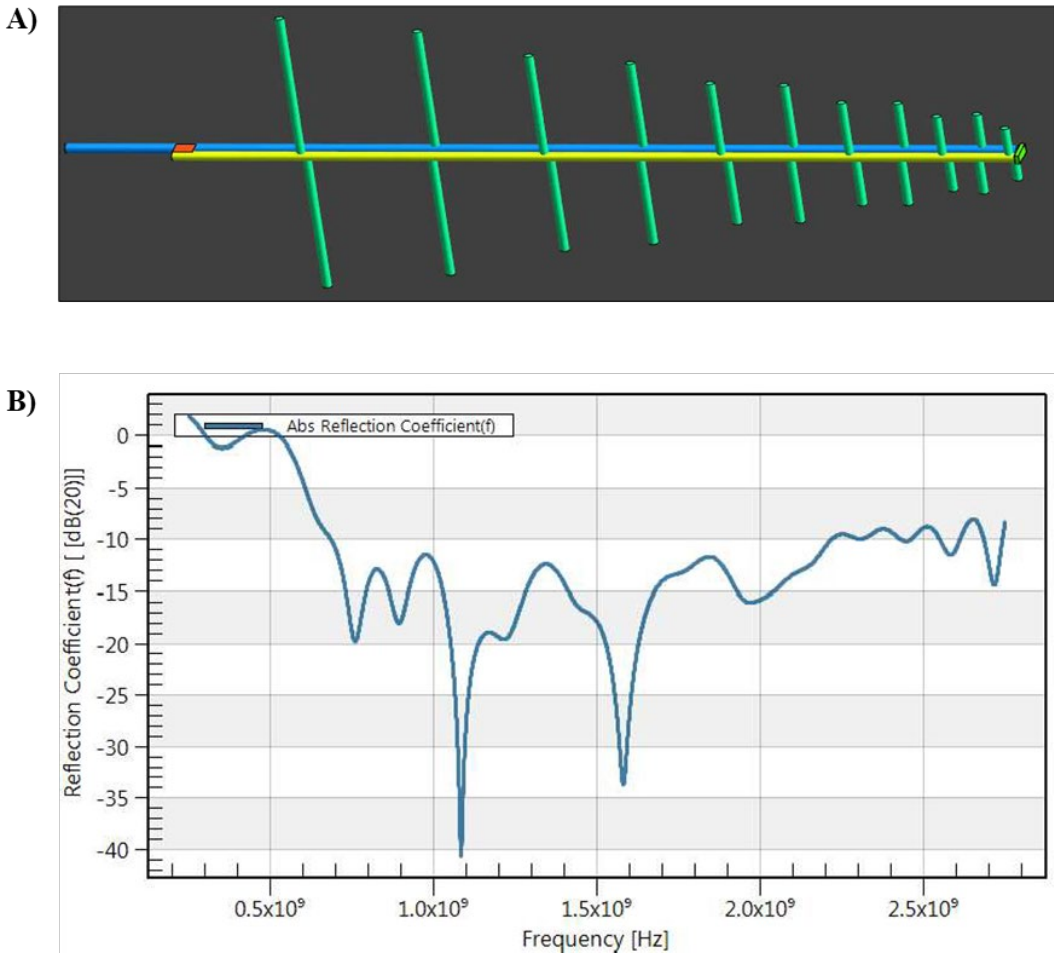

Figure A-30. (A) Log Periodic Antenna Computer-aided Design Model and (B) Reflection Coefficient

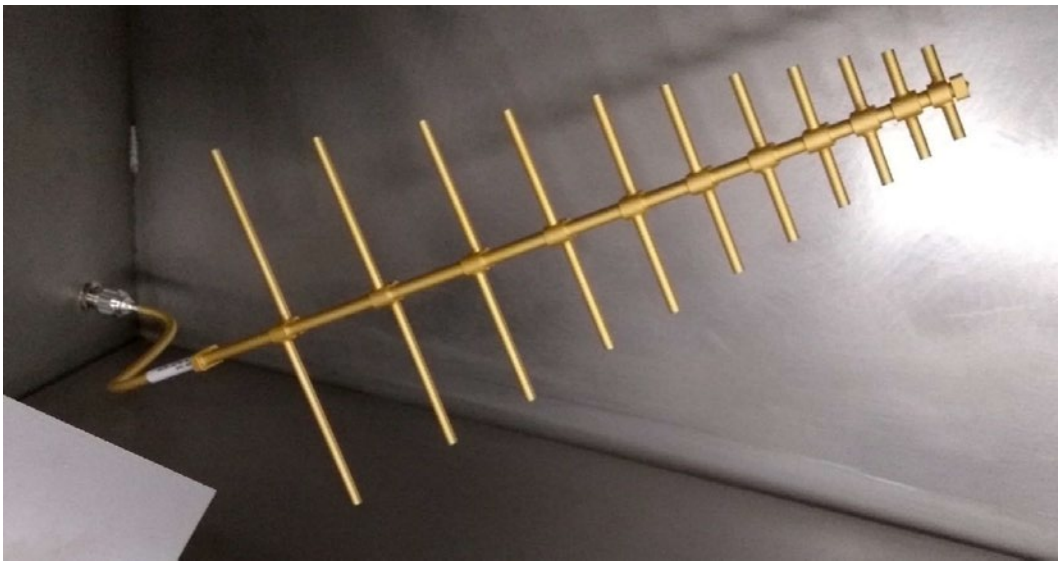

Figure A-31. Log Periodic Antenna Installed in One of the Chambers

A.7.5. Exposure Control

The exposure level in any given chamber depended on (i) the number of amplifiers connected to the chamber, (ii) the output power from the amplifiers, (iii) the number and weight of the animals in the chamber, and (iv) the amount of bedding and feed in each chamber. The number of amplifiers connected to the different chambers depended on which time slot was being used and the required SAR for that chamber. Typically, the first 10-minute time slot had all three amplifiers connected to the high-power chamber (Chamber 1), with each amplifier connected to a different antenna (i.e., the chamber was used as a cavity power combiner). In the second 10-minute slot, two amplifiers were connected to the medium-power chamber (Chamber 2) and the third amplifier was connected to the low-power chamber (Chamber 3). Therefore, each amplifier's output power was individually controlled, which was achieved by controlling the input power to each amplifier in each 10-minute time period. The controller facilitated this by varying the input to a set of voltage-controlled attenuators, which in turn set the output power to the required value under computer control. The control level was calculated based on the measured field strength in a given chamber. In addition to the level set by the computer control, further levels of control were integrated. These included a limiter to ensure that the maximum output power level did not exceed the safe operation level for each amplifier and that the maximum reflected power did not exceed the set threshold, as this would increase the dissipation within the amplifier with the potential for permanent damage. The block diagram for the controller is given in Figure A-32. The software generated warnings if the measured fields and calculated SAR deviated from the target by more than a given threshold, to alert staff to a potential problem. To ensure the safety of the animals, the exposure would be aborted if the SAR exceeded a second set of programmable thresholds, which were set in consultation with the testing facility and NIEHS/DTT scientists.

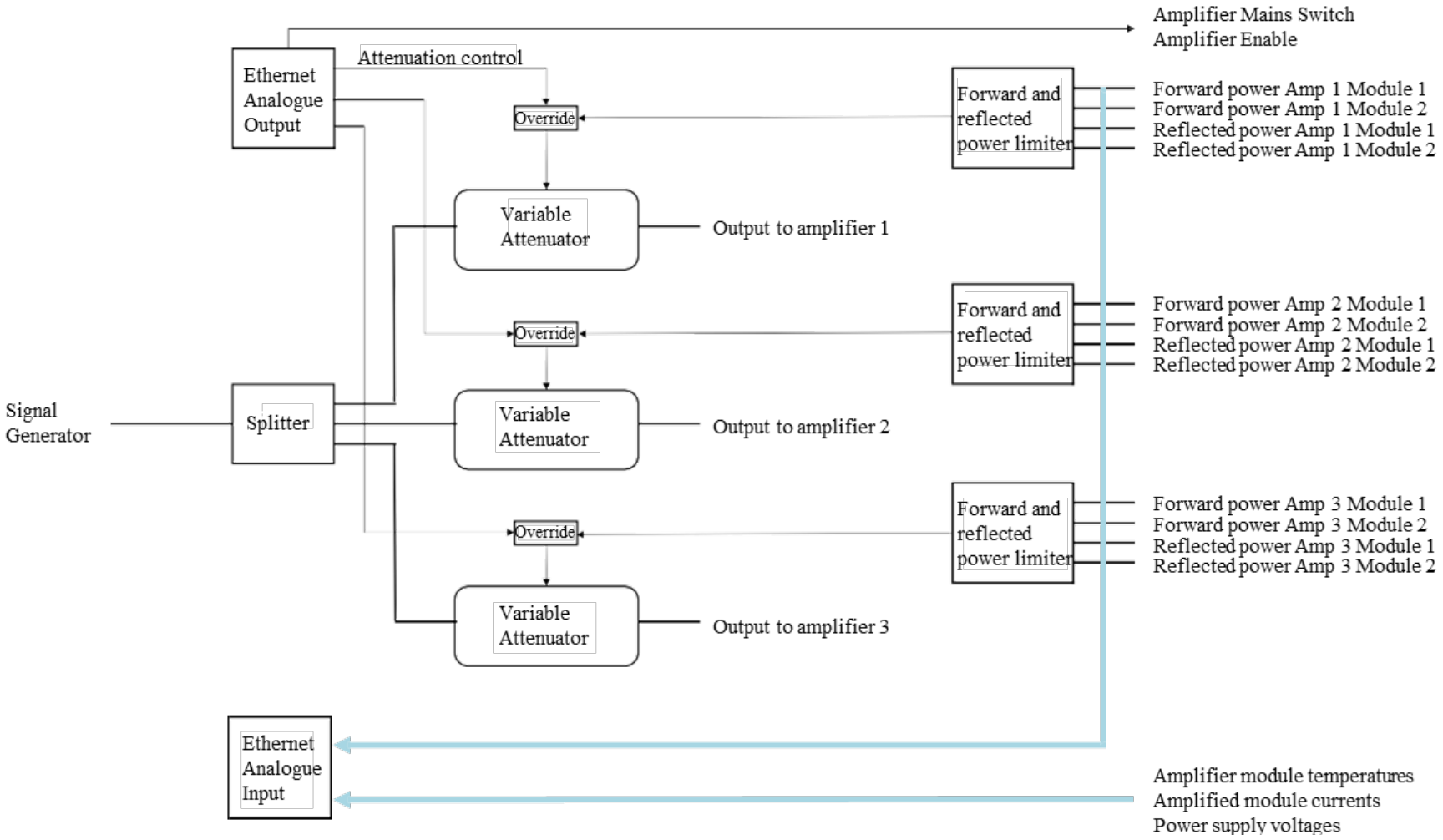

Figure A-32. Radiofrequency Amplifier Level-Control System

A.8. Chamber Quality Factor and Stirring Performance

A.8.1. Insertion Loss Measurements

A vector network analyzer (VNA), Agilent 8753B, connected to two antennas in the reverberation chamber was used to characterize the losses due to the individual chamber contents, such as racks, bedding, and feed. These measurements were important for calculation of the power needed to meet the required field strengths in the chambers.

A.8.1.1. Measurement Uncertainty

The measurement repeatability was assessed for the VNA S21 measurements using sets of five repeated measurements of 10,025 points (i.e., measurement locations) spaced over 124/125 rotations of the two stirrers. The maximum standard deviation observed at either 900 MHz or 1,900 MHz was 0.05 dB.

The stated uncertainty of the Agilent 8753B transmission measurement assuming a typical insertion loss of 20 dB, a source and load match of −10 dB, and response calibration is 0.8 dB (k = 2). The overall uncertainty for the measurement is summarized in Table A-5.

Table A-5. Overall Uncertainty of the Measurement

Equipment	Uncertainty	Distribution	Divisor × Coverage	Standard Uncertainty
Agilent 8753B	±0.8 dB	Normal (k = 2)	2	±0.4 dB
Stirrer Modulation	±0.05 dB	Normal	1	±0.05 dB
Combined Standard Uncertainty				±0.4 dB

The combined standard uncertainty was 0.4 dB or 9.7% for the S21 and effective quality (Q) values calculated in the following sections. On the basis of the insertion loss measurements for the chamber with each additional element inserted, the following effective Q values were determined for 900 MHz and 1,900 MHz. The overall Q value for any combination of elements can be calculated with the following expression:

$$Q_T = \left(\frac{1}{Q_0} + \frac{1}{Q_1} + \frac{1}{Q_2} + ... \frac{1}{Q_n} \right)^{-1}$$

The equivalent Q values of elements in the empty and fully loaded reverberation chambers are given in Table A-6 and Table A-7, respectively. The measured S-parameters are shown in Figure A-33 and Figure A-34. For correct operation of a reverberation chamber, the points in the plots, which correspond to discrete stirrer positions, should be equally distributed across all four quadrants of the S21 (transmission between two antennas in a single chamber) plots, as any bias in a given direction would indicate the presence of unstirred energy, which would degrade the homogeneity of the exposure. In addition, analysis of the magnitude of S21 allows information on the Q factor of the chamber to be determined. The equivalent Q values of components in the fully loaded reverberation chamber are summarized in Table A-8.

Table A-6. Equivalent Q Values of Elements in the Empty Reverberation Chamber

Empty Chamber	900 MHz	1,900 MHz
Quality Factor	1,121	1,624
Stirred to Unstirred Energy	9.7 dB	14.2 dB
Average Reflection Coefficient	−8.3 dB	−12.2 dB

Table A-7. Equivalent Q Values of Elements in the Fully Loaded Reverberation Chamber

Fully Loaded Chamber	900 MHz	1,900 MHz
Quality Factor	157	385
Stirred to Unstirred Energy	24.1 dB	14.5 dB
Average Reflection Coefficient	−11.4 dB	−17.0 dB

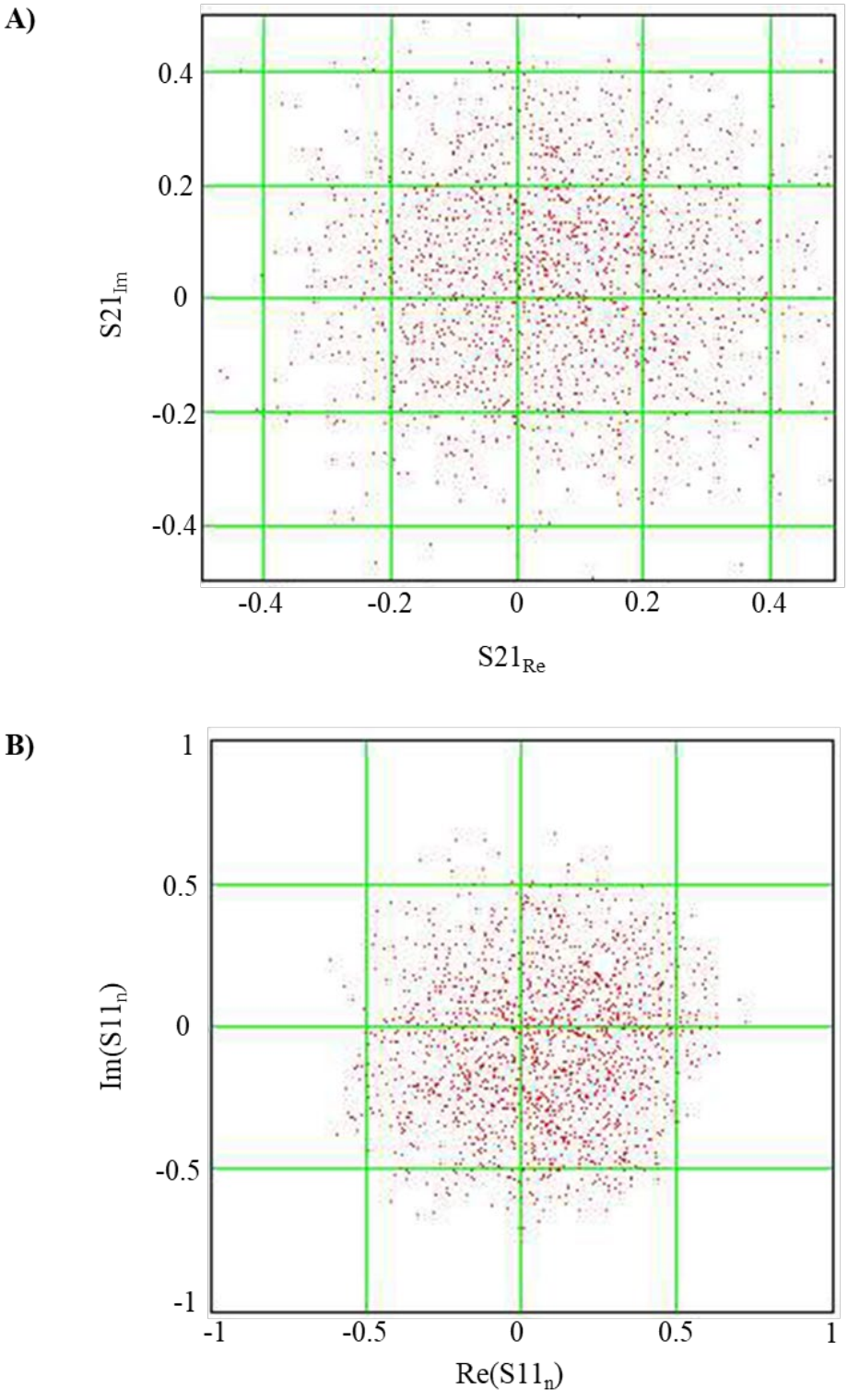

Figure A-33. 900 MHz S-Parameter Plots

A)

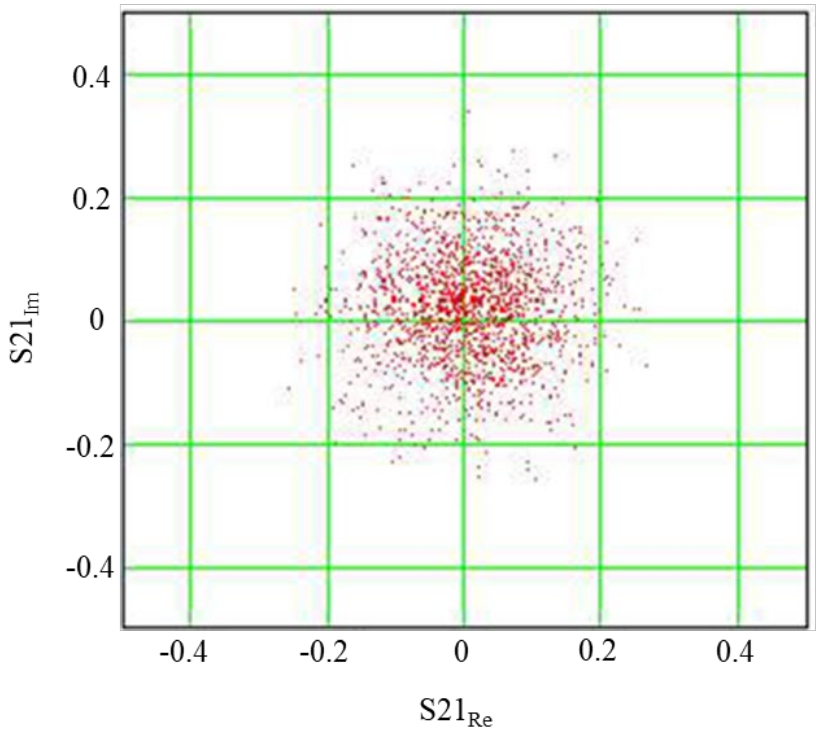

B)

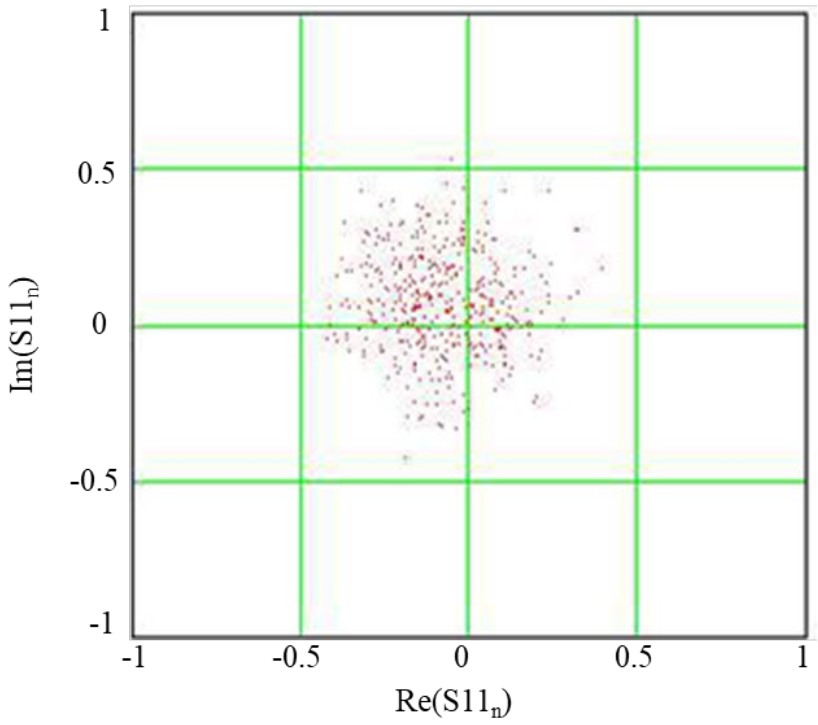

Figure A-34. 1,900 MHz S-Parameter Plots

Table A-8. Equivalent Q Values of Components in the Fully Loaded Reverberation Chamber

Component	900 MHz	1,900 MHz
Empty Chamber	1,121	1,624
Racks	1,072	1,029
Cages	17,117	6,859
Bedding	1,331	2,517
Feed	6,667	9,649
Phantoms	268	2,752

The following expression from the NIST Technical Note 1506[42] allows the Q value to be related to input power and field strength:

$$E^2 = \frac{Q \cdot P \cdot \eta_{TX}}{2 \cdot \pi \cdot f \cdot \varepsilon_0 \cdot Vol}$$

On the basis of the Q values evaluated, the relative power absorptions obtained for 10 rats and 10 mice with assumed maximum weights of 550 g/rat at 900 MHz and 55 g/mouse at 1,900 MHz, respectively, are listed in Table A-9.

Table A-9. Relative Power Absorptions for Ten Rats and Ten Mice

Element	Power Dissipation[a]	
	900 MHz	1,900 MHz
Chamber Walls, Lights, Stirrers	13.7%	23.7%
Racks	14.3%	37.4%
Cages	0.9%	5.6%
Bedding	11.5%	15.3%
Feed	2.3%	4.0%
Phantoms	57.3%	14.0%

[a]Obtained assuming a maximum weight for rats of 550 g/rat and a maximum weight for mice of 55 g/mouse.

On the basis of the Q values evaluated, the power requirements for 10 rats and 10 mice with maximum weights of 550 g and 55 g, respectively, are listed in Table A-10. The maximum efficiency is 57% for rats and 14% for mice.

Table A-10. Power Requirements for Ten Rats and Ten Mice

	Maximum SAR	Power Absorbed by Animal	Average Power Delivered to Chamber	Peak Power Delivered to Chamber
Rats[a]	8 W/kg	44 W	77 W	640 W
Mice[b]	15 W/kg	8.25 W	59 W	490 W

[a]Obtained assuming a maximum weight for rats of 550 g/rat.
[b]Obtained assuming a maximum weight for mice of 55 g/mouse.

A.9. Field Uniformity Measurement

A.9.1. Measurement Uncertainty

The requirements for field uniformity form a key element of the specification of the chamber, and a large number of measurements must be made over the working volume, both with the chamber empty and fully loaded with racks and phantoms, to assess the uniformity. Unlike VNA S-parameter measurements, field measurements are time consuming. Thus, two elements of the measurement were assessed, namely, the measurement repeatability and the increase in uncertainty as the number of points (i.e., measurement locations) is reduced and the measurement speed is increased.

The repeatability was assessed on the basis of 3,440 stirrer positions over 4/5 rotations of the two stirrers. The standard deviation of sets of 900 MHz measurements was <0.2 dB for the total field and 0.3 dB for any given component of the field. The standard deviation of the sets of 1,900 MHz measurements was 0.22 dB for the total field and 0.37 dB for any given orthogonal field component. The overall uncertainty for the field strength measurements was calculated from the individual uncertainty elements as shown in Table A-11.

Table A-11. Standard Uncertainty in Measurements of E-fields and H-fields

Equipment	Uncertainty	Distribution	Divisor × Coverage	Standard Uncertainty
Absolute Accuracy of the E- and H-field Probes	±0.26 dB	Normal	1	±0.26 dB
Frequency Linearity	±0.2 dB	Rectangular	√3	±0.12 dB
Dynamic Range Linearity	±0.2 dB	Rectangular	√3	±0.12 dB
Isotropy	±0.4 dB	Rectangular	√3	±0.12 dB
Stirrer Modulation/ Repeatability	±0.22 dB	Normal	1	±0.22 dB
Combined Standard Uncertainty				±0.40 dB

A.9.2. Homogeneity Measurements

The measurements were performed on a grid $\Delta X = 150$ mm, $\Delta Y = 95$ mm, and $\Delta Z = 135$ mm with 12 measurement locations inside each cage apart from two areas close to the fixed probes integrated into each chamber where only six measurement locations could be measured.

The homogeneity measurement was performed with six EF3DV3 E-field probes (SPEAG, Switzerland) supported by Rohacell ($\varepsilon_r \approx 1.1$) inside a modified cage with parts close to the probe tips removed (Figure A-35). The jig was placed in the chamber facing forward and

rearward to measure all 12 locations (Figure A-36). When the data acquisition electronics (DAE) units were at the rear, the lower shelves had to be removed to allow access.

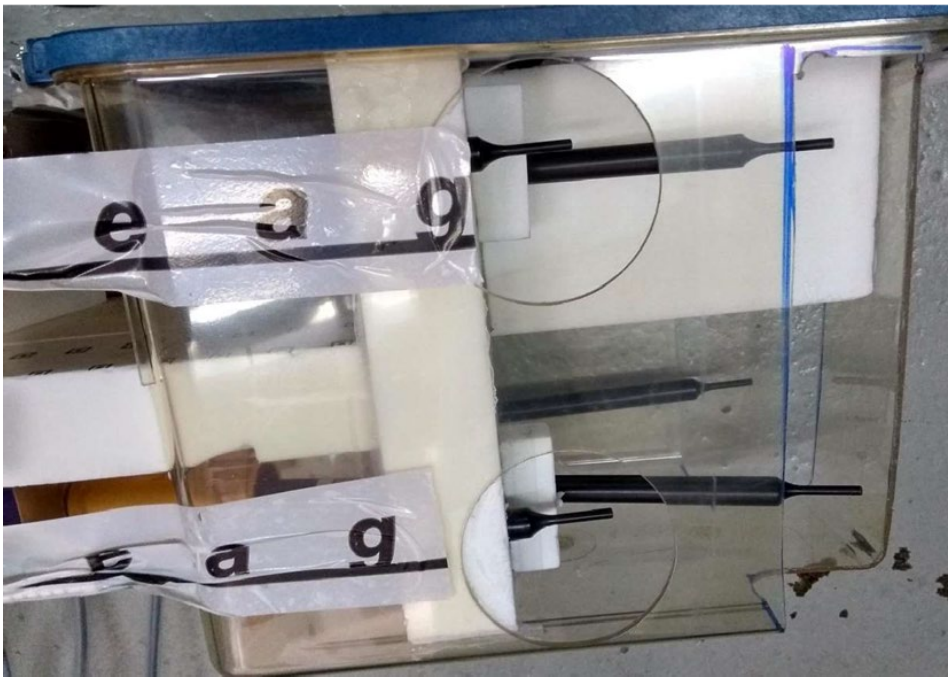

Figure A-35. Measurement Jig in a Modified Cage with Six E-field Probes

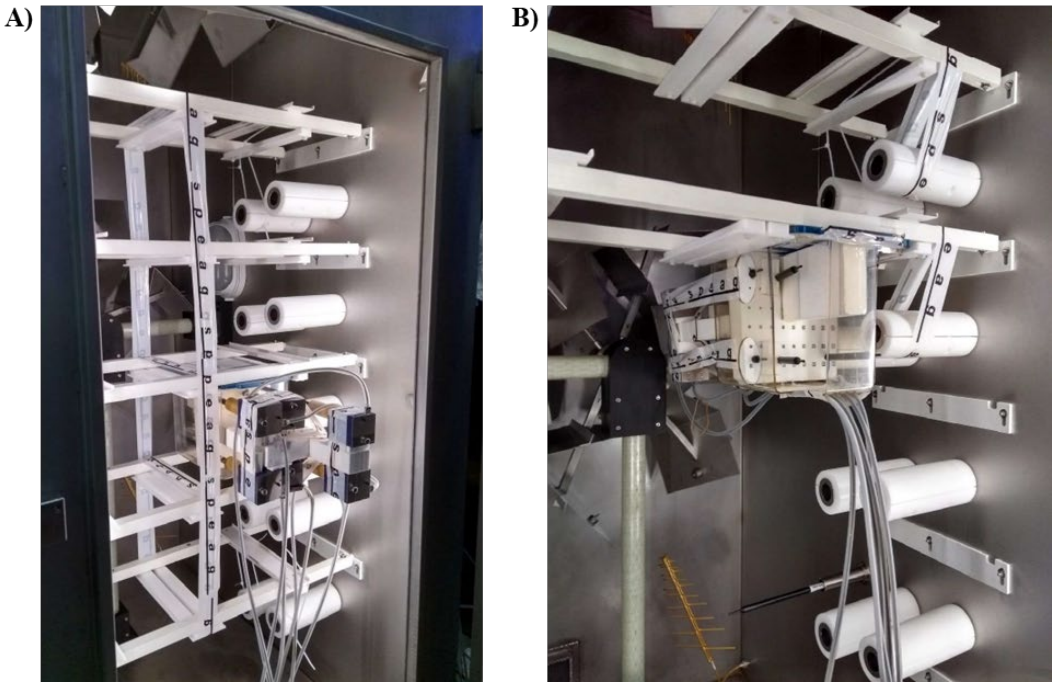

Figure A-36. Measurement Jig, (A) Forward-facing and (B) Rearward-facing

For homogeneity with the chamber loaded with phantoms, one cage was removed to allow the probe jig to be inserted. It was inserted only from the front, as there was no space for the optical connections when all shelves were present, which prevented the use of rear-facing DAE configurations (Figure A-37).

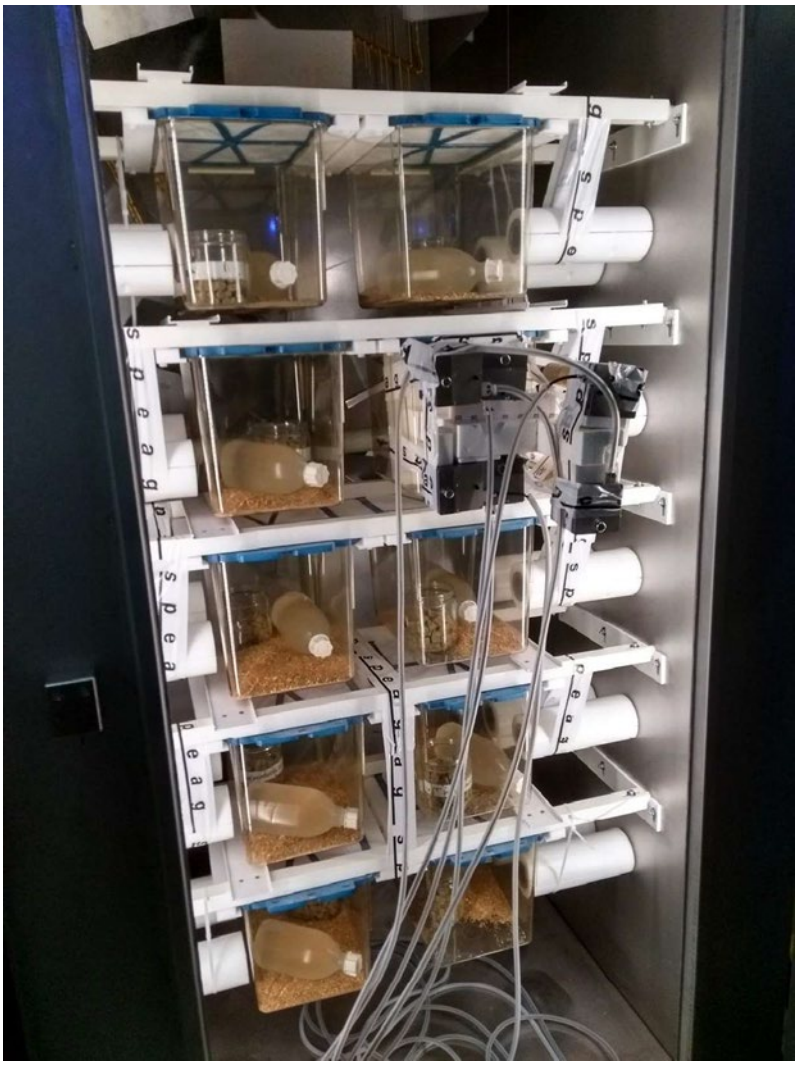

Figure A-37. Chamber Loaded with Rat Phantoms, One Cage Removed to Allow Probes to Be Inserted

Measurements were normalized with respect to the field measured by the integrated E-field probes to account for variations in the field with time. The field samples were obtained over a 2-minute period at each location and involved an integral number of stirrer rotations, namely, five for the top stirrer and seven for the rear stirrer. The field was sampled continuously over this period.

A.9.2.1. Homogeneity – 900 MHz

Table A-12. Empty Chamber, 108 Measurement Locations

	E_X	E_Y	E_Z	E_{Total}	$E_{X,Y,Z}$
Average (dB)	−0.44	−0.54	−0.23	−0.40	−0.40
StDev (dB)	1.27	1.34	0.80	0.73	1.16
Min (dB)	−3.36	−4.68	−2.54	−1.50	−4.82
Max (dB)	2.72	3.22	2.53	1.78	3.08

Table A-13. Loaded Chamber, 60 Measurement Locations

	E_X	E_Y	E_Z	E_{Total}	$E_{X, Y, Z}$
Average (dB)	−0.21	−0.05	0.17	−0.03	−0.03
StDev (dB)	1.43	1.31	1.01	0.84	1.26
Min (dB)	−5.85	−3.90	−3.21	−2.17	−6.03
Max (dB)	3.55	2.84	2.81	2.06	3.37

For the empty chamber (Table A-12), the key figures were:

- Homogeneity = 0.73 dB
- Isotropy = 1.16 dB
- All measurement locations within ±2.5 dB

For the loaded chamber (Table A-13), the key figures were:

- Homogeneity = 0.84 dB
- Isotropy = 1.26 dB

Field maps were evaluated at 900 MHz over three vertical planes at rear, middle, and front locations in the cages, for the empty chamber without cages, bedding, and phantoms. For the locations that could not be measured, average fields were substituted. Figure A-38, Figure A-39, and Figure A-40 show the contours at the rear, middle, and front planes, respectively.

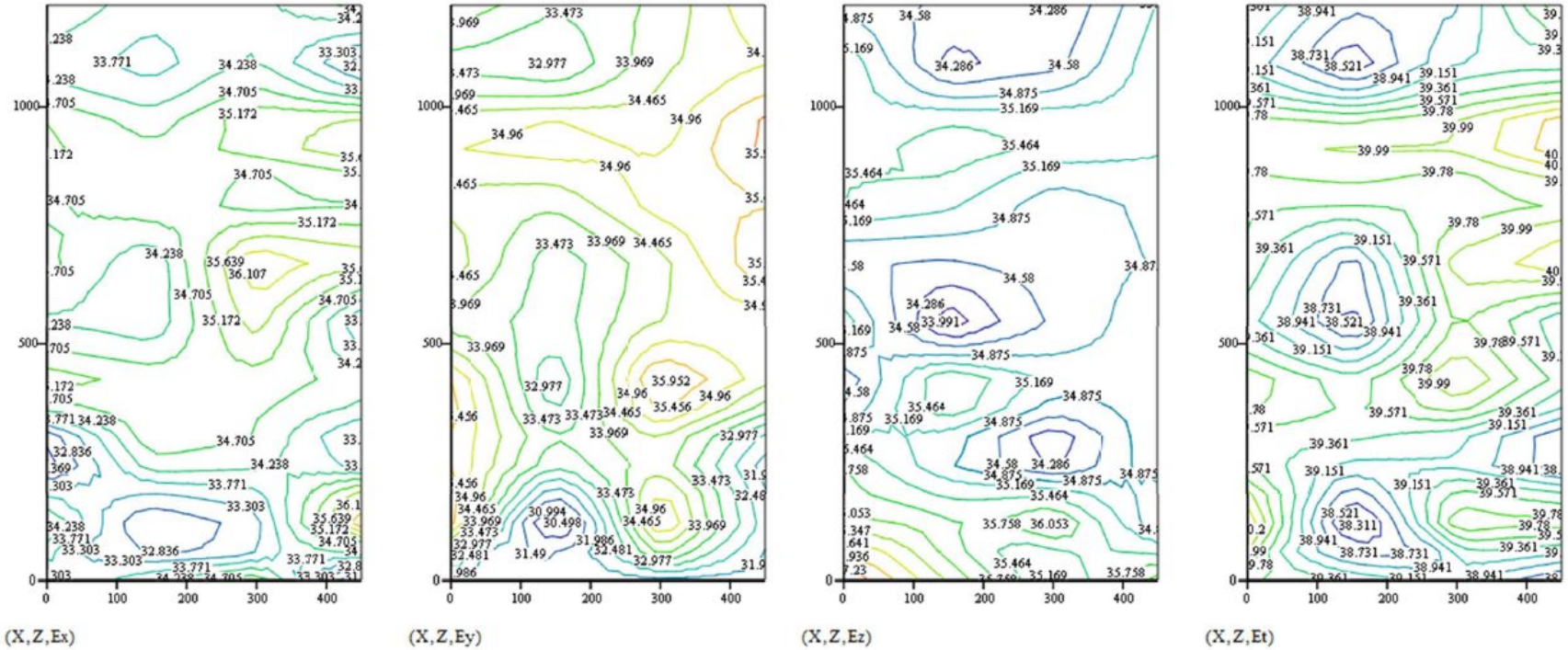

Figure A-38. Rear Plane at Y = 0 mm – 900 MHz

Colored contours in the figure show the directed components of the E-field (X-Component, Y-Component, and Z-Component, or Ex, Ey, and Ez), and total E-field (Et) in dBV/m in the plots from left to right. Axes show distance in millimeters.

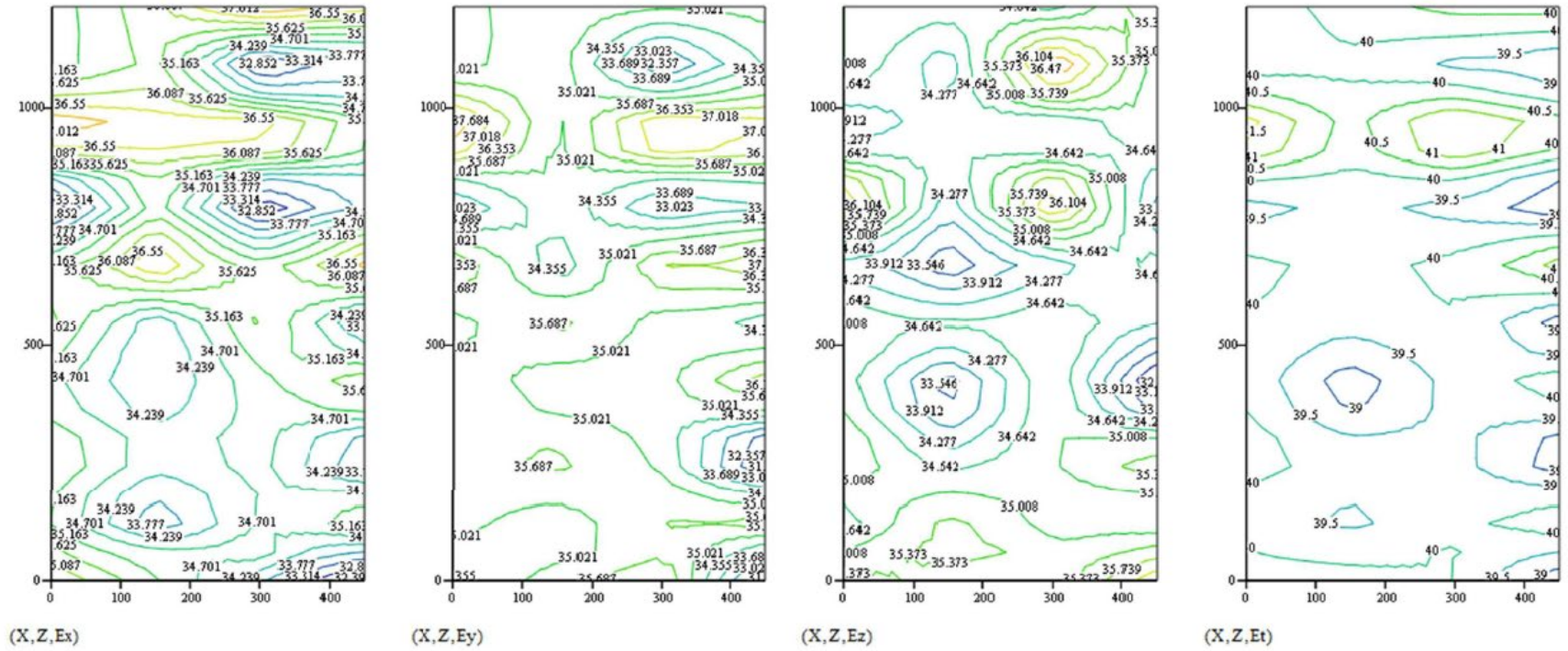

Figure A-39. Middle Plane at Y = 95 mm – 900 MHz

Colored contours in the figure show the directed components of the E-field (X-Component, Y-Component, and Z-Component, or Ex, Ey, and Ez), and total E-field (Et) in dBV/m in the plots from left to right. Axes show distance in millimeters.

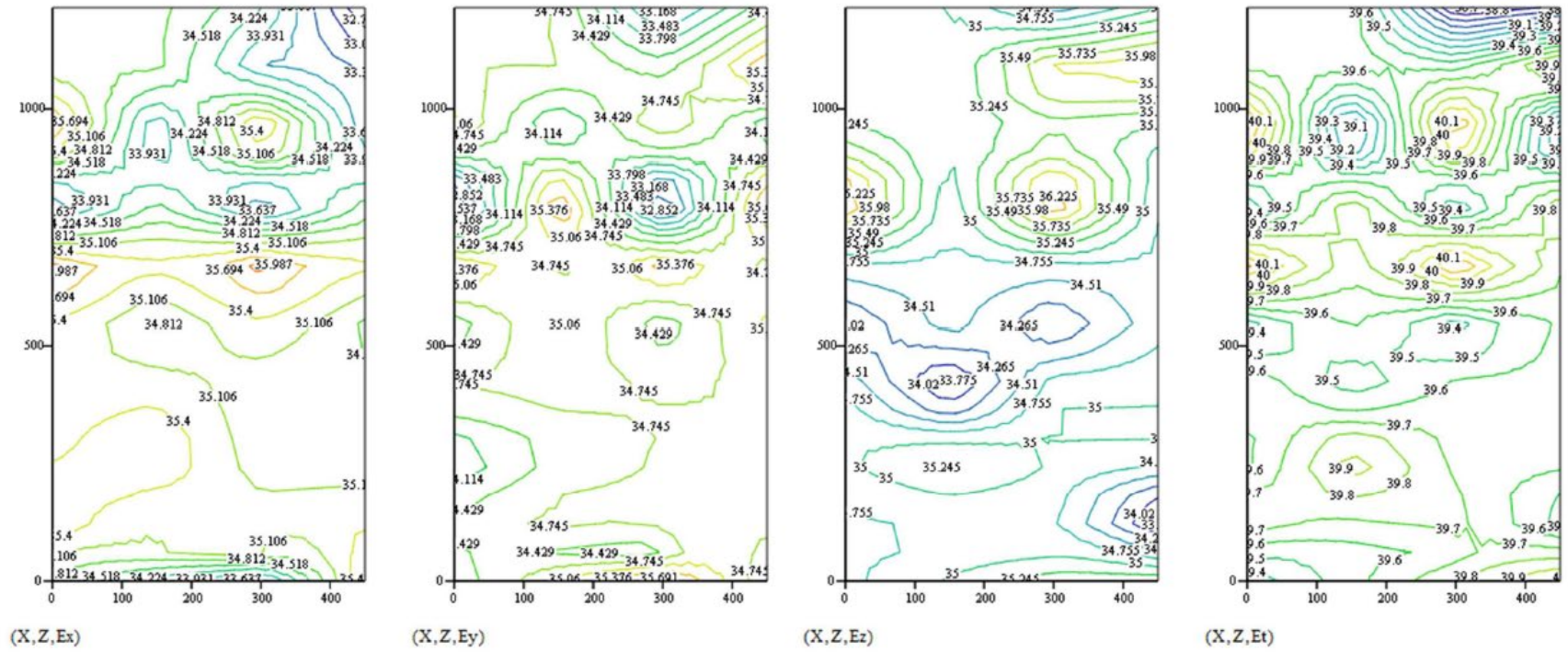

Figure A-40. Front Plane at Y = 190 mm – 900 MHz

Colored contours in the figure show the directed components of the E-field (X-Component, Y-Component, and Z-Component, or Ex, Ey, and Ez), and total E-field (Et) in dBV/m in the plots from left to right. Axes show distance in millimeters.

A.9.2.2. Homogeneity – 1,900 MHz

Table A-14. Empty Chamber, 108 Measurement Locations

	E_X	E_Y	E_Z	E_{Total}	$E_{X,Y,Z}$
Average (dB)	0.35	0.55	0.35	0.42	0.42
StDev (dB)	0.62	0.66	0.68	0.44	0.66
Min (dB)	−1.34	−1.44	−2.10	−0.94	−2.17
Max (dB)	1.82	1.73	1.99	1.18	1.92

Table A-15. Loaded Chamber, 60 Measurement Locations

	E_X	E_Y	E_Z	E_{Total}	$E_{X,Y,Z}$
Average (dB)	0.19	0.32	−0.26	0.09	0.09
StDev (dB)	0.70	0.81	0.81	0.60	0.80
Min (dB)	−1.55	−1.78	−1.95	−1.23	−2.30
Max (dB)	1.62	2.36	2.27	1.79	2.59

For the empty chamber (Table A-14), the key figures were:

- Homogeneity = 0.44 dB
- Isotropy = 0.66 dB
- All measurement locations within ± 1.2 dB

For the loaded chamber (Table A-15), the key figures were:

- Homogeneity = 0.60 dB
- Isotropy = 0.80 dB

Field maps were evaluated at 1,900 MHz over three vertical planes at rear, middle, and front locations in the cages, for the empty chamber without cages, bedding, and phantoms. For the locations that could not be measured, average fields were substituted. Figure A-41, Figure A-42, and Figure A-43 show the contours at the rear, middle, and front planes, respectively.

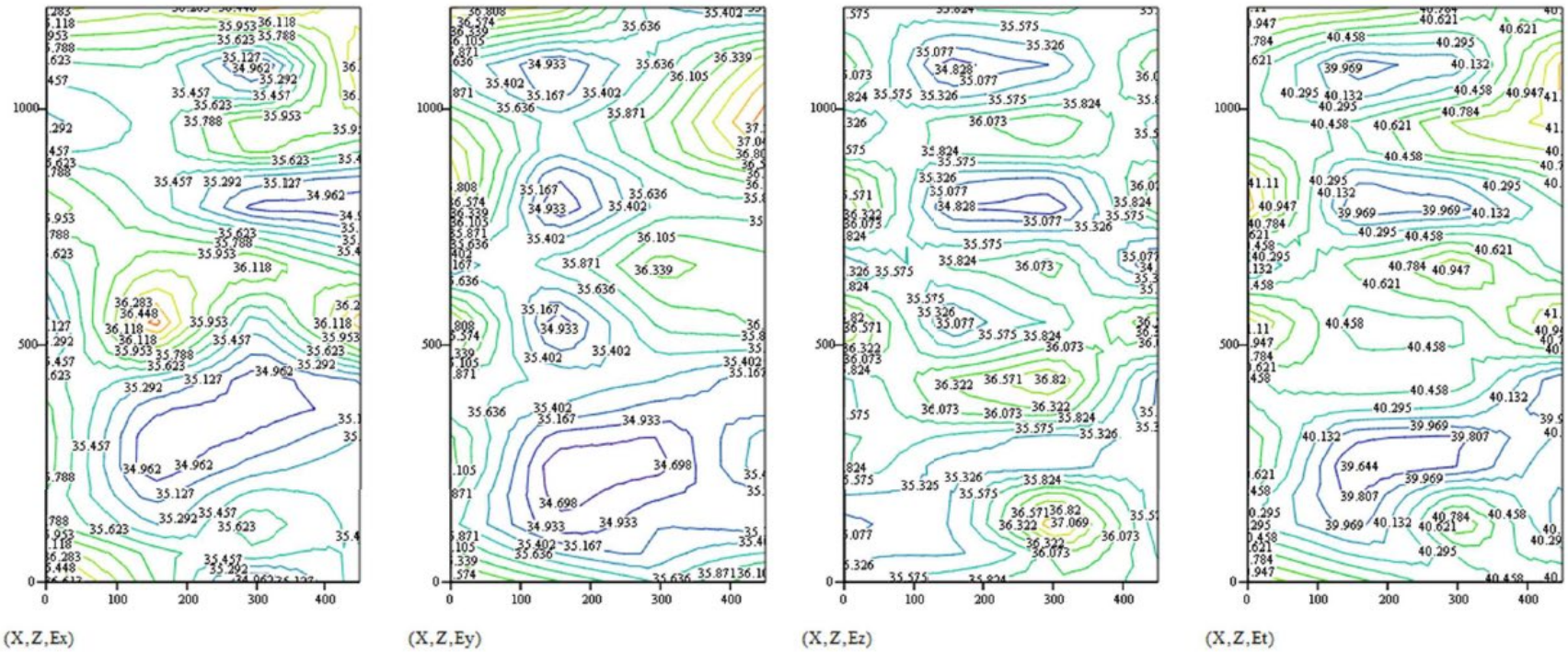

Figure A-41. Rear Plane at Y = 0 mm – 1,900 MHz

Colored contours in the figure show the directed components of the E-field (X-Component, Y-Component, and Z-Component, or Ex, Ey, and Ez), and total E-field (Et) in dBV/m in the plots from left to right. Axes show distance in millimeters.

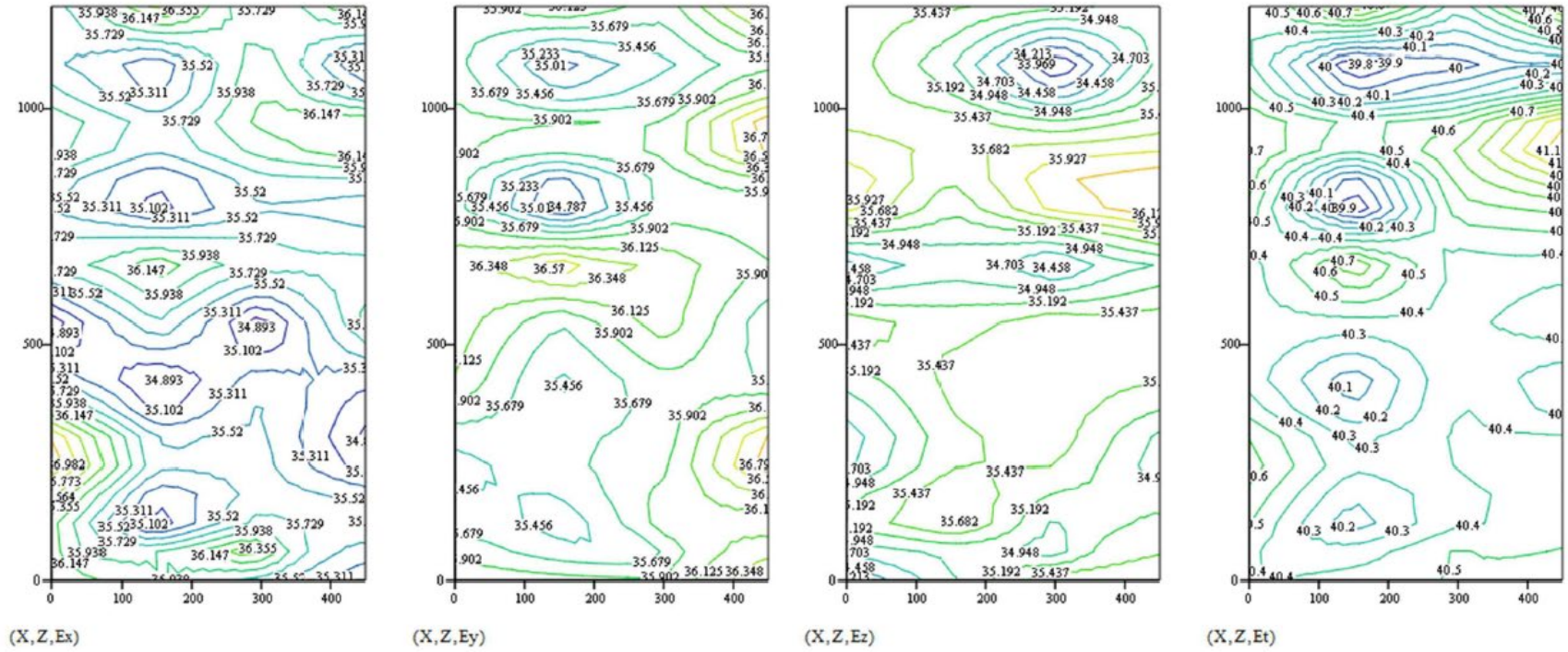

Figure A-42. Middle Plane at Y = 95 mm – 1,900 MHz

Colored contours in the figure show the directed components of the E-field (X-Component, Y-Component, and Z-Component, or Ex, Ey, and Ez), and total E-field (Et) in dBV/m in the plots from left to right. Axes show distance in millimeters.

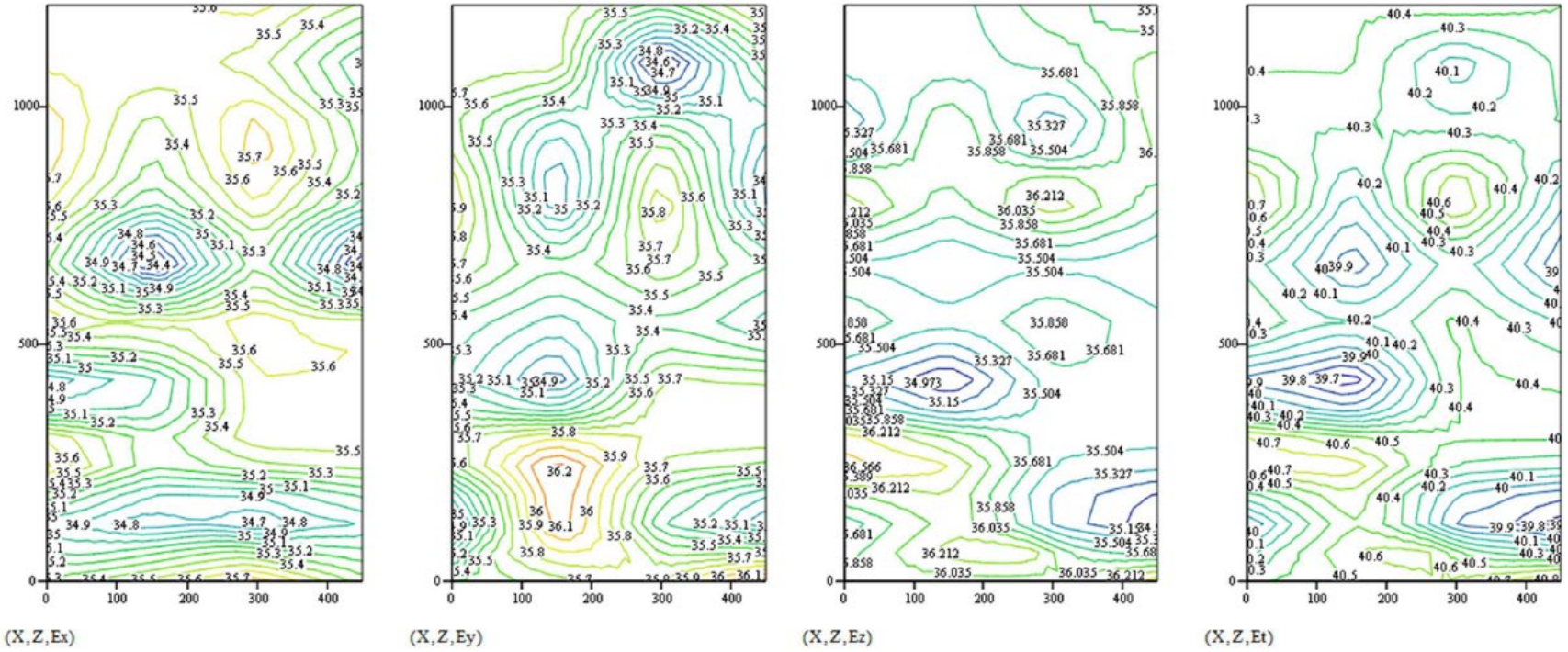

Figure A-43. Front Plane at Y = 190 mm – 1,900 MHz

Colored contours in the figure show the directed components of the E-field (X-Component, Y-Component, and Z-Component, or Ex, Ey, and Ez), and total E-field (Et) in dBV/m in the plots from left to right. Axes show distance in millimeters.

A.10. Stirrer Modulation

The aim of these NIEHS/DTT studies was to mimic mobile handset-like exposure conditions inside the reverberation chambers, as in the previous NTP studies. The modulation of the RF carrier is one element; the second is how the output power of a handset varies within the communication network. In these studies, one of two different digital cellular communication signals (GSM and IS-95 CDMA) was applied within the chambers. This section includes the rationales for the signal concepts and proposed methodologies to achieve exposure conditions inside the chambers that could mimic the real-life power control variations.

A.10.1. GSM Mobile Station Signal

The signal from GSM mobile handsets is mainly determined by the multiple access method applied. GSM facilitates both frequency division multiple access (FDMA) and time division multiple access (TDMA). For FDMA, the GSM band is divided into channels 200 kHz wide. As a complement to FDMA, a TDMA mechanism enables up to eight time slots (voice channels) per frequency channel (i.e., a mobile handset transmits in only one out of eight available channels during a voice communication), which introduces a pulsed signal shape with a pulse repetition rate of 217 Hz. Such a TDMA frame has a length of 4.6 ms, and 26 TDMA frames make up a multiframe with a 120 ms duration. During a multiframe, a mobile handset transmits in 25 out of 26 possible time slots. This TDMA frame structure causes significant low-frequency components to be superimposed on the RF carrier at 8.3 and 217 Hz. In GSM, the duplexing between the uplink (handset transmits to the base station) and downlink (base station transmits to the handset) is implemented in the frequency and time domains, and the frequency spacing between uplink and downlink frequencies is kept constant. The downlink frequency is chosen according to the cell (i.e., the area covered by a base station into which the mobile handset is allocated). To minimize interference between neighboring cells, a frequency reuse policy is applied. This policy implies that when a mobile handset is handed over (i.e., moves from one cell to another), the frequencies in the uplink and downlink change, and the transmit frequency changes. The power levels after power control signal from the base station exhibit a stepwise response. The power control has a dynamic range of 30 dB subdivided into 2 dB power level steps. The power control is typically implemented by means of a slow associated-control channel, which facilitates a power-control update rate no faster than every four multiframes (i.e., every 480 ms). Once a target power level is received, the mobile station is able to regulate its power in 2 dB steps every 60 ms (i.e., a power regulation over 15 steps [full dynamic range] takes 900 ms). GSM base stations, however, typically average the received signal strength from a mobile handset over 1 s, such that the actual power regulation usually takes place after multiples of 480 ms.

In summary, the main extremely low-frequency (ELF) component of the GSM system is composed of a 217 Hz TDMA frame, 8.3 Hz multiframe, 2 Hz discontinuous transmission (DTx), and <1 Hz power control.

A.10.2. Interim Standard 95 (i.e., CDMA) Mobile Station Signal

IS-95 (also known as TIA-EIA-95) is the first CDMA-based digital cellular communication standard. The system's multiple access is based entirely on code division separation of mobile stations as well as base stations, which implies that the signal structure is significantly different

from that of GSM. In the forward downlink, a set of 64 Walsh codes, which are deterministic and orthogonal, are applied to spread and separate the individual channels in the downlink of a cell. After orthogonal spreading, a short 16-bit pseudo noise (PN) code is applied to further spread the signal and identify the cell. Hence, separation of neighboring cells in the frequency domain is no longer necessary.

Eventually, there is no need for the mobile station to change its transmission frequency during the transition from one cell to another. Since Walsh codes require a synchronous system in the reverse uplink, only long 42-bit PN codes are applied. As with GSM, duplexing between the forward and reverse links is implemented in the frequency domain. In CDMA systems, efficient power control is crucial. Because all mobile stations transmit and interfere in the same frequency channel, each mobile decreases the signal to noise ratio of all the other mobiles. Hence, the output power of a mobile handset should be kept to the minimum level that guarantees good voice quality. On the other hand, when moving around, the mobile handset is subject to slow and fast fading, shadowing, and external interferences. To keep the output power low and compensate for the effects of changing communication channel loss, fast power control is necessary. When an IS-95 (i.e., CDMA) mobile station is actively communicating, a closed-loop power control is applied. The base station monitors the signal quality in the reverse link and inserts power control bits in the communication channel, which facilitates power control over a dynamic range of 48 dB in 1 dB steps with an update rate of 800 Hz. The power control is implemented by sending a binary value of 1 to regulate the transmit power by 1 dB down and a value of 0 to regulate the transmit power by 1 dB up. A quasi-static power level is therefore implemented with an alternating 0101 power control pattern.

A.10.3. Mobile Station Signals in Real Networks

To determine the time-domain signal behavior (i.e., the ELF components from the power control and frame structure superimposed on the RF carrier), mobile stations in real networks were evaluated. The System Network and Handset Analyzer (SYNEHA; Figure A-44) was used to evaluate mobile stations in real networks. The mobile system measures the output power of mobile phones attached to phantom heads while moving through a cellular network. The system is able to measure variations in mobile phone output power at rates of up to 2 kHz.

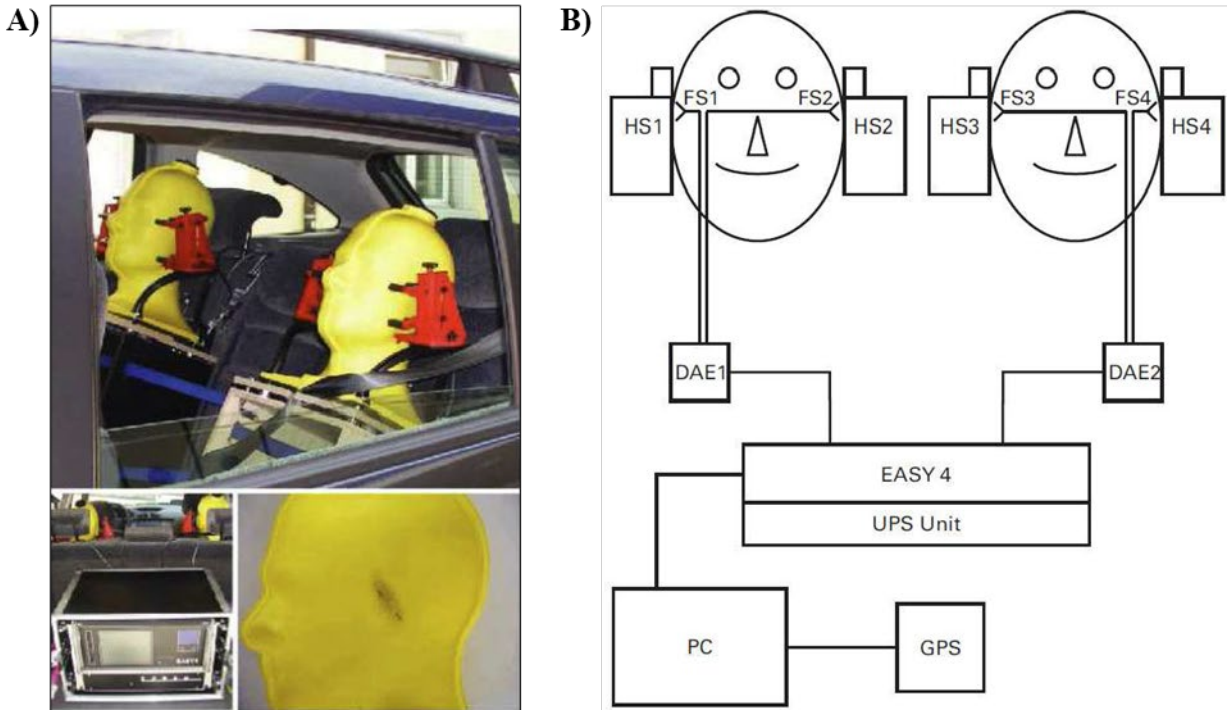

Figure A-44. System Network and Handset Analyzer

(A) Phantom heads with mobile phones and System Network and Handset Analyzer (SYNEHA) data acquisition system mounted inside the measurement vehicle. (B) Block diagram of the SYNEHA measurements system. Examples shown are the two specific anthropomorphic mannequin phantom heads with mobile phone handsets (HS) attached to each ear. The field sensors (FS) measure the E-field inside the phantom. This field is analog-to-digital converted and optically forwarded by the data acquisition electronics (DAE). The Exposure Acquisition System (EASY4) is used as a data logger for the field values. The personal computer (PC) controls the system and stores the field and position data. Figure adapted from Capstick et al.[17]
UPS = uninterruptible power supply; GPS = global positioning system.

In Figure A-45, the ELF components resulting from a GSM mobile phone moving through a highway and an urban environment are shown. Despite the different environments, significant low-frequency components resulting from the access scheme (time slots and data frames) and handovers can be identified at 8.3 Hz (multiframe) as well as in the sub-Hz range. In contrast to GSM, in IS-95 (i.e., CDMA), no such significant components can be identified in the ELF spectrum moving through suburban environments (Figure A-46).

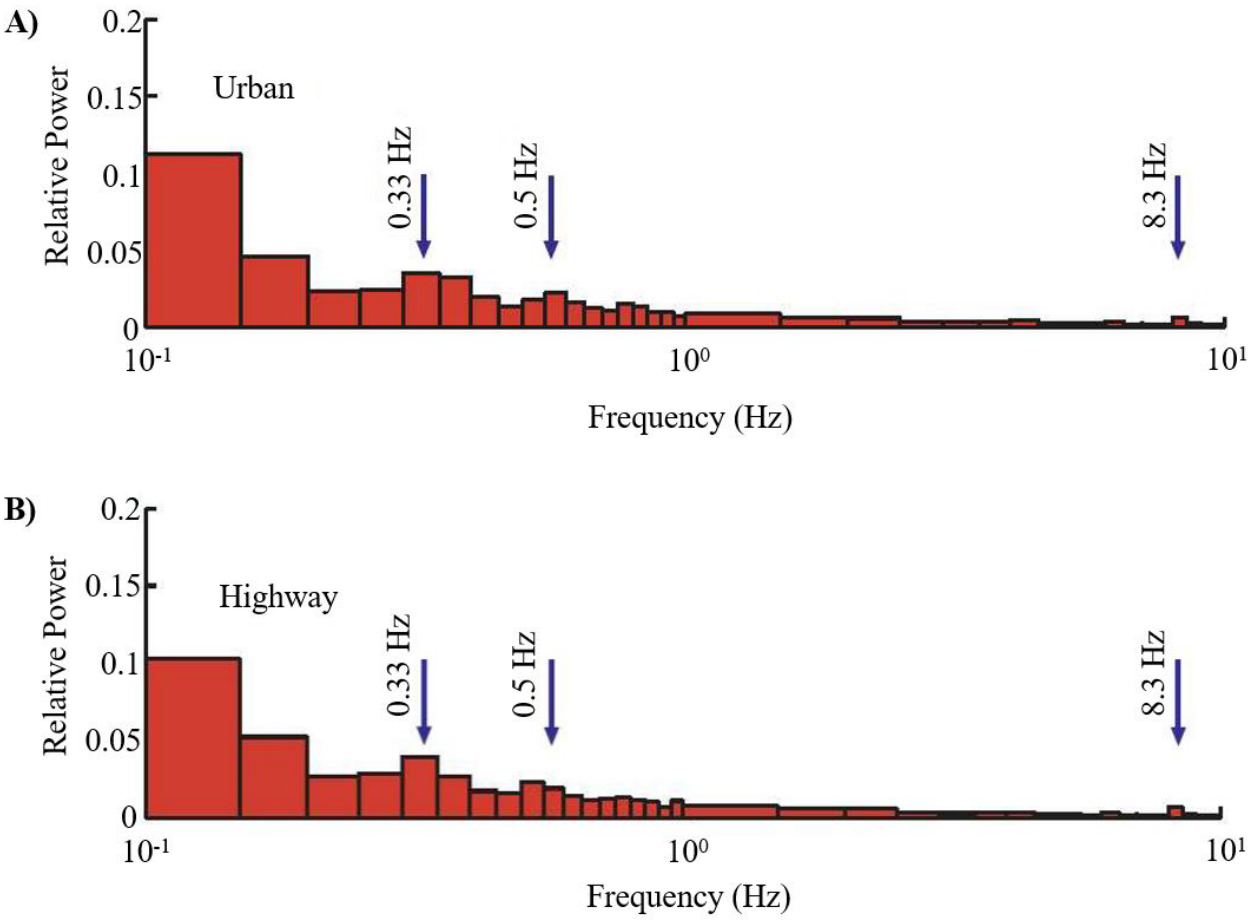

Figure A-45. GSM Extremely Low-Frequency Components in Urban and Highway Environments

Figure adapted from Capstick et al.[17] GSM = Global System for Mobile Communications-modulated cell phone radiofrequency radiation.

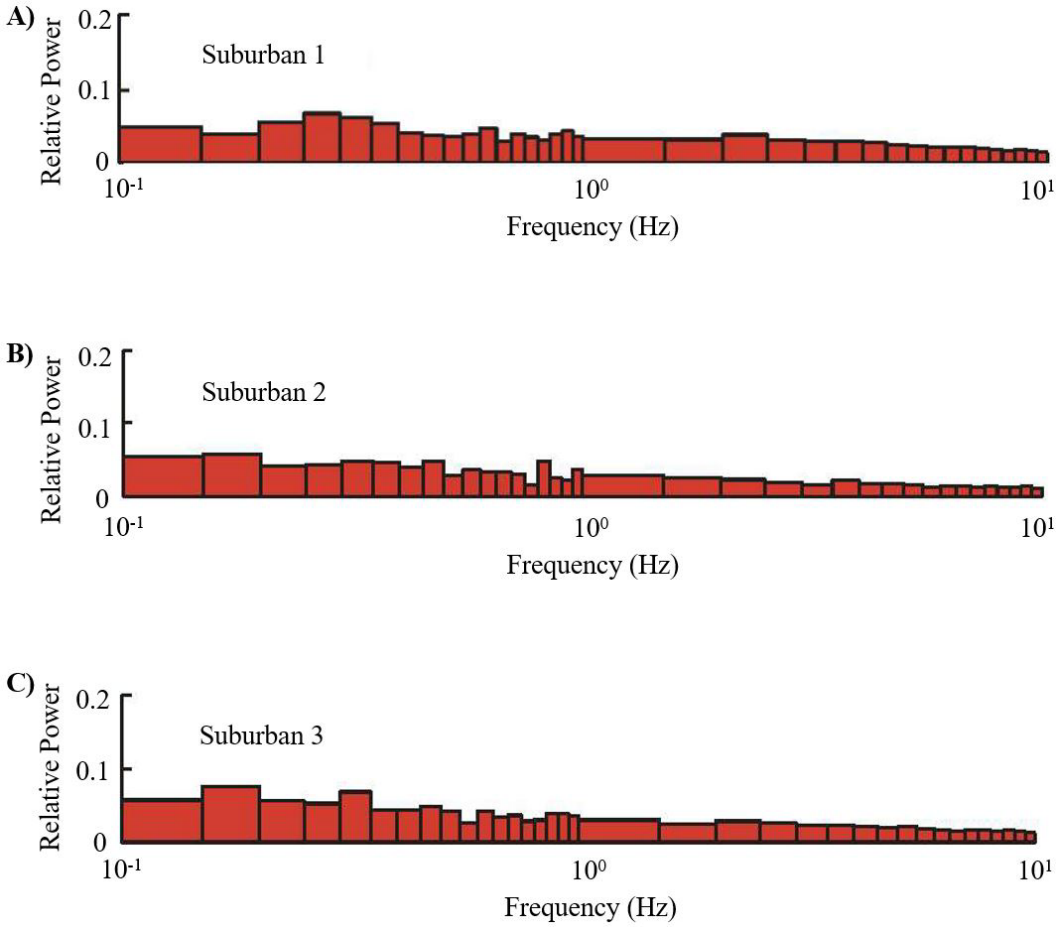

Figure A-46. Interim Standard 95 (i.e., CDMA) Extremely Low-Frequency Components in Suburban Environments

Figure adapted from Capstick et al.[17] CDMA = Code Division Multiple Access-modulated cell phone radiofrequency radiation.

A.10.4. Signals in the Experiment

In the experiment, the GSM and IS-95 (i.e., CDMA) signals provided by the signal generators represent a standard voice call with a PN data sequence being transmitted. To also mimic the ELF components of GSM and IS-95 (i.e., CDMA) mobile phones in a real network, the appropriate stirrer speeds were determined. The time-domain field variations of a continuous wave (CW) signal applied to the fully loaded chamber were measured with an antenna placed in the chamber. Time-domain sampling was performed over a period of 60 or 120 s with a diode detector and a digital oscilloscope to allow an integral number of stirrer rotations to be sampled. The detector voltages were then converted to powers, and fast Fourier transform was performed to obtain the frequency domain low-frequency power distribution of the stirrer modulation. Many combinations of stirrer speeds were measured, and those that best represented the ELF components because of power control were selected for the exposure experiments. The chosen stirrer speeds shown in Table A-16 indicate the figures corresponding to the resulting spectra.

Table A-16. Horizontal and Vertical Stirrer Speed Combinations for GSM and IS-95 (i.e., CDMA) Modulation

Frequency	Modulation	Horizontal (rpm)	Vertical (rpm)	Figure
900 MHz	GSM	6.0	4.0	Figure A-47
900 MHz	IS-95 CDMA	7.0	9.0	Figure A-48
1,900 MHz	GSM	2.85	5.70	Figure A-49
1,900 MHz	IS-95 CDMA	4.5	5.0	Figure A-50

GSM = Global System for Mobile Communications-modulated cell phone radiofrequency radiation; IS-95 = International Standard 95; CDMA = Code Division Multiple Access-modulated cell phone radiofrequency radiation.

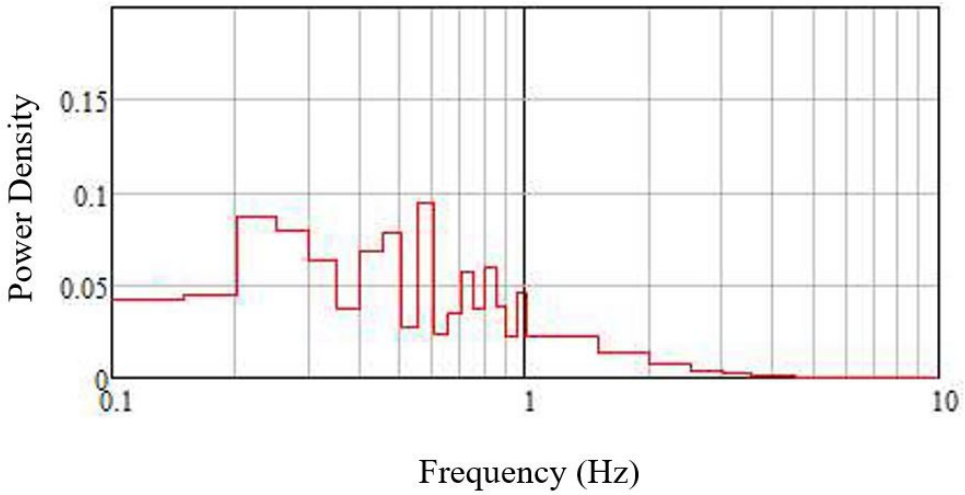

Figure A-47. 900 MHz GSM

GSM = Global System for Mobile Communications-modulated cell phone radiofrequency radiation.

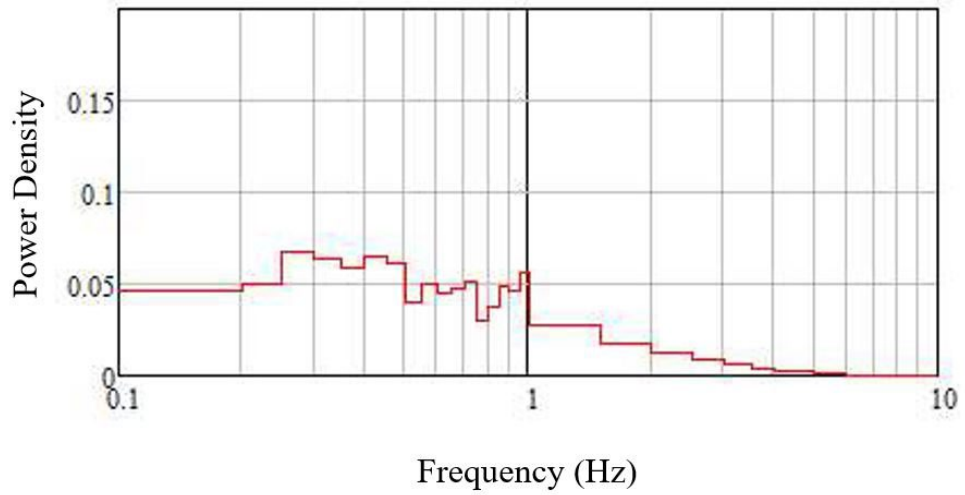

Figure A-48. 900 MHz Interim Standard 95 (i.e., CDMA)

CDMA = Code Division Multiple Access-modulated cell phone radiofrequency radiation.

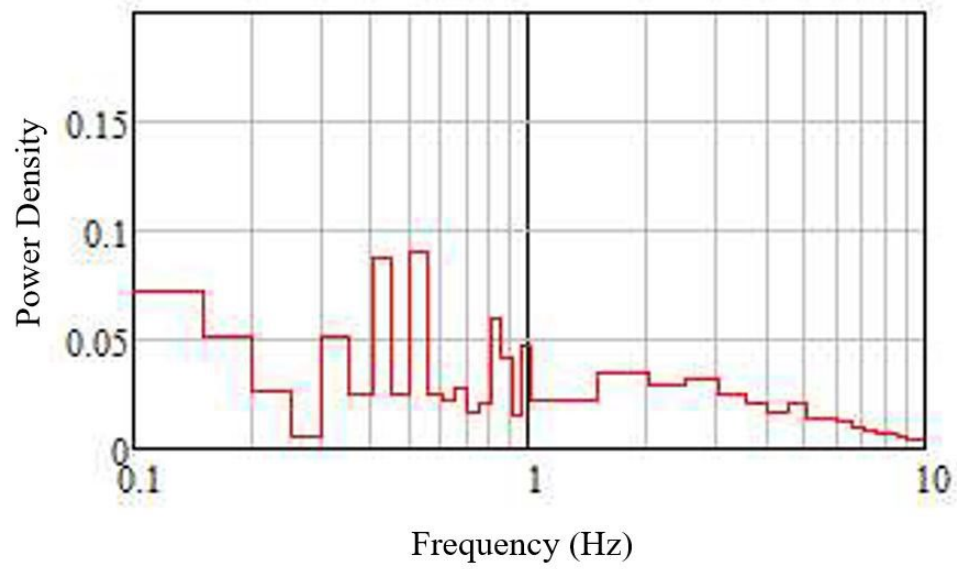

Figure A-49. 1,900 MHz GSM

GSM = Global System for Mobile Communications-modulated cell phone radiofrequency radiation.

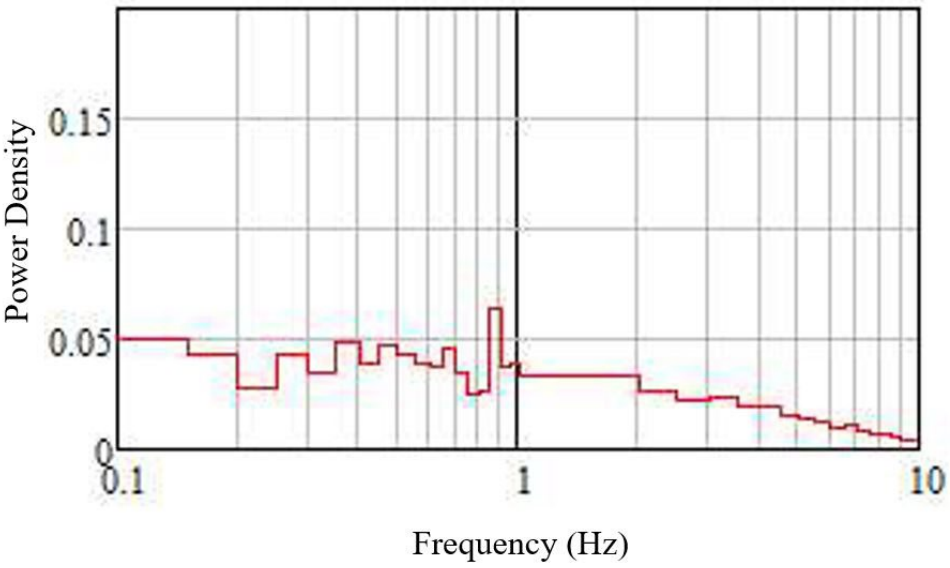

Figure A-50. 1,900 MHz Interim Standard 95 (i.e., CDMA)

CDMA = Code Division Multiple Access-modulated cell phone radiofrequency radiation.

A.11. Dosimetry

Dosimetry in the fields of health physics and radiation protection is the measurement, calculation and assessment of internal exposure to the body. Nonionizing radiation dosimetry within the RF range is quantified as the SAR. The SAR is expressed in W/kg body weight (W/kg). It is not possible to measure induced fields or SAR directly in a subject (humans or animals); thus, the electromagnetic fields that a subject is exposed to are measured and numerical simulations using different postures of anatomical models are performed representing different species, sexes, and age groups (numerical dosimetry). If the incident field is well characterized, the correlation between incident field conditions and the fields induced in the different tissues and organs can be established. However, the correlation needs to be verified experimentally using homogeneous phantoms (experimental dosimetry).

The numerical dosimetry for both rats and mice was reported in Gong et al.[18] and relates to the SAR induced in the bodies (whole-body and tissue specific) for a given incident field strength within a reverberation chamber environment as a function of the animal's body weight (Figure A-51).

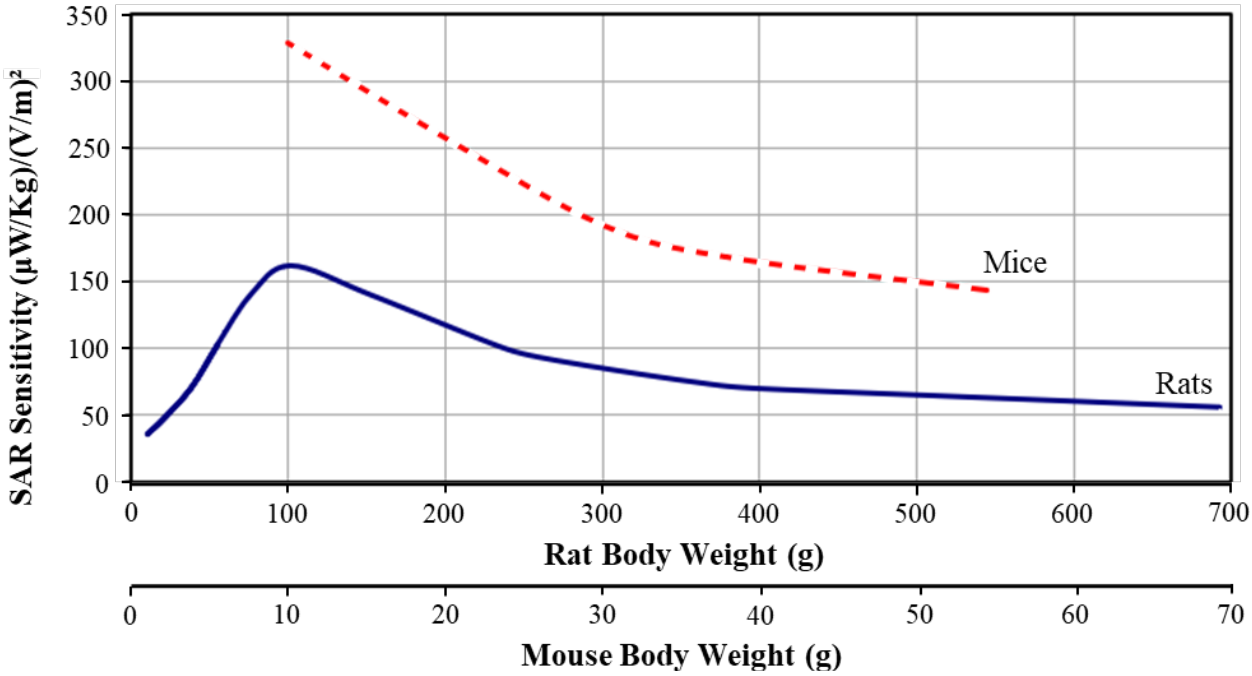

Figure A-51. Specific Absorption Rate Sensitivity for Rats at 900 MHz and Mice at 1,900 MHz as a Function of Body Weight Based on Numerical Dosimetry Using Anatomical Models

Figure adapted from Gong et al.[18] SAR = specific absorption rate.

A.11.1. Experimental Dosimetry Phantoms

Experimental dosimetry was performed in the study chambers using the control system designed and fabricated for these studies. During system testing, animal surrogates, or "phantoms" were used. Each phantom consisted of a container with a low-dielectric-constant, low-loss material filled with an appropriate volume of tissue-simulating liquid. The appropriate tissue-simulating liquid was selected following simulations of the whole-body average SAR (SAR_{WB}) efficiency

achieved with liquids of varying dielectric constants and loss tangents compared to that of the actual full anatomical body model of the animal with the same weight.

Simulations of full anatomical models of the rat or mouse provided the SAR distribution across all tissues, which was then averaged to provide the overall average SAR. The overall average SAR was then normalized to an incident field strength of 1 V/m to provide the SAR_{WB} sensitivity. Simulations of the phantoms filled with a selection of tissue-simulating liquids were performed, and the tissue-simulating liquid that provided the closest average SAR value was selected. The chosen liquids were not meant to represent the average tissue properties of a rat or mouse but to represent the same absorption, which is related not only to individual tissue properties within the anatomical model but also the inhomogeneous field distribution.

For the male rats, a nominal 0.5 L bottle filled to the top with approximately 550 mL tissue-simulating liquid was used for the male rat phantom. The specific tissue-simulating liquid used for the rat was head-simulating liquid (HSL) 900 (SPEAG, Switzerland), with properties $\varepsilon_r = 41.5$, $\sigma = 0.97$ S/m, which provided a good match to the whole-body anatomical rat. Figure A-52 shows the physical rat phantom and the corresponding model used for numerical dosimetry.

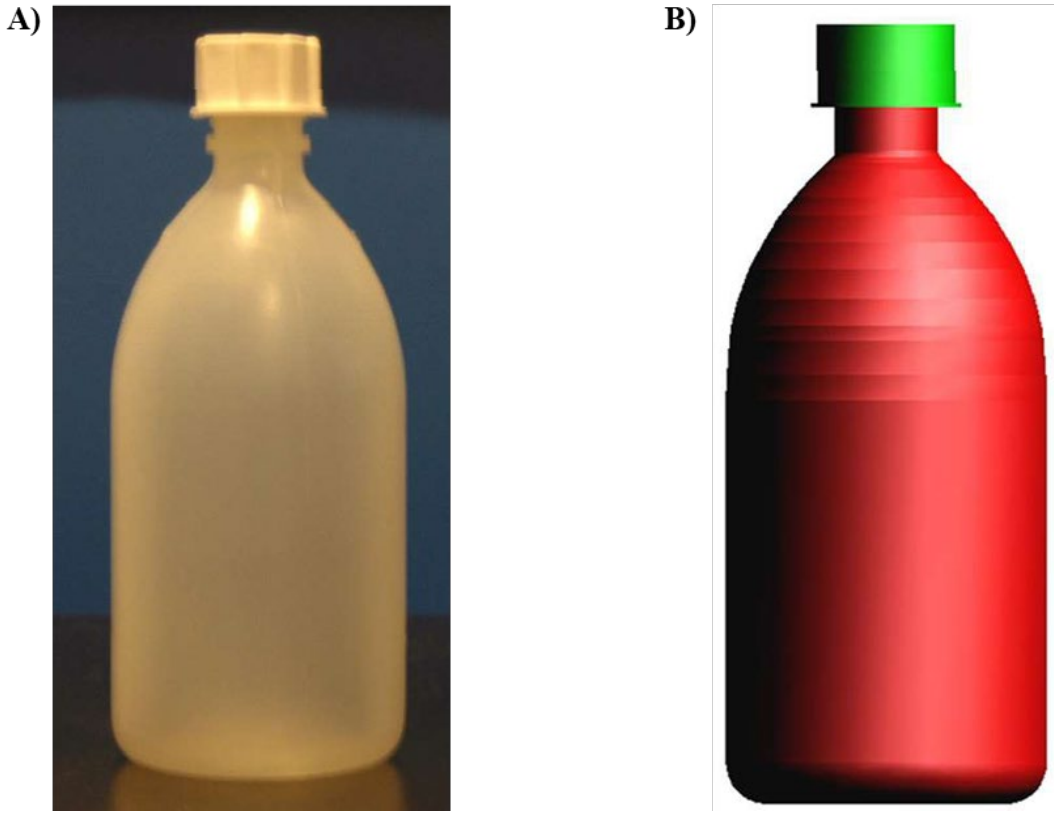

Figure A-52. (A) Rat Phantom and (B) SEMCAD Model of the Rat Phantom

From the simulations, the average SAR_{WB} efficiency could be determined. Figure A-53 illustrates the SAR distribution induced by the isotropic field from which the whole-body average was calculated and the SAR efficiency determined. For the male rat phantom filled with 550 mL HSL900, the SAR_{WB} efficiency was 5.556×10^{-5} (W/kg)/(V^2/m^2).

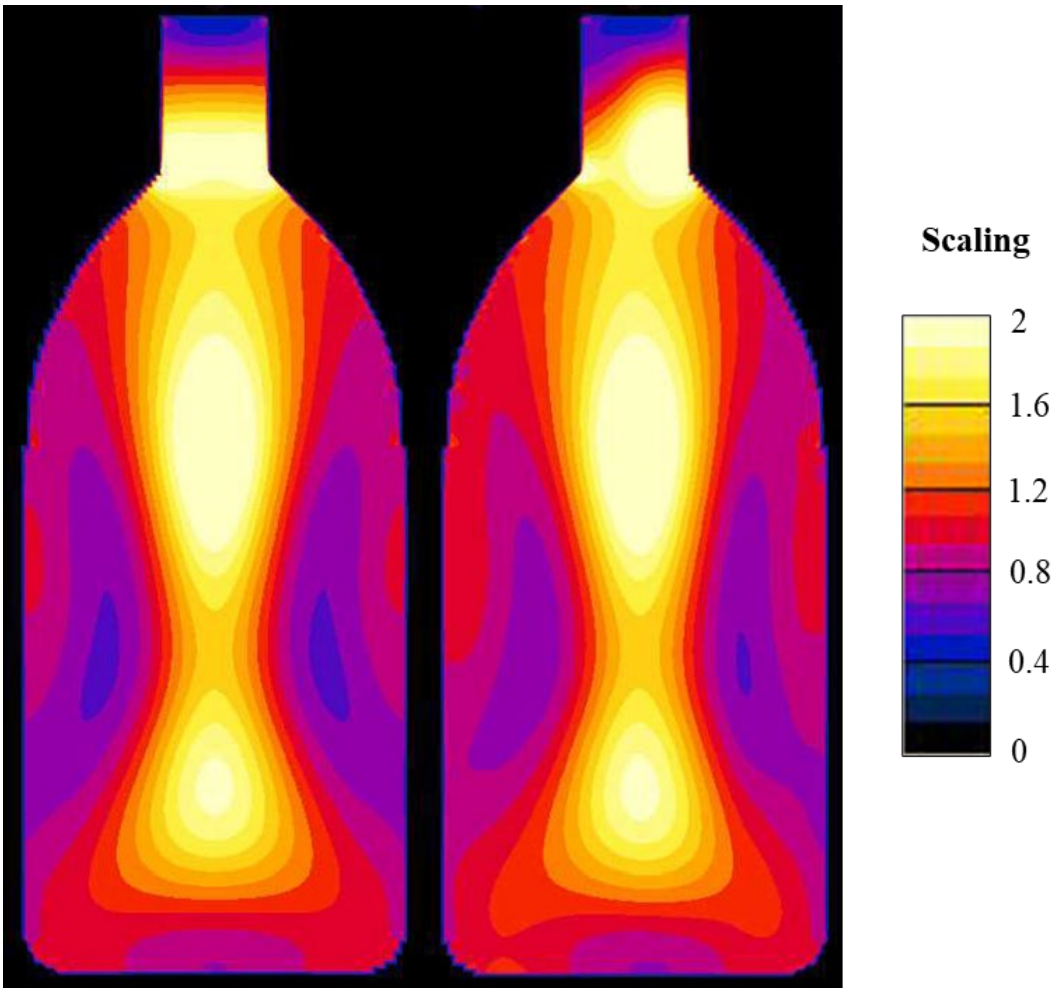

Figure A-53. Male Rat Phantom Specific Absorption Rate Distribution

For the physical mouse phantom, a nominal 50 mL conical centrifuge tube filled to the top with 55 mL of HSL1900 (SPEAG, Switzerland) was used. HSL1900 is the tissue-simulating liquid, with properties $\varepsilon_r = 40.0$, $\sigma = 1.40$ S/m, that provided the best match to the SAR_{WB} efficiency of the mouse. The average SAR_{WB} efficiency for the mouse phantom was 1.50×10^{-4} $(W/kg)/(V^2/m^2)$.

Figure A-54 shows the physical mouse phantom, the corresponding SEMCAD model, and the simulated SAR distribution in the phantom.

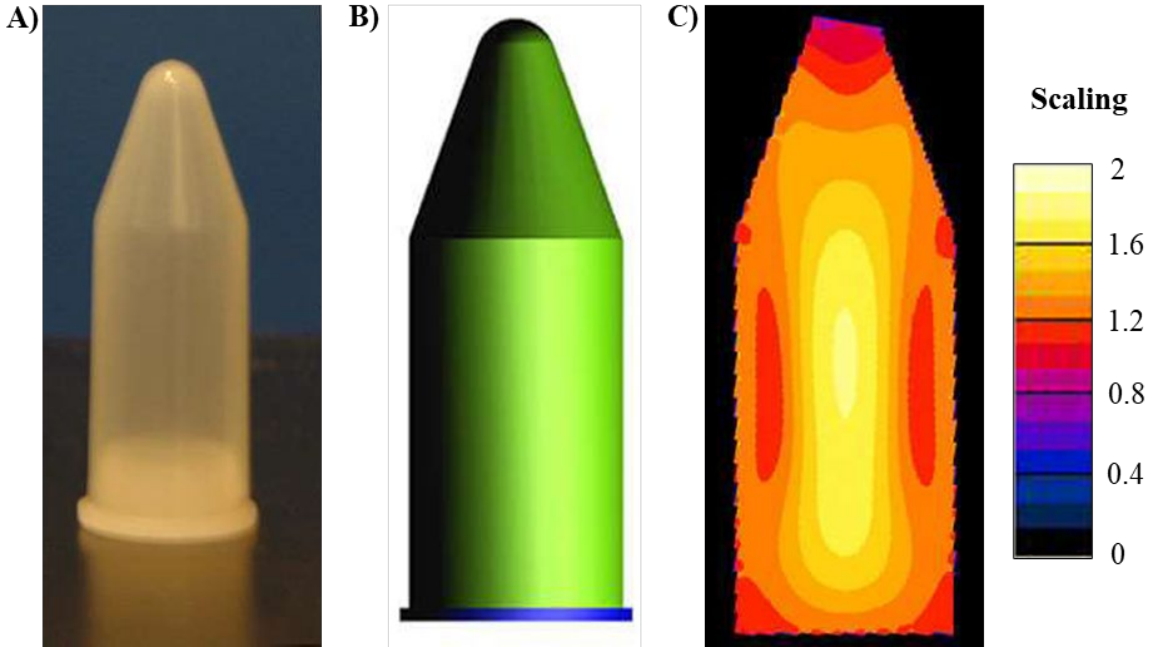

Figure A-54. (A) Mouse Phantom, (B) Sim4Life Phantom Model, and (C) Simulated Specific Absorption Rate Distribution in the Phantom

A.11.2. Temperature Method

The SAR in the animal phantoms was assessed experimentally using the temperature method. In this method, animal phantoms were exposed to RFR in a chamber while the temperature of the liquid was monitored. When a liquid phantom was exposed to RF, the temperature change was measured during the applied RFR (i.e., the heating phase), and after RF was switched off (i.e., the cooling phase), and the heat transfer time constant τ was determined. By applying the lumped-heat-capacity method described in *Heat Transfer*,[19] the liquid temperature follows the differential equation below, based on cooling to the ambient temperature of the environment and RF heating, encompassing a cooling term due to heat loss to the environment and a heating term due to power absorption:

$$\frac{dT}{dt} = \frac{-\left(T_{liquid} - T_{ambient}\right)}{\tau} + \frac{SAR_{WB}}{C_{liquid}}$$

where C_{liquid} is the heat capacity of the tissue-simulating liquid, T is temperature, t is time, τ is the time constant, and ΔT is the temperature increase in the liquid (i.e., $T_{liquid} - T_{ambient}$). Two processes are possible: (1) when RF is on, the liquid temperature increases until an equilibrium state is reached, whereby the rate of heat absorbed due to the RF exposure and the rate of heat loss due to convection are equal; (2) when RF is off, the liquid cools through heat convection toward the lower temperature of the environment. SAR values were determined by solving the differential equation for long exposure times ($t >> \tau$) of the heating curve equation when the system is in an equilibrium temperature state:

$$SAR_{WB} = C_{liquid}\frac{\Delta T}{\tau}$$

where C_{liquid} is the heat capacity of the tissue-simulating liquid, τ is the time constant, and ΔT is the temperature increase in the liquid. The determination of SAR_{WB} requires that the temperature of the environment remains constant, coupled with measurements of the absolute temperature of the dummy liquid, measurements of the room temperature, and determination of the time constant τ. The latter was determined by fitting the theoretical curve to the recorded temperature change in the dummy liquid during the heating process.

The time constant of the process can be calculated from either the heating or cooling curve; however, the RF power during the warm-up phase of the power amplifiers can vary by several dB, resulting in increased uncertainty. Consequently, use of the cooling curve is preferred. The stated uncertainty of the temperature probes used in these measurements is ±0.2°C.

A.11.3. Verification of Rat Dosimetry

The 10 male rat phantoms were placed in cages and positioned in the chamber. Two phantoms were equipped with fixed temperature sensors to evaluate the heating and cooling time constants, Figure A-55 and Figure A-56. The target field strength was set to 400 V/m. The E-field strength, air temperature, and phantom temperature were recorded during the course of the dosimetry. To ensure that the ambient temperature did not change significantly, air was circulated through the chamber and cooler outside air let into the room periodically.

Figure A-55. Rat Phantom with Temperature Sensor

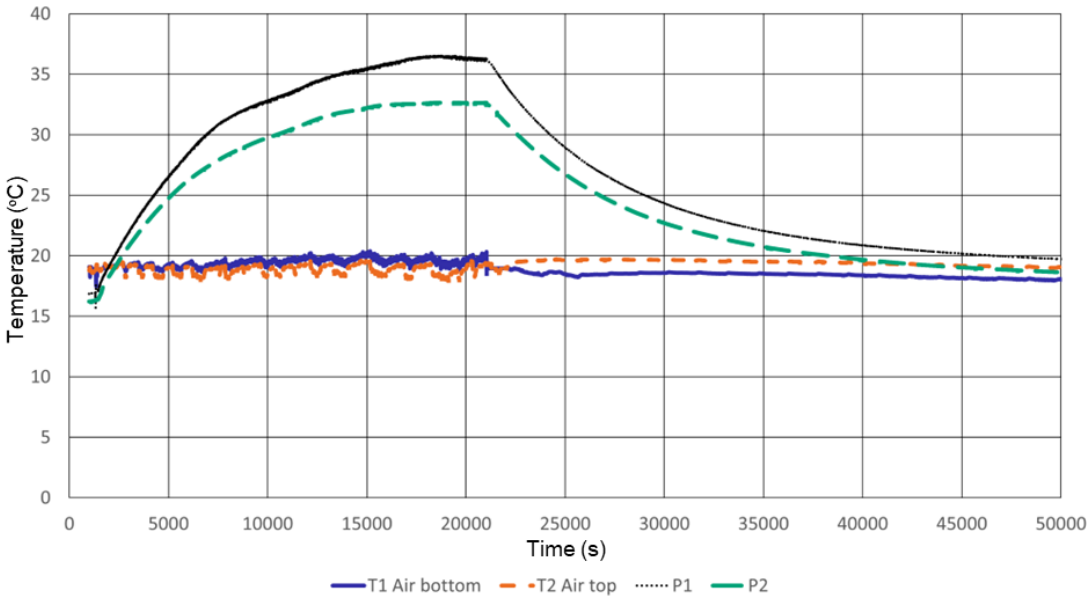

Figure A-56. Typical Rat Phantom (Phantoms P1 and P2) Heating and Cooling Curves

Figure shows ΔT as a function of time and ambient air temperature at two locations.

The SAR uniformity was determined by measuring the phantoms immediately after the power was shut off in as short a time as possible. The cooling of the phantoms was corrected via reference to the phantom(s) using fixed temperature probes that were present throughout the experiment. The data in Table A-17 show excellent agreement—a difference of about 0.36 dB—between the SAR calculated from the field strength present and the SAR measured.

Table A-17. Rat Dosimetry: Comparison of Calculated and Measured Specific Absorption Rate

Rat Dosimetry	Value
Calculated SAR	
E-field (V/m)	402.25
SAR Efficiency ((W/kg)/(V^2/m^2))	5.56×10^{-5}
SAR (mW/mL)	8.99
Measured SAR	
CW (J/kg*K)	3,766
ΔT (°C)	15.97
τ (s)	7,169
SAR (mW/g)	8.28
Difference in SAR (dB)	−0.36

SAR = specific absorption rate.

The uniformity in the male rat phantoms was assessed in the eight phantoms without fixed temperature sensors by measuring the final temperature. The uniformity (standard deviation) in the SAR was 0.36 dB and was within ±0.6 dB of the mean with all phantoms.

A.11.3.1. 900 MHz Dosimetry Uncertainty

The uncertainty for the rat dosimetry (Table A-18) was based on the values provided for the measurement instrumentation and observed variations in room temperature and time constant.

Table A-18. Uncertainty in the Rat Dosimetry

Equipment/Factor	Uncertainty Distribution	Divisor ×	Coverage	Standard Uncertainty
Absolute Accuracy of the E- and H-field Probe	±0.26 dB	Normal	1	±0.26 dB
Frequency Linearity	±0.2 dB	Rectangular	√3	±0.12 dB
Dynamic Range Linearity	±0.2 dB	Rectangular	√3	±0.12 dB
Isotropy	±0.4 dB	Rectangular	√3	±0.12 dB
Temperature Probe Accuracy	±0.05°C	Normal	1	±0.02 dB
Room Temperature Fluctuations	±0.12 dB	Normal	1	±0.12 dB
Field Control	±0.2 dB	Normal	1	±0.20 dB
Time Constant Uncertainty	±0.12 dB	Normal	1	±0.12 dB
Combined Standard Uncertainty				±0.47 dB

A.11.4. Verification of Mouse Dosimetry

Ten mouse phantom positions within the chamber were measured using two phantoms with temperature sensors installed (Figure A-57). The temperature was monitored to determine when it approached a constant value at each location, before the phantoms were moved to the next location, which was repeated five times to get 10 positions (i.e., one position in each cage). The

final temperature was determined by fitting the "best fit" theoretical curve to each portion of the temperature curves. The time constant was determined from the cooling curve (Figure A-58).

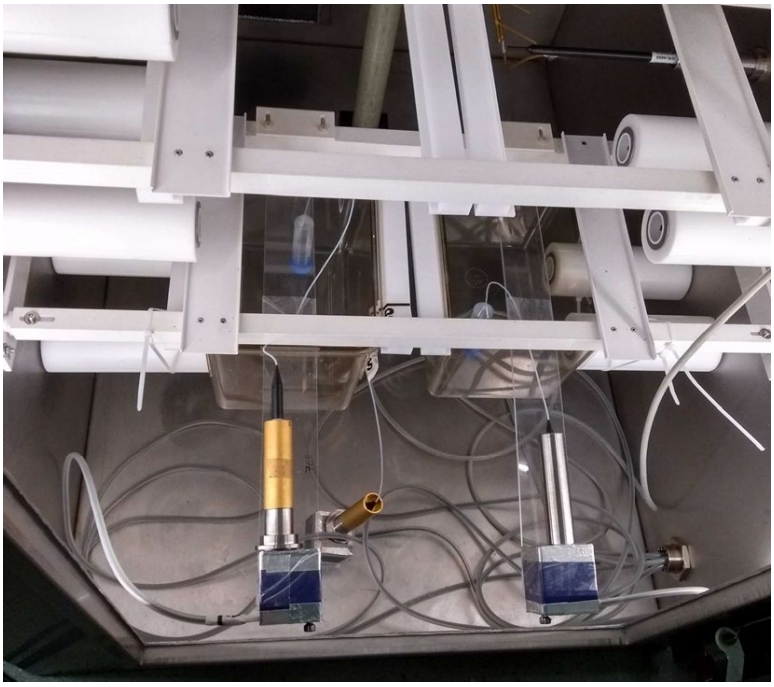

Figure A-57. Mouse Phantoms with Temperature Sensors

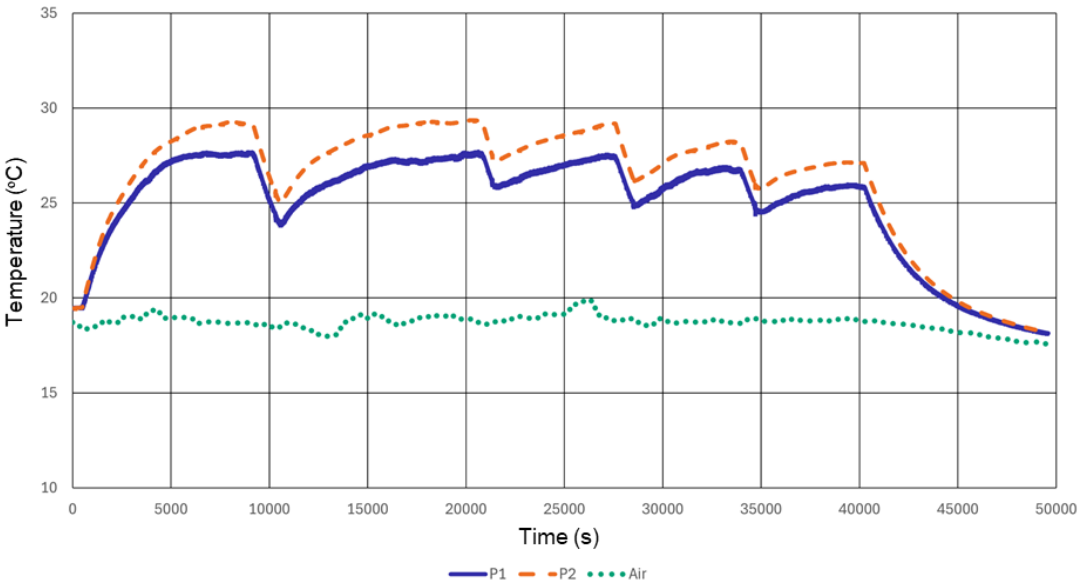

Figure A-58. Mouse Phantoms (Phantoms P1 and P2) and Air Temperature Plots

Figure shows ΔT as a function of time and ambient air temperature at ten locations using two phantoms.

The SAR uniformity was determined by measuring and estimating the final temperatures of all phantoms. The cooling time constant was then used to calculate the SAR with temperature probes present throughout the experiment. The data in Table A-19 show excellent agreement—a difference of about 0.2 dB—between the SAR calculated from the field strength present and the SAR measured.

Table A-19. Mouse Dosimetry: Comparison of Calculated and Measured Specific Absorption Rate

Mouse Dosimetry	Value
Calculated SAR	
E-field (V/m)	301
SAR Efficiency ((W/kg)/(V^2/m^2))	1.50×10^{-4}
SAR (mW/g)	13.58
Measured SAR	
CW (J/kg*K)	3,767
ΔT (°C)	9.52
τ (s)	2,526
SAR (mW/mL)	14.19
Difference in SAR (dB)	0.18

SAR = specific absorption rate.

The uniformity (standard deviation) in the SAR was 0.5 dB and within ±0.9 dB of the mean with all phantoms. Hence, the uniformity for the mouse is also considered excellent.

A.11.4.1. 1,900 MHz Dosimetry Uncertainty

The uncertainty in the mouse dosimetry (Table A-20) is based on the values provided for the measurement instrumentation and observed variations in room temperature and time constant.

Table A-20. Uncertainty in the Mouse Dosimetry

Equipment/Factor	Uncertainty Distribution	Divisor ×	Coverage	Standard Uncertainty
Absolute Accuracy of the E- and H-field Probe	±0.26 dB	Normal	1	±0.26 dB
Frequency Linearity	±0.2 dB	Rectangular	√3	±0.12 dB
Dynamic Range Linearity	±0.2 dB	Rectangular	√3	±0.12 dB
Isotropy	±0.4 dB	Rectangular	√3	±0.12 dB
Temperature Probe Accuracy	±0.05°C	Normal	1	±0.02 dB
Room Temperature Fluctuations	±0.34 dB	Normal	1	±0.34 dB
Field Control	±0.2 dB	Normal	1	±0.20 dB
Time Constant Uncertainty	±0.21 dB	Normal	1	±0.21 dB
Combined Standard Uncertainty				±0.59 dB

A.11.5. Verification of the Effect of the Water System on the Dosimetry

The fields around the water system were measured with respect to the fields measured by the two fixed probes in the chamber (Figure A-59).

Figure A-59. Field Probe Arrangement

At 900 MHz, the field strength at the lixit was well below the nominal chamber field strength, showing that the rats would be safe (i.e., that exposure would not be higher than the target SAR) while drinking (Table A-21). The field at the flange was slightly above that of the nominal field but within the variation measured during the homogeneity measurement of the empty chamber, which was up to 3 dB higher than the average field strength.

Table A-21. E-fields Determined at 900 MHz

$E_{average}$	Flange	Lixit
245 V/m	279 V/m	177 V/m
	1.1 dB	−2.8 dB

Similarly, at 1,900 MHz, the field strength at the lixit was well below the nominal chamber field strength, showing that the mice would be safe (i.e., that exposure would not be higher than the target SAR) while drinking (Table A-22). The field strength at the flange was also lower than that of the nominal field but within the variation measured during the homogeneity measurement within the empty chamber, which was as much as 2.1 dB lower than the average field strength.

Table A-22. E-fields Determined at 1,900 MHz

$E_{average}$	Flange	Lixit
283 V/m	265 V/m	149 V/m
	−0.6 dB	−5.6 dB

In summary, variations in the field strength close to the periphery of the flange on the choke tube—at 1.1 and 0.6 dB with respect to the fixed probes—were well within the variations seen in the empty chamber for both frequencies, 900 MHz and 1,900 MHz. The field strength close to the lixit was always reduced compared to the field strength in the chamber, indicating that the animals would be protected during drinking. The measurement uncertainty is the same as that for the chamber homogeneity (i.e., 0.4 dB).

A.11.5.1. Water System Numerical Dosimetry

The water system employed inside the chambers was based on that used in the previous NTP studies as well as on a system designed by the IT'IS Foundation and developed as part of a European project for use in small desktop chambers. However, as this configuration was new, both numerical and experimental dosimetry were performed using the same methods as employed in the previous NTP studies. Simulations were performed using the FDTD solver in SIM4LIFE (Zurich MedTech, Zürich, Switzerland), using anatomical rat and mouse models from the Virtual Zoo (IT'IS Foundation, Zürich, Switzerland). To determine the potential influence of the water system, results were compared for the rat or mouse drinking from and in the absence of the lixit structure. The scope of the numerical dosimetry was extended to elicit information on the frequency bands over which the water system could be expected to perform safely. The frequency responses for the mouse and rat are shown in Figure A-60 and Figure A-61, respectively. The response bandwidth for the rat water system was much narrower than that of the mouse system and more sensitive to all variations in dimension and posture; hence, operation at frequencies other than that intended was not recommended. The response bandwidth for the mouse water system is broader band, and the system could be operated over the frequency range of 1.8 to 2 GHz. Figure A-62 and Figure A-63 show the details of the SAR distributions from the simulations in the center slice at the center frequency of operation for the mouse and the rat, respectively. The SAR scales are the same throughout, with a scale of 0 to −25 dB, where 0 dB = 1 mW/kg for the field strength of a peak at 1 V/m.

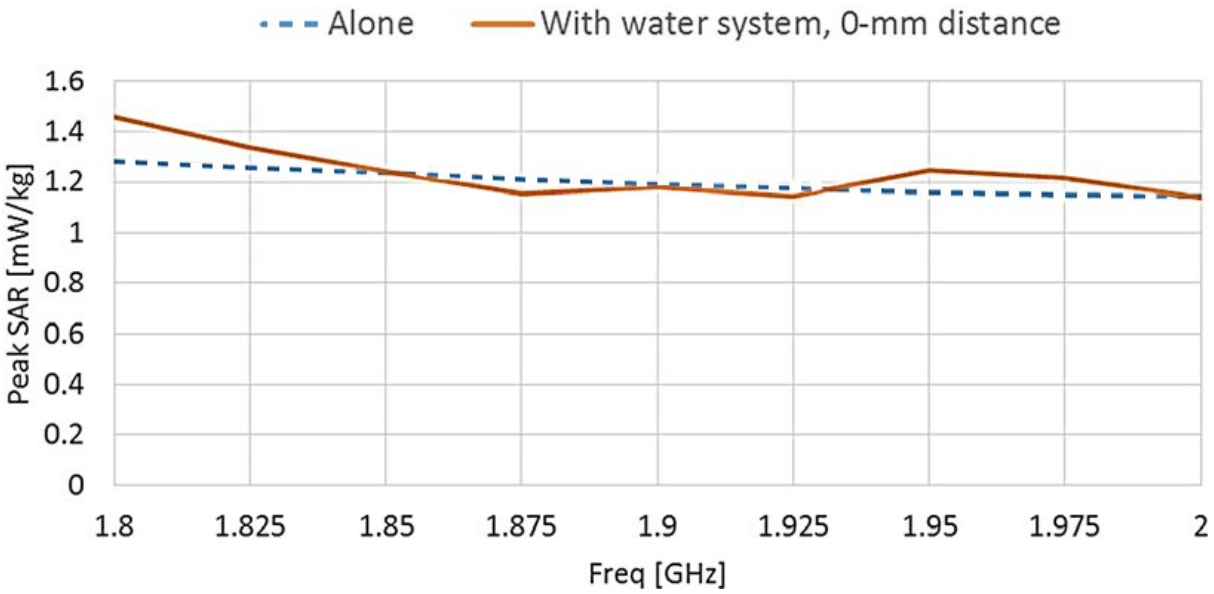

Figure A-60. Variation in the Peak Specific Absorption Rate in the Mouse When Drinking as a Function of Frequency

Figure shows the variation when the mouse was alone without a lixit water system (blue, dashed line) and when the mouse was touching the lixit water system (orange, solid line). SAR = specific absorption rate.

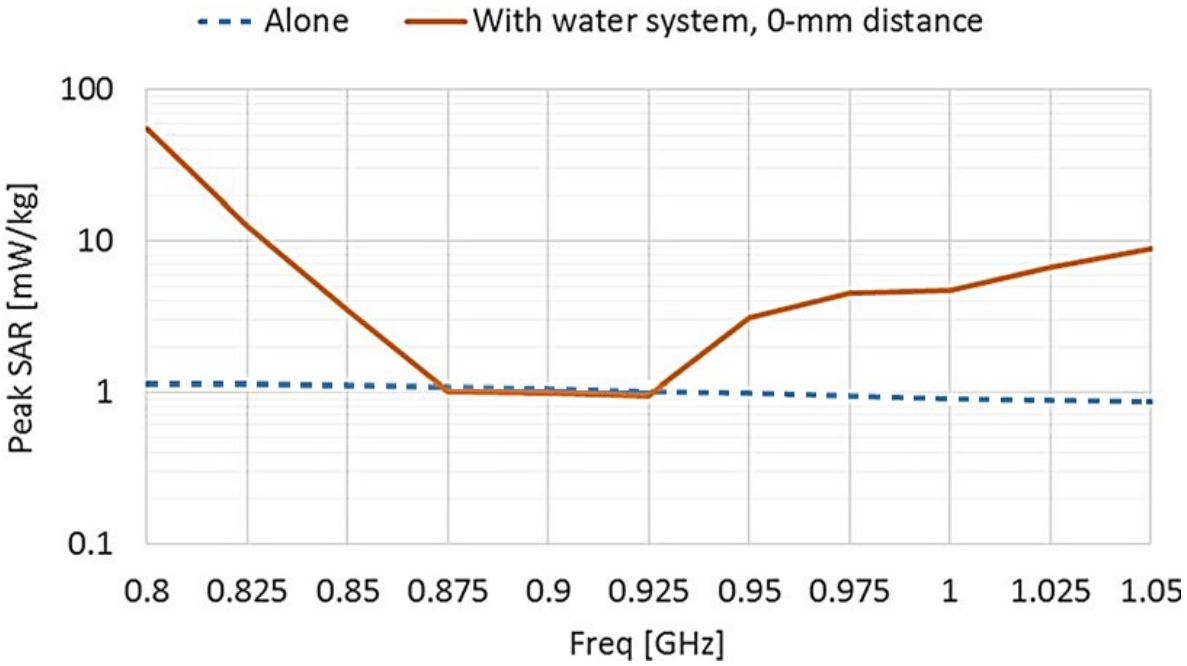

Figure A-61. Variation in the Peak Specific Absorption Rate in the Rat When Drinking as a Function of Frequency

Figure shows the variation when the rat was alone without a lixit water system (blue, dashed line) and when the rat was touching the lixit water system (orange, solid line). SAR = specific absorption rate.

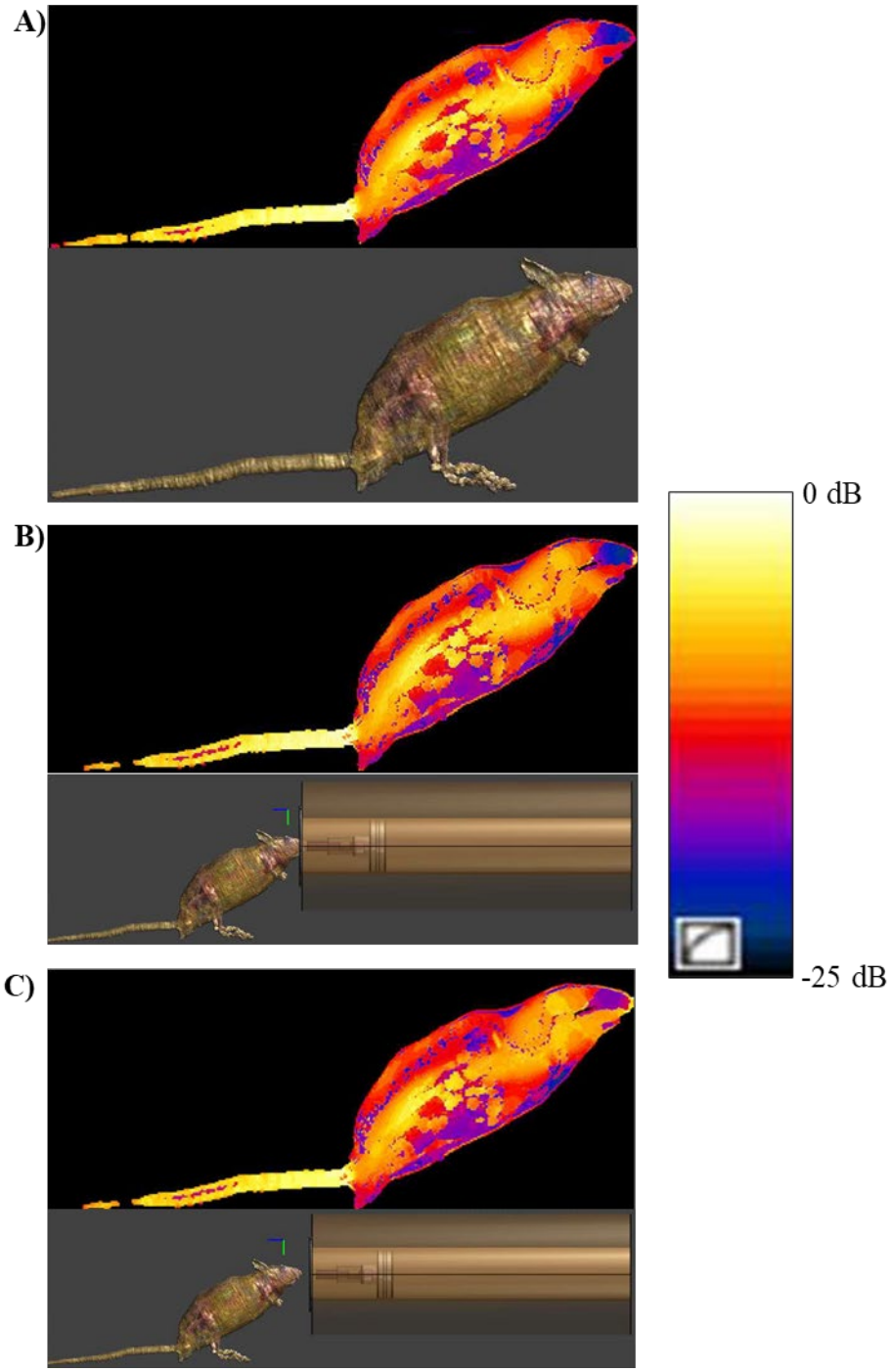

Figure A-62. Simulated Specific Absorption Rate Distributions in the Center Slice of the Mouse for Different Locations with Respect to the Water System

(A) Mouse alone. (B) Mouse drinking. (C) Mouse 10 mm from the water system. Scale is in dB relative to the peak specific absorption rate.

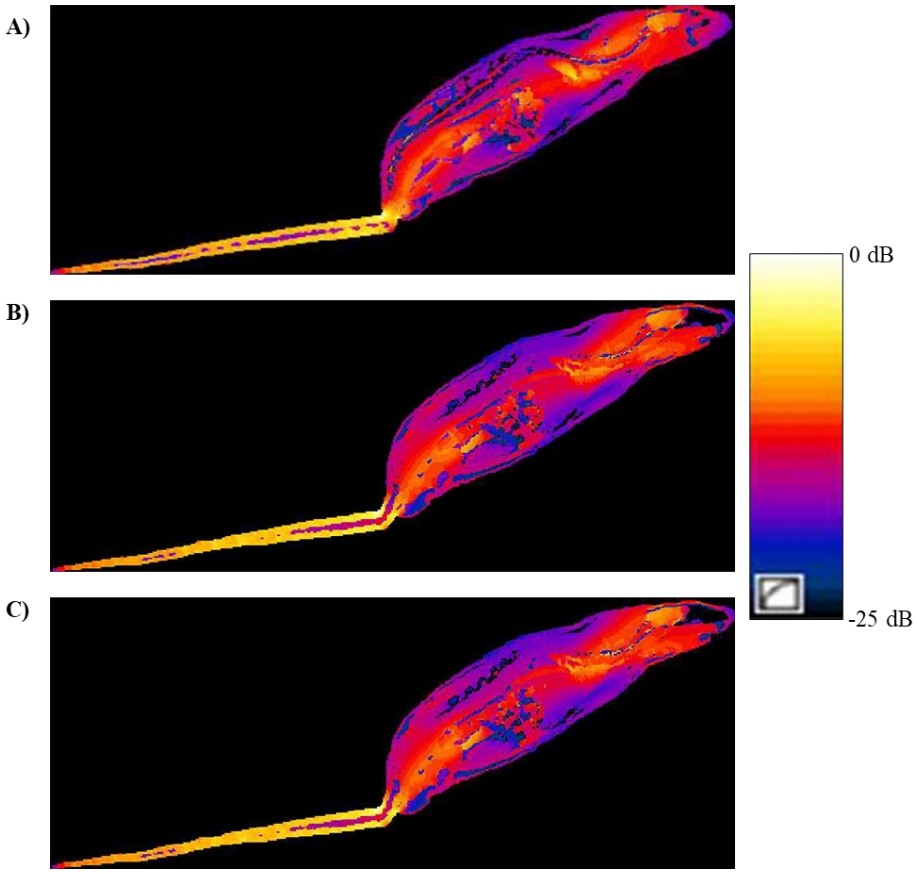

Figure A-63. Simulated Specific Absorption Rate Distributions in the Center Slice of the Rat for Different Locations with Respect to the Water System

(A) Rat alone. (B) Rat drinking. (C) Rat 10 mm from the water system. Scale is in dB relative to the peak specific absorption rate.

A.11.5.2. Water System Experimental Dosimetry: SAR in Gel Phantoms, Touching and Away from the Water System

Gel phantoms were made to assess the SAR when drinking and well away from the water system for rats at 900 MHz and mice at 1,900 MHz. The relative magnitude of the SAR was determined by observing the rate of temperature change at different locations within the phantom, namely, at the mouth, the head, and the center of the body. A 3D printed shell based on the anatomical models used for the numerical dosimetry was utilized for the rat, whereas a simplified shape was used for the mouse. Evaporation from the exposed gel surface was found to be a confounding process that could reduce the temperature increase at the mouth if the surface was not covered by a plastic membrane. For 900 MHz, the phantom can be seen in Figure A-64 with a close up of the mouth parts touching the lixit.

A)

B)

Figure A-64. Gel Rat Phantom

Panel (A) shows a detailed view of the rat phantom touching the lixit. Panel (B) shows a wide view of the reverberation chamber with the rat phantom touching the lixit.

The results of the rat water system dosimetry can be seen in Table A-23, showing that the SAR in the mouth and head were lower than in the case when the animal is not close to the water system (approximately 100 mm away) and confirming that the animal would be safe (i.e., that the exposure when the animal was drinking water was not higher than the target SAR).

Table A-23. Dosimetry of the Rat Water System

	SAR (mK/s)		Relative SAR	
	Touching Lixit	Not Touching Lixit	Touching Lixit	Not Touching Lixit
Body	4.58	3.90	1.00	1.00
Head	2.51	4.84	0.55	1.24
Mouth	2.27	1.92	0.50	0.49

The gel mouse phantom used for dosimetry at 1,900 MHz is shown in Figure A-65.

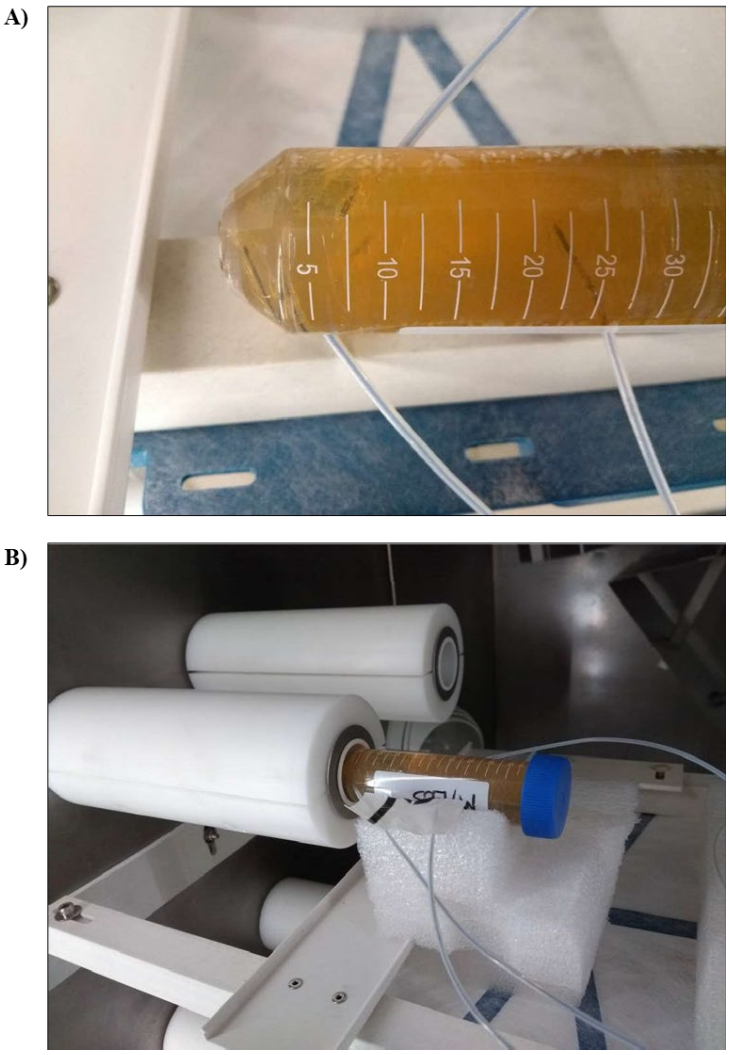

Figure A-65. Gel Mouse Phantom

Panel (A) shows a detailed view of the mouse phantom. Panel (B) shows a wide view of the reverberation chamber with the mouse phantom touching the lixit.

The results for the mouse dosimetry are presented in Table A-24, which shows that the SAR in the head was the same as when the animal is not close to the water system. The mouth shows a small increase, although the SAR is lower than that in the head. Despite this small increase in the SAR, it is clear that the increase would not be sufficient to cause RF burns or other detrimental effects.

Table A-24. Dosimetry of the Mouse Water System

	SAR (mK/s)		Relative SAR	
	Touching Lixit	Not Touching Lixit	Touching Lixit	Not Touching Lixit
Body	3.73	4.66	1.00	1.00
Head	5.64	6.98	1.51	1.50
Mouth	4.55	3.96	1.22	0.85

SAR = specific absorption rate.

The uncertainty associated with the exposure field for the short-term exposures used in this assessment (Table A-25) was higher than that used within other assessments as there was not an integral number of stirrer rotations; the stirrer modulation aspect was increased from 0.22 dB to 0.33 dB to reflect the increased uncertainty. The highest uncertainty came from the homogeneity within the chamber as the animal phantom was moved from one location to another, as may be observed in the variation in absolute SAR in the same region within the animal. This effect will also be reflected in the relative SAR values. None of the measurements were outside these variation limits.

Table A-25. Uncertainties for the Water System Dosimetry

Equipment/Factor	Uncertainty Distribution	Divisor ×	Coverage	Standard Uncertainty
Absolute Accuracy of the E- and H-field Probe	±0.26 dB	Normal	1	±0.26 dB
Frequency Linearity	±0.2 dB	Rectangular	√3	±0.12 dB
Dynamic Range Linearity	±0.2 dB	Rectangular	√3	±0.12 dB
Isotropy	±0.4 dB	Rectangular	√3	±0.12 dB
Temperature Probe Accuracy	±0.05°C	Normal	1	±0.02 dB
Homogeneity	±0.65 dB	Normal	1	±0.65 dB
Field Control	±0.2 dB	Normal	1	±0.20 dB
Stirrer Modulation	±0.33 dB	Normal	1	±0.33 dB
Combined Standard Uncertainty				±0.85 dB

A.11.6. Implantable Temperature Sensors

Implantable temperature sensors (Star-Oddi, Gardebaer, Iceland) were needed to monitor body temperature during both exposure and nonexposure periods. Two features, safety and compatibility, were considered important. From a safety perspective, the presence of the implant should not lead to an increase in the SAR and hence heating. From a compatibility perspective, the implanted sensor should report the correct temperature without interference from electromagnetic fields. Any sensor that failed to meet one of these criteria would be deemed incompatible and/or not fit for purpose. To help elucidate safety and compatibility issues, dummy sensors with no internal electronics (i.e., with a shell filled only with epoxy) were used for comparison to the actual temperature sensors. The method involved placing a fiber temperature sensor close to the part of the implant considered to have the highest field enhancement; for micro-T and nano-T sensors, this position is close to the end of the visible

internal metal parts. For the micro-HRT sensor, a position close to one of the electrodes was chosen.

A.11.6.1. Rat Implantable Sensors

A.11.6.1.1. Micro-T Sensor

For the micro-T implantable sensors, a dummy sensor was supplied. Figure A-66 shows the dummy sensor (with no visible internal metal parts) compared to the real sensor, which contained several metal parts (i.e., a battery, temperature sensor, and electronics) to log the readings to be read out at a later time. To allow the real micro-T sensor to be compared to the dummy sensor, both were placed in the same rat phantom symmetrically about the center, with the fiber temperature sensors close to the end of the visible internal metal parts (Figure A-67).

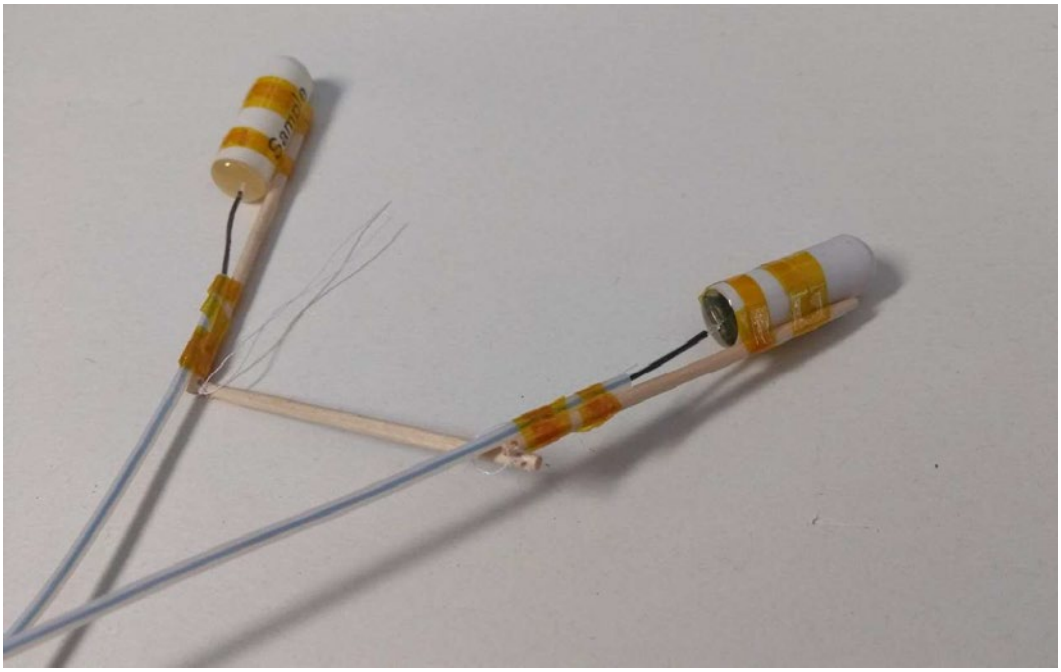

Figure A-66. Micro-T Sensor and the Dummy Sensor with Fiber Temperature Sensors

Figure shows the dummy sensor (white object, on the left, with no visible internal metal parts) compared to the real micro-T sensor (white object, on the right). For this comparison, the fiber temperature sensors (black fiber objects) are each positioned close to the end of the micro-T and dummy sensors.

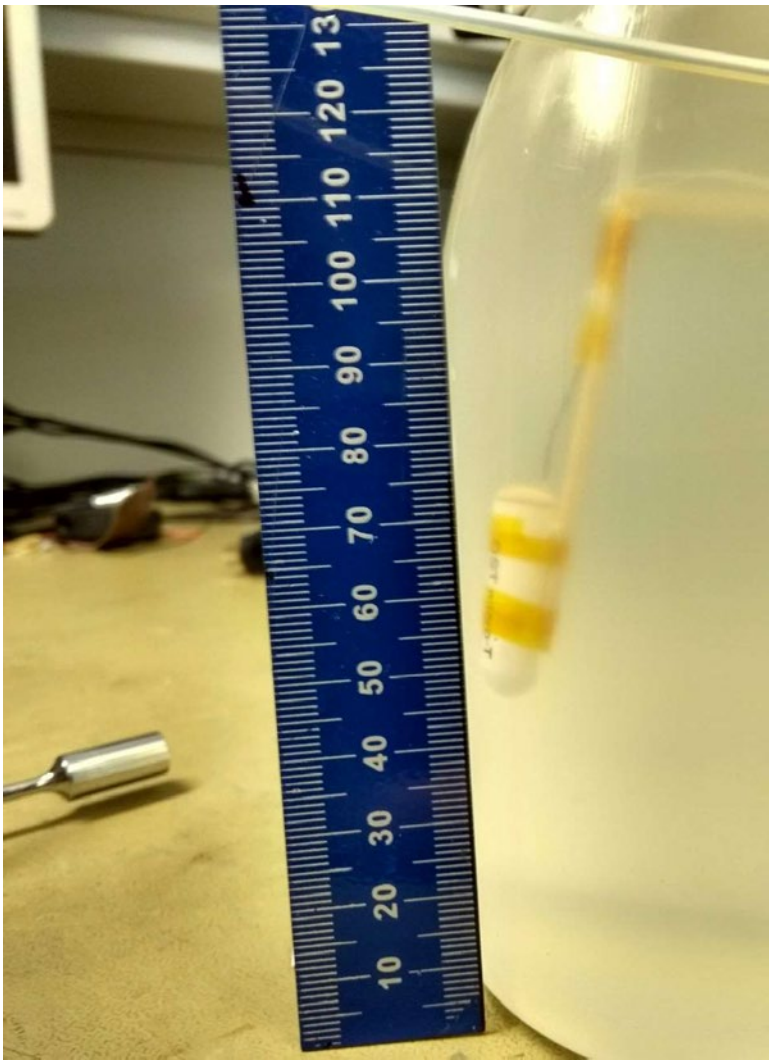

Figure A-67. Placement of the Implantable Micro-T Sensor within the Rat Phantom

Figure shows placement of the fiber temperature sensor near the end of the implantable micro-T sensor within a rat phantom. On the opposite side of the same rat phantom, a dummy sensor was placed within the phantom (not shown).

The rate of temperature increase (SAR) was determined in two experiments; the averaged results are presented in Table A-26. The implantable micro-T temperature sensor recorded an increase in the SAR by 50% over that of the dummy sensor, indicating a potential for detrimental effects. The increased SAR exhibited by the real sensor is due to the metal conductors within the sensor. The metal conductors can short out the electric field, which leads to a field enhancement outside the implantable sensor. This can occur alongside field enhancements associated with the shape of the metallic parts, particularly any sharp edges or pointed structures. Any field enhancement will lead to increases in SAR and the potential for higher-than-expected temperature rises.

Table A-26. Comparison of Micro-T and Dummy Temperature Sensors in the Rat

	ΔT (mK/s)	Ratio (dB)
Micro-T	1.44	1.48
Dummy	0.97	1.7

A.11.6.1.2. Micro-HRT Sensor

For the micro-HRT, an implantable temperature and heart rate sensor and a dummy sensor with no internal electronics were supplied. To allow the real micro-HRT sensor to be compared to the dummy sensor, both the micro-HRT and dummy sensors were placed in the same rat phantom symmetrical about the center, with the fiber temperature sensors close to one of the surface electrodes (Figure A-68).

Figure A-68. Placement of the Implantable Micro-HRT Sensor within the Rat Phantom

Figure shows placement of the fiber temperature sensor near the electrodes on the implantable micro-HRT sensor within a rat phantom. A dummy sensor was also placed into the same rat phantom in a similar placement (not shown).

Table A-27 shows the results for the rate of temperature increase (SAR) close to the end of the micro-HRT implant. The area around the electrodes also showed increased SAR; while not as high as the value at the end of the implant, the SAR was still notably higher (36%). The SAR at the end of the micro-HRT implant increased by approximately 50%, similar to that observed with the micro-T implant presented in Table A-26.

Table A-27. Comparison of Micro-HRT and Dummy Heart Rate Sensors in the Rat

	ΔT (mK/s)	Ratio (dB)
Micro-HRT	1.6305	1.36
Dummy	1.2005	1.3

A.11.6.2. Mouse Implantable Sensors

In the case of the nano-T sensor, which can be implanted in either rats or mice, no dummy sensor was supplied. Thus, the nano-T sensor was compared to the background SAR at the same location in a second phantom. Two measurements were made with the relative positions of the

phantoms reversed to account for chamber homogeneity. The measurement setup is shown in Figure A-69.

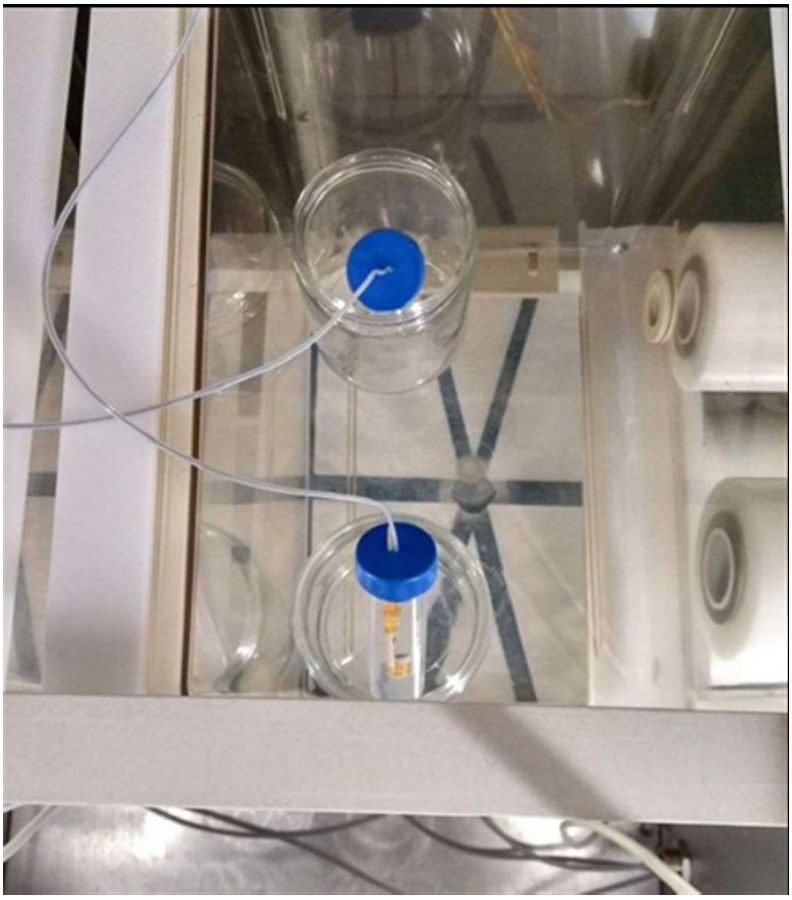

Figure A-69. Measurement Setup with Nano-T Sensor in Mouse Phantom

Table A-28 details the SAR results. There is little difference between the SAR with and without the implant, showing that the nano-T sensor was safe to implant within the rodents (i.e., that the temperature was not higher due to the presence of the sensor).

Table A-28. Temperature Increase Measured with Nano-T Sensor

	ΔT (mK/s)	Ratio (dB)
Nano-T	7.53	1.03
No sensor	7.33	0.12

A.11.6.3. Electromagnetic Compatibility of the Temperature Sensing

The ability of the implantable temperature sensors to report the temperature in the presence of the high-field strengths expected within the highest SAR chambers is of high importance for the temperature sensor to be fit for this purpose. To assess the potential for malfunction, the sensor was placed in a rat phantom for the exposures at 900 MHz and in a mouse phantom for the exposures at 1,900 MHz. The operation during GSM (pulsed) exposure and CW exposure was investigated, as these exposure conditions were the two extremes. The micro-size sensors (i.e.,

micro-T and micro-HRT) showed significant susceptibility to electromagnetic interference, particularly under GSM-pulsed exposure (Figure A-70 and Figure A-71, for micro-T and micro-HRT, respectively). With CW, the temperature level spiked only at the onset of exposure; however, this meant that the micro-size sensors were not considered appropriate for use in these experiments. The nano-T sensor also showed a small amount of interference with GSM signals, but the increase in temperature was reported with reasonable fidelity (Figure A-72). Based on these results, the nano-T sensors were considered appropriate for use in the planned experiments.

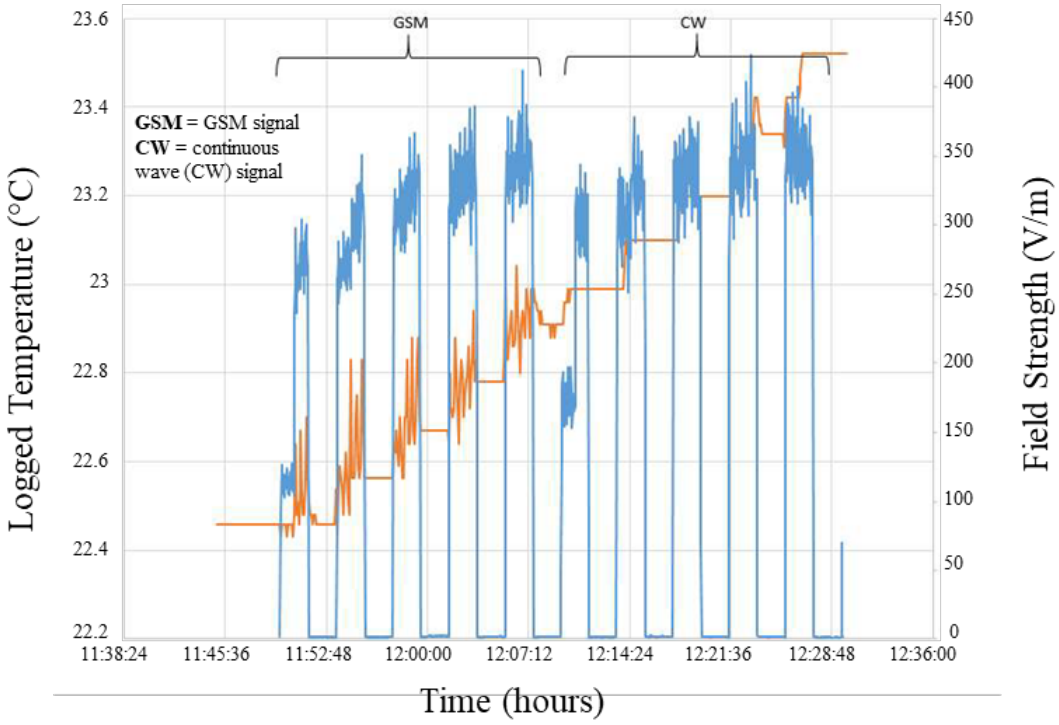

Figure A-70. Micro-T Sensor Logged Temperature Values and the Applied Field Strength

Figure shows the temperature values (orange) and the applied field strength (blue) for GSM and CW signals. GSM = Global System for Mobile Communications-modulated cell phone radiofrequency radiation; CW = continuous wave.

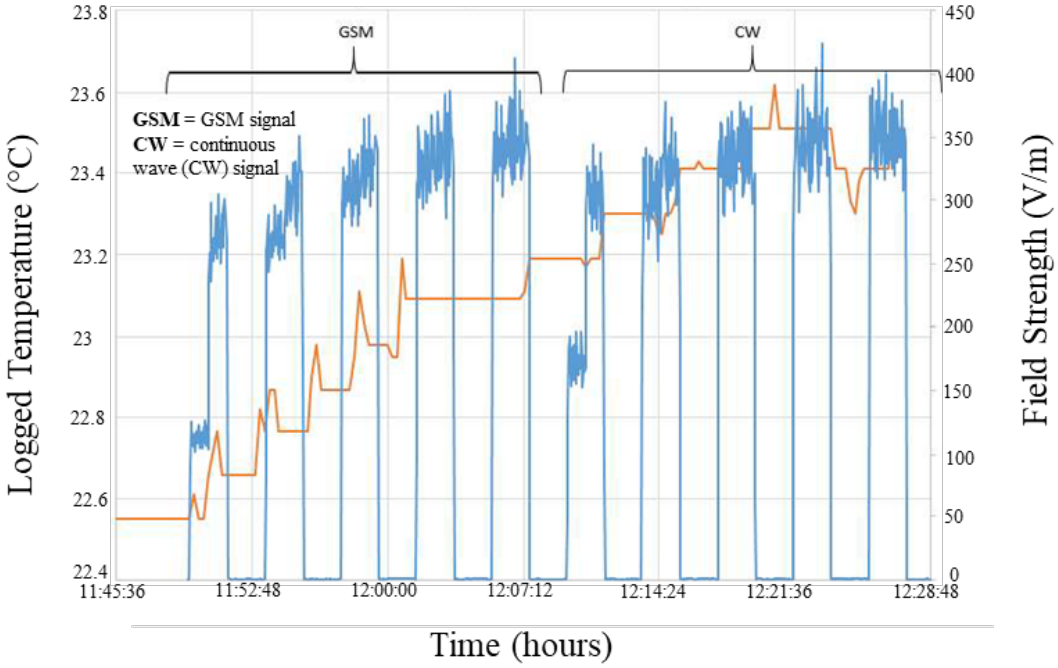

Figure A-71. Micro-HRT Sensor Logged Temperature Values and the Applied Field Strength

Figure shows the temperature values (orange) and the applied field strength (blue) for GSM and CW signals. GSM = Global System for Mobile Communications-modulated cell phone radiofrequency radiation; CW = continuous wave.

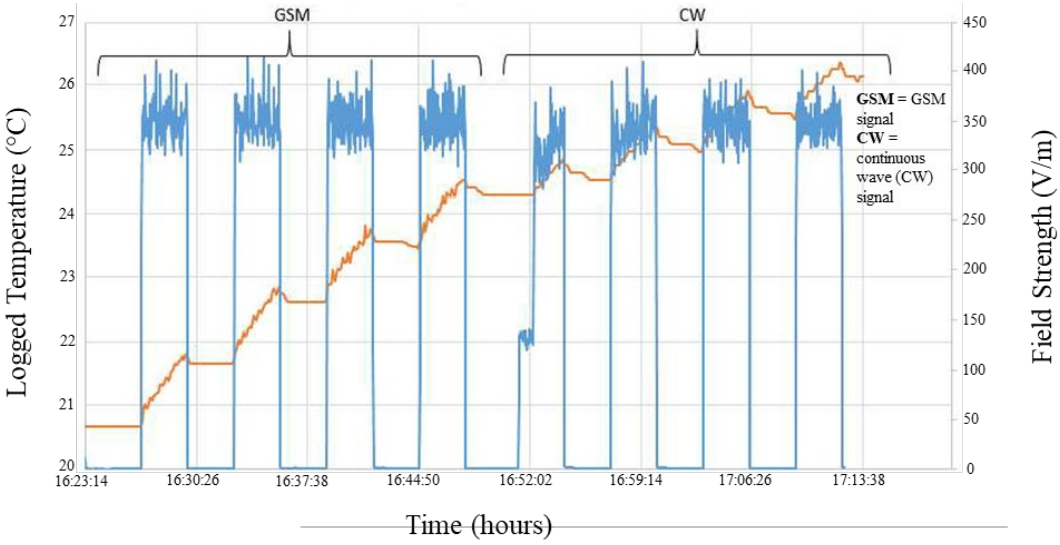

Figure A-72. Nano-T Sensor Logged Temperature Values and the Applied Field Strength

Figure shows the temperature values (orange) and the applied field strength (blue) for GSM and CW signals. GSM = Global System for Mobile Communications-modulated cell phone radiofrequency radiation; CW = continuous wave.

A.12. Infrared Cameras

The infrared (IR) camera chosen was the Transcend DrivePro Body 1080p camera (Figure A-73). The cameras were placed within Faraday boxes to provide shielding for error and artifact-free operation in the high-field environment of the reverberation chamber. Furthermore, because of the all-metal construction, there was no absorption of energy, and the incident field was scattered. As the reverberation chamber environment was designed to give maximum scattering of the fields, the camera had no impact on the exposures provided. The cameras were placed more than half a wavelength from the nearest cage, and because the cameras were mounted on the metallic door, their presence had no impact on the RF field.

Figure A-73. The Transcend DrivePro Body 1080p Camera

Appendix B. Verification of Electromagnetic Field Exposure Values in Reverberation Chambers and Measurement of Ambient Fields

Table of Contents

Figures

B.1. Introduction

This appendix describes the independent verification of the radiofrequency radiation (RFR) exposure system by the National Institute of Standards and Technology (NIST). To verify the parameters of RFR exposures recorded by the data-capture component exposure system, technical experts from NIST conducted an independent verification of the system following installation and initial testing of the exposure system by the Foundation for Research on Information Technologies in Society (IT'IS Foundation, Zürich, Switzerland) and the testing facility. Specifically, NIST evaluated RFR exposure fields, chamber characteristics (field uniformity), and signal quality.

The Spectrum Technology and Research Division of the NIST Communications Technology Laboratory was tasked to provide an independent verification of the radiofrequency (RF) field characteristics that directly affected animal exposure and dosimetry. These characteristics included electric field intensity, field uniformity throughout the chamber, and quality of the modulation. The NIST measurements were compared to the corresponding values reported by the IT'IS-developed automated control system. The power delivered to each chamber—and hence the exposure field level—was determined through a feedback loop using electric field probes located inside the chamber. These IT'IS field probes provided real-time monitoring of exposure levels. For these exposure verification tests, a NIST-calibrated field probe and an antenna system (Figure B-1) were installed in each chamber simultaneously to verify the field intensity reported by the IT'IS probes. These field intensity measurements were performed in each active chamber (total of three: Chambers 1, 2, and 3), and each chamber was tested at 900 MHz with rat cages and rat phantoms (i.e., animal surrogates) and at 1,900 MHz with mouse cages and mouse phantoms. For each configuration, tests were performed for Global System for Mobile Communications (GSM) and Interim Standard 95 (i.e., IS-95, or Code Division Multiple Access [CDMA]), as well as simple continuous wave (CW) signals. The NIST evaluations at the testing facility in West Jefferson, OH, were performed during the weeks of August 5, 2019, and September 16, 2019. The measurement details and data processing techniques are outlined in this appendix, along with the final measurement results of these tests.

The RF signals generated by the exposure system were generally within the estimated uncertainty bounds, indicating that the chamber fields measured by NIST agreed with the measurements provided by the exposure system's integrated probes. The magnitude of field variation throughout the volume of the chambers was also consistent with values reported for the chambers in the previous National Toxicology Program (NTP) studies. The quality of the modulated signals was found to be acceptable with regard to distortion and harmonic content. Overall, the NIST evaluation confirmed that the exposure system was operating correctly and RFR exposures were within specifications. These activities were conducted prior to the initiation of any animal studies. Additionally, NIST measured ambient levels of RFR at various locations in the facility to assess any potential differences at different locations across the facility. The data demonstrated that there were no marked differences in exposures among the sites evaluated across the facility. This appendix contains full details of the procedures for measurements and calculations.

B.2. Reverberation Chambers

An electromagnetic reverberation chamber is an electrically large, high quality factor (Q), multimoded complex cavity in which electromagnetic energy can become statistically uniform by changing boundary conditions, in particular by moving large reflective surfaces or paddles. The field parameter that is directly proportional to the specific absorption rate (SAR) is the square of the time-average electric or magnetic field (power density) in the chamber. The average field was determined by sampling the electric field response of calibrated probes and/or antennas over complete rotations of the revolving metal paddles in each chamber. The variability of the average field throughout the volume of the chamber is the metric used to quantify the field (and hence the SAR) uniformity in the chamber.

B.3. Field Comparisons

The NIST field measurements for each of the three active chambers were compared to the values returned by the IT'IS system. These data included the effects of the independent probe calibrations, slightly different sampling rates, and the variability (or uniformity) of the average field. The field validation measurements were performed with cages and phantoms in the chamber because the isotropy and homogeneity initially measured by IT'IS were similar for the loaded and unloaded chambers, and it was best to evaluate the chambers in a manner consistent with general operation. The photograph in Figure B-1 includes the NIST receiving antenna and the small three-axis probe in the chamber. The antenna received the signal from the chamber, which was processed by a spectrum analyzer to return total channel power for each sample, which could then be used to estimate the electric field.

Figure B-1. One of the Reverberation Test Chambers at the Testing Facility

Each chamber could be configured with either 10 mouse cages or 10 rat cages. This picture shows a chamber configured with nine rat cages, with the tenth cage space occupied by a dual-ridged horn antenna and each cage containing a phantom that simulates the electromagnetic properties of a rat.

The three-axis probe gave three different direct current (DC) voltages that were related to the field incident on each of the three dipole antennas aligned with the orthogonal Cartesian axes of the probe. These DC voltages were then converted to E-field values using calibration data to determine the equivalent field strength for each sample. The probe had a slow response time. To minimize sampling errors due to fields changing as the paddles rotated, the paddles were held at a fixed position during measurement of each sample. (Note: The paddles turned continuously during the animal tests to give the most uniform time-averaged SAR exposure; here the paddles were stopped only to allow the most accurate recording of the field strength within the constraints of the instrumentation.) Probe voltages and received power from the antenna were recorded at 100 different positions of the paddles.

The IT'IS system used similar three-axis probes, with two E-field probes in each chamber. These probes were calibrated by IT'IS to give their estimate of the fields in the chamber.

B.4. Measurement Uncertainty

By far, the largest contributor to the overall uncertainty of these measurements was the uniformity of the individual chambers. IT'IS reported uniformities (standard deviation of the mean field over multiple locations) in the empty chamber of 1.2 dB (referred to as isotropy in Appendix A) for a Cartesian component of the field at 900 MHz and 0.7 dB (referred to as homogeneity) for the total field. Each value was 0.1 dB higher in the loaded chamber. At 1,900 MHz, IT'IS reported uniformities of 0.7 dB for a Cartesian component of the field and 0.4 dB for the total field. These values were slightly higher (0.8 and 0.6 dB, respectively) for the loaded chamber.

Another source of uncertainty was the use of a limited number (n = 100) of sample positions. Given a Rayleigh distribution, which typically describes the Cartesian fields in a reverberation chamber, 100 samples will result in uncertainties of approximately 0.45 dB. A final large contributor to the uncertainty was the calibration of the probe, which was estimated to be approximately 0.4 dB. These three terms combined to give an estimated standard uncertainty of approximately 1.4 dB for measurements of Cartesian field at 900 MHz, 1.0 dB for the Cartesian field at 1,900 MHz, and approximately 1.0 dB for measurements of the total field. The expanded uncertainty, assuming a coverage factor of 2 (95% confidence), is approximately 3.0 dB for measurements of Cartesian field and 2.0 dB for measurements of the total field (conservatively). These uncertainties represented how accurate the measurements were expected to be, and agreement between the various measurement systems within this range indicated acceptable performance of the field probes.

B.5. General Processing

Rather than deal with a wide variety of measured values (Cartesian or total field, electric or magnetic field, and received power) and to allow for easier comparison, all measurements were converted to an estimated equivalent total electric field. From a measurement of mean Cartesian electric field $<|E_C|>$, the mean total field $<|E_T|>$ can be estimated by multiplying by 15/8[43]:

$$<|E_T|> \approx \frac{15}{8} <|E_C|>$$

Finally, from the power measured from the receiving antenna, the mean Cartesian electric field can be estimated as:

$$<|E_C|> \approx \frac{8\pi}{\lambda}\left\langle\sqrt{5P_R}\right\rangle$$

By multiplying $<|E_C|>$ by 15/8 as shown above, the mean total field can be estimated as:

$$<|E_T|> \approx \frac{15\pi}{\lambda}\left\langle\sqrt{5P_R}\right\rangle$$

In this way, similar values will always be compared.

B.6. Measurement Results

The estimated total electric field based on measurements of mean Cartesian field is presented first. Each individual Cartesian component is used to estimate an equivalent total electric field using the above relationships. As mentioned earlier, each chamber contained two IT'IS E-field probes. Two charts of the results are given below in Figure B-2. In Figure B-2A all the individual readings and the mean field strength are shown for each configuration; in Figure B-2B, all the field measurements are normalized to the average measured value (mean), and only the deviation from that target is presented. As mentioned above, the expanded uncertainties of such measurements are approximately 3 dB, and appropriate error bars are placed around the mean in each chamber. These charts also show the total field estimate based on measurements of received power from a dual-ridged horn antenna, giving an independent confirmation of the measurements. Overall, the measurements were within the expected range. Given the field uniformity data provided by IT'IS, slightly smaller variations for measurements taken at 1,900 MHz than for measurements taken at 900 MHz might be expected. However, this is not obvious in the data shown in Figure B-2B.

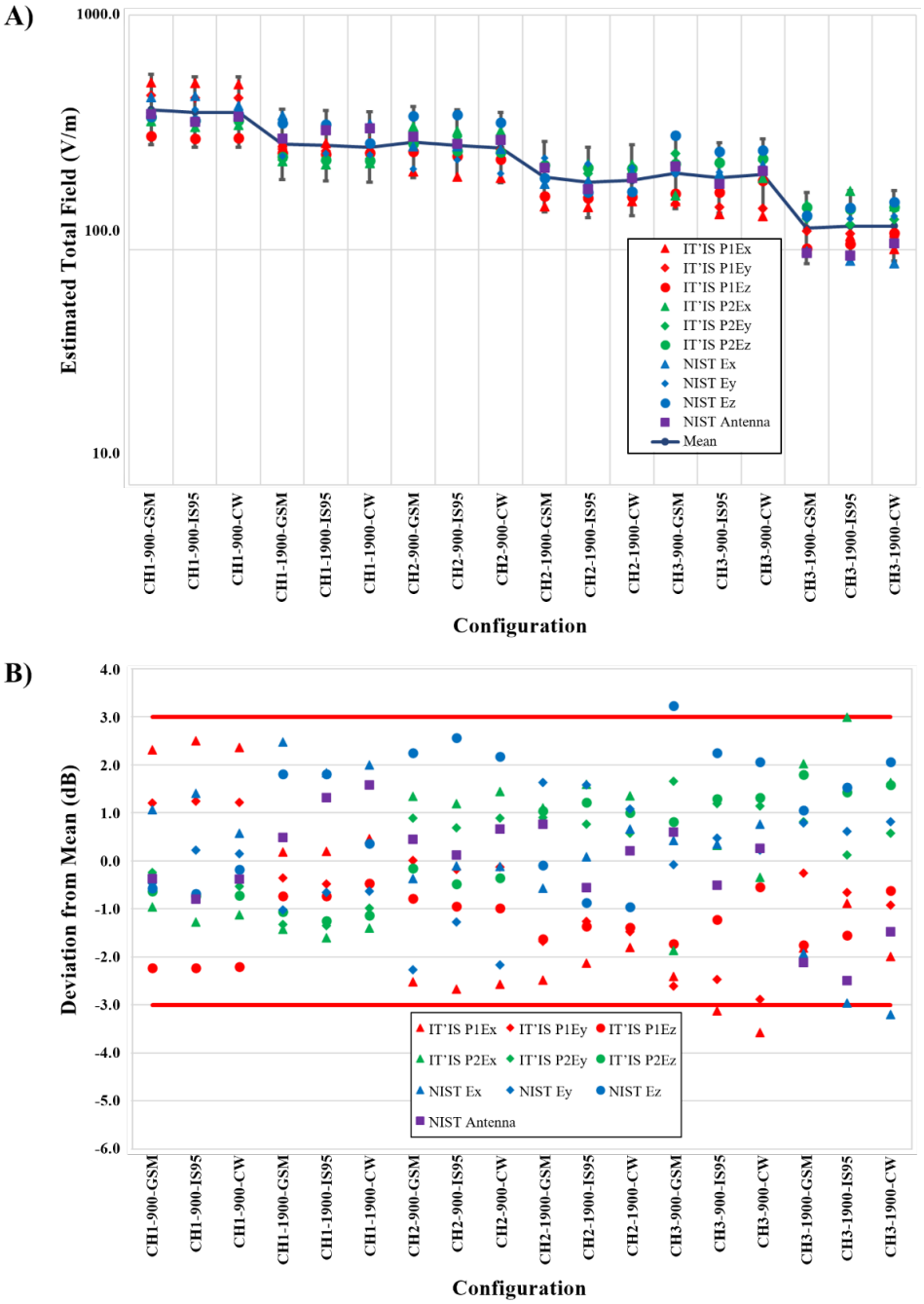

Figure B-2. Total Electric Field Estimated from Each Individual Measured Cartesian Field Component Compared to the Mean and Associated Uncertainty

Panel (A) shows the actual field strength in each chamber. Panel (B) is normalized to the mean and shows only the deviation from that value. The abbreviations shown in the legends of each panel equate to which probe generated the data (IT'IS or NIST), the probe number in the case of the IT'IS data (P1 or P2), and the Cartesian axis of the electrical field component (Ex, Ey, or Ez). For example, "IT'IS P1Ex" corresponds to the x-axis electric field component ("Ex") of IT'IS probe number 1 ("P1"). Different configurations were derived from the three possible chambers (CH1, CH2, CH3), the two possible frequencies (900 or 1,900 MHz), and the three possible modulations (GSM, IS-95 CDMA, CW). CDMA = Code Division Multiple Access-modulated cell phone radiofrequency radiation; CH1 = Chamber 1; CH2 = Chamber 2; CH3 = Chamber 3; CW = continuous wave; GSM = Global System for Mobile Communications-modulated cell phone radiofrequency radiation; IS-95 = International Standard 95.

Measurements of the total electric field calculated directly (root-sum-square) from the individual measured Cartesian field components are examined next. Two charts of the results are given below in Figure B-3. Figure B-3A shows the actual field values, and Figure B-3B is normalized to the mean field strength and shows only the deviation from that target. Here the uncertainties are somewhat reduced to 2.0 dB, and again the measurements generally fall within the expected range. It is interesting to note, however, that there is a difference between IT'IS Probe 1 in Chambers 2 and 3 (note: Probe 1 in Chamber 2 is physically different from Probe 1 in Chamber 3) and the other two probes. The same trend is also apparent in Figure B-2, which shows that all three axes of Probe 1 appear to be biased low relative to all the other data. The total field measured on Probe 1 is still almost within 2.0 dB of the mean field; such an offset is within the range of possibility, but the consistency in the plots is unexpected. It might be possible to verify this by swapping Probe 1 with Probe 2 in Chambers 2 and 3 or by swapping probes between chambers. Regardless, a 2.0 dB offset is unexpected but not problematic.

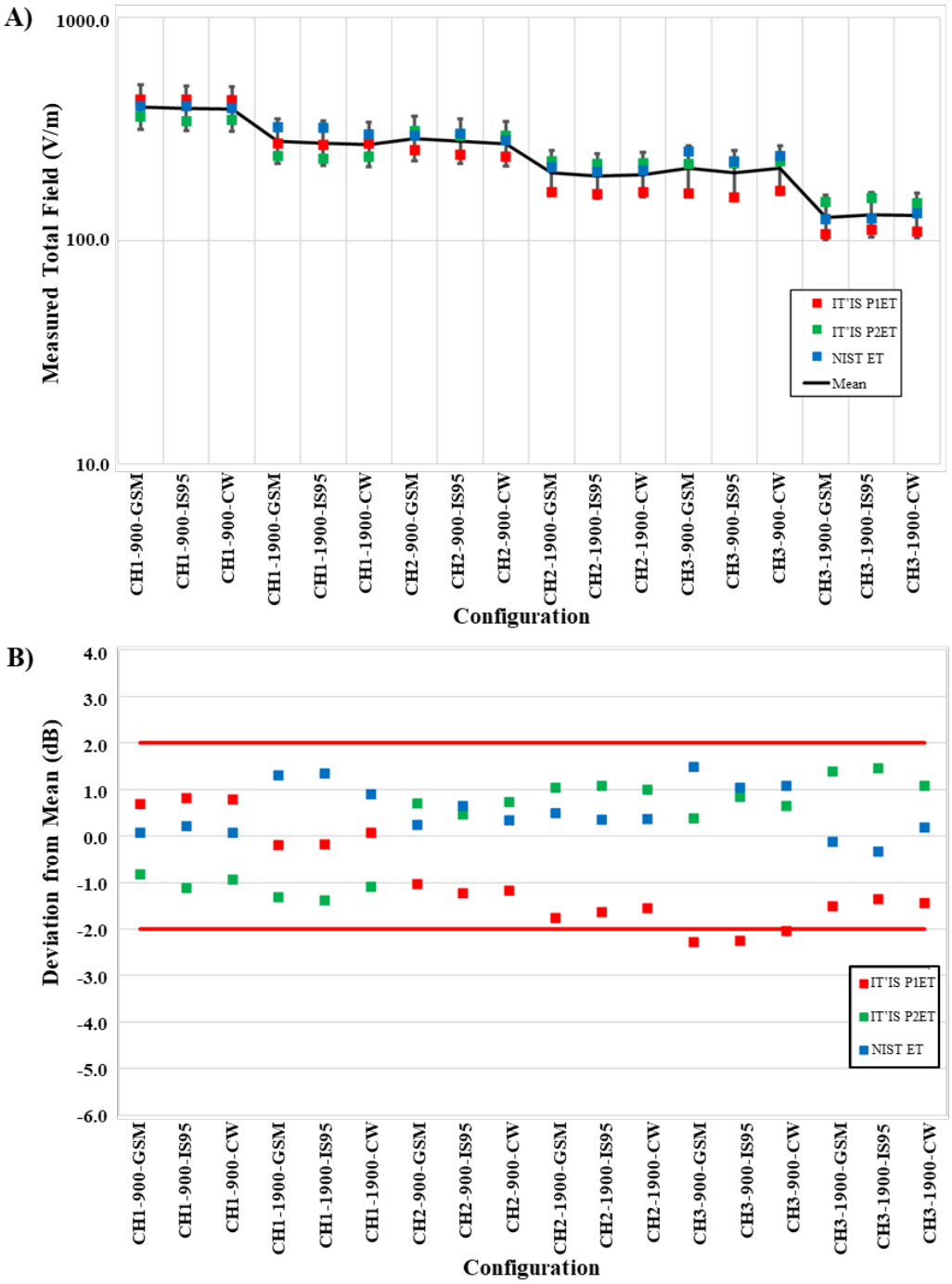

Figure B-3. Total Electric Field Calculated Directly (Root-Sum-Square) from the Individual Measured Cartesian Field Components Compared to the Mean and Associated Uncertainty

Panel (A) shows the actual field strength in each chamber. Panel (B) is normalized to the mean and shows only the deviation from that value. The abbreviations shown in the legends of each panel equate to which probe generated the data (IT'IS or NIST), the probe number in the case of the IT'IS data (P1 or P2), and the total Cartesian electric field (i.e., ET). For example, "IT'IS P1ET" corresponds to the total electric field ("ET") of IT'IS probe number 1 ("P1"). Different configurations were derived from the three possible chambers (CH1, CH2, CH3), the two possible frequencies (900 or 1,900 MHz), and the three possible modulations (GSM, IS-95 CDMA, CW). CDMA = Code Division Multiple Access-modulated cell phone radiofrequency radiation; CH1 = Chamber 1; CH2 = Chamber 2; CH3 = Chamber 3; CW = continuous wave; GSM = Global System for Mobile Communications-modulated cell phone radiofrequency radiation; IS-95 = International Standard 95.

B.7. Field Uniformity in a Fully Loaded Chamber

IT'IS performed a very detailed evaluation of the uniformity of the test chambers, both of empty chambers and chambers loaded with phantoms, with the field being sampled at many locations throughout the chamber (Appendix A). During the evaluation summarized above, three electric field probes (one NIST probe and two IT'IS probes) were placed at different locations in each chamber, and each probe contained three dipole antennas, giving nine separate readings of the Cartesian component of the field or three separate readings of the total field. An antenna placed in the chamber gave an additional indication of the Cartesian field. The spread in measured results shown in Figure B-2 and Figure B-3 is consistent with the uniformity evaluation given by IT'IS, supporting its determination of the uniformity.

B.8. Ambient Fields

In addition to the test exposure fields within the chambers, the ambient field in and around the test chambers, as well as other locations throughout the building, were also of interest since the animals would be exposed to these signals whenever they were not inside the test chambers. For these results, a lower-frequency disc-cone antenna was connected to one spectrum analyzer, and a higher-frequency disc-cone antenna was connected to a second spectrum analyzer. The measurement setup is shown in Figure B-4. The lower-frequency antenna was scanned from 10 MHz to 1 GHz, and the higher-frequency antenna was scanned from 1 to 6.5 GHz. Each spectrum analyzer was set to a max-hold condition to capture the peak signals, and frequency sweeps were taken over a 24-hour period at each location. Only the peak power observed in each location over the measurement period is reported. Because all measurements were taken indoors, there is no knowledge of the angles-of-arrival for the observed signals and there is no way to convert received power to field levels. Similarly, there is no method to convert measurements of received power to SAR without detailed knowledge of any target animal. The results are considered representative of typical results in each area, but it is possible that there were different levels (either higher or lower) outside the time window in which these measurements were taken.

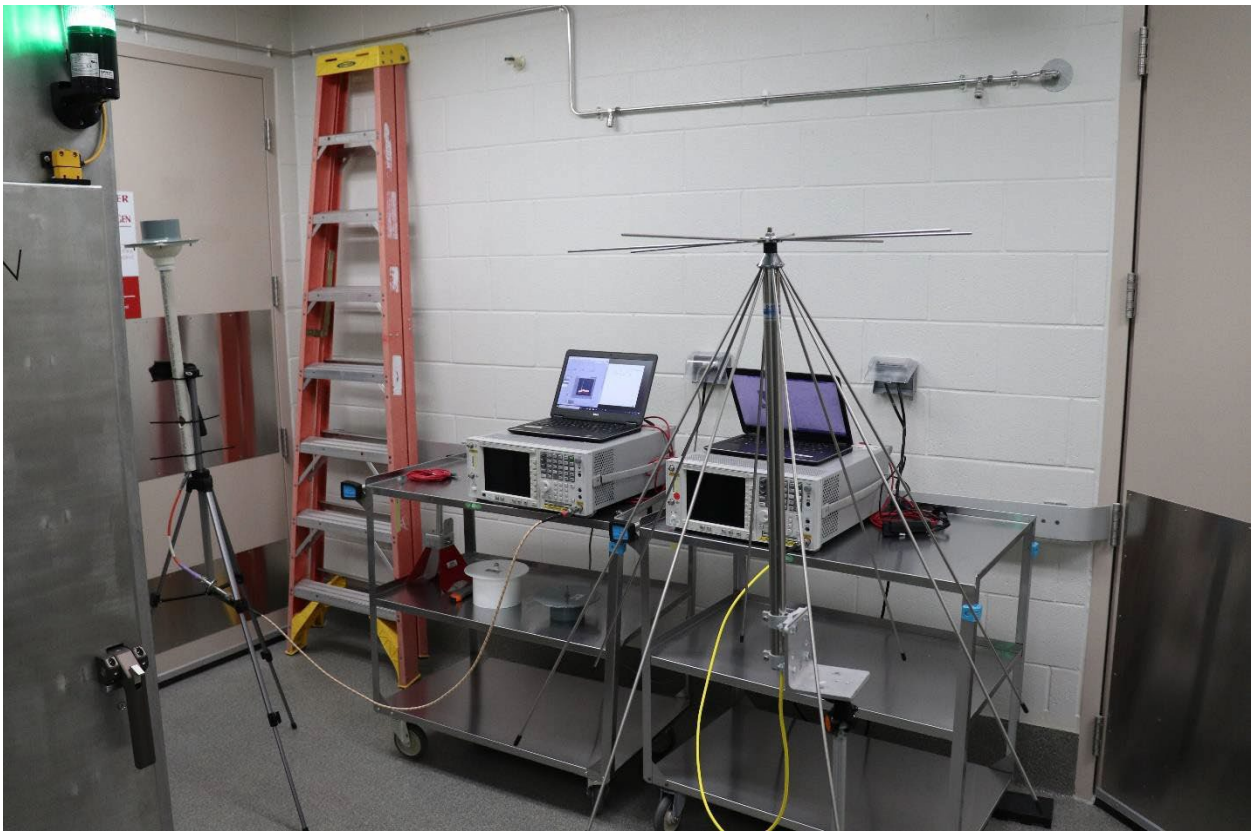

Figure B-4. The Ambient Field Measurement Setup

The antenna made of wire rods, on the right, is a low-frequency disc-cone antenna. The smaller antenna, on the left, is a high-frequency disc-cone antenna. Measurements were taken at four separate locations within the testing facility. The locations included the radiofrequency radiation exposure room and three other locations that represented a large geographic distribution throughout the facility.

Figure B-5 shows the peak received power over 24 hours in the low-frequency band at each of four different locations. Overall, the electromagnetic environments in all locations were similar. The highest observed signals were in the cellular frequency bands around 750 MHz and 873 MHz in Location 2. For reference, the lowest expected test field at the time of this evaluation was approximately 194 V/m at 900 MHz, which would give an average received power of approximately +26 dBm or 46 dB higher than observed at the worst-case location.

Similar results for the high-frequency band are shown in Figure B-6. Once again, the highest levels were observed in Location 2, with the highest signal being cellular signals around 2.1 GHz and general communication signals for wireless networks around 2.4 and 5.2 GHz. The lowest expected test field was approximately 132 V/m at 1,900 MHz, which would give an average received power of approximately +16 dBm or, again, 46 dB higher than that observed at the worst-case location.

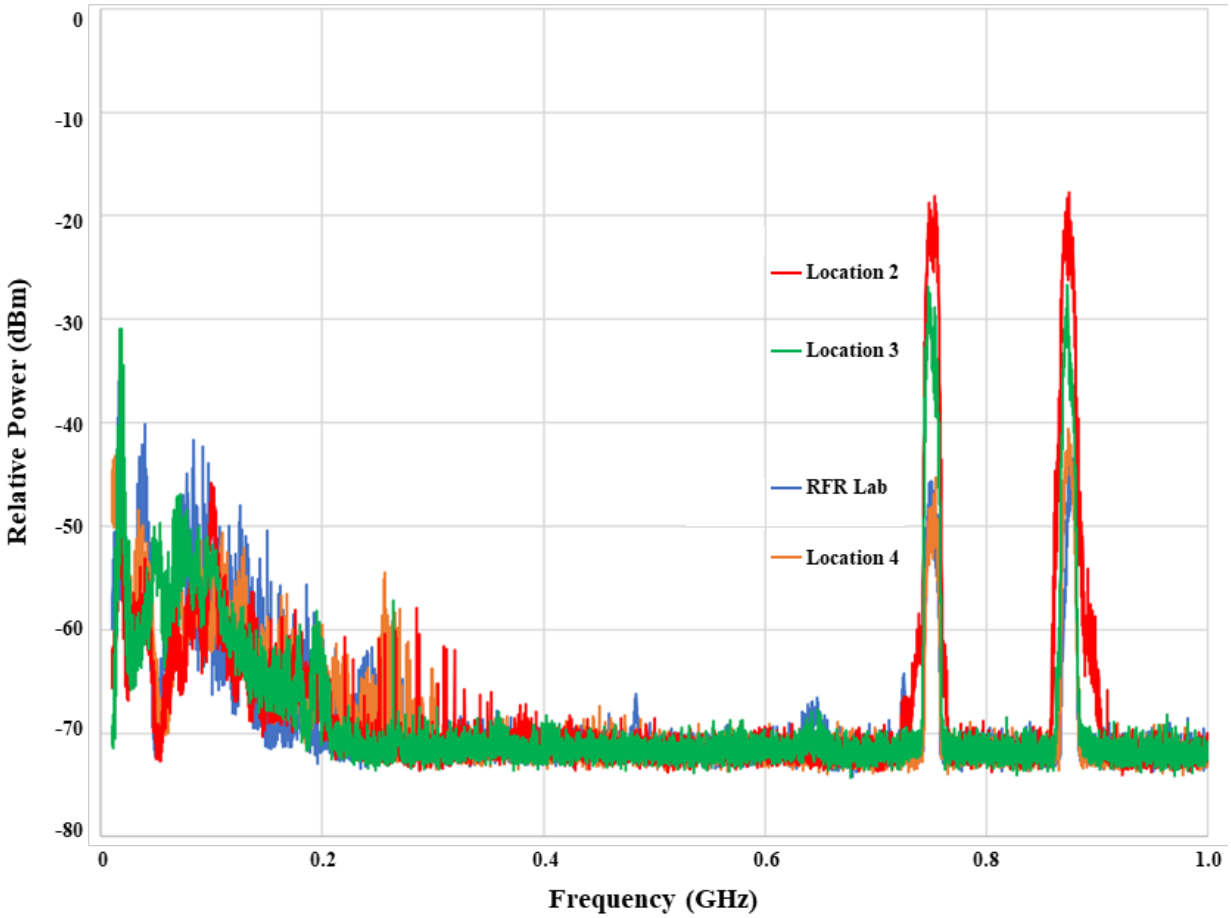

Figure B-5. Peak Received Power over 24 Hours in Each of Four Separate Locations in the Low-frequency Band

The locations tested included the room housing the reverberation chambers (i.e., radiofrequency radiation laboratory, or "RFR lab") and three other locations throughout the testing facility. In general, received power at each of the four locations was similar. Here, the highest observed signal (shown in red) was in Location 2. Other signals were mostly negligible and difficult to distinguish from each other.

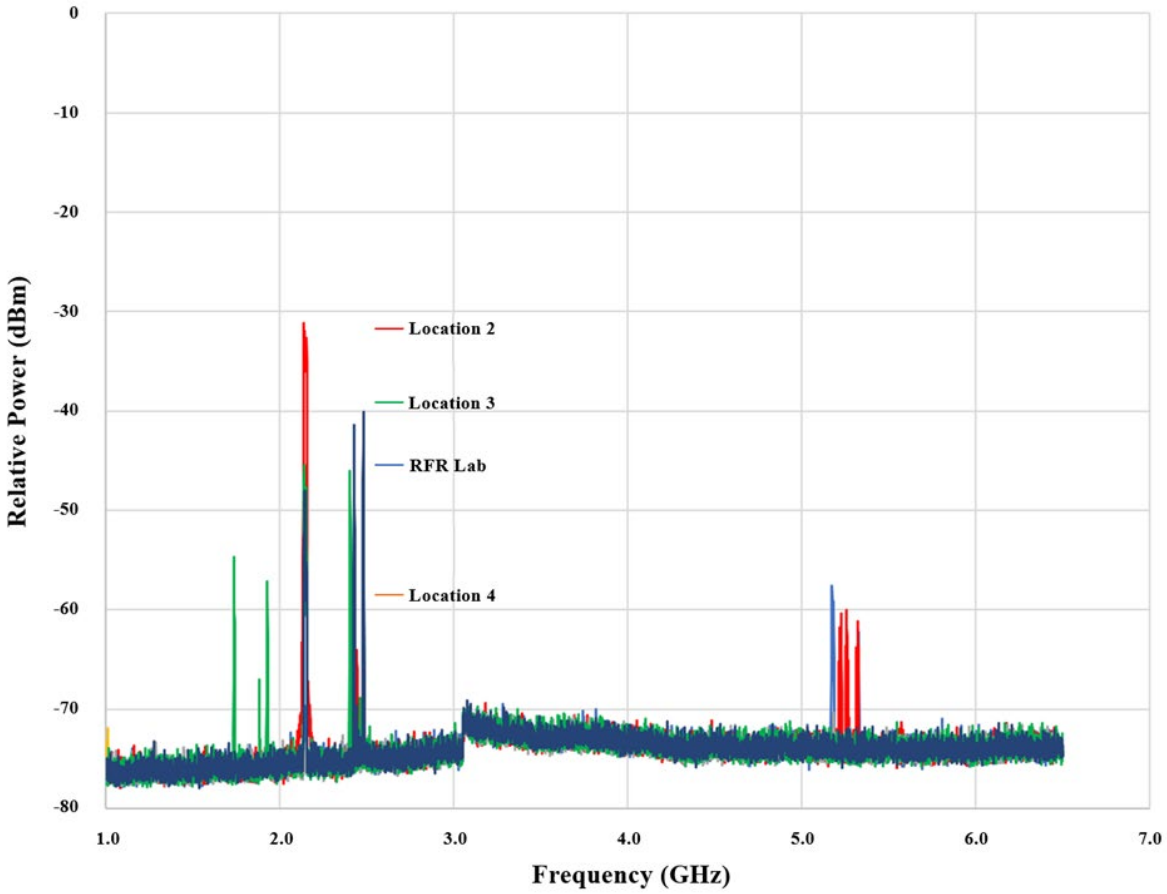

Figure B-6. Peak Received Power over 24 Hours in Each of Four Separate Locations in the High-frequency Band

The locations tested included the room housing the reverberation chambers (i.e., radiofrequency radiation laboratory, or "RFR lab") and three other locations throughout the testing facility. In general, received power at each of the four locations was similar. Here, the highest observed signal (shown in red) was in Location 2. Other signals were mostly negligible and difficult to distinguish from each other.

B.9. Distortion Measurements of the Modulated Signals

Measurements of the spectra of the modulated signals in high-power chambers were carried out to assess the level of both intermodulation distortion and harmonic distortion. The high-power chambers were studied because the amplifiers used to increase the signal levels in these chambers are generally pushed closer to their nonlinear range when compared to their use in the lower-power chambers. Typically, power amplifiers operating in the nonlinear regime are the primary source of distortion in the electronics of the transmit chain.

Standards organizations judge the level of distortion in a modulated signal by comparing the signal level in the main channel (the desired signal) to the signal level in the adjacent channel (distortion). Often, a "spectrum mask" is provided that specifies the acceptable maximum signal level in the adjacent channel relative to the main channel. An example of this mask from the European Telecommunications Standards Institute (ETSI) for the GSM specification is given in Figure B-7 below. In Figure B-7, the measured power 200 kHz from the center frequency should

be at least 30 dB below that in the main channel. This number was used to quantify an acceptable level of distortion in the GSM chamber measurements. The IS-95 (i.e., CDMA) specifications are not based on open standards. They are kept by the Telecommunications Industry Association (TIA), a trade organization. However, the spectrum mask for the CDMA2000 and IMT-2000 (International Mobile Telecommunications-2000) specifications is similar to the mask for the GSM specification and is used here to judge the maximum acceptable level of distortion in the chamber measurements. According to Annex 1, "Unwanted Emission Characteristics for IMT-2000 CDMA Direct Spread Radio Interface,"[44] the spectrum emission mask requirement is approximately 35 dB below the level in the main channel for the adjacent channel.

Typically, harmonic distortion is not considered in specifications documents since bandpass filters are required that only let the main channel signals through the transmitting system. The signal levels in the harmonics were measured only because they gave an indication of the purity of the generated modulated signals. Values below 50 dB or so from those in the main channel should be low enough to affect the signals only minimally. A signal whose level is 50 dB below the main channel is 100,000 times weaker. This signal level would be hard to detect over and above the main channel signal.

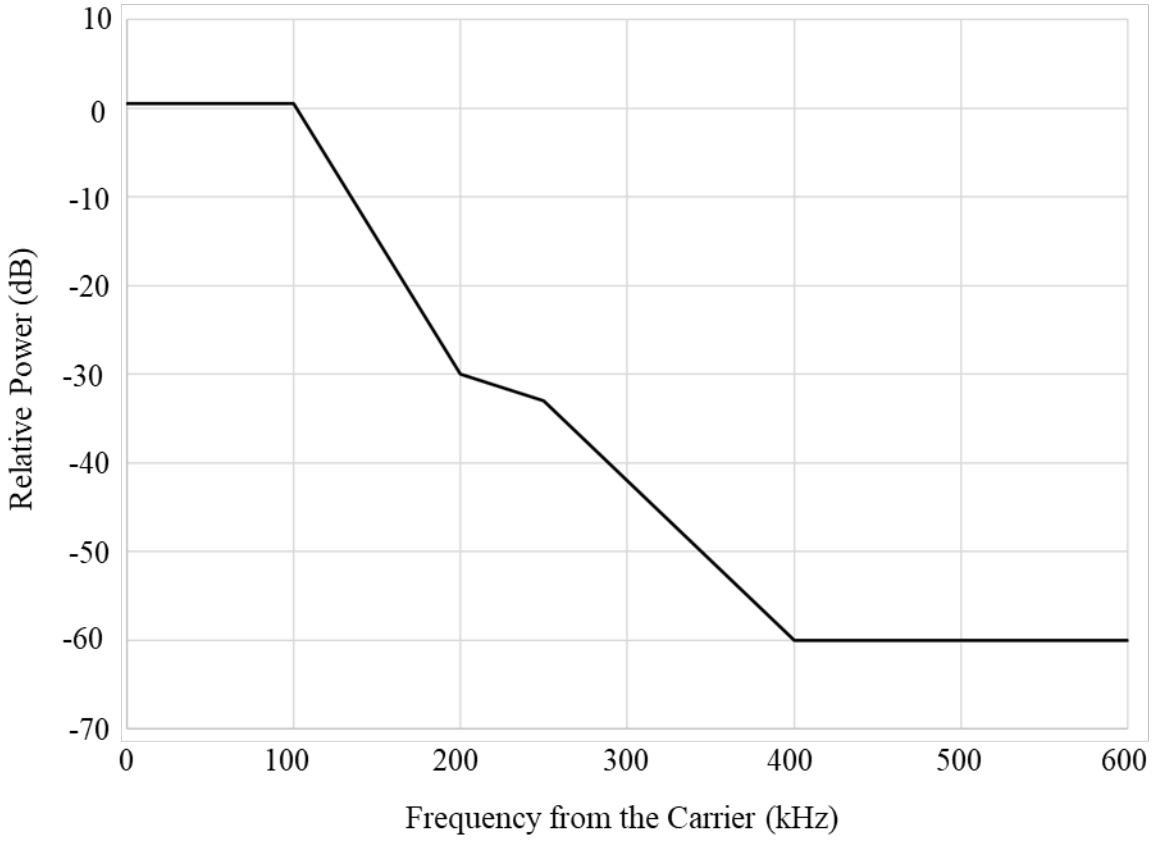

Figure B-7. GSM Spectrum Mask from "Radio Transmission and Reception," GSM 05.05 May 1996, Version 5.1.0

Figure based on specifications from the European Telecommunications Standards Institute.[45] GSM = Global System for Mobile Communications.

B.9.1. Modulation Measurement Results

In the following, representative results of both harmonic distortion and intermodulation distortion measurements are shown. The measurements were carried out using a spectrum analyzer and a dual-ridge guide directional antenna. The measurement parameters for the spectrum analyzer are noted in the figure captions. The antenna was placed in the chamber and its output was fed to the spectrum analyzer through a bulkhead. The unloaded chambers were excited with their respective modulated signals at their specified power levels. The spectrum analyzer "peak hold" feature was enabled so the maximum signal levels were acquired over a period of time in order to assess the distortion.

Figure B-8A shows that the maximum signal level in the adjacent channel (approximately 200 kHz from the center frequency of 900 MHz) is more than 35 dB lower than the signal level at the center frequency, which is below the limit of the acceptable range specified in the GSM specification shown in Figure B-7. Figure B-8B shows that the signal level at the second harmonic at 1,800 MHz is around 60 dB below that of the signal at 900 MHz, which is well within the acceptable range.

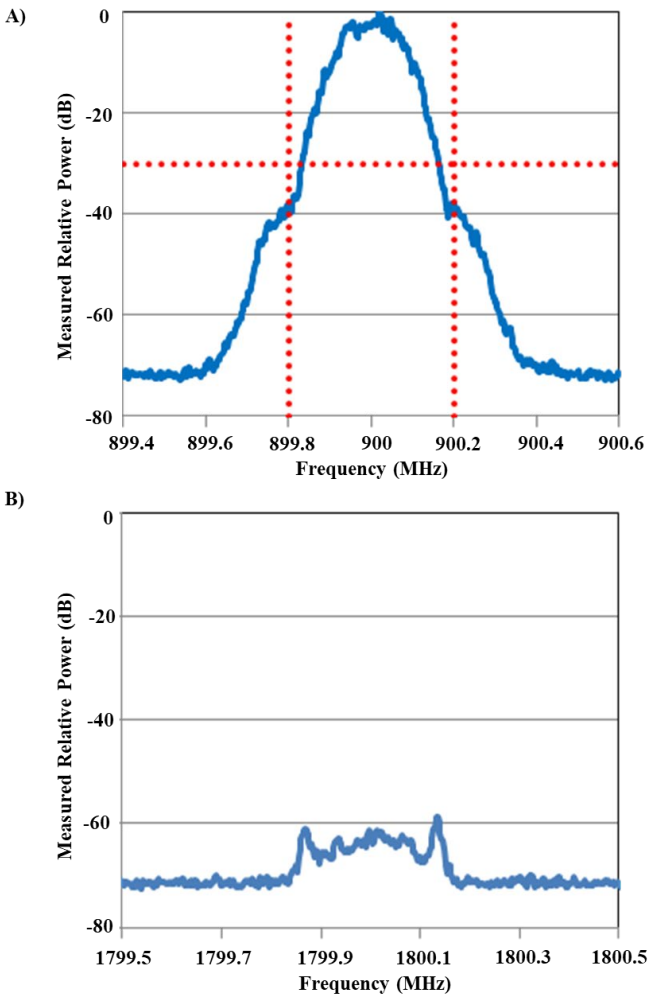

Figure B-8. 900 MHz GSM Spectra Measured in a High-power Chamber, Normalized to the Highest Measured Power

(A) Fundamental frequency band, peak hold on. The spectral mask limits for GSM transmissions are denoted by the red, dotted lines on the plot. (B) Second harmonic, peak hold on. The spectrum analyzer frequency resolution was approximately 2 kHz. GSM = Global System for Mobile Communications-modulated cell phone radiofrequency radiation.

Figure B-9 shows the GSM spectra in a high-power mouse chamber at 1,900 MHz. Again, the level of intermodulation distortion (signal level in the adjacent channel around the carrier frequency of 1,900 MHz) in Figure B-9A is approximately 35–37 dB below the maximum. These results are very close to the published specification found in the GSM 05.05[45] and shown in Figure B-7, as depicted by the dotted red lines in Figure B-9A. Any signal levels near this level will have an insignificant contribution to the total power in the signal. The level of harmonic distortion in Figure B-9B is well within acceptable ranges.

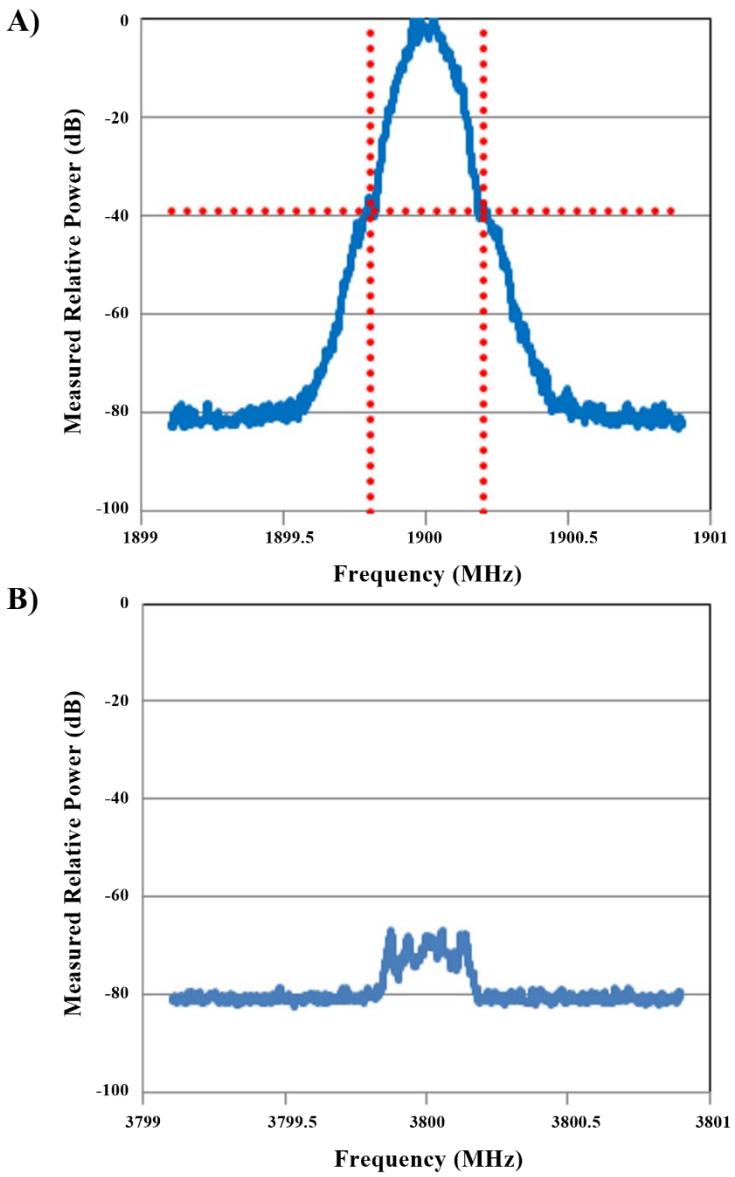

Figure B-9. 1,900 MHz GSM Spectra Measured in a High-power Chamber

(A) Fundamental, peak hold on. The spectral mask limits for GSM transmissions are denoted by the red, dotted lines on the plot. (B) Second harmonic, peak hold on. The spectrum analyzer frequency resolution was approximately 200 Hz. GSM = Global System for Mobile Communications-modulated cell phone radiofrequency radiation.

The intermodulation distortion in the highest-power rat and mouse chambers was also measured for the IS-95 (i.e., CDMA) excitation. It is noteworthy that the asymmetry in the lower adjacent channel compared to that of the upper adjacent channel, most noticeably in Figure B-10B, which is not uncommon when wideband modulated signals are amplified. Figure B-10 shows the signal levels in both upper and lower adjacent channels (marked by the vertical dotted lines) are within the specification of approximately 35 dB below the main channel over a 30 kHz frequency bandwidth. The horizontal dotted lines indicate the amplitude threshold limit. Outside the channel, signals need to be below this threshold.

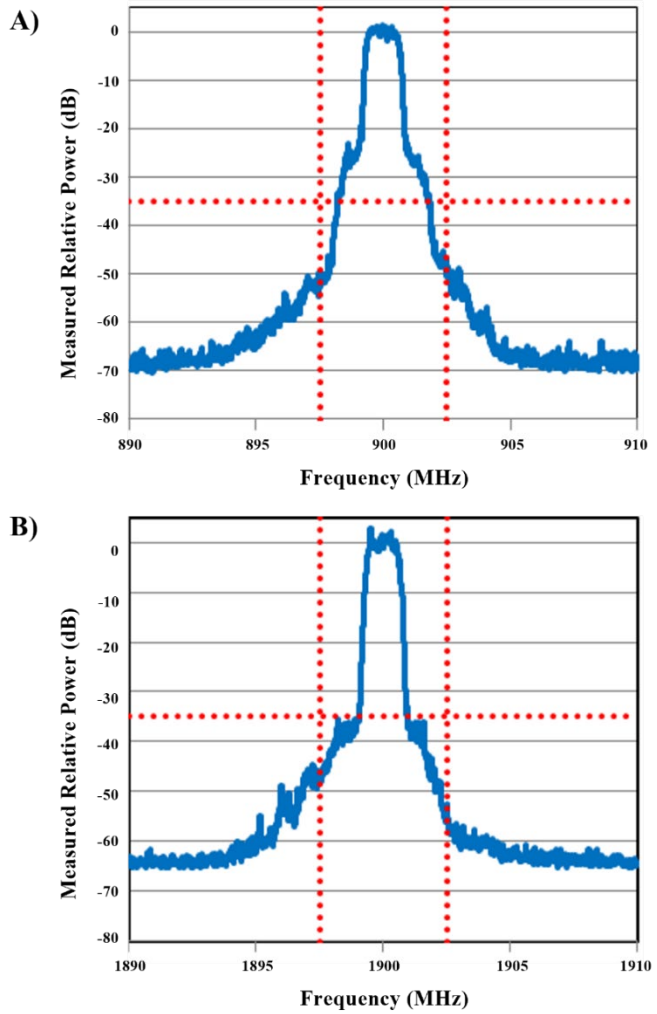

Figure B-10. Interim Standard 95 (i.e., CDMA) Spectrum Measured in a High-power Chamber for (A) 900 MHz and (B) 1,900 MHz

Measurements were conducted in the high-power chamber (Chamber 1). The spectrum analyzer peak hold feature was "on," and the signal was acquired over several minutes' time. The spectrum analyzer frequency resolution was approximately 2.4 kHz. CDMA = Code Division Multiple Access-modulated cell phone radiofrequency radiation.

Finally, the time-domain waveform associated with the GSM signal in the highest-power rat chamber was measured. Again, the paddles were turning, and the dual-ridge guide antenna was placed in the chamber. The spectrum analyzer was set to "zero span" to acquire the time-domain trace. These measurements were taken to assess possible leakage of signals intended for other chambers through the electronic switches into the chamber of interest.

Figure B-11 shows the maximum level of several repeat measurements overlaid. In each case, the paddle was in a different position, so in some cases the signals were stronger than in other cases. No leak-through was observed, indicating that the maximum possible leak-through signals were at least 70 dB lower than the signals in the desired excitation time slot. High-power radiofrequency switches typically have isolation ratings between 20 and 30 dB between switched channels. The isolation measurements show that the switch exceeded the manufacturer's specifications.

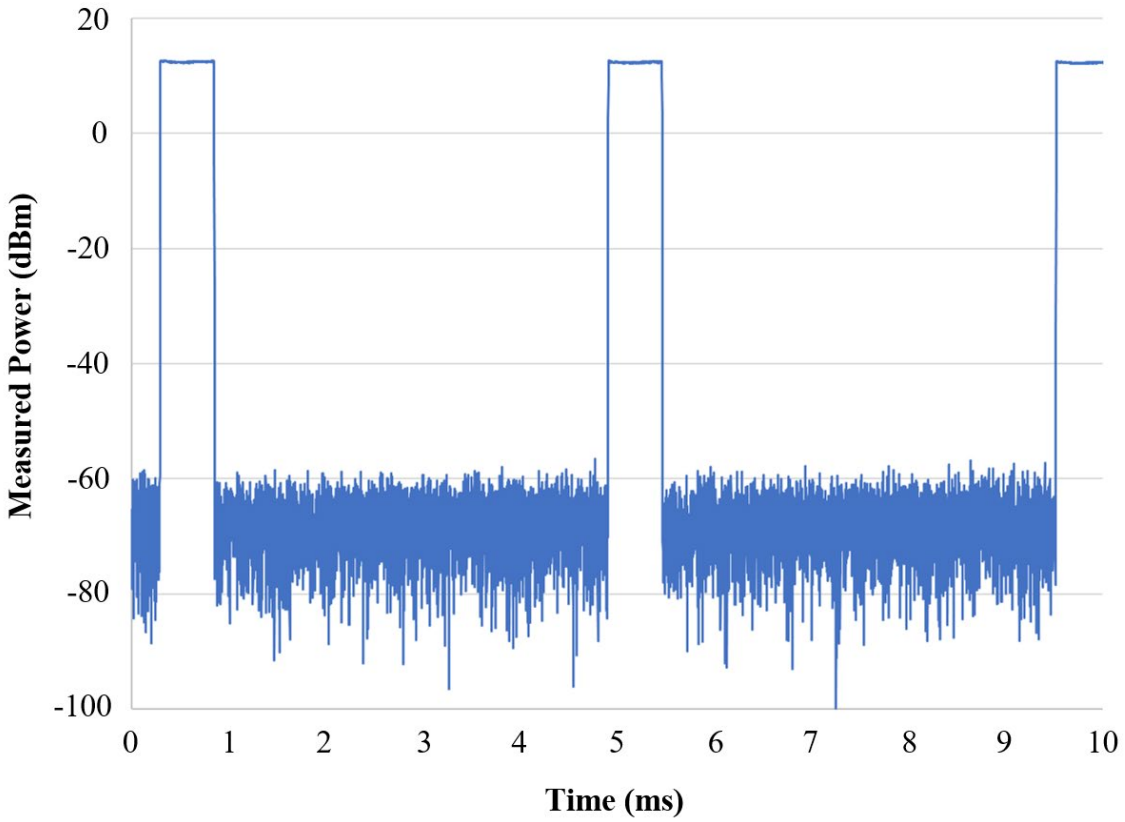

Figure B-11. Time-domain Waveform Showing Principal Timeslots (High Level) and Timeslots for Other Chambers (Lower Levels)

The spectrum analyzer was set to "zero span" to measure the time-domain waveform.

This appendix indicates that the distortion in the transmission systems used to excite the chambers was minimal. The harmonic distortion was low enough to have a negligible contribution to the total signal power. The intermodulation distortion measured in the adjacent channel was consistent with the spectrum mask for both the GSM and IS-95 (i.e., CDMA) signals. The leak-through from the switches used to excite other chambers was less than 47 dB, well within the specification of such switches and low enough that interference to the main channel should not have been an issue.

B.10. Conclusions

Overall, each of the chambers behaved as expected. The chamber/IT'IS probe readings were consistent with the calibrated NIST probes, the field uniformity was within expected bounds, and the signal quality was acceptable.

Significant findings include:

- With the exception of a few measured points outside the uncertainty bounds (shown in Figure B-2 and Figure B-3), the electric field measurements agreed within the estimated uncertainty bounds, which indicates that the chamber fields measured by the NIST probe, the NIST reference antenna, and the IT'IS probes agreed within the

reported accuracy of each system. For the limited number of measurements outside the uncertainty bounds, they only narrowly exceed the bounds and do not warrant additional concern. The reported exposure field in the chamber was therefore considered reliable.

- The magnitude of field variation throughout the volume of a fully loaded chamber was consistent with earlier values reported on the prototype chamber. However, there may have been up to ±2 dB of variation in the exposure field depending on location in the cage racks. A simple way to mitigate any effect of this exposure variation would be to routinely rotate the cages to various locations in the racks.
- The quality of the modulated signals was found to be acceptable with regard to distortion and harmonic content. The power delivery system appeared to be functioning well within acceptable limits with only minimal leak-through in the switching system.

The overall conclusion is that the system was operating correctly and capable of performing the exposure study.

Appendix C. Exposure Monitoring Data

Table of Contents

Tables

C.1. Overview

Exposure data are reported for animals exposed to whole-body radiofrequency radiation (RFR) via signal modulations of Code Division Multiple Access (CDMA) or Global System for Mobile Communications (GSM). Target exposure levels, and acceptable ranges, for rats and mice are reported in Table C-1. Exposure data include specific absorption rate (SAR) levels (W/kg body weight, or W/kg) (Table C-2, Table C-4, Table C-6, and Table C-8), and electric field (E-field) measurements (V/m) (Table C-3, Table C-5, Table C-7, and Table C-9). Fields were measured continuously throughout the studies and measurements were automatically recorded approximately every 20 seconds. For every 20-second interval, the SAR was calculated based on the average E-field data. The data presented for each exposure parameter include the mean and standard deviation [expressed in decibels (dB), W/kg or V/m], the total number of measurements recorded during the identified period of exposure (468/day); the lowest (minimum) and highest measurement (maximum) recorded during the given exposure period; the number of measurements that were within the acceptable range; and the ratio of all measurements within range.

The data reported for SAR also include the animal body weights (g) and the selected target SAR (W/kg) for each group. The data reported for E-field strength include the target range of the field required to maintain appropriate SAR exposures. The minimum and maximum exposure values reported represent a single recorded measurement over the 5-day exposure period. The SAR and chamber field in the control chamber and exposure chambers were within the target ranges (defined as ±2 dB) for 100% of recorded measurements over the course of the study; 100% of E-field exposures in the control chamber and exposure chambers were within the target ranges.

The dB represents a mathematical transformation of a number or numerical ratio using base 10 logarithms. Multiplication of ratios is transformed into addition of dBs; raising a number to a power is transformed into multiplication of dBs.

In general, dB(power) = 10 × log(R) and dB(field) = 20 × log(R). The formulas differ by a factor of 2 because power or SAR varies as the square of the fields. For SAR (in W/kg), the dB formula is calculated as:

$$\text{SAR (dB)} = 10 \times \log(\text{SAR}_M/\text{SAR}_T)$$

where SAR_M is the measured value and SAR_T is the target value, and

$$-2 \text{ dB} = 10 \times \log(\text{SAR}_L/\text{SAR}_T), \text{ where } \text{SAR}_L \text{ (low)} = \text{SAR}_T \times 10^{-0.2}$$

$$+2 \text{ dB} = 10 \times \log(\text{SAR}_H/\text{SAR}_T), \text{ where } \text{SAR}_H \text{ (high)} = \text{SAR}_T \times 10^{0.2}$$

Therefore, the ±2 dB range specified by the National Institute of Environmental Health Sciences Division of Translational Toxicology (NIEHS/DTT) translates to the ranges described in Table C-1 for each SAR used in the 5-day studies.

Table C-1. Target Specific Absorption Rate Levels and Acceptable Specific Absorption Rate Range for the Five-day Studies of Radiofrequency Radiation

Target SAR Level (W/kg)	Acceptable SAR Level Range (W/kg)[a]
Rats	
3	1.89 to 4.75
6	3.79 to 9.51
9	5.68 to 14.26
Mice	
5	3.15 to 7.92
10	6.31 to 15.85
15	9.46 to 23.77

SAR = specific absorption rate.
[a]The acceptable SAR range was ±2 dB from the target SAR.

C.2. Results

C.2.1. Five-day Studies in Male Mice Exposed to CDMA-modulated Cell Phone Radiofrequency Radiation

Table C-2. Summary of CDMA-modulated Cell Phone Radiofrequency Radiation Exposure Data for Male Mice-Specific Absorption Rate

Chamber	Animal Weight (g)	Target (W/kg)	Mean (W/kg)	Stdev (dB)	Min (dB)	Max (dB)	In Range/Total	Ratio
July 22, 2020								
1[a]	39.5	15.000	15.013	0.25	−0.71	0.57	468/468	1.000
2	41.3	10.000	10.006	0.13	−0.55	0.59	458/458	1.000
3	40.5	5.000	5.006	0.21	−0.60	0.58	458/458	1.000
4	40.7	0.000	0.000	–	–	–	468/468	1.000
July 23, 2020								
1	39.5	15.000	15.011	0.24	−0.67	0.66	468/468	1.000
2	41.3	10.000	10.011	0.14	−0.41	0.63	475/475	1.000
3	40.5	5.000	5.008	0.21	−0.58	0.55	475/475	1.000
4	40.7	0.000	0.000	–	–	–	468/468	1.000
July 24, 2020								
1	39.5	15.000	15.013	0.23	−0.55	0.58	468/468	1.000
2	41.3	10.000	10.008	0.15	−0.50	1.06	459/459	1.000
3	40.5	5.000	5.001	0.19	−0.57	0.47	459/459	1.000
4	40.7	0.000	0.000	–	–	–	468/468	1.000
July 25, 2020								
1	39.5	15.000	14.998	0.24	−0.62	0.56	472/472	1.000
2	41.3	10.000	10.006	0.13	−0.36	0.50	470/470	1.000
3	40.5	5.000	5.005	0.20	−0.51	0.57	470/470	1.000

Chamber	Animal Weight (g)	Target (W/kg)	Mean (W/kg)	Stdev (dB)	Min (dB)	Max (dB)	In Range/Total	Ratio
4	40.7	0.000	0.000	–	–	–	472/472	1.000
July 26, 2020								
1	39.5	15.000	15.006	0.24	−0.66	0.61	466/466	1.000
2	41.3	10.000	10.005	0.13	−0.59	0.50	465/465	1.000
3	40.5	5.000	5.004	0.20	−0.61	0.52	465/465	1.000
4	40.7	0.000	0.000	–	–	–	466/466	1.000

CDMA = Code Division Multiple Access-modulated cell phone radiofrequency radiation.
[a]Exposures occurred in 10-minute on, 10-minute off cycles, and due to system power constraints, the 0 W/kg and 15 W/kg groups (Chambers 4 and 1, respectively) were exposed during opposite 10-minute intervals than the 5 W/kg and 10 W/kg (Chambers 2 and 3, respectively) groups.

Table C-3. Summary of CDMA-modulated Cell Phone Radiofrequency Radiation Exposure Data for Male Mice-Averaged E-field

Chamber	Target (V/m)	Mean (V/m)	Stdev (dB)	Min (dB)	Max (dB)	In Range/Total	Ratio
July 22, 2020							
1[a]	304.4	304.4	0.25	−0.71	0.57	468/468	1.000
2	252.1	252.1	0.13	−0.54	0.59	458/458	1.000
3	177.2	177.2	0.21	−0.61	0.58	458/458	1.000
4	0.0	0.0	–	–	–	468/468	1.000
July 23, 2020							
1	304.4	304.3	0.24	−0.67	0.66	468/468	1.000
2	252.1	252.2	0.15	−0.41	0.63	475/475	1.000
3	177.2	177.2	0.22	−0.58	0.55	475/475	1.000
4	0.0	0.0	–	–	–	468/468	1.000
July 24, 2020							
1	304.4	304.4	0.24	−0.55	0.58	468/468	1.000
2	252.1	252.2	0.14	−0.50	1.06	459/459	1.000
3	177.2	177.1	0.19	−0.57	0.47	459/459	1.000
4	0.0	0.0	–	–	–	468/468	1.000
July 25, 2020							
1	304.4	304.2	0.24	−0.62	0.56	472/472	1.000
2	252.1	252.1	0.13	−0.36	0.50	470/470	1.000
3	177.2	177.2	0.20	−0.51	0.57	470/470	1.000
4	0.0	0.0	–	–	–	472/472	1.000
July 26, 2020							
1	304.4	304.3	0.24	−0.66	0.61	466/466	1.000
2	252.1	252.1	0.13	−0.59	0.51	465/465	1.000
3	177.2	177.2	0.21	−0.62	0.53	465/465	1.000
4	0.0	0.0	–	–	–	466/466	1.000

CDMA = Code Division Multiple Access-modulated cell phone radiofrequency radiation.
[a]Exposures occurred in 10-minute on, 10-minute off cycles, and due to system power constraints, the 0 W/kg and 15 W/kg groups (Chambers 4 and 1, respectively) were exposed during opposite 10-minute intervals than the 5 W/kg and 10 W/kg (Chambers 2 and 3, respectively) groups.

C.2.2. Five-day Studies in Male Rats Exposed to CDMA-modulated Cell Phone Radiofrequency Radiation

Table C-4. Summary of CDMA-modulated Cell Phone Radiofrequency Radiation Exposure Data for Male Rats-Specific Absorption Rate

Chamber	Animal Weight (g)	Target (W/kg)	Mean (W/kg)	Stdev (dB)	Min (dB)	Max (dB)	In Range/Total	Ratio
October 21, 2021								
1[a]	388.8	9.000	9.004	0.20	−0.59	0.65	462/462	1.000
2	388.1	6.000	6.002	0.18	−0.67	0.62	455/455	1.000
3	384.7	3.000	3.002	0.16	−0.60	0.54	455/455	1.000
4	382.4	0.000	0.000	–	–	–	462/462	1.000
October 22, 2021								
1	388.8	9.000	9.003	0.19	−0.72	0.59	477/477	1.000
2	388.1	6.000	6.008	0.19	−0.70	1.04	477/477	1.000
3	384.7	3.000	3.002	0.16	−0.64	0.91	477/477	1.000
4	382.4	0.000	0.000	–	–	–	477/477	1.000
October 23, 2021								
1	388.8	9.000	9.026	0.22	−0.72	0.86	473/473	1.000
2	388.1	6.000	6.004	0.21	−1.02	0.82	473/473	1.000
3	384.7	3.000	3.003	0.17	−0.57	0.72	473/473	1.000
4	382.4	0.000	0.000	–	–	–	473/473	1.000
October 24, 2021								
1	388.8	9.000	9.004	0.19	−0.59	0.60	477/477	1.000
2	388.1	6.000	6.003	0.18	−0.62	0.82	477/477	1.000
3	384.7	3.000	3.001	0.16	−0.88	0.61	477/477	1.000
4	382.4	0.000	0.000	–	–	–	477/477	1.000
October 25, 2021								
1	388.8	9.000	9.014	0.22	−0.96	0.89	461/461	1.000
2	388.1	6.000	6.014	0.21	−0.96	0.86	475/475	1.000
3	384.7	3.000	3.003	0.17	−0.72	0.59	475/475	1.000
4	382.4	0.000	0.000	–	–	–	461/461	1.000

CDMA = Code Division Multiple Access-modulated cell phone radiofrequency radiation.
[a]Exposures occurred in 10-minute on, 10-minute off cycles, and due to system power constraints, the 0 W/kg and 9 W/kg groups (Chambers 4 and 1, respectively) were exposed during opposite 10-minute intervals than the 3 W/kg and 6 W/kg (Chambers 2 and 3, respectively) groups.

Table C-5. Summary of CDMA-modulated Cell Phone Radiofrequency Radiation Exposure Data for Male Rats-Averaged E-field

Chamber	Target (V/m)	Mean (V/m)	Stdev (dB)	Min (dB)	Max (dB)	In Range/Total	Ratio
October 21, 2021							
1[a]	341.6	341.6	0.21	−0.59	0.65	462/462	1.000
2	278.8	278.8	0.18	−0.67	0.62	455/455	1.000
3	196.6	196.7	0.16	−0.60	0.55	455/455	1.000
4	0.0	0.0	–	–	–	462/462	1.000

Chamber	Target (V/m)	Mean (V/m)	Stdev (dB)	Min (dB)	Max (dB)	In Range/Total	Ratio
October 22, 2021							
1	341.6	341.6	0.19	−0.72	0.59	477/477	1.000
2	278.8	278.9	0.19	−0.70	1.04	477/477	1.000
3	196.6	196.7	0.16	−0.63	0.91	477/477	1.000
4	0.0	0.0	–	–	–	477/477	1.000
October 23, 2021							
1	341.6	342.0	0.22	−0.71	0.86	473/473	1.000
2	278.8	278.8	0.21	−1.03	0.81	473/473	1.000
3	196.6	196.7	0.17	−0.57	0.72	473/473	1.000
4	0.0	0.0	–	–	–	473/473	1.000
October 24, 2021							
1	341.6	341.6	0.19	−0.59	0.60	477/477	1.000
2	278.8	278.8	0.18	−0.62	0.81	477/477	1.000
3	196.6	196.6	0.17	−0.89	0.60	477/477	1.000
4	0.0	0.0	–	–	–	477/477	1.000
October 25, 2021							
1	341.6	341.8	0.22	−0.96	0.89	461/461	1.000
2	278.8	279.0	0.21	−0.96	0.86	475/475	1.000
3	196.6	196.7	0.17	−0.73	0.59	475/475	1.000
4	0.0	0.0	–	–	–	461/461	1.000

CDMA = Code Division Multiple Access-modulated cell phone radiofrequency radiation.
[a]Exposures occurred in 10-minute on, 10-minute off cycles, and due to system power constraints, the 0 W/kg and 9 W/kg groups (Chambers 4 and 1, respectively) were exposed during opposite 10-minute intervals than the 3 W/kg and 6 W/kg (Chambers 2 and 3, respectively) groups.

C.2.3. Five-day Studies in Female Rats Exposed to CDMA-modulated Cell Phone Radiofrequency Radiation

Table C-6. Summary of CDMA-modulated Cell Phone Radiofrequency Radiation Exposure Data for Female Rats-Specific Absorption Rate

Chamber	Animal Weight (g)	Target (W/kg)	Mean (W/kg)	Stdev (dB)	Min (dB)	Max (dB)	In Range/Total	Ratio
November 18, 2021								
1[a]	277.0	9.000	9.006	0.17	−0.54	0.61	465/465	1.000
2	275.1	6.000	5.999	0.18	−1.07	0.64	471/471	1.000
3	267.0	3.000	2.999	0.16	−0.57	0.58	471/471	1.000
4	266.5	0.000	0.000	–	–	–	465/465	1.000
November 19, 2021								
1	277.0	9.000	9.006	0.18	−0.73	0.57	477/477	1.000
2	275.1	6.000	5.999	0.15	−0.59	0.62	477/477	1.000
3	267.0	3.000	3.001	0.14	−0.54	0.59	477/477	1.000
4	266.5	0.000	0.000	–	–	–	477/477	1.000

Chamber	Animal Weight (g)	Target (W/kg)	Mean (W/kg)	Stdev (dB)	Min (dB)	Max (dB)	In Range/Total	Ratio
November 20, 2021, First Period[b]								
1	277.0	9.000	8.998	0.09	−0.14	0.22	18/18	1.000
2	275.1	6.000	5.976	0.11	−0.22	0.17	18/18	1.000
3	267.0	3.000	3.012	0.12	−0.27	0.25	18/18	1.000
4	266.5	0.000	0.000	–	–	–	18/18	1.000
November 20, 2021, Second Period[b]								
1	277.0	9.000	9.002	0.14	−0.65	0.60	441/441	1.000
2	275.1	6.000	6.000	0.13	−0.56	0.56	446/446	1.000
3	267.0	3.000	3.002	0.11	−0.32	0.61	446/446	1.000
4	266.5	0.000	0.000	–	–	–	441/441	1.000
November 21, 2021[c]								
1	277.0	9.000	8.995	0.13	−0.29	0.34	99/99	1.000
2	275.1	6.000	6.006	0.12	−0.27	0.50	99/99	1.000
3	267.0	3.000	3.000	0.10	−0.25	0.33	99/99	1.000
4	266.5	0.000	0.000	–	–	–	99/99	1.000
November 22, 2021								
1	277.0	9.000	9.006	0.16	−0.50	0.63	461/461	1.000
2	275.1	6.000	6.002	0.16	−0.68	0.59	474/474	1.000
3	267.0	3.000	3.003	0.16	−0.56	0.57	474/474	1.000
4	266.5	0.000	0.000	–	–	–	461/461	1.000
November 23, 2021, First Period[b]								
1	277.0	9.000	8.933	0.13	−0.26	0.28	18/18	1.000
2	275.1	6.000	5.983	0.15	−0.38	0.14	18/18	1.000
3	267.0	3.000	2.997	0.06	−0.12	0.09	18/18	1.000
4	266.5	0.000	0.000	–	–	–	18/18	1.000
November 23, 2021, Second Period[b]								
1	277.0	9.000	9.004	0.16	−0.68	0.55	441/441	1.000
2	275.1	6.000	6.001	0.17	−0.77	0.58	446/446	1.000
3	267.0	3.000	3.003	0.15	−0.49	0.47	446/446	1.000
4	266.5	0.000	0.000	–	–	–	441/441	1.000

CDMA = Code Division Multiple Access-modulated cell phone radiofrequency radiation.

[a]Exposures occurred in 10-minute on, 10-minute off cycles, and due to system power constraints, the 0 W/kg and 9 W/kg groups (Chambers 4 and 1, respectively) were exposed during opposite 10-minute intervals than the 3 W/kg and 6 W/kg (Chambers 2 and 3, respectively) groups.

[b]On November 20 and 23, 2021, exposure ceased prematurely and was restarted. The first period exposed animals for approximately 30 minutes, and the second period exposed for 8 hours and 30 minutes.

[c]On November 21, 2021, exposure ceased prematurely because Chamber 1 (9 W/kg) was not properly closed following afternoon animal husbandry activities and exposure did not resume until the next day, leading to an exposure of only approximately 2 hours for each chamber. Therefore, animals were exposed for an additional day.

Table C-7. Summary of CDMA-modulated Cell Phone Radiofrequency Radiation Exposure Data for Female Rats-Averaged E-field

Chamber	Target (V/m)	Mean (V/m)	Stdev (dB)	Min (dB)	Max (dB)	In Range/Total	Ratio
November 18, 2021							
1[a]	309.6	309.7	0.17	−0.54	0.61	465/465	1.000
2	252.3	252.2	0.18	−1.07	0.65	471/471	1.000
3	176.9	176.8	0.16	−0.58	0.58	471/471	1.000
4	0.0	0.0	–	–	–	465/465	1.000
November 19, 2021							
1	309.6	309.7	0.18	−0.73	0.57	477/477	1.000
2	252.3	252.3	0.15	−0.59	0.62	477/477	1.000
3	176.9	176.9	0.14	−0.54	0.59	477/477	1.000
4	0.0	0.0	–	–	–	477/477	1.000
November 20, 2021, First Period[b]							
1	309.6	309.6	0.09	−0.14	0.22	18/18	1.000
2	252.3	251.8	0.11	−0.22	0.17	18/18	1.000
3	176.9	177.2	0.12	−0.27	0.26	18/18	1.000
4	0.0	0.0	–	–	–	18/18	1.000
November 20, 2021, Second Period[b]							
1	309.6	309.6	0.14	−0.65	0.60	441/441	1.000
2	252.3	252.3	0.13	−0.55	0.56	446/446	1.000
3	176.9	176.9	0.11	−0.31	0.61	446/446	1.000
4	0.0	0.0	–	–	–	441/441	1.000
November 21, 2021[c]							
1	309.6	309.5	0.13	−0.29	0.34	99/99	1.000
2	252.3	252.4	0.12	−0.27	0.50	99/99	1.000
3	176.9	176.9	0.10	−0.25	0.34	99/99	1.000
4	0.0	0.0	–	–	–	99/99	1.000
November 22, 2021							
1	309.6	309.7	0.16	−0.50	0.63	461/461	1.000
2	252.3	252.3	0.16	−0.68	0.60	474/474	1.000
3	176.9	176.9	0.16	−0.55	0.57	474/474	1.000
4	0.0	0.0	–	–	–	461/461	1.000

Chamber	Target (V/m)	Mean (V/m)	Stdev (dB)	Min (dB)	Max (dB)	In Range/Total	Ratio
November 23, 2021, First Period[d]							
1	309.6	308.4	0.14	−0.26	0.28	18/18	1.000
2	252.3	251.9	0.15	−0.38	0.14	18/18	1.000
3	176.9	176.8	0.06	−0.11	0.08	18/18	1.000
4	0.0	0.0	–	–	–	18/18	1.000
November 23, 2021, Second Period[b]							
1	309.6	309.7	0.16	−0.68	0.55	441/441	1.000
2	252.3	252.3	0.18	−0.78	0.57	446/446	1.000
3	176.9	176.9	0.15	−0.49	0.47	446/446	1.000
4	0.0	0.0	–	–	–	441/441	1.000

CDMA = Code Division Multiple Access-modulated cell phone radiofrequency radiation.
[a]Exposures occurred in 10-minute on, 10-minute off cycles, and due to system power constraints, the 0 W/kg and 9 W/kg exposure groups (Chambers 4 and 1) were exposed during opposite 10-minute intervals than the 3 W/kg and 6 W/kg exposure (Chambers 2 and 3) groups.
[b]On November 20 and 23, 2021, exposure ceased prematurely and was restarted. The first period exposed animals for approximately 30 minutes, and the second period exposed for 8 hours and 30 minutes.
[c]On November 21, 2021, exposure ceased prematurely because Chamber 1 (9 W/kg) was not properly closed following afternoon animal husbandry activities and exposure did not resume until the next day, leading to an exposure of only approximately 2 hours for each chamber. Therefore, animals were exposed for an additional day.

C.2.4. Five-day Studies in Male Rats Exposed to GSM-modulated Cell Phone Radiofrequency Radiation

Table C-8. Summary of GSM-modulated Cell Phone Radiofrequency Radiation Exposure Data for Male Rats-Specific Absorption Rate

Chamber	Animal Weight (g)	Target (W/kg)	Mean (W/kg)	Stdev (dB)	Min (dB)	Max (dB)	In Range/Total	Ratio
September 30, 2021								
1[a]	373.2	9.000	9.001	0.20	−0.62	0.74	468/468	1.000
2	360.2	6.000	5.997	0.18	−0.85	0.55	468/468	1.000
3	377.4	3.000	3.001	0.17	−0.77	0.59	468/468	1.000
4	377.7	0.000	0.000	–	–	–	468/468	1.000
October 1, 2021								
1	373.2	9.000	9.002	0.21	−0.87	0.81	477/477	1.000
2	360.2	6.000	6.005	0.18	−0.54	0.61	477/477	1.000
3	377.4	3.000	3.004	0.19	−0.69	0.80	477/477	1.000
4	377.7	0.000	0.000	–	–	–	477/477	1.000
October 2, 2021, First Period[b]								
1	373.2	9.000	8.987	0.15	−0.36	0.39	67/67	1.000
2	360.2	6.000	5.990	0.12	−0.22	0.41	60/60	1.000
3	377.4	3.000	3.005	0.15	−0.44	0.45	60/60	1.000
4	377.7	0.000	0.000	–	–	–	67/67	1.000

Chamber	Animal Weight (g)	Target (W/kg)	Mean (W/kg)	Stdev (dB)	Min (dB)	Max (dB)	In Range/Total	Ratio
October 2, 2021, Second Period[b]								
1	373.2	9.000	9.001	0.22	−0.69	0.78	378/378	1.000
2	360.2	6.000	6.010	0.21	−0.61	0.68	378/378	1.000
3	377.4	3.000	3.002	0.18	−0.57	0.91	378/378	1.000
4	377.7	0.000	0.000	–	–	–	378/378	1.000
October 3, 2021								
1	373.2	9.000	9.011	0.22	−0.71	0.75	477/477	1.000
2	360.2	6.000	6.009	0.20	−0.61	0.97	477/477	1.000
3	377.4	3.000	3.002	0.18	−0.86	0.51	477/477	1.000
4	377.7	0.000	0.000	–	–	–	477/477	1.000
October 4, 2021								
1	373.2	9.000	9.014	0.21	−0.79	0.78	470/470	1.000
2	360.2	6.000	6.012	0.21	−0.73	0.82	467/467	1.000
3	377.4	3.000	3.004	0.18	−0.72	0.68	467/467	1.000
4	377.7	0.000	0.000	–	–	–	470/470	1.000

GSM = Global System for Mobile Communications-modulated cell phone radiofrequency radiation.
[a]Exposures occurred in 10-minute on, 10-minute off cycles, and due to system power constraints, the 0 W/kg and 9 W/kg groups (Chambers 4 and 1, respectively) were exposed during opposite 10-minute intervals than the 3 W/kg and 6 W/kg (Chambers 2 and 3, respectively) groups.
[b]On October 2, 2021, exposure was disrupted because of a facility power outage, and the system did not expose for approximately 33 minutes. The first period exposed animals for 1 hour and 20 minutes, and the second period exposed for 7 hours and 10 minutes.

Table C-9. Summary of GSM-modulated Cell Phone Radiofrequency Radiation Exposure Data for Male Rats-Averaged E-field

Chamber	Target (V/m)	Mean (V/m)	Stdev (dB)	Min (dB)	Max (dB)	In Range/Total	Ratio
September 30, 2021							
1[a]	337.6	337.5	0.20	−0.61	0.73	468/468	1.000
2	272.8	272.7	0.18	−0.85	0.55	468/468	1.000
3	195.5	195.5	0.18	−0.77	0.59	468/468	1.000
4	0.0	0.0	–	–	–	468/468	1.000
October 1, 2021							
1	337.6	337.5	0.21	−0.87	0.81	477/477	1.000
2	272.8	272.9	0.18	−0.54	0.61	477/477	1.000
3	195.5	195.6	0.19	−0.70	0.80	477/477	1.000
4	0.0	0.0	–	–	–	477/477	1.000
October 2, 2021, First Period[b]							
1	337.6	337.3	0.15	−0.36	0.39	67/67	1.000
2	272.8	272.6	0.12	−0.21	0.41	60/60	1.000
3	195.5	195.7	0.15	−0.44	0.46	60/60	1.000
4	0.0	0.0	–	–	–	67/67	1.000

Chamber	Target (V/m)	Mean (V/m)	Stdev (dB)	Min (dB)	Max (dB)	In Range/Total	Ratio
October 2, 2021, Second Period[b]							
1	337.6	337.5	0.23	−0.70	0.77	378/378	1.000
2	272.8	273.0	0.21	−0.61	0.68	378/378	1.000
3	192.5	195.6	0.18	−0.57	0.91	378/378	1.000
4	0.0	0.0	–	–	–	378/378	1.000
October 3, 2021							
1	337.6	337.7	0.22	−0.71	0.75	477/477	1.000
2	272.8	273.0	0.20	−0.62	0.97	477/477	1.000
3	195.5	195.6	0.18	−0.85	0.51	477/477	1.000
4	0.0	0.0	–	–	–	477/477	1.000
October 4, 2021							
1	337.6	337.8	0.21	−0.79	0.78	470/470	1.000
2	272.8	273.0	0.21	−0.74	0.81	467/467	1.000
3	195.5	195.6	0.18	−0.73	0.69	467/467	1.000
4	0.0	0.0	–	–	–	470/470	1.000

GSM = Global System for Mobile Communications-modulated cell phone radiofrequency radiation.
[a]Exposures occurred in 10-minute on, 10-minute off cycles, and due to system power constraints, the 0 W/kg and 9 W/kg groups (Chambers 4 and 1, respectively) were exposed during opposite 10-minute intervals than the 3 W/kg and 6 W/kg (Chambers 2 and 3, respectively) groups.
[b]On October 2, 2021, exposure was disrupted because of a facility power outage, and the system did not expose for approximately 33 minutes. The first period exposed animals for 1 hour and 20 minutes, and the second period exposed for 7 hours and 10 minutes.

Appendix D. Genetic Toxicology

Table of Contents

Tables

D.1. Comet Assay

D.1.1. Evaluation Protocol

This report considers biological as well as statistical factors to determine an overall result for the comet assay.

D.1.2. Collection of Tissue Samples for Genotoxicity Testing

Exposures to Global System for Mobile Communications (GSM)- or Code Division Multiple Access (CDMA)-modulated cell phone radiofrequency radiation continued briefly on the day of necropsy to minimize the time between exposure and collection of tissues for the comet assay. Subsets of animals were removed during successive "off" exposure periods, with representation across exposure groups during each "off" period. Exposures continued for animals that remained in the reverberation chambers until all animals were removed. All animals were necropsied and all tissues of interest were collected within approximately 2 hours and 4 minutes for mice and 2 hours and 50 minutes for rats. Animals were necropsied in the following order: one animal from each exposure group starting with the chamber control group, moving through each of the exposed groups, then rotating back to the chamber control group; animals were necropsied in numerical order within each exposure group. Six different tissues (cerebellum, frontal cortex, hippocampus, liver, heart, and blood) were collected from each animal for the comet assay. The amount of time that elapsed between euthanizing the animal and submerging dissected tissues in cold mincing solution on ice did not exceed 8 minutes for mice and 13 minutes for rats. Specifically, for CDMA mice, all tissues except brain tissues (i.e., cerebellum, frontal cortex, hippocampus) were submerged within 5 minutes; all brain tissues were submerged within 8 minutes. For CDMA male rats, heart tissue was submerged within 13 minutes, and brain tissues were submerged within 6 minutes; all other tissues from CDMA male rats were submerged within 5 minutes. For CDMA female rats, all tissues were submerged within 7 minutes. For GSM male rats, all tissues were submerged within 8 minutes.

D.1.3. Comet Assay Protocol

Tissue and peripheral blood samples were analyzed by Integrated Laboratory Systems, LLC, an Inotiv company (ILS; Research Triangle Park, NC) for determination of DNA damage. At termination of the 5-day studies of radiofrequency radiation (RFR), a 50 µL sample of blood was transferred to a tube containing 1 mL of freshly prepared cold mincing buffer ([Mg^{+2}, Ca^{+2}, and phenol-free Hank's Balanced Salt Solution [Life Technologies, Carlsbad, CA] with 20 mM EDTA [ethylenediaminetetraacetic acid], pH 7.3 to 7.5, and 10% v/v fresh dimethyl sulfoxide [DMSO]), then frozen in liquid nitrogen. The frontal cortex, hippocampus, cerebellum, liver, and heart were rinsed with cold mincing buffer to remove residual blood, then transferred to individual weigh boats containing sufficient fresh, cold mincing buffer to submerge the tissue and held on ice briefly (≤5 minutes) until processed. Several frozen cubes were prepared from each tissue by cutting small pieces of tissue (3 to 4 mm) and dropping them immediately into a weigh boat containing liquid nitrogen. Tissue cubes were given adequate time to freeze completely and were then transferred to labeled microfuge tubes maintained on dry ice. All samples were subsequently transferred to a −80°C freezer for storage until shipment by overnight

courier on dry ice to the analytical laboratory. Upon receipt, all samples were immediately placed in a −80°C freezer for storage until further processing.

Microcentrifuge tubes containing frozen tissue chunks were removed from the −80°C freezer and kept on dry ice until preparation of single cell suspensions in mincing buffer. One milliliter of cold mincing solution was aliquoted into a labeled microcentrifuge tube for each cubed, flash-frozen sample of frontal cortex, cerebellum, liver, and heart (right atrium and ventricle). Because of the small size of the tissue, 0.5 mL of cold mincing solution was aliquoted into a labeled microcentrifuge for each sample of hippocampus. Tubes with cold mincing solution were maintained on ice. Working rapidly to avoid tissue thawing, tissue cubes were transferred to tubes containing the cold mincing solution and rapidly minced until finely dispersed. Minced tissues were immediately processed onto slides. Frozen diluted blood was thawed on ice for immediate processing onto slides.

During slide preparation, freshly prepared minced tissues were maintained on ice and frozen blood samples were allowed to thaw on ice. Just before use, each sample was shaken gently to mix the cells and placed back on ice for 15 to 30 seconds to allow clumps to settle. A portion of the supernatant was empirically diluted with 0.5% low melting point agarose (Lonza, Walkersville, MD) dissolved in Dulbecco's phosphate buffer (Ca^{+2}, Mg^{+2}, and phenol-free) at 37°C and layered onto each well of a 2-well or 3-well CometSlide™ (Trevigen, Gaithersburg, MD). For each tissue, slides were prepared in batches of up to 10 animals and then immediately transferred to a refrigerator at 1°C–10°C to solidify the agarose.

Slides were immersed in cold lysing solution (2.5 M NaCl, 100 mM Na_2EDTA, 10 mM tris(hydroxymethyl)aminomethane (Tris), pH 10, containing freshly added 10% DMSO [Fisher Scientific, Pittsburgh, PA], and 1% Triton X-100) overnight in a refrigerator, protected from light. The following day, the slides were rinsed in 0.4 M Trizma base (pH 7.5), randomly placed onto the platform of a horizontal electrophoresis unit, and treated with cold alkali solution (300 mM NaOH, 1 mM Na_2EDTA, pH > 13) for 20 minutes to allow DNA unwinding, then electrophoresed at 4°C to 9°C for 20 minutes at 25 V (0.7 V/cm), with a current of approximately 300 mA. After electrophoresis, slides were neutralized with 0.4 M Trizma base (pH 7.5) for 5 minutes and then dehydrated by immersion in absolute ethanol (Pharmco-AAPER, Shelbyville, KY) for at least 5 minutes and allowed to air dry. Slides were prepared in a laboratory with a relative humidity of no more than 60% and stored at room temperature in a desiccator with a relative humidity of no more than 60% until stained and scored; stained slides were stored in a desiccator. NaCl, Na_2EDTA, Triton X-100, and Trizma base were purchased from Sigma-Aldrich (St. Louis, MO); NaOH was purchased from Fisher Scientific (Pittsburgh, PA).

After staining with SYBR® Gold (Molecular Probes, Life Technologies, Grand Island, NY), the slides, which were independently coded to mask exposure, were scored using Comet Assay IV Imaging Software, Version 4.3.1 (Perceptive Instruments, Ltd., Suffolk, UK), validated for Good Laboratory Practice Part 11 compliance.[46] In the alkaline (pH > 13) comet assay, damaged nuclear DNA fragments undergo unidirectional migration through the agarose gel within an electrical field, forming an image that resembles a comet, and greater fragmentation leads to increased DNA migration. The image analysis software partitions the intensity of the fluorescent signal of the DNA in the entire comet image into the percentage attributable to the comet head and the percentage attributable to the tail. Manual adjustment of the automated detection of head

and tail features is sometimes required. To evaluate DNA damage levels, the extent of DNA migration was characterized for 150 scorable comet figures per animal/tissue as the percent tail DNA (intensity of all tail pixels divided by the total intensity of all pixels in the comet, expressed as a percentage).

Comet figures are classified during the scoring process as scorable (evaluated for the percent tail DNA), nonscorable (because of inability to evaluate the percent tail DNA, for example, if comets overlapped), and "hedgehog." Hedgehogs either have no defined head (i.e., all DNA appears to be in the tail), or the head and tail appear to be separated. Hedgehogs may represent cells that have sustained high levels of DNA damage and may be apoptotic, although certain data suggest they may represent cells with high levels of repairable DNA damage. Hedgehogs were included in the scoring if they could be adequately recognized by the software. The frequency of hedgehogs was determined by tabulating the number observed in a separate group of 150 cells per animal/tissue.

Although there was no concurrent positive control group in these cell phone RFR studies, slides were made with human TK6 cells treated with ethyl methanesulfonate (standard positive control compound for the comet assay) and were included in each electrophoresis run with each slide set as an internal technical positive control.

D.1.4. Data Analysis for the Comet Assays

For evaluation of the percent tail DNA, the nonparametric statistical tests selected for trend and for pairwise comparisons with the control group do not make any assumptions about the underlying distribution of measurements and do not require equal variances among the groups. The Jonckheere test is used to test for linear trend and the Dunn test[47] is used for pairwise comparisons of each RFR-exposed group with the chamber control group. To correct for multiple pairwise comparisons, the p value for each comparison with the control group is multiplied by the number of comparisons made. If this product is greater than 1.00, it is replaced with 1.00. The room control group was compared to the chamber control group using a two-sided Wilcoxon rank-sum test, and results are considered statistically significant if the p value is $p \leq 0.05$.

A result is considered positive if the trend test is significant and if at least one exposed group is significantly increased over the control group, or if two or more exposed groups are significantly increased over the corresponding control group. A response is equivocal if only the trend test is significant or if only a single exposed group is significantly increased over the control group. To maintain the overall significance level at 0.05 for positive and equivocal calls, the trend and pairwise differences are considered statistically significant if the one-sided p value is ≤ 0.025 (0.05/2).

Although the percent hedgehogs is reported, comet assay results (positive, equivocal, negative) are based solely on the percent tail DNA.

D.1.5. Results

DNA damage from exposure to RFR was assessed in frontal cortex, hippocampus, cerebellum, liver, blood, and heart cell samples from male mice and male and female rats using the comet assay (Table D-1, Table D-2, Table D-3, and Table D-4). For CDMA male mice, there were no

significant increases in DNA damage, measured as the percent tail DNA, in cells sampled from the three brain regions, blood, and heart tissue; there was a significant trend test for the percent tail DNA in liver cells that is of uncertain biological significance. For CDMA male and CDMA female rats, no significant increases in the percent tail DNA were observed for any tissue. For GSM male rats, there were no significant increases in DNA damage, measured as the percent tail DNA, in cells sampled from frontal cortex, cerebellum, liver, blood, or heart tissue; there was a significant trend test for the percent tail DNA in hippocampal cells that is of uncertain biological significance.

The percent tail DNA for room control animals and chamber control animals was not significantly different for 20 of the 24 tissues examined in the 5-day studies. For CDMA male mice, the percent tail DNA was lower in the frontal cortex and higher in the heart in the room control group compared to the chamber control group. For GSM male rats and CDMA female rats, the percent tail DNA in heart tissue was lower in the room control group compared to the chamber control group. For these four instances in which significant differences in the percent tail DNA were detected between the two control groups, the differences did not reach twofold (1.5–1.6-fold) except for the frontal cortex cells in CDMA male mice, which showed a twofold difference in the chamber control group over the room control that may be considered biologically relevant. Notably, negative results were observed in the dose-response studies for each of these four tissues (i.e., heart and frontal cortex in CDMA male mice and heart in GSM male rats and CDMA female rats).

Table D-1. DNA Damage in Male Mice Exposed to Whole-body CDMA-modulated Cell Phone Radiofrequency Radiation for Five Days

	Exposure Level (W/kg)	Percent Tail DNA[a]	P Value[b]	Percent Hedgehogs[a]
Frontal Cortex	Room Control[c]	0.46 ± 0.11	0.008	1.60 ± 0.39
	0	0.91 ± 0.10		3.20 ± 1.01
	5	1.15 ± 0.24	1.000	1.60 ± 0.44
	10	0.77 ± 0.12	1.000	2.00 ± 0.57
	15	1.34 ± 0.30[d]	0.954	1.33 ± 0.61[d]
	Trend[e]	p = 0.401		
Hippocampus	Room Control	6.62 ± 1.16	0.940	2.87 ± 0.66
	0	6.89 ± 1.49		4.47 ± 2.06
	5	9.19 ± 0.94	0.175	3.87 ± 1.18
	10	4.94 ± 0.89	1.000	3.40 ± 0.72
	15	7.17 ± 1.42	1.000	2.60 ± 1.24
	Trend	p = 0.727		
Cerebellum	Room Control	3.13 ± 0.47	0.174	1.00 ± 0.27
	0	2.50 ± 0.60		0.53 ± 0.17
	5	2.55 ± 0.28	0.566	1.07 ± 0.30
	10	3.37 ± 0.95	0.936	0.60 ± 0.12
	15	4.28 ± 2.37[d]	1.000	0.74 ± 0.28[d]
	Trend	p = 0.550		

	Exposure Level (W/kg)	Percent Tail DNA[a]	P Value[b]	Percent Hedgehogs[a]
Liver	Room Control	4.78 ± 0.78	0.326	8.87 ± 1.80
	0	6.05 ± 0.93		12.07 ± 3.23
	5	6.94 ± 1.88	1.000	7.40 ± 1.67
	10	11.80 ± 2.35	0.080	9.20 ± 2.14
	15	10.58 ± 1.50	0.080	14.27 ± 3.19
	Trend	p = 0.010		
Heart	Room Control	7.73 ± 0.92	0.004	2.93 ± 0.81
	0	4.78 ± 0.43		1.27 ± 0.36
	5	4.95 ± 0.29	1.000	2.00 ± 0.38
	10	4.98 ± 0.45	1.000	2.73 ± 0.76
	15	5.60 ± 0.22[d]	0.123	2.07 ± 0.84[d]
	Trend	p = 0.054		
Blood	Room Control	1.02 ± 0.16	0.650	1.47 ± 0.47
	0	0.91 ± 0.13		1.13 ± 0.47
	5	1.10 ± 0.10	0.389	1.27 ± 0.32
	10	1.06 ± 0.14	0.701	1.60 ± 0.46
	15	1.19 ± 0.10	0.144	1.33 ± 0.36
	Trend	p = 0.077		

CDMA = Code Division Multiple Access-modulated cell phone radiofrequency radiation.
[a]Data are presented as mean ± standard error; n = 10.
[b]Pairwise comparisons for exposed groups with 0 W/kg chamber control group performed using one-sided Dunn test ($p \leq 0.025$).
[c]Pairwise comparison for the room control group compared to the 0 W/kg chamber control group performed using the two-sided Wilcoxon rank-sum test ($p \leq 0.05$).
[d]n = 9.
[e]Exposure-related trends evaluated by one-sided Jonckheere test ($p \leq 0.025$). The room control group was excluded from the trend test.

Table D-2. DNA Damage in Male Rats Exposed to Whole-body CDMA-modulated Cell Phone Radiofrequency Radiation for Five Days

	Exposure Level (W/kg)	Percent Tail DNA[a]	P Value[b]	Percent Hedgehogs[a]
Frontal Cortex	Room Control[c]	13.14 ± 1.15	0.450	17.07 ± 1.86
	0	11.54 ± 1.01		20.53 ± 1.86
	3	14.39 ± 0.86	0.139	22.27 ± 1.53
	6	12.34 ± 1.15	1.000	15.89 ± 1.09
	9	14.28 ± 1.57	0.331	18.80 ± 2.27
	Trend[d]	p = 0.265		
Hippocampus	Room Control	11.55 ± 0.86	0.450	11.27 ± 2.80
	0	13.14 ± 1.04		11.00 ± 1.33
	3	14.41 ± 1.76	0.737	14.47 ± 3.77
	6	15.43 ± 2.08	0.869	16.53 ± 3.50
	9	14.07 ± 1.38	0.908	11.27 ± 1.74
	Trend	p = 0.298		

	Exposure Level (W/kg)	Percent Tail DNA[a]	P Value[b]	Percent Hedgehogs[a]
Cerebellum	Room Control	6.14 ± 0.48	0.450	0.93 ± 0.35
	0	5.76 ± 0.48		0.73 ± 0.29
	3	5.16 ± 0.31	1.000	1.73 ± 0.86
	6	5.43 ± 0.52	1.000	1.20 ± 0.36
	9	5.49 ± 0.32	1.000	1.27 ± 0.61
	Trend	p = 0.414		
Liver	Room Control	5.07 ± 0.66	0.151	14.00 ± 4.20
	0	5.96 ± 0.46		14.93 ± 2.30
	3	7.62 ± 0.40	0.064	20.33 ± 2.46
	6	7.75 ± 0.82	0.133	19.50 ± 2.20
	9	5.97 ± 0.90	1.000	10.13 ± 2.48
	Trend	p = 0.481		
Heart	Room Control	8.76 ± 0.65	0.326	6.88 ± 1.15
	0	7.53 ± 0.79		5.00 ± 0.68
	3	8.55 ± 0.88	0.888	4.87 ± 1.08
	6	7.80 ± 0.28	1.000	4.32 ± 0.91
	9	8.49 ± 0.79	0.426	3.43 ± 0.79
	Trend	p = 0.161		
Blood	Room Control	6.78 ± 1.98	0.096	9.07 ± 3.55
	0	11.29 ± 2.39		22.13 ± 4.82
	3	6.15 ± 0.71	1.000	11.33 ± 1.86
	6	5.61 ± 0.60	1.000	8.80 ± 1.11
	9	4.90 ± 0.51	1.000	5.67 ± 1.16
	Trend	p = 0.997		

CDMA = Code Division Multiple Access-modulated cell phone radiofrequency radiation.
[a]Data are presented as mean ± standard error; n = 10.
[b]Pairwise comparisons for exposed groups with 0 W/kg chamber control group performed using one-sided Dunn test ($p \leq 0.025$).
[c]Statistical analysis for the room control group compared to the 0 W/kg chamber control group performed using the two-sided Wilcoxon rank-sum test ($p \leq 0.05$).
[d]Exposure-related trends evaluated by one-sided Jonckheere test ($p \leq 0.025$). The room control group was excluded from the trend test.

Table D-3. DNA Damage in Female Rats Exposed to Whole-body CDMA-modulated Cell Phone Radiofrequency Radiation for Five Days

	Exposure Level (W/kg)	Percent Tail DNA[a]	P Value[b]	Percent Hedgehogs[a]
Frontal Cortex	Room Control[c]	8.32 ± 0.83	0.762	15.07 ± 3.97
	0	8.69 ± 1.07		13.80 ± 3.54
	3	9.73 ± 1.08	0.523	12.60 ± 3.30
	6	11.43 ± 1.61	0.189	12.47 ± 2.12
	9	10.95 ± 0.95	0.169	12.80 ± 1.94
	Trend[d]	p = 0.043		
Hippocampus	Room Control	6.71 ± 0.59	0.597	3.00 ± 0.52
	0	7.63 ± 0.85		3.07 ± 0.83
	3	8.15 ± 1.07	1.000	3.00 ± 0.62
	6	9.90 ± 1.58	0.538	5.93 ± 1.17
	9	10.26 ± 2.57	0.908	5.20 ± 1.36
	Trend	p = 0.235		
Cerebellum	Room Control	3.36 ± 0.21	0.940	7.60 ± 1.35
	0	3.69 ± 0.53		6.87 ± 1.15
	3	3.99 ± 0.65	1.000	7.33 ± 2.42
	6	3.77 ± 0.47	1.000	7.67 ± 1.27
	9	4.45 ± 0.59	0.413	7.73 ± 1.51
	Trend	p = 0.167		
Liver	Room Control	9.61 ± 0.62	0.226	22.20 ± 2.50
	0	10.85 ± 0.78		23.20 ± 2.42
	3	9.45 ± 1.08	1.000	15.60 ± 1.41
	6	8.93 ± 0.58	1.000	18.80 ± 3.24
	9	10.11 ± 0.82	1.000	19.93 ± 2.81
	Trend	p = 0.773		
Heart	Room Control	8.88 ± 0.98	0.013	6.20 ± 1.57
	0	13.50 ± 1.21		9.88 ± 2.97
	3	11.95 ± 1.38	1.000	11.60 ± 2.57
	6	13.92 ± 1.88	1.000	8.67 ± 1.90
	9	10.58 ± 1.44[e]	1.000	7.04 ± 1.90[e]
	Trend	p = 0.904		
Blood	Room Control	2.13 ± 0.39	0.364	8.80 ± 1.61
	0	1.64 ± 0.34		6.20 ± 1.27
	3	2.54 ± 0.56	0.253	8.93 ± 1.71
	6	1.89 ± 0.74	1.000	7.60 ± 1.89
	9	2.83 ± 0.39	0.061	28.47 ± 11.63
	Trend	p = 0.092		

CDMA = Code Division Multiple Access-modulated cell phone radiofrequency radiation.
[a]Data are presented as mean ± standard error; n = 10.
[b]Pairwise comparisons for exposed groups with 0 W/kg chamber control group performed using one-sided Dunn test ($p \leq 0.025$).
[c]Statistical analysis for the room control group compared to the 0 W/kg chamber control group performed using the two-sided Wilcoxon rank-sum test ($p \leq 0.05$).
[d]Exposure-related trends evaluated by one-sided Jonckheere test ($p \leq 0.025$). The room control group was excluded from the trend test.
[e]n = 9.

Table D-4. DNA Damage in Male Rats Exposed to Whole-body GSM-modulated Cell Phone Radiofrequency Radiation for Five Days

	Exposure Level (W/kg)	Percent Tail DNA[a]	P Value[b]	Percent Hedgehogs[a]
Frontal Cortex	Room Control[c]	6.96 ± 0.48	0.326	4.27 ± 0.90
	0	7.85 ± 0.65		1.87 ± 0.60
	3	7.22 ± 0.56	1.000	2.60 ± 0.71
	6	7.68 ± 0.60	1.000	1.80 ± 0.28
	9	8.93 ± 0.38	0.196	3.27 ± 1.13
	Trend[d]	p = 0.064		
Hippocampus	Room Control	6.82 ± 0.39	0.650	0.13 ± 0.09
	0	6.75 ± 0.41		3.60 ± 1.42
	3	6.43 ± 0.37	1.000	1.47 ± 0.50
	6	8.54 ± 0.64	0.073	3.40 ± 1.10
	9	9.24 ± 1.12	0.064	2.60 ± 1.24
	Trend	p = 0.002		
Cerebellum	Room Control	3.98 ± 0.48	0.450	3.00 ± 0.75
	0	3.47 ± 0.38		2.27 ± 0.52
	3	3.26 ± 0.47	1.000	2.40 ± 0.51
	6	3.28 ± 0.51	1.000	1.60 ± 0.33
	9	3.80 ± 0.54	1.000	2.87 ± 0.53
	Trend	p = 0.386		
Liver	Room Control	5.90 ± 0.84	0.880	3.27 ± 0.52
	0	5.35 ± 0.43		2.33 ± 0.30
	3	6.80 ± 0.86	0.990	4.07 ± 0.88
	6	3.59 ± 0.56	1.000	1.53 ± 0.33
	9	3.50 ± 0.40	1.000	2.80 ± 0.52
	Trend	p = 0.996		
Heart	Room Control	3.19 ± 0.37	0.007	3.27 ± 0.46
	0	5.04 ± 0.38		4.07 ± 0.48
	3	4.42 ± 0.26	1.000	2.93 ± 0.74
	6	5.41 ± 0.57	0.949	4.93 ± 0.76
	9	4.28 ± 0.28	1.000	2.47 ± 0.47
	Trend	p = 0.808		
Blood	Room Control	5.87 ± 0.75	0.326	4.87 ± 2.17
	0	7.90 ± 1.43		18.53 ± 6.17
	3	7.92 ± 0.77	1.000	15.53 ± 3.10
	6	7.36 ± 1.04	1.000	19.80 ± 2.87
	9	11.08 ± 1.47	0.123	23.80 ± 5.33
	Trend	p = 0.053		

GSM = Global System for Mobile Communications-modulated cell phone radiofrequency radiation.
[a]Data are presented as mean ± standard error; n = 10.
[b]Pairwise comparisons for exposed groups with 0 W/kg chamber control group performed using one-sided Dunn test ($p \leq 0.025$).
[c]Statistical analysis for the room control group compared to the 0 W/kg chamber control group performed using the two-sided Wilcoxon rank-sum test ($p \leq 0.05$).
[d]Exposure-related trends evaluated by one-sided Jonckheere test ($p \leq 0.025$). The room control group was excluded from the trend test.

Appendix E. Ingredients, Nutrient Composition, and Contaminant Levels in NTP-2000 Rat and Mouse Ration

Table of Contents

Tables

E.1. NTP-2000 Feed

Table E-1. Ingredients of NTP-2000 Rat and Mouse Ration

Ingredients	Percent by Weight
Ground Hard Winter Wheat	23.00
Ground #2 Yellow Shelled Corn	22.44
Wheat Middlings	15.0
Oat Hulls	8.5
Alfalfa Meal (Dehydrated, 17% Protein)	7.5
Purified Cellulose	5.5
Soybean Meal (49% Protein)	4.0
Fish Meal (60% Protein)	4.0
Corn Oil (without Preservatives)	3.0
Soy Oil (without Preservatives)	3.0
Dried Brewer's Yeast	1.0
Calcium Carbonate (USP)	0.9
Vitamin Premix[a]	0.5
Mineral Premix[b]	0.5
Calcium Phosphate, Dibasic (USP)	0.4
Sodium Chloride	0.3
Choline Chloride (70% Choline)	0.26
Methionine	0.2

USP = United States Pharmacopeia.
[a]Wheat middlings as carrier.
[b]Calcium carbonate as carrier.

Table E-2. Vitamins and Minerals in NTP-2000 Rat and Mouse Ration

	Amount[a]	Source
Vitamins		
Vitamin A	4,000 IU	Stabilized vitamin A palmitate or acetate
Vitamin D	1,000 IU	D-activated animal sterol
Vitamin K	1.0 mg	Menadione sodium bisulfite complex
α-Tocopheryl Acetate	100 IU	–
Niacin	23 mg	–
Folic Acid	1.1 mg	–
d-Pantothenic Acid	10 mg	d-Calcium pantothenate
Riboflavin	3.3 mg	–
Thiamine	4 mg	Thiamine mononitrate

	Amount[a]	Source
B_{12}	52 µg	–
Pyridoxine	6.3 mg	Pyridoxine hydrochloride
Biotin	0.2 mg	d-Biotin
Minerals		
Magnesium	514 mg	Magnesium oxide
Iron	35 mg	Iron sulfate
Zinc	12 mg	Zinc oxide
Manganese	10 mg	Manganese oxide
Copper	2.0 mg	Copper sulfate
Iodine	0.2 mg	Calcium iodate
Chromium	0.2 mg	Chromium acetate

[a]Per kg of finished diet.

Table E-3. Nutrient Composition of NTP-2000 Rat and Mouse Ration

Nutrient	Mean ± Standard Deviation	Range	Number of Samples
Protein (% by Weight)	14.45 ± 0.191	14.3–14.7	4
Crude Fat (% by Weight)	8.1 ± 0.0816	8.0–8.2	4
Crude Fiber (% by Weight)	9.96 ± 0.312	9.68–10.4	4
Ash (% by Weight)	5.31 ± 0.252	5.07–5.53	4
Amino Acids (% of Total Diet)			
Arginine	0.807 ± 0.070	0.67–0.97	32
Cystine	0.220 ± 0.021	0.15–0.25	32
Glycine	0.704 ± 0.037	0.62–0.8	32
Histidine	0.340 ± 0.067	0.27–0.68	32
Isoleucine	0.546 ± 0.037	0.43–0.66	32
Leucine	1.095 ± 0.060	0.96–1.24	32
Lysine	0.698 ± 0.100	0.31–0.86	32
Methionine	0.407 ± 0.039	0.26–0.49	32
Phenylalanine	0.628 ± 0.035	0.54–0.72	32
Threonine	0.513 ± 0.039	0.43–0.61	32
Tryptophan	0.168 ± 0.070	0.11–0525	32
Tyrosine	0.425 ± 0.063	0.28–0.54	32
Valine	0.668 ± 0.042	0.55–0.77	32
Essential Fatty Acids (% of Total Diet)			
Linoleic	3.920 ± 0.242	3.49–4.55	32
Linolenic	0.224 ± 0.134	0.004–0.35	32

Nutrient	Mean ± Standard Deviation	Range	Number of Samples
Vitamins			
Vitamin A (IU/kg)	3,353 ± 69	2,390–4,040	4
α-Tocopherol (ppm)	74.38 ± 23.62	20.3–124.0	32
Thiamine (ppm)[a]	7.075 ± 0.492	6.7–7.8	4
Riboflavin (ppm)	8.02 ± 3.46	1.1–17.5	32
Niacin (ppm)	81.46 ± 10.62	66.4–107.0	32
Pantothenic Acid (ppm)	28.61 ± 10.7	17.4–81.0	32
Pyridoxine (ppm)[a]	9.60 ± 2.46	2.3–14.3	32
Folic Acid (ppm)	1.65 ± 0.47	1.15–3.27	32
Biotin (ppm)	0.323 ± 0.112	0.0–0.704	32
B_{12} (ppb)	50.57 ± 33.14	18.3–174.0	32
Choline (as Chloride) (ppm)	2,537 ± 628	1,160–3,790	32
Minerals			
Calcium (%)	0.065 ± 0.09	0.954–1.15	4
Phosphorus (%)	0.614 ± 0.026	0.577–0.635	4
Potassium (%)	0.662 ± 0.035	0.569–0.733	32
Chloride (%)	0.395 ± 0.068	0.3–0.688	32
Sodium (%)	0.192 ± 0.026	0.153–0.283	32
Magnesium (%)	0.216 ± 0.052	0.185–0.49	32
Iron (ppm)	181.8 ± 46.27	21–311	32
Manganese (ppm)	49.87 ± 8.97	21.0–73.1	32
Zinc (ppm)	51.13 ± 9.64	18.4–78.5	32
Copper (ppm)	7.70 ± 2.42	3.21–16.3	32
Iodine (ppm)	0.50 ± 0.236	0–1.0	32
Chromium (ppm)	0.72 ± 0.66	0.249–3.97	31
Cobalt (ppm)	0.215 ± 0.146	0.086–0.864	30

[a]As hydrochloride.

Table E-4. Contaminant Levels in NTP-2000 Rat and Mouse Ration

	Mean ± Standard Deviation	Range	Number of Samples
Contaminants			
Arsenic (ppm)	0.185 ± 0.020	0.169–0.214	4
Cadmium (ppm)	0.062 ± 0.0167	0.47–0.085	4
Lead (ppm)	0.085 ± 0.0104	0.02–0.08	4
Mercury (ppm)	0.01 ± 0.0034	0.005–0.0129	4
Selenium (ppm)	0.0098 ± 0.0034	0.107–0.24	4

	Mean ± Standard Deviation	Range	Number of Samples
Aflatoxins (ppb)[a]	<5.0	–	4
Nitrate Nitrogen (ppm)[b]	9.58 ± 1.42	8.67–11.7	4
Nitrite Nitrogen (ppm)[b]	0.212 ± 0.112	0.122–0.355	4
BHA (ppm)[c]	1.0175 ± 0.035	1.0–1.07	4
BHT (ppm)[a,c]	<1.0	–	4
Aerobic Plate Count (CFU/g)[d]	<10.0	–	4
Coliform (MPN/g)[d]	<3	–	4
Escherichia coli (MPN/g)[d]	<3	–	4
Salmonella sp. (MPN/g)	Negative	–	4
Total Nitrosamines (ppb)[e]	7.325 ± 3.45	3.4–11.7	4
N-Nitrosodimethylamine (ppb)[e]	2.625 ± 1.86	1.5–5.4	4
N-Nitrosopyrrolidine (ppb)[e]	4.7 ± 2.173	1.7–6.3	4
Pesticides (ppm)[f]			
Methyl Chlorpyrifos	0.0315 ± 0.0075	0.024–0.039	2
Deltamethrin	0.12 ± 0.0100	0.11–0.13	2
Malathion	0.172 ± 0.0814	0.068–0.27	4
Piperonyl Butoxide	2.4	2.4–2.4	1
THPI	0.015	0.015–0.015	1

All samples were irradiated.
BHA = butylated hydroxyanisole; BHT = butylated hydroxytoluene; CFU = colony-forming units; MPN = most probable number; THPI = 1,2,3,6-Tetrahydrophthalimide.
[a]All values were below the detection limit. The detection limit is given as the mean.
[b]Sources of contamination include alfalfa, grains, and fish meal.
[c]Sources of contamination include soy oil and fish meal.
[d]Results of microbiological analyses were less than the limit of detection.
[e]All values were corrected for percent recovery.
[f]Only pesticides above the limit of quantitation (LOQ) are listed. All pesticides tested can be found in the Chemical Effects in Biological Systems (CEBS) database.[36]

Appendix F. Sentinel Animal Program

Table of Contents

Tables

F.1. Methods

Rodents used in National Institute of Environmental Health Sciences Division of Translational Toxicology studies are produced in optimally clean facilities to eliminate potential pathogens that might affect study results. The Sentinel Animal Program is part of the periodic monitoring of animal health that occurs during the toxicological evaluation of test agents. Under this program, the disease state of the rodents is monitored via sera or feces from extra (sentinel) or exposed animals in the study rooms. The sentinel animals and the study animals are subject to identical environmental conditions. Furthermore, the sentinel animals come from the same production source and weanling groups as the animals used for the studies of test agents.

Blood samples were collected from each sentinel animal via dried blood spot sampling technology. Additionally, fecal samples were collected and tested for endoparasites and *Helicobacter* species. Pelt swabs were evaluated for the presence of ectoparasites. All samples were processed appropriately with serology, ectoparasites, endoparasites, and *Helicobacter* testing performed by IDEXX BioAnalytics (formerly Rodent Animal Diagnostic Laboratory [RADIL], University of Missouri), Columbia, MO, for determination of the presence of pathogens.

The laboratory methods and agents for which testing was performed are tabulated below; the times at which samples were collected during the studies are also listed (Table F-1, Table F-2).

F.2. Results

Rats: All test results were negative.

Mice: All test results were negative.

Table F-1. Methods and Results for Sentinel Animal Testing in Male and Female Rats

Five-day Studies	
Collection Time Points	**Pre-exposure**
Number Examined (Males/Females)	5/5
Method/Test	
Multiplex Fluorescent Immunoassay (MFI)	–
Kilham rat virus (KRV)	–
Lymphocytic choriomeningitis virus (LCMV)	–
Mycoplasma pulmonis	–
Pneumocystis carinii	–
Pneumonia virus of mice (PVM)	–
Rat coronavirus/sialodacryoadenitis virus (RCV/SDA)	–
Rat minute virus (RMV)	–
Rat parvo virus (RPV)	–
Rat theilovirus (RTV)	–

Five-day Studies	
Reovirus Type 3 (REO3)	–
Sendai	–
Theiler's murine encephalomyelitis virus (TMEV)	–
Toolan's H-1	–
Fecal Polymerase Chain Reaction (PCR)	
Helicobacter spp.	–
Helicobacter bilis	–
Helicobacter ganmani	–
Helicobacter hepaticus	–
Helicobacter mastomyrinus	–
Helicobacter rodentium	–
Helicobacter typhlonius	–
Aspiculuris tetraptera	–
Syphacia muris	–
Syphacia obvelata	–
Pelt Swabs	
Myocoptes	–
Radfordia/Myobia	–

– = negative.

Table F-2. Methods and Results for Sentinel Animal Testing in Male Mice

Five-day Study	
Collection Time Points	**Pre-exposure**
Number Examined (Males)	5
Method/Test	
Multiplex Fluorescent Immunoassay (MFI)	
Ectromelia virus (ECTV)	–
Epizootic diarrhea of infant mice (EDIM)	–
Lymphocytic choriomeningitis virus (LCMV)	–
Minute virus of mice (MVM)	–
Mouse hepatitis virus (MHV)	–
Mouse norovirus (MNV)	–
Mouse parvovirus (MPV)	–
Mycoplasma pulmonis	–
Pneumonia virus of mice (PVM)	–
Reovirus Type 3 (REO3)	–

Five-day Study	
Sendai	–
Theiler's murine encephalomyelitis virus (TMEV)	–
Fecal Polymerase Chain Reaction (PCR)	
Helicobacter spp.	–
Helicobacter bilis	–
Helicobacter ganmani	–
Helicobacter hepaticus	–
Helicobacter mastomyrinus	–
Helicobacter rodentium	–
Helicobacter typhlonius	–
Aspiculuris tetraptera	–
Syphacia muris	–
Syphacia obvelata	–
Pelt Swabs	
Myocoptes	–
Radfordia/Myobia	–

– = negative.

Appendix G. Supplemental Data

Tables with supplemental data can be found here: https://doi.org/10.22427/NIEHS-DATA-NIEHS-RFRA.[36]

G.1. Cage Grommet Modification Experiment – Male Rats

I04 – Body Weight Analysis: Evaluation of Male Rats in Different Housing Conditions Following Cage Grommet Modification
I04_Body_Weight_Analysis_ Evaluation_of_Male_Rats_in_Different_Housing_Conditions_Following_Cage_Grommet_Modification.pdf

I04 – Body Weight Analysis: Evaluation of Male Rats in Different Housing Conditions
I04_Body_Weight_Analysis_ Evaluation_of_Male_Rats_in_Different_Housing_Conditions.pdf

G.2. CDMA Male Mice

G01 – In Vivo Alkaline Comet Assay Summary Data
G08015E_G01_In_Vivo_Alkaline_Comet_Assay_Summary_Data_CDMA_Male_Mice.pdf

I01 – Animal Removal Summary
C0801501_I01_Animal_Removal_Summary_CDMA_Male_Mice.pdf

I02 – Animal Removals
C0801501_I02_Animal_Removals_CDMA_Male_Mice.pdf

I04 – Body Weight Analysis
C0801501_I04_Body_Weight_Analysis_RFR_2.0_5-day_CDMA_Male_Mice.pdf

I05 – Clinical Observations Summary
C0801501_I05_Clinical_Observations_Summary_CDMA_Male_Mice.pdf

Individual Animal Body Weight Data
C0801501_Individual_Animal_Body_Weight_Data_CDMA_Male_Mice.xlsx

Individual Animal Clinical Observations Data
C0801501_Individual_Animal_Clinical_Observations_Data_CDMA_Male_Mice.xlsx

Individual Animal Removal Reasons Data
C0801501_Individual_Animal_Removal_Reasons_Data_CDMA_Male_Mice.xlsx

Video Clinical Observations AM Off
Five_Day_Study_Video_Observations_AM_Off_CDMA_Male_Mice.xlsx

Video Clinical Observations AM On
Five_Day_Study_Video_Observations_AM_On_CDMA_Male_Mice.xlsx

Video Clinical Observations PM Off
Five_Day_Study_Video_Observations_PM_Off_CDMA_Male_Mice.xlsx

Video Clinical Observations PM On
Five_Day_Study_Video_Observations_PM_On_CDMA_Male_Mice.xlsx

G.3. CDMA Rats

G01 – In Vivo Alkaline Comet Assay Summary Data - Female
G08015E_G01_In_Vivo_Alkaline_Comet_Assay_Summary_Data_CDMA_Female_Rats.pdf

G01 – In Vivo Alkaline Comet Assay Summary Data - Male
G08015E_G01_In_Vivo_Alkaline_Comet_Assay_Summary_Data_CDMA_Male_Rats.pdf

I01 – Animal Removal Summary
C0801502_I01_Animal_Removal_Summary_CDMA_Rats.pdf

I02 – Animal Removals
C0801502_I02_Animal_Removals_CDMA_Rats.pdf

I04 – Body Weight Analysis
C0801502_I04_Body_Weight_Analysis_CDMA_Rats.pdf

I05 – Clinical Observations Summary
C0801502_I05_Clinical_Observations_Summary_CDMA_Rats.pdf

Individual Animal Body Weight Data
C0801502_Individual_Animal_Body_Weight_Data_CDMA_Rats.xlsx

Individual Animal Clinical Observations Data
C0801502_Individual_Animal_Clinical_Observations_Data_CDMA_Rats.xlsx

Individual Animal Removal Reasons Data
C0801502_Individual_Animal_Removal_Reasons_Data_CDMA_Male_Rats.xlsx

Video Clinical Observations AM Off
Five_Day_Study_Video_Observations_AM_Off_CDMA_Rats.xlsx

Video Clinical Observations AM On
Five_Day_Study_Video_Observations_AM_On_CDMA_Rats.xlsx

Video Clinical Observations PM Off
Five_Day_Study_Video_Observations_PM_Off_CDMA_Rats.xlsx

Video Clinical Observations PM On
Five_Day_Study_Video_Observations_PM_On_CDMA_Rats.xlsx

G.4. GSM Male Rats

G01 – In Vivo Alkaline Comet Assay Summary Data
G08013E_G01_In_Vivo_Alkaline_Comet_Assay_Summary_Data_GSM_Male_Rats.pdf

I01 – Animal Removal Summary
C0801302_I01_Animal_Removal_Summary_GSM_Male_Rats.pdf

I02 – Animal Removals
C0801302_I02_Animal_Removals_GSM_Male_Rats.pdf

I04 – Body Weight Analysis
C0801302_I04_body_weight_Analysis_GSM_Male_Rats.pdf

I05 – Clinical Observations Summary
C0801302_I05_Clinical_Observations_Summary_GSM_Male_Rats.pdf

Individual Animal Body Weight Data
C0801302_Individual_Animal_Body_Weight_Data_GSM_Male_Rats.xlsx

Individual Animal Clinical Observations Data
C0801302_Individual_Animal_Clinical_Observations_Data_GSM_Male_Rats.xlsx

Individual Animal Removal Reasons Data
C0801302_Individual_Animal_Removal_Reasons_Data_GSM_Male_Rats.xlsx

Video Clinical Observations AM Off
Video_Clinical_Observations_AM_Off_GSM_Male_Rats_508c.xlsx

Video Clinical Observations AM On
Video_Clinical_Observations_AM_On_GSM_Male_Rats_508c.xlsx

Video Clinical Observations PM Off
Video_Clinical_Observations_PM_Off_GSM_Male_Rats_508c.xlsx

Video Clinical Observations PM On
Video_Clinical_Observations_PM_On_GSM_Male_Rats_508c.xlsx

G.5. Current Pesticides Analyzed in Rodent Feed

Current Pesticides Analyzed in Rodent Feed
Current Pesticides Analyzed in Rodent Feed.pdf

National Institute of
Environmental Health Sciences
Division of Translational Toxicology
Office of Policy, Review, and Outreach
P.O. Box 12233
Durham, NC 27709